University of Strathclyde

Department of Electrical and Electronic Engineering

Model-Free Non-Invasive Health Assessment for Battery Energy Storage Assets

By

Joanna Sobon

A thesis presented to the fulfilment of the requirements for the degree

of

Doctor of Philosophy

2023

Originality and Copyright Declaration

This thesis is the result of the author's original research. It has been composed by the author, except where states otherwise by reference or acknowledgement. The work presented here has not been previously submitted for examination, which has led to the award of a degree.

Abstract

Increasing penetration of renewable energy generation in the modern power network introduces uncertainty about the energy available to maintain a balance between generation and demand due to its time-fluctuating output that is strongly dependent on the weather. With the development of energy storage technology, there is the potential for this technology to become a key element to help overcome this intermittency in a generation. However, the increasing penetration of battery energy storage within the power network introduces an additional challenge to asset owners on how to monitor and manage battery health. The accurate estimation of the health of this device is crucial in determining its reliability, power-delivering capability and ability to contribute to the operation of the whole power system. Generally, doing this requires invasive measurements or computationally expensive physics-based models, which do not scale up cost-effectively to a fleet of assets.

As storage aggregation becomes more commonplace, there is a need for a health metric that will be able to predict battery health based only on the limited information available, eliminating the necessity of installation of extensive telemetry in the system. This work develops a solution to battery health prognostics by providing an alternative, a non-invasive approach to the estimation of battery health that estimates the extent to which a battery asset has been maloperated based only on the battery-operating regime imposed on the device. The model introduced in this work is based on the Hidden Markov Model, which stochastically models the battery limitations imposed by its chemistry as a combination of present and previous sequential charging actions, and articulates the preferred operating regime as a measure of health consequence.

The resulting methodology is demonstrated on distribution network level electrical demand and generation data, accurately predicting maloperation under a number of battery technology scenarios. The effectiveness of the proposed battery maloperation model as a proxy for actual battery degradation for lithium-ion technology was also tested against lab tested battery degradation data, showing that the proposed health measure in terms of maloperation level reflected that measured in terms of capacity fade. The developed model can support condition monitoring and remaining useful life estimates, but in the wider context could also be used as the policy function in an automated scheduler to utilise assets while optimising their health.

Acknowledgements

I would like to express my sincere gratitude to my supervisor, Dr Bruce Stephen, for providing valuable support, advice and guidance at any point in my Ph. D study.

I want to express my appreciation to all my friends and colleagues from the University of Strathclyde who, in some way, played a part in this project for their valuable assistance, support and encouragement. I want to express special thanks to my best friends Renan, Syiska and Xu for always being when I needed them.

Thank you, Allison, Susan, Eleni, Syiska, and Tania from 'The mothers pursuing PhD support Group' for always being with me when I needed support and reassurance. Pursuing a PhD and being a full-time mum of two was extremely challenging. It was great to be able to share with you my 'ups' and 'downs', knowing that you fully understand what I am going through.

I would like to offer my special thanks to Dr Helena Gleskova for the opportunity of being involved in teaching one of her classes. The chance to interact with students during the classes, share my knowledge and enthusiasm for the subject with them, observing how their knowledge and confidence in the subject were developing was a wonderful experience that I enjoyed.

I also would like to acknowledge ETC Ltd. Company for co-funding my PhD studies. I want to express a special thanks to John Bingham and Euan McPherson, engineers from this company, for their support during the first year of my PhD. I would like to also thank the technicians at ETC Ltd. for their help with connecting my equipment.

This thesis is dedicated to my beloved Husband and my wonderful daughters, Nicola and Emily. I could never finish this work if it were not for your support, patience, understanding, encouragement and unwavering belief in me.

TABLE OF CONTENTS

List of Figures

List of Tables

Glossary and Abbreviations

AC	Alternating Current
ANN	Artificial Neural Network
AR	Autoregressive
ARIMA	Autoregressive Integrated Moving Average
BES	Battery Energy Storage
BIC	Bayesian Information Criterion
BMS	Battery Management Systems
BPNN	Backpropagation Neural Network
DC	Direct Current
DNN	Deep Neural Network
EIS	Electrochemical Impedance Spectroscopy
EKF	Extended Kalmar Filter
EM	Expectation-Maximization Algorithm
EMD	Empirical Mode Decomposition
EMD-ARIMA	Empirical Mode Decomposition ARIMA
FFNN	Feed-Forward Neural Network
FN	False Negatives
FP	False Positives
FVS-SVR	Feature Vector Selection - Support Vector Regression
GBM	Gradient Boost Machine
GPR	Gaussian Process Regression
HI	Health Index
HMM	Hidden Markov Model
IOHMM	Input-Output Hidden Markov Model

KF	Kalman Filter
KiBaM	Kinetic Battery Model
LSTM-RNN	Long-Short-Term Memory Recurrent Neural Network
LV	Low Voltage
MAPE	Mean Absolute Percentage Error
MC	Markov Chain
MDP	Markov Decision Process
MLE	Maximum Likelihood Estimation
NaS	Sodium Sulphur Battery
ND-AR	Nonlinear Degradation Autoregressive
NiCd	Nickel Cadmium Battery
NiMH	Nickel Metal Hybrid Battery
NN	Neural Network
PF	Particle Filter
PKNN	Prior-Knowledge Neural Network
PNN	Probabilistic Neural Network
PV	Photovoltaic
RNN	Recurrent Neural Network
RUL	Remaining Useful Life
SNN	Structural Neural Network
SoC	State of Charge
SoH	State of Health
SSE	Sum of Squared Errors
SVR	Support Vector Regression
SVM	Support Vector Machine
TN	True Negatives

TP	True Positives
VRFB	Vanadium Redox Flow Battery
VRLA	Valve-Regulated Lead-Acid Battery
Zn/Br_2	Zinc–Bromine Flow Battery

CHAPTER 1

1. Introduction

This thesis contributes to the design of a battery model that automatically recognizes the violation of battery health due to the action set by a Battery Energy Storage (BES) scheduler, which in a practical context can be used as the cost function when optimising the operation of a system comprising this device. Additionally, it investigates the influence of electrical demand forecasting performances on the battery schedules generated based on such forecasts, the battery state of health and the ability of this device to perform its dedicated function.

1.1 Research Background and Motivations

In the past, the power system in the UK was characterized by centralised infrastructure where large conventional, coal, nuclear, gas and oil-fired power plants provided continuous and reliable electricity that then was transported over a distance to the consumers through an electric power grid. Operation of such a system was planned centrally by scheduling the power plant outputs according to a forecast of aggregated demand, additionally incorporating a sufficient level of security margin in transmission and generation to ensure that system could withstand a single contingency (loss of a generator, a transmission line or a transformer). Recently, the power network of Great Britain has been undergoing an intensive transformation toward smart grid infrastructure that is characterized by generation distributed within the network and a greater share of renewable energy generation. Unfortunately, renewable energy generation provides time fluctuating power availability against time, dictated by weather, time of day, season and climate, introducing uncertainty about the availability of energy to maintain a balance

between generations and demand [1]. Electrical load disaggregation, from the national level to the Low Voltage (LV) feeder level, due to a decentralization of the power network introduces a higher level of uncertainty to the system when planning to balance load and generation. This is dictated by a much lower accuracy of load prediction on the local and disaggregated levels compared with the national level. As we are moving closer to the end-user, short-term, day-ahead forecasting of demand becomes more challenging due to its more volatile and noisy character on the disaggregated level [2]. With the decrease in load aggregation, the Mean Absolute Percentage Error (MAPE) in the load prediction increases significantly from around 3% at the national level, through 10% for the secondary substation, 15 – 20% for the LV feeder to 25 - 30% for end-user [2][3]. The significantly lower effectiveness of demand prediction and the uncertainty originating from unknown generation outputs become an important challenge that needs to be addressed to ensure the continuity of energy provision efficiently and reliably and that the security[1] of the system is maintained [4]. The reliability of the small power systems with high penetration of embedded renewable generation can be enhanced by accurate and timely forecasting with resulting demand-side response [5][6]. Rapid technology development in the area of energy storage places this device as a promising element of the future power network, which is capable of not only playing a prominent role in overcoming the problems of generation intermittency by providing the ability to shift demand to times when generation is available, but can also provide the ability to shift the power from off-peak hours to meet demand during peak hours by storing excess of energy and releasing it when required [7][8][9].

The increasing penetration of battery energy storage within the power network introduces an additional challenge to the asset owners on how to monitor and manage battery health to ensure the safe and reliable operation of this device despite its ageing (i.e. a gradual performance deterioration over time). Proper estimation of the battery health is of vital importance, as consequences of unexpected battery failures can result in

[1] Power system security refers to the ability of power network to withstand system contingencies without loss of supply to the customers.

economic losses and can lead to hazards for people and other equipment in the power network. Appropriate health management can help to prevent premature battery failures or catastrophic hazards, thus improving battery durability. To facilitate effective health management, the battery management system (BMS) should accurately monitor the health of the device [10] by observing health indicators (HI) such as capacity, internal resistance [11][12], State-of-Health (SoH), which is the measure of the general condition of the battery cell compared to the condition of the brand new device [13]. Accurate estimation of battery health is crucial in estimating the battery's reliability, its power-delivering capability and proper operation of the whole system comprising this device [14][15]. As the batteries age, they experience gradual degradation of performance, which results in a decline in capacity and an increase in resistance over time, due to an operating regime resulting from the user requirements and battery application, power availability for recharging, ambient conditions and battery design [16][17]. Additionally, the degradation of this device and its ageing can be accelerated if it is subject to the stress factors such as; temperature, a high or low state of charge, high depth of discharge, cycling under a partial state of charge and long intervals between recharging to fully charged state [18][19]. The processes behind the deterioration of the battery performance are very complex and depend on both the external factors mentioned above and battery chemistry, and consequently are strictly battery type dependent. They are also very difficult to measure and quantify and have an important influence on the changes observed in the HI.

A battery as an electrochemical device is subject to a different chemical reaction when operated/cycled and stored, depending on its technology, design and chemistry. Those electrochemical processes are physically difficult to observe by direct measurements introducing requirements to apply other techniques to monitor or predict a battery state. A common choice of battery state and health estimation is modelling based on the critical battery variables such as voltage, internal battery resistance, current, battery and ambient temperature and operating time and other variables collected or measured from experiments. An important drawback of this approach is that it cannot be done online during normal battery operation. Moreover, some variables are very difficult to measure,

such as internal battery temperature or internal resistance. It is impossible to measure internal battery temperature directly. This is possible only by using the sensor mounted to the surface of the battery cell with the assumption that the measured value approximates the mean cell temperature, or by using the measured value in conjunction with the thermal model [20]. The research on the possibility of measuring internal battery temperature using internally embedded thermocouples (temperature sensors) was carried out by Li et al. [21], Mutyala et al. [22] and Mörtel et al. [23]. However, this approach introduces additional manufacturing challenges and can result in increased costs for the battery systems. Proper modelling of battery health often requires a substantial amount of training data that needs to be available; additionally resulting model often requires multiple inputs for predicting battery health, such as current, voltage, temperature and others, depending on how the model was structured. This introduces the need for the installation of additional telemetry for gathering the required input data for the model to allow its application. Another option for battery state and health monitoring is a direct (online) observation of the voltage, current and temperature of this device. This introduces the need for the installation of numerous sensors to measure indicative variables. In a situation when we deal with the rising number of BES incorporated within the system, this can introduce significant costs, increase the level of maintenance required to ensure the proper operation of such sensors, and will introduce a substantial amount of data to be processed. Moreover, online measurements suffer from signal noise and quality that can result from sensor degradation due to harsh working environments [24]. This in turn, reduces the efficiency of estimation of battery health leading often to inaccurate results. The accuracy of the sensor can also affect the estimation of the battery's health. For example, the measuring of the voltage with sensors of a low accuracy cannot capture small changes in voltages leading to inaccurate impedance calculation [25] and internal resistance estimation leading to a wrong assessment of battery health.

As storage aggregation becomes more commonplace, the management of the constituent battery assets will require health metrics in order to ensure ongoing contractual turn-up and turn-down commitments are fulfilled to their agreed capacity and that the

system operates safely and in a reliable manner. As the current battery health monitoring solutions are not ideal, they often add extra telemetry installation costs, require impractical volumes of data, or are burdened with high computational costs; there is a need for a new health metric for batteries that will:

- Minimise input data requirements eliminating the necessity of installation of extensive telemetry,
- Be able to provide information if the battery is operated in a way that can prolong its life instead leading to the premature replacement of this device based only on the limited information available, for example, simple knowledge of the battery charging regime.

This work aims to provide a solution to the battery health prognostics by providing an alternative way of assessing battery health by capturing cumulative maloperation level as a proxy for cell health, articulated via the strong influence misuse has on the internal chemical state.

1.2 Research Objective

Primary objective: This work aims to develop an alternative, non-invasive approach to the estimation of battery health that estimate the extent to which a battery asset has been maloperated based only on the battery operating regime: the charge/discharge/hold actions set by a BES scheduler. This approach is proposed to address the common problems of lack of asset monitoring data, eliminate the requirement of installing telemetry, avoid potential problems due to missed reading in measurements, and reduce requirements for maintenance of the system comprising battery energy storage with extensive telemetry.

Secondary objective: To study and understand the effect of demand forecast errors on the battery energy storage schedule effectiveness and provision of functions (self-consumption increase in the system and reduction in the export energy to the grid) and the health of the storage asset.

1.3 The Original Contribution of the Thesis

This thesis provides the following contribution to knowledge:

- Cross-cutting research into battery chemistries, covered in Chapter 2, has led to the heuristic rule formulation that allowed the generation of the novel health indexes of the battery device that is based on the battery chemical preference in the context of charging action and state of charge.

- The health of battery energy storage is usually expressed and assessed in terms of capacity fading and internal resistance increase. In this work, an alternative way of measuring the battery's state of health was proposed in Chapter 4. This work alternatively proposes capturing cumulative maloperation as a proxy for cell health, motivated by the strong influence misuse has on the internal state of the battery.

- The Input-Output Hidden Markov Model (IOHMM) framework was not previously applied in the area of battery health prediction. It has wide usage in the processing of grammatical inference problems [26], synthesis of facial animation from audio [27], hand gesture recognition [28], modelling of financial returns series [29], modelling of forecasting of electricity prices [30] and fault diagnosis and prognosis of diesel generators [31]. This work proposes, designs and validates the IOHMM battery model that automatically recognizes the violation of battery health due to the action sets by a BES scheduler, the subject of Chapter 4. The model automatically recognizes violations of chemistry-specific usage preferences from observed charging actions and can constitute the metric to the cost function for charge schedule optimization.

- Increasing understanding of the effect of demand forecasting error on the effectiveness of battery energy storage schedule and battery health with the application of developed IOHMM battery maloperation model in conjunction with

designed generic parametrized forecasting and energy storage scheduling tool for small power parks and microgrid applications, the subject of Chapter 5.

1.4 Publications

The following peer reviewed works have been published during the course of this PhD:

- J. Sobon and B. Stephen, "Model-Free Non-Invasive Health Assessment for Battery Energy Storage Assets", IEEE Access, Apr. 2021. This publication is based on the work discussed in chapters two, three and four and covers the first three contributions of work presented in this thesis.
- J. Sobon, A. Roscoe, and B. Stephen, "Energy storage day-ahead scheduling to reduce grid energy export and increase self-consumption for micro-grid and small power park applications," in *2017 52nd International Universities Power Engineering Conference, UPEC 2017*, 2017. This conference paper partially covers the last contribution of the work presented in this thesis. The expanded version of this publication is presented in Chapter 5.

1.5 Thesis Overview

This thesis is structured as follows:

Chapter 2: In this chapter, an extensive technical review of contemporary battery technologies often used in energy storage applications in the power sector is carried out, followed by the derivation of heuristic rules that were used to generate novel health indexes required for model training and testing.

Chapter 3: In this chapter, the state-of-art in battery health modelling is discussed. The shortcomings of currently used methods in battery health prognostics as well as the overall problem of the lack of suitable datasets are discussed here. The gaps in the battery health monitoring are identified, and an alternative solution is proposed, which is then implemented in consecutive chapter.

Chapter 4: This chapter consists of the development of the IOHMM of BES based on the rules formulated in Chapter 2. It describes the full procedure of model development, starting from data generation through model training and ending with the validation of the developed battery maloperation model against a publicly available data set. This chapter contributed to the design of a novel machine-learning model employing the IOHMM, which captures battery degradation mechanisms without considering the detailed chemistry and physics of the asset.

Chapter 5: This chapter comprises the development of parametrized availability-based battery energy storage scheduling tool, which employs different demand forecasting models, and produces a charge/discharge schedule that reduces export to the grid and increases self-consumption energy in the microgrid or small power park applications. In this chapter, the influence of the forecast error on the effectiveness of the BES schedule and the fulfilment of the main functions by this device is investigated. Additionally, the influence of the BES schedule based on different demand forecast models and associated errors in demand prediction on the battery maloperation level is examined. This chapter demonstrated the operational practicality of the battery maloperation model developed in the preceding chapter. It contributed to an increasing understanding of how the error in forecasted demand influenced the effectiveness of the battery schedules generated based on this forecast and how it is reflected in the battery maloperation level.

Chapter 6: The subsequent chapter concludes the work presented in this thesis. Finally, further work is discussed, followed by appendixes and references to work cited in this thesis.

CHAPTER 2

This chapter and the next two consecutive chapters constitute an extended version of a journal paper published in IEEE Access Journal in 2021 by Joanna Sobon and Bruce Stephen, titled: "Model-Free Non-Invasive Health Assessment for Battery Energy Storage Assets" [32].

2. Battery Technology Review and Heuristics Rules Formulation for Battery Model Training.

A rechargeable battery, also known as a secondary battery, is an electrochemical device that is capable of storing energy and releasing it when required. It comprises electrochemical cells that are connected in series and/or parallel to achieve the required capacity and voltage. In the battery cell, electrical energy is converted into chemical energy through the electrochemical reactions during the charging processes and converted back to electrical energy when discharged. The simplified schematic of the battery cell with reactions that takes place at electrodes during the charge and discharge processes is shown in Fig. 1. The *k* electrons are released from the reductant (R_1) at the anode (1). The electrons, which are excess in the anode, now flow to the cathode through the external load connected to the battery cell. At the same time, at the cathode, j electrons are accepted by an oxidant (O_2) (2).

$$R_1 \rightarrow O_1 + ke^- \quad \text{(Reactions at the anode during discharge)} \qquad (1)$$

$$O_2 + je^- \rightarrow R_2 \quad \text{(Reactions at the cathode during discharge)} \qquad (2)$$

The product of the oxidation of the anode, cations (positive ions) flow to the cathode through the electrolyte. Simultaneously the anions (negative ions), the product of reduction at the cathode, flow through the electrolyte to the anode, Fig. 1.

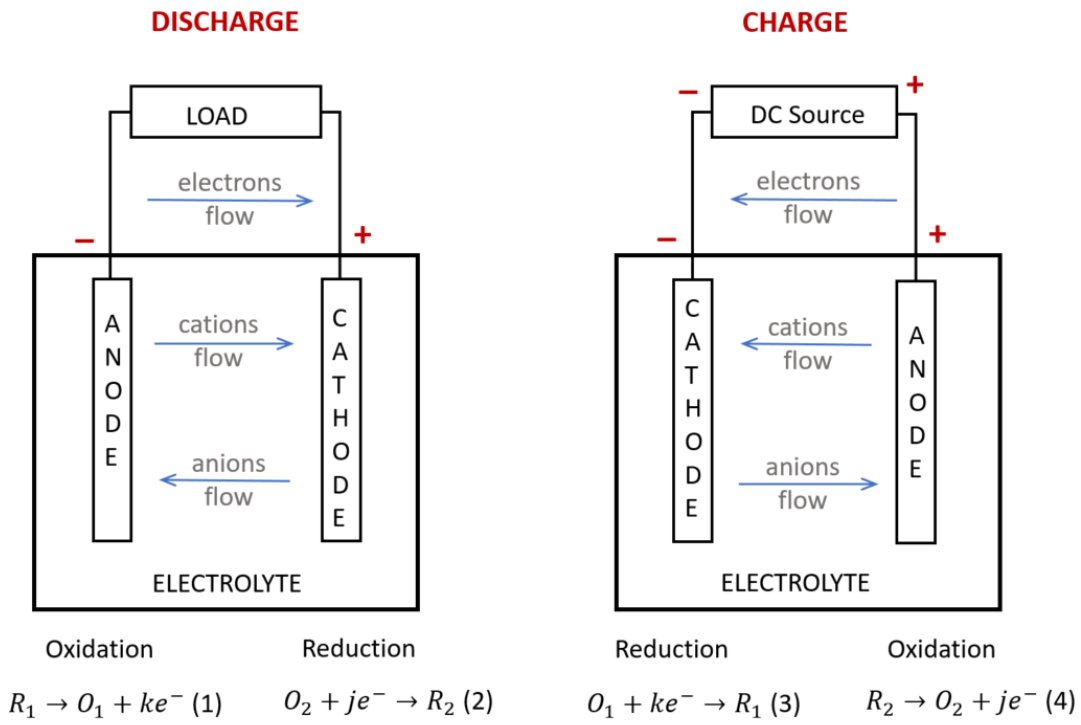

Figure 1 Simplified schematics of the rechargeable battery cell showing a flow of ions, electrons and reactions during the charging and discharging processes. The *O* in the equation means oxidant, *R* stands for reductant, j and k are the numbers of electrons, and e means electron.

During the charging process, the reactions are reversed. When the direct current (DC) source is connected to the battery, the negative terminal of the DC source to the cathode and the positive to the anode, the electrons are injected into the cathode. The reduction reaction takes place at the cathode (3) and the oxidation at the anode (4).

$$O_1 + ke^- \rightarrow R_1 \quad \text{(Reactions at the cathode during charge)} \qquad (3)$$

$$R_2 \rightarrow O_2 + je^- \quad \text{(Reactions at the anode during charge)} \qquad (4)$$

Due to reduction processes, cathode material regains its previous state. Similarly, the anode material regains electrons due to the oxidation of the anode and comes back to its state before discharge [33].

To understand the following sections, where the review of different technologies of rechargeable batteries will be discussed, a battery vocabulary needs to be introduced first. The glossary terms with their explanations, that are used to describe battery design, characteristics and operation are presented in Table 1 and Table 2, respectively.

Table 1 General glossary terms used to describe the battery.

General Terms	Definition
Anode	The negative electrode of the electrochemical cell (in discharging mode).
Charging	The process of conversion of the electrical energy supplied to the battery into the chemical energy that is stored and then reused.
Cathode	The positive electrode of the electrochemical cell (in discharging mode).
Discharging	The process of converting chemical energy stored in the battery into electrical energy that is used by the load connected to the battery.
Electrolyte	A non-metallic conductor of electricity placed between the anode and cathode of the battery cell: can be liquid, solid, molten mass, gas or vacuum.
Gassing	The evolution of the gas from one or both electrodes of the cell resulted due to the electrolysis of water during over-discharge.
Oxidation	A chemical reaction that involves electron release by the active material of battery cell electrode, anode during discharge and cathode during charge processes.
Reduction	A chemical reaction that results in the acceptance of electrons by an active material of battery cell electrode, cathode during discharge and anode during charge processes.
Separator	The permeable membrane that is placed between electrodes, anode and cathode, to prevent electrical contact between them and simultaneously allow the passage of ions.
Thermal runaway	A condition in the battery that leads to damage to the device. It occurs when the rate of heat production inside the battery due to operation is much higher than the rate of heat dissipation through the case of the battery.

Table 2 Battery characteristics glossary terms.

Terms	Definition
Capacity	The measure of the amount of energy that can be delivered during one discharge episode, usually given in amp-hour or watt-hour units, where watt-hour is equivalent to amp-hour multiplied by the battery voltage.
C rate	The measure of the rate at which the battery is discharged in relation to its maximum capacity. For example, a discharge rate equal to 1C for a 1Ah (ampere-hour) battery means that the discharge current of 1A will discharge the battery fully for 1 hour. Similarly, with the C rate of 0.5C, we will be able to provide 0.5A through 2 hours.
High-rate discharge	Drawing a large current for a short interval of time.
Low-rate discharge	Drawing a small current for a long interval of time.
Cycle	One sequence of charge and discharge.
Cycle Life	The total number of charge/discharge cycles the cell can sustain before it fails to meet specific performance criteria. The end of life of the battery is typically considered to be reached when the cell or battery delivers only 80% of its rated capacity.
Depth of discharge	The amount of energy taken from the battery cell is usually expressed as a percentage of the total battery capacity.
Deep cycle	A cycle in which the discharge of the battery is continued until its cut-off voltage is reached.
Shallow cycle	A cycle in which the discharge does not allow the battery to approach its cut-off voltage.
State of Charge	Describes the remaining capacity of the battery as a percentage of the initial capacity.
State of health	This term describes the remaining lifetime of the battery as a percentage of the lifetime of the new device.
Internal resistance	Describes the level of resistance to the flow of the electric current inside the battery.
Energy density	Measures how much energy a battery can store in a given size of the battery in watt-hours per litre (Wh/L).
Self -Discharge	The type of discharge that takes place while the battery is in an open-circuit condition.
Memory Effect	Reversible process of temporary loss of remaining capacity due to not operating in successive cycles to the full depth of discharge. Occurs in Nickel-cadmium (NiCd) cells.
Cut-off voltage	The voltage at which the battery is considered to be fully discharged. At this voltage, the load should be disconnected from the battery to prevent over-discharging.

2.1 Overview of Contemporary Rechargeable Battery Technology

Electrochemical cells can be divided into three groups: primary batteries, secondary batteries and fuel cells, Fig. 2. All electrochemical cells and batteries (multiple cells connected in parallel, series or series-and-parallel configuration) are capable of converting chemical energy into electrical energy through electrochemical reactions. The fundamental difference between batteries and fuel cells is that the fuel cell, to provide electrical energy through an electrochemical reaction, requires a continuous supply of fuel (hydrogen) and oxygen (usually from the air). In the case of batteries, the chemical energy comes from chemical materials already present in this device. Fuel cells were excluded from the scope of this work as the focus is on the devices that can store energy and provide electricity to the system without the need for supplying external fuel. For fuel cells to provide electricity first require external fuel to be available (supplied or generated), which introduces the need for additional infrastructure for hydrogen production that adds additional complexity to the modelled system. The primary batteries cannot be recharged after discharging and need to be discarded after use as the electrochemical reactions taking place inside this device are not reversible. Primary batteries are used as the power source for portable electronic devices, toys, lighting and other applications, but because they have no applications for grid-scale storage, they are out of the scope of this thesis. The secondary batteries, also called rechargeable batteries, in contrary to the primary type, can be alternately discharged and charged electrically by passing the current in the opposite direction during these processes. The taxonomy of secondary batteries is summarised in Fig.2. The red entries indicate the battery technologies that found application in the grid- scale battery energy storage systems and are the subject of this chapter. The remaining secondary battery types, black entries in Fig.2, due to the lack of application in grid-scale BES, are out of the scope of this work. The secondary batteries are also called storage batteries or accumulators. They are used as energy storage devices in power systems, vehicles, and electrical equipment such as mobile phones, laptops and other applications.

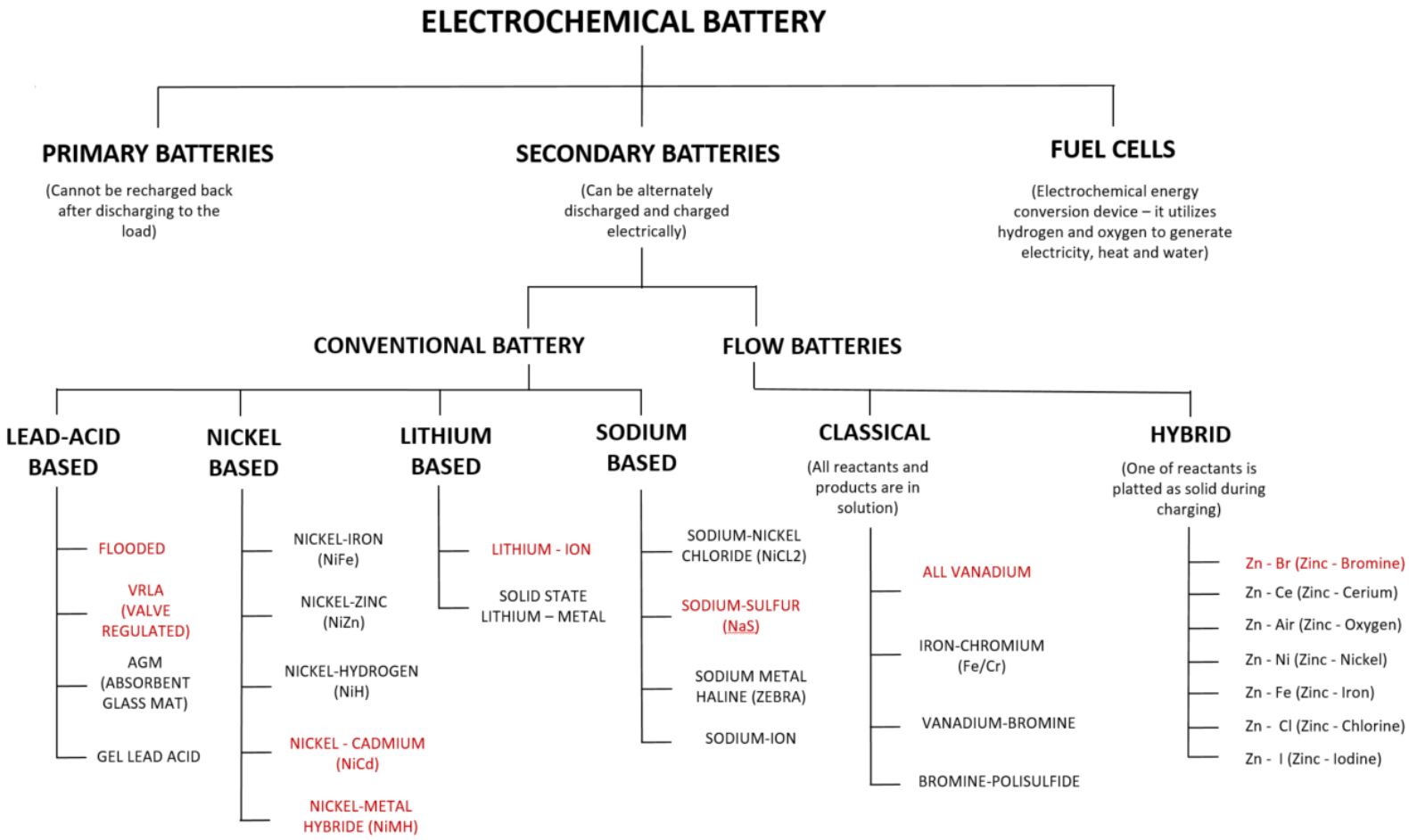

Figure 2 Battery technologies. (Red entries indicate the battery technologies that are considered in this thesis) [34]–[38]

Among secondary batteries, we have conventional and flow batteries. A fundamental difference between those two types of batteries is in the component that provides rechargeability. The energy is stored in the solid electrode in conventional batteries compared with flow battery technology in which the energy is stored in the electrolyte liquids. The construction of a classical flow battery differs from the conventional rechargeable batteries, as can be seen in Fig. 3(b)(c) and Fig.3(a), respectively. The conventional battery, Fig. 3(a), consists of electrodes (anode-negative and cathode-positive) and the medium that enables the ions to flow between electrodes, called an electrolyte. The electrolyte is usually in the form of liquid composed of water or other solvents with dissolved salts, alkalis or acids that provide ionic conduction. Some batteries have a solid-state electrolyte. This type of battery is called a solid-state battery. Contrary to conventional batteries, Figure 3(a), flow batteries, Fig. 3(b) and 3(c), consist of two external tanks with active material in liquid form that is pumped through the cell with the ion exchange membrane. The reduction/oxidation takes place on both sides of this membrane resulting in electrical potential in this type of battery [35][39].

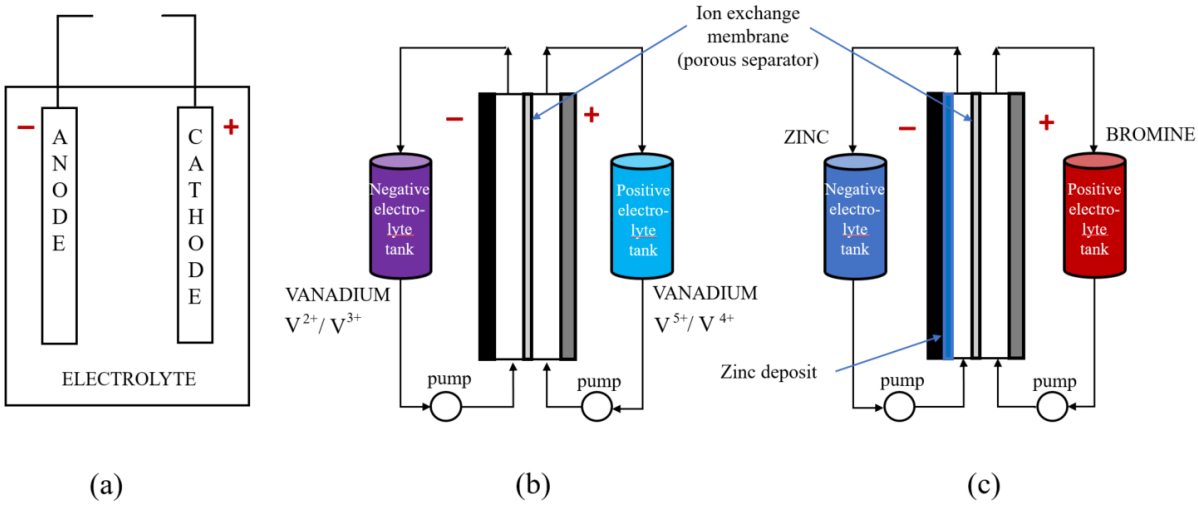

Figure 3 Difference in the construction of the conventional battery (a), classical flow battery - VRFB (b) and hybrid flow battery – Zn/Br_2 (c). (+) indicates a positive electrode (cathode), and (-) indicates a negative electrode (anode).

Flow batteries further can be divided into two groups: classical and hybrid flow batteries, Fig. 3(b) and 3(c), respectively, depending on if all reactants and products are in solution or active material is deposited on one of the electrodes. In classical flow battery such as Vanadium Redox Flow Battery (VRFB), the active material in the form of redox flow solutions are stored in separate tanks and are pumped through a stack of electrochemical cells where the solutions are separated by an ion-exchange membrane that prevents mixing of the two solutions [40]. The hybrid flow battery system, such as zinc-bromine (Zn/Br_2) also consists of two electrolyte solutions, but contrary to classical flow batteries, it involves the deposition of metal at the negative electrode during charging, Fig. 3(c) [34].

The construction of the battery has an important influence on the battery energy capacity and power of the battery system [41]. It can also have an important influence on the battery cycle life and its state of health. The voltage of the battery cell is controlled by battery chemistry [33][35]. In conventional batteries, energy capacity is governed by the weight of the active material in electrodes, and system power depends on the area of electrodes [41]. In redox flow batteries, the system power is determined by the size of the cell stack [35][42]. In this type of battery, the reactants and products are in the solution phase during charging; therefore no metal deposition occurs. This implies that the capacity of such a system is mainly determined by the size of the electrolyte tanks. In hybrid flow batteries such as zinc-bromine, during charging layer of zinc is deposited on the negative electrode; thus the total energy capacity of this type of battery is limited by the available area of the electrode (quantity of zinc metal deposited on the negative electrode) [35]. The aforementioned three parameters, voltage, capacity and power along with the thermal properties of the battery cells, are affected by the internal impedance of the cell, which is dependent on the layout of the components in the current path and their resistance and on the electrolyte conductivity. Therefore, the performance of the battery cell is affected by its construction (size, shape and materials used) [35]. Additionally, battery construction can influence the battery cycle life and its state of health. The changes that occur in the electrodes materials of conventional batteries result in their degradation over time, which limits the cyclic lifetime of this device [39][43][44]. In the flow batteries, the active

material is stored in separate tanks dissolved in liquid, thus this type of battery is free of the processes leading to mechanical breakdown of the active material, offering longer cycle life under deep discharge operation than conventional secondary batteries [35]. The summary of cycle efficiency, self-discharge rate and life cycle for the seven battery chemistries considered in this work are shown in Fig. 4, and the comparison of the battery's energy density is listed in Table 3.

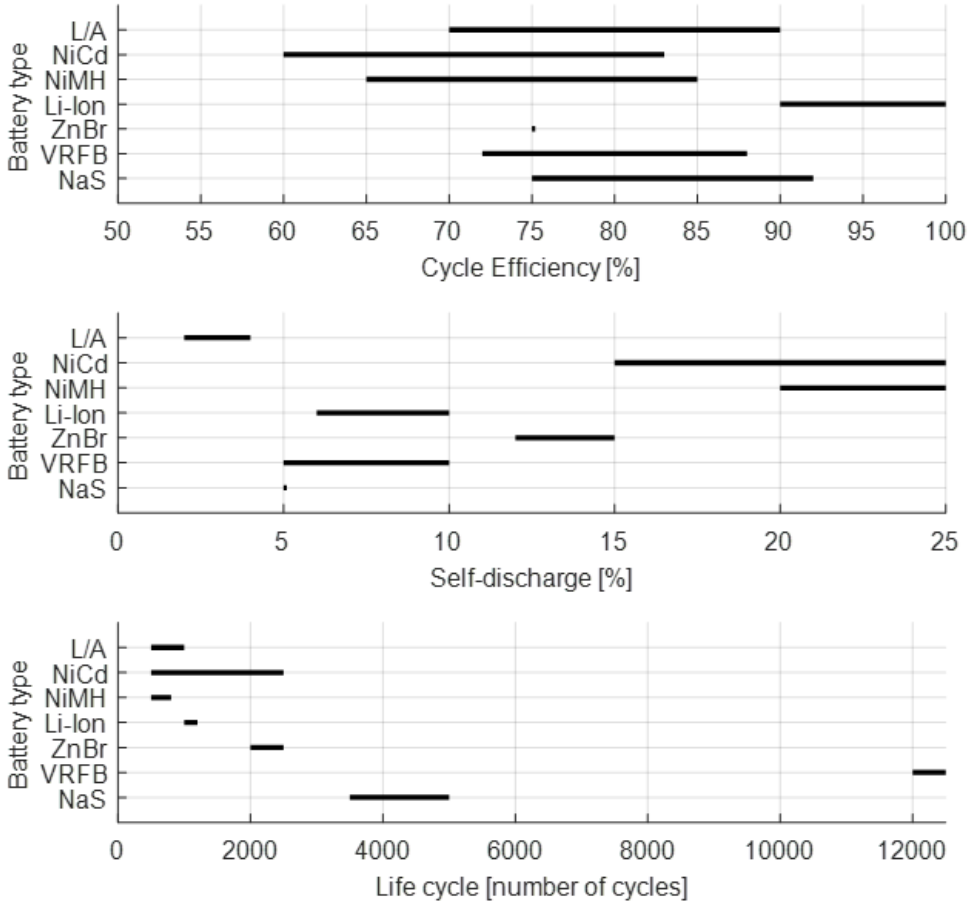

Figure 4 Cell performance for the commonly used battery chemistries in contemporary BES [45]–[48].

Table 3 Energy densities [45][46].

Battery Technology	Energy density By Weight [Wh/kg]	Energy density By Volume [Wh/ L]
Lead-acid	30-50	70-110
NiCd	50-75	100-150
NiMH	60-80	200-350
Lithium-ion	75-200	200-500
Zn/Br_2	30-50	30-60
VRFB	10-30	16-33
NaS	150-240	150-250

Both battery chemistry and battery design have a significant impact on the battery performance and preferences to the way it is operated. The review of different battery technologies used or potentially used in energy storage applications is carried out in the following sections with the aim of providing knowledge-based battery preferences to the operating regime. The following battery technologies are considered in this work: lead-acid, lithium-ion, sodium sulphur (NaS), Nickel Metal-Hybrid (NiMH), Nickel Cadmium, Zinc Bromine Flow Battery and Vanadium Redox Flow Battery.

2.1.1 Lead-acid

The lead-acid battery is one of the most mature battery types presently used. The history of this technology dates back to 1859 when it was invented by the French physicist Gaston Plante [33][49]. It was the first type of rechargeable battery ever designed [50]. Of all the lead-acid technologies available, only two dominant forms, valve-regulated lead-acid battery (VRLA-sealed lead acid) and flooded lead-acid battery, are the subject of this work as they are the most matured and are often used in battery energy storage applications. From a chemical point of view, both battery types mentioned above are alike but have

fundamental differences in construction, impacting the battery behaviour during cycling operation and the possible applications. The lead-acid batteries are sensitive not only to overcharging and over-discharging but also do not like to be chronically under-charged (i.e. not charged to the full state of charge before discharging again) [19][51]. Different chemical reactions take place inside the cell during the device cycling operation, influencing the degradation of its performance.

Storing the lead-acid battery in a not-fully charged state, self-discharge and chronically undercharging of this type of battery have a negative influence on its performance due to the harmful build-up of the sulphate crystals on the plates in a process called sulphation [18][52]. The sulphate discharge products that are deposited on the electrodes during these events result in the rise of battery internal resistance impacting negatively device performance; sulphate crystals act as an insulator to the flow of electricity in the battery [18]. When the process of sulphation is prolonged, the sulphate crystals formed can reach a size that cannot be easily broken down by the charge processes [53], and as a result, the battery becomes unserviceable. This is the reason why the lead-acid battery should be stored in the fully charged state when not used, with a charge applied every six months to prevent battery performance deterioration due to the sulphation process occurring through self-discharge of the cell. Examples of the positive and negative plates covered by the sulphate crystals (white patches on the surface of the plates) are shown in Fig. 5.

The over-discharging of the lead-acid battery or storing the battery in the discharged state for too long leads to performance deterioration due to the occurrence of the hydration process. In this process, the lead hydrates, formed during the dissolving of the lead and its compound in the water of discharged cells, are deposited on the separators leading to permanent damage to the battery from short circuits between negative and positive plates during the recharging process [33][52].

The consequences of the overcharging depend on the lead-acid battery technology and constitute the key difference between the two types of batteries considered here. In the case of the valve regulated and flooded lead-acid battery, when the cell is close to the full state of charge, the charging current is converted into electrochemical energy that is

responsible for the process of electrolysis of the water in the electrolyte, known as gassing. This process leads to the production of free oxygen and hydrogen gas that is vented from the battery in case of the flooded lead-acid battery or is subject to recombination process in VRLA type. In flooded batteries, the gassing leads to the loss of water that needs to be replenished to restore the original battery performance, in comparison to sealed lead-acid batteries, process of recombination takes place that eliminates the loss of electrolyte and necessitates replenishing the water [33][51].

Figure 5 Positive and negative sulphated plates of Lead-acid battery. (Figure reproduced from Karami et al. [54])

The lead-acid battery prefers long charging times. High-rate charge promotes the early evolution of hydrogen, and this significantly reduces the charging efficiency of the plates [47].

The lead-acid battery does not like deep cycling, which reduces its cycling life [55]. The active material of the lead-acid battery becomes soft and less cohesive over time. This process is accelerated by the deep cycling of the battery and leads to capacity loss [56]. The depth of discharge of the lead-acid battery has an important influence on the cycle

life of this device, where the cycle life is a log function of the depth of discharge [57]. Compared with lithium and nickel-based batteries, the lead-acid battery is less durable when deep cycled.

Expansion and corrosion of the positive grid structure due to oxidation of the grid and plate materials is one of the main factors leading to performance deterioration and shortening of the life of this type of battery [56][58]. Those processes lead to an increase in the internal resistance of the cell and reduce the cell's capacity. To more severe consequence of the change in the volume of the material and the increase in its corrosion is a distortion of the grid resulting in short circuits [56].

Fig. 6 shows the effect of the corrosion on the positive plate of the VRLA battery. The elevated temperature during the overcharging process increases the positive plate corrosion rate and, in the case of the VRLA, increases the risk of a thermal runaway that can lead to permanent damage to the battery [59][60].

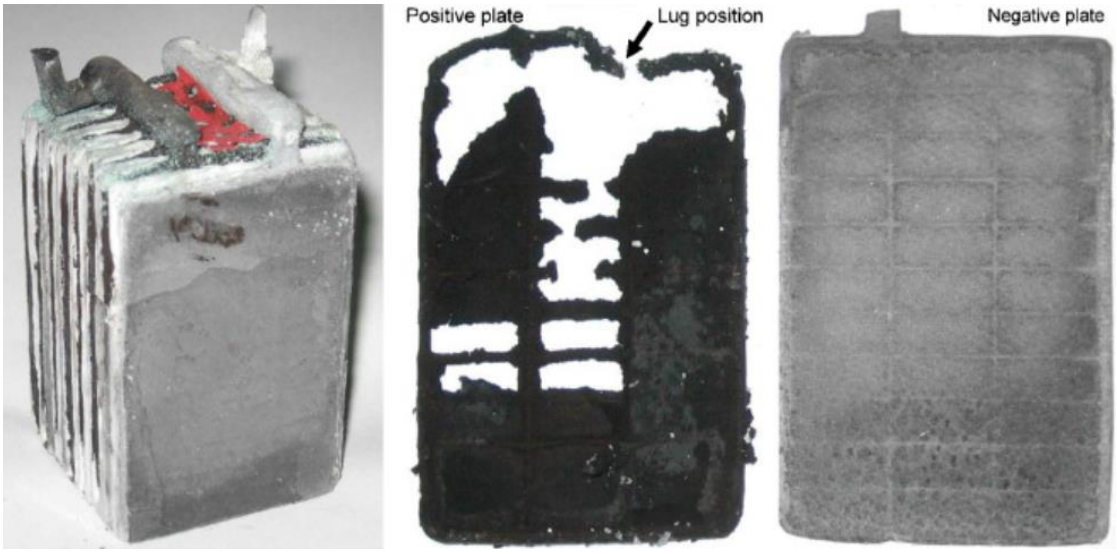

Figure 6 Severe corrosion on a Lead Acid positive grid. (Figure reprinted from Guo et al. [61])

During extensive or prolonged overcharge, the process of oxygen recombination significantly drops causing water loss, which in turn leads to rapid saturation of the

separators and a significant rise in internal resistance. If the battery reaches the point when the internally generated heat will no longer be dissipated through the casing, thermal runaway occurs [59][62]. When the temperature of the battery reaches 90°C a plastic case will become soft and start to deform due to internal pressure, as seen in Fig. 7. A more serious effect of thermal runaway is possible ignition fire or explosion due to hydrogen being released through safety vents [59][60]. All the above-mentioned changes are damaging to this device, inevitably to a point beyond economic repair, resulting in the end of the asset life.

Figure 7 VRLA battery showing runaway conditions (Figure reprinted from Hoff et al. [60]).

2.1.2 Nickel Cadmium

Due to the excellent stability of the active material, the nickel-cadmium battery (NiCd) has the potential to maintain stable capacity over long cycling. It can last over 1000 cycles until the rise in self-discharge interferes with the performance of this device [38]. This battery technology is also characterised by the low internal resistance that remains almost constant as the function of the cycling life and state of charge [38]. Unfortunately, nickel-

cadmium batteries experience a memory effect when repeatedly shallow cycled. This limits the possible applications of this battery to those that allow deep cycling operation or permit conditioning. The loss of capacity due to repeated charging of the battery before it is fully discharged can be reversed by conditioning charging (performing a couple of charge cycles after the full discharge of the battery) [38].

The charging process of the NiCd battery can be divided into three stages characterised by different voltage, temperature and charging efficiency. The charging efficiency of the nickel-cadmium battery is influenced by different chemical mechanisms occurring during each stage of the charging. In the first stage of the charging process, the loss of energy occurs. It is linked with the process of transferring a significant part of the active material into a non-usable form that takes place during this stage. With the input charge increasing, the efficiency of the charging also increases until the point when it remains almost constant during some period of time. This takes place in the second stage of charging. When the cell is close to reaching the full state of charge, the last stage of charging, the input current starts to more contribute to the oxygen production from the charging of the positive active material. The first two stages of charging are strongly endothermic as the battery cools during the charging. During the last stage, when the cell approaches a full state of charge, an increase in cell temperature occurs. This is the result of the oxygen evolution processes taking place at the positive electrode (production of oxygen) and the oxygen reduction occurring at the negative electrode (consumption of oxygen) [33]. Both mentioned above chemical reactions contribute to the cell temperature rise during the overcharging process of the NiCd battery. Similarly to the lead-acid and lithium-ion battery technologies, NiCd batteries are also prone to thermal runaway, although this phenomenon for NiCd batteries is governed by different mechanisms than in lead-acid and lithium-ion batteries. For lead-acid and lithium-ion batteries, the runaway is triggered by extensive or long-term overcharging. In the case of NiCd battery, supplementary reactions need to occur in addition to overcharge to lead to this phenomenon [63]. The thermal runaway in NiCd batteries takes place due to the acceleration of the recharging reaction in the battery and electrodes decomposition due to long recharge and

overcharging of the battery, which is connected with the drop in internal battery resistance due to heating up of the cell [64]. It was shown by [63][65] that in addition to the aforementioned mechanism, two supplementary reactions inside the battery need to occur to cause the thermal runaway. The first one is the powerful exothermic recombination of the atomic hydrogen that was accumulated in the electrodes as a result of a long operation of the battery [66][65]. An additional cause is an accumulation of the dendrites on the cadmium electrode; dendrite growth up through the separator leads to a change in the current density and an increase in electrode temperature due to a decrease in the distance between the electrodes [67].

The NiCd cell performance can be compromised due to water loss occurring during battery cycling operation, thus necessitating maintenance to retain the performance of the battery at acceptable levels [33].

2.1.3 Nickel Metal Hybride

A nickel-metal hybride battery (NiMH) was designed to eliminate the memory effect that is a shortcoming of the nickel-cadmium battery by using hydrogen-absorbing metal as the negative electrode in exchange for cadmium that was used in NiCd cells. As a result, the NiMH cell is less prone to the memory effect than the NiCd cell. Compared to the NiCd battery, it has a limited cycling life and a high self-discharge rate, which can be seen in Fig. 4, summarising the cell performance of different battery chemistries, which is included in Section 2.1. The cycle life of the NiMH battery is strongly influenced by deep discharge, overcharging and elevated temperature [68]. NiMH battery is more sensitive to overcharging than NiCd batteries. The temperature is an important factor affecting the performance and the service life of this type of battery which is related to the nature of heat generated during operation in the battery itself [38][69]. A large amount of heat is generated during fast charging and high-load discharging, which limits the application of this battery technology to those that allow the slower rate of charging and eliminates the possible high-load discharging events [69].

Both NiCd and NiMH batteries are relatively less prone to thermal runaway due to overcharging compared with the VRLA battery [64]. The runaway of the NiMH battery is associated with the intensive oxygen evolution process occurring at the positive electrode with a simultaneous significant reduction of hydrogen production at the negative electrode leading to the transfer of the excess electric energy pumped during overcharging into the heat, rising internal temperature of the cell [64].

No loss of water occurs during cycling operation in this type of battery compared to the NiCd. Water is consumed at the positive and then produced at the negative electrode during charging, and this process is reversed during the discharging of the cell [70]. Due to water recovery, the requirement for maintenance for this battery technology is minimized.

As a consequence of the over-discharging of NiMH cells, the process called voltage reversal can take place. This process involves a change in the potential of a negative electrode that becomes, as a result, more positively charged than the positive one. This can happen when the cell is discharged beyond the capacity of the positive electrode. The main effect of this process is hydrogen formation. The produced hydrogen then diffuses to what was the negative electrode and oxidizes to form water [64][68].

The charging rate of the NiMH battery above 0.5 C can be dangerous due to the rapid rise in internal battery temperature. Additionally, charging at 0.5 C is not recommended if the ambient temperature is above 23°C. Charging at higher rates, 1 C, is inefficient and causes a reduction of standard battery capacity to less than 65% before overcharging occurs [69].

2.1.4 Lithium-ion

The lithium-ion battery technology is characterised by the highest energy density of all battery technologies, see Table 3. It also has a higher cycle efficiency, reaching almost 100%, as shown in Fig. 4. Compared to nickel-cadmium technologies, Lithium-ion battery does not suffer the memory effect, and unlike lead-acid and nickel-cadmium systems, it does not require scheduled cycling to prolong its life.

Lithium-ion batteries are highly sensitive to overcharge and over-discharge which is closely related to the nature of the lithium chemistries. During the overcharging of the lithium-ion cell or charging the cell above its upper voltage limit, 4.2V, excess energy is produced due to the exothermic decomposition of the cathode material leading to oxygen production [71][72]. Additionally, combustion gases are produced during this process due to thermal electrolyte decomposition. The presence of both combustive gases and oxygen leads to a violent reaction inside the cell [73][74][75]. The excess energy produced during overcharging cannot be consumed by any side reaction in the cell, as there is no side reaction that can consume this excess of energy, leading to the rise of the temperature inside the device [76]. Due to high temperature, the separator can melt leading to internal short [75]. During overcharging the heat generated inside the cell becomes higher than can be dissipated by the cell leading to the thermal runaway, which introduces the fire and explosion hazard [76][74].

Overdischarging the lithium-ion cell or discharging below its low voltage threshold value (2.7V) compromises the battery performance due to the collapse of the lithium lattice [76]. Overdischarging or extremely low voltages introduce potential risks due to the electrolyte reduction process and the production of combustion gases during these events [76]. Recharging of the over-discharged cell can lead to short circuits within the cell due to dendrites formed on the negative electrode and consequently to irreversible damage to the battery [76][77].

The lithium-ion battery is characterised by the quick response to the change in load condition. This battery can be charged at relatively fast rates, 1C or 2C, only if the upper charge voltage limit is not reached [78]. This battery technology tolerates microcycles; minimal charging can actually prolong its life [78].

2.1.5 Sodium Sulphur

The sodium sulphur battery (NaS) belongs to high-temperature battery technology and operates at temperatures in the range of 300-350 °C to maintain the molten state of the

positive and negative electrodes, made of sulphur and sodium respectively [79][80]. The beta-alumina ceramic electrolyte, in the solid state, separates the active material of molten electrodes and allows sodium ions to flow from the negative to the positive electrode during charging processes and in the opposite direction during discharging of the cell [81]. The schematic construction of the NaS battery is shown in Fig. 8. When the battery is running, the heat that is produced during the discharging process and the cooling effect that takes place during the charging of the battery is enough to maintain the operational temperature of this device [48].

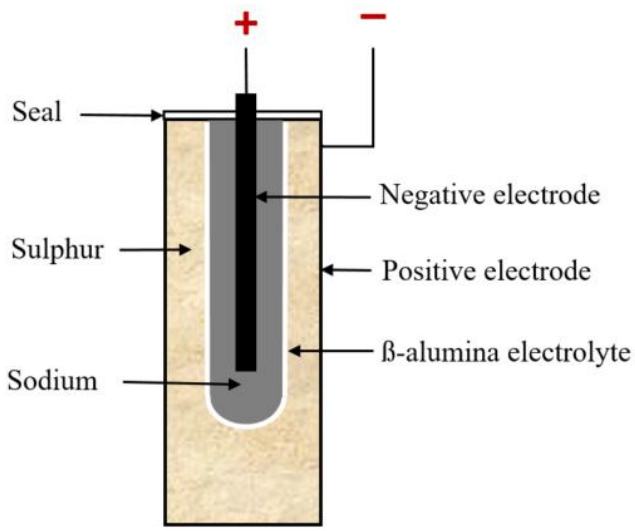

Figure 8 Schematic of the Sodium-Sulphur battery.

This battery type is characterized by a very low rate of self-discharge due to the characteristics of the beta-alumina solid electrolyte. This chemical material has good conductivity for the sodium ions but plays as the insulator for the electrons, not allowing cross mixing of active materials from electrodes to occur [80]. NaS battery has a high cycling efficiency of 80-90% [82], with only a small portion of the energy used to maintain battery operational temperature, see Fig. 4 [81]. Sodium Sulphur battery has a long cycle life in a range of 3500 to 5000 cycles at 80% depth of discharge [82] due to the absence

of morphological changes of electrodes due to their molten state [33][83] what is the limiting factor for the batteries with the solid electrodes.

Sodium Sulphur battery is averse to being either overcharged or over-discharged. During overcharging processes, the solid electrolyte can be damaged due to ceramic breakdown and the cell voltage can be reduced due to the insulating properties of the molten Sulphur, the final product of charging [81]. The over-discharging of NaS battery leads to irreversible chemical changes in the Sulphur electrode, where solid Na_2S_2 with high electric resistance is formed, leading to poor recharging processes and even structural damage [81][84].

One of the important advantages of this battery is its flexible operation. This battery can operate over a wide range of conditions, such as different charging/discharging rates and depths of discharge [33].

2.1.6 Vanadium Redox Flow Batteries

The Vanadium Redox Flow battery (VRFB) belongs to the classical redox flow battery group in which the chemical energy required for exchange during charging and discharging processes comes from two chemical compounds dissolved in liquids that circulate in separate systems, Fig. 3(b). The energy exchange between compounds takes place through an ion-permeable membrane. This battery uses single metal ions, vanadium, in the four different oxidation states to store chemical energy. The V^{4+}/V^{5+} and V^{2+}/V^{3+} redox couples are stored in positive and negative half-cells respectively [43]. The usage of the same metal ions in both half-cells prevent cross-contamination, leading to a lower self-discharge rate in this battery technology, compared with the Zinc-bromine flow battery, for which mentioned process has a substantial influence on self-discharge [85]. An additional factor influencing the low self-discharge of VRFB is storing compounds dissolved in electrolytes separated from each other [86]. When the battery is not in use, only a small fraction of the electrolyte is present in the cell where cross-mixing between species through a separator takes place. The majority of the electrolyte is kept in separate tanks, thus limiting the degree of cross-mixing, resulting in a lower self-discharge rate of

this battery technology [87]. It is worth mentioning that the cross-contamination of compounds can accelerate the degradation of the battery [40][88], but in the case of the VRFB battery, it has no detrimental effect on this battery technology longevity because the mixed electrolytes revert to the unchanged state and then can be easily recharged [44][86].

The cycle life of the VRFB battery can reach 12000-13000 cycles [45][88], as can be seen in Fig. 4, and is not directly influenced by the depth of discharge as long as the battery is operated within its voltage limits. When the VRFB battery undergoes charging/discharging cycles, the electrodes do not experience any changes as it is in the case of the conventional battery because all changes take place in the active material that is dissolved in the electrolyte. The changes that occur in the electrodes materials of conventional batteries result in their degradation over time, which limits the cyclic lifetime of these devices [39][43][44]. The VRFB does not experience life degradation due to repeated deep discharges and additionally can be stored completely discharged for long periods without a negative effect on its performance [39][44]. This type of battery can be over-discharged within the limits of the capacity of the electrolytes, but overcharging must be prevented [39]. During the overcharge of the cell, the oxygen and hydrogen evolution occurs at the positive and negative electrodes respectively. These processes can interrupt the electrolyte flow leading to the limitation in the operational state of charge and decreasing battery efficiency [89]. Additionally, the resistance of the cell increases due to gases evolution during the overcharge of the cell and the oxidation of the carbon electrode due to oxygen evolution can also occur [90].

The VRFB can be charged and discharged at any rate [91]; however, the cycle efficiency decreases when the charging rate is too high due to oxygen and hydrogen evolution, the gassing process occurring during rapid recharge. It is also claimed that vanadium redox battery can withstand fluctuating power demand without any signs of performance deterioration [39].

Similarly to the lithium-ion battery, the performance of VRFB is not affected by micro cycling. Unlike the flooded lead-acid battery, this battery requires very low maintenance [39][92].

2.1.7 Zinc Bromine Flow Battery

Zinc Bromine Flow Battery (Zn/Br_2) is a hybrid flow battery where one of the electro-active compound, zinc, is deposited as a solid layer on the electrode during charging processes, the second one, bromine, is dissolved in the liquid solvent, and the ion exchange takes place through the ion-permeable membrane, Fig. 3(c) [35]. This battery is characterised by a quick response and a lower energy density compared with standard rechargeable batteries, see Table 3, and it has a higher self-discharge rate compared with conventional flow batteries like VRFB, refer to Fig. 4.

Zn/Br_2 has a cycle life in the range of 2000 cycles, which is not affected by the depth of discharge as it is in the case of the lead-acid battery, Fig. 4. This battery can be deep cycled up to 100% depth of discharge on a daily basis without negative effects on the cycle life and battery performances [44][93]. A deep discharge actually promotes battery health by removing zinc deposits from the negative electrode, deposited during charging processes, as well as zinc dendrites from the positive electrode [44][93]. This conditioning of the battery is important because when the battery is charged, metallic zinc, which is plated on the electrode during this process, is often deposited non-uniformly, and the dendrites can be formed on the anode which degrades the battery stability and its performance. Examples of the non-uniform dendrite formation on the anode and possible damage in the separator due to dendrites formation are shown in Fig. 9. The risk associated with dendrite formation is possible damage of the membrane by puncture and occurrence of electrical short circuits [35][93]. If the operating regime of the battery does not allow full discharge of the battery every cycle, then it needs to be fully discharged every couple of days to mitigate zinc dendrites produced during charging processes and to maintain battery life [93].

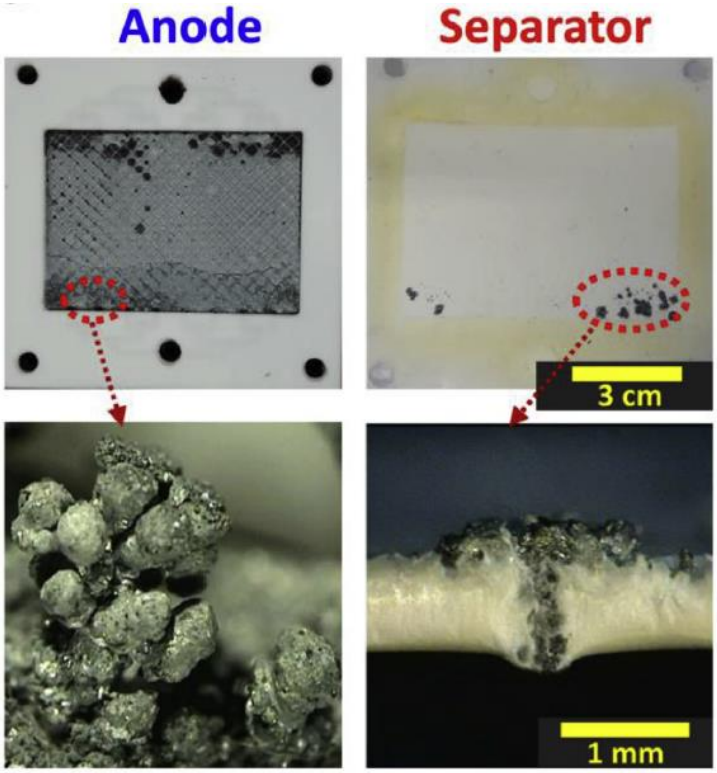

Figure 9 Cylindrical dendrites deposited on the anode, lower left, and the dendrite attached to the separator and piercing it, lower right, in Zn/Br_2. (Figure reprinted from Yang et al. [85])

The major problem of the zinc-bromine flow battery is its high self-discharge rate [39][44]. The self-discharge mechanism in this type of battery is associated with the diffusion of the Br_2 from the bromine side electrode, across the membrane, to the zinc electroplated electrode and subsequent oxidization of the plated zinc leading to a decline of the battery charge when stored unused in the fully charged state. This battery should not be kept in a charged state at rest for an extended period of time due to the aforementioned reactions, instead, it is better to store it in the fully discharged state, in contrast to the lead-acid battery whose performance can be compromised by storing it in an empty state [93][94]. The Zn/Br_2 flow battery does not like to be overcharged as this process, in the extreme case, leads to electrolysis of the electrolyte and the production of oxygen and hydrogen, leading to irreversible damage to the battery cell [35][43].

The charging and discharging rate have an important impact on the performance of the zinc-bromine flow battery. The cycle efficiency is inversely proportional to the discharge/charge rate, which means that an increase in the rate of charge/discharge decreases the cycle efficiency of this technology [93].

2.2 Battery Technology, What is Needed Versus What is Available

Ideally, the battery energy storage in power system applications should provide as much energy as required to meet the energy demand and be able, at any time, to accommodate as much energy as possible when excess energy is generated by power-generating units in the system. The key features that should characterise such an ideal BES are as follows:

- The ability to provide all required functions (for example, peak shaving, shifting energy in time from when it is generated in excess to time of energy deficit in the system, auxiliary services and others),
- Ability to be deep or shallow cycled when required without negative influence on device performance and health,
- Being insensitive to the rate of charge and discharge,
- Becoming unaffected by infrequent events of overcharging and over-discharging caused by mis-scheduled actions,
- Being insensitive to micro-cycling if this is a battery application requirement in a particular application,
- Highly efficient, preferably 100%.

Unfortunately, battery technology that possesses all the listed above features does not exist yet. The review of battery technologies currently used in the grid-scale BES system applications carried out in the preceding part of this chapter clearly showed how battery chemistries differ from each other. The batteries have their preferences for the way they should be run to ensure the longevity of these devices is preserved, and their performances are not compromised. As it was shown, these preferences are different for different battery

technology and are battery chemistry dependent. When planning the BES installation, it is important to consider battery preferences and choose the technology suitable to the planned application/installation and its intended functions in the power network. The running of the battery against its preferences negatively affects the health and performance of this device and the system including this device. In the following section, the tabular summary of the battery operational preferences is included with the potential application for the knowledge gained in the preceding sections about seven battery technologies.

2.3 Rules Formulation Based on Battery Chemistries Review

The overview of the battery preferences dictated by device chemistry carried out in the previous sections constitutes the base for the formulation of the rules required for the model training. Table 4 summarizes the battery operating preferences and constitutes the base for the definition of rules dictating the favoured operation from the battery health point of view, which then are learned by the developed BES model.

Table 4 Battery Operating Preferences

Type	**Charge Sensitivity**	**Cycle Preference**	**Micro-Cycle**	**Charge Condition**	**Idle SoC**
Lead Acid	o/c, o/d, u/c	Shallow	No	Full	Full
NiCd	o/c	Deep	No	Empty	-
NiMH	o/c, o/d	Shallow	No	-	-
Li-Ion	o/c, o/d	-	Yes	-	-
VRFB	o/c	-	Yes	-	-
Zn/Br_2	o/c	Deep	No	Empty	Empty
NaS	o/c, o/d	-	No	-	-

Notation: o/c – overcharge, o/d – over-discharge, u/c – undercharge

The preferences listed in Table 4 are dictated by battery chemistry and therefore are different for each battery type. They are the results of the chemical changes that take place inside the battery due to cycling that can either positively or negatively affect battery

performance and its health. Some similarities in preferences between different battery technologies can be seen. For example, both Zn/Br_2 and NiCd batteries prefer to be fully discharged before recharging again. Although this preference is the same for both batteries, it is dictated by completely different chemical reactions taking place inside the cells when running contrary to preference (specifically the memory effect for NiCd battery and dendrite formation in Zn/Br_2). For a better understanding of the preferences included in Table 4, some explanation of the terms used to describe the preferences is required. The charge sensitivity term describes the preference of the battery to not being overcharged (charged above the maximum energy battery can safely accept), over-discharged (drawing energy from the empty device), under-charged (partially charging the battery, not charging the battery to its full capacity before discharging again, this is particularly important for the Lead-acid battery as it can lead to a build-up of sulphate crystals). The cycle preferences describe how deep the battery can be discharged. The battery can either be deep cycled ('deep' in Table 4), shallow cycled ('shallow' in Table 4) or does not have a preference ('-' in Table 4). Batteries with the preference for deep cycling like to be continuously discharged until the device is fully discharged, which is usually considered when the battery cell reaches its cut-off voltage, typically at 80% of the discharge. Battery with a preference for shallow cycling likes to be discharged until some point, for example, 50% of the state of charge. The depth of discharge is particularly important for lead-acid and zinc-bromine batteries. In the case of the first battery technology, the cell prefers to be shallow cycled as deep cycling can accelerate softening of active material leading to capacity loss [95]. Deep cycling is preferred by second battery technology as it removes the zinc dendrites from the battery cell, positively influencing battery health conditions [93]. Some battery technologies have a preference to reach a particular state of charge before charging or discharging again to ensure device's healthy operation: 'empty' in Table 4 means a preference for discharging until fully discharged, and 'full' means the preference for charging until fully charged state is achieved. This is described by the charge condition term in this work. The lead-acid battery is an example of battery chemistry that prefers to be fully charged before discharging again, as it

positively influences device health by preventing sulfation occurrence within the battery cell [18]. The Zn/Br_2 battery technology, contrary to the lead-acid chemistry, prefers to be fully discharged following the charging process to break down the Zinc dendrites created during battery cycling operation [93]. Micro-cycling describes the battery's preference to be constantly charged and discharged without the necessity of firstly fully charging or fully discharging this device; in other words, the battery likes the frequent change of the direction of battery current. The last term, idle SoC, describes the preference of the battery to the state of charge in which the battery prefer to be kept when at rest. The lead-acid battery is a good example of a battery that prefers to be kept fully charged when at rest to prevent deterioration of its performance due to the sulphation process occurring because of the self-discharge of the cell [96].

Before the formulation of the rules is discussed in detail, it is worth mentioning that the battery operational preferences summarised in Table 4 also have another potential practical application, namely as the supporting information for system designers/engineers in the battery technology selection process. With the knowledge of the system where BES will be added and the required function that this device will perform in the application, the applicability of each battery technology can be assessed. The battery function that this device will perform dictates the way it will be operated. The potential way that the battery will be operated and the battery requirements in the planned system can be assessed against battery operational preferences, covered in Table 4, allowing the choice of the best match of the battery technology to the intended application.

2.3.1 Rules Formulation

During the formulation of rules and defining the preference indexes, some assumptions were made, namely:

1. Temperature influence on battery degradation was not considered during battery modelling. It was assumed that the BES operating environment was not hostile to this device and that the sole threat to asset life was through misuse. This is dictated

by the fact that in the grid storage applications, regardless if the battery is stored in containers, dedicated rooms in the building or if we deal with ready-to-install systems, the system is always equipped with a temperature management system, which maintains the optimum conditions for the batteries. The addition of the temperature into the model can help extend the application of the developed model into those applications where the battery is not operating in the controlled environment and constitute potential further work.

2. Each battery type is assumed to be new and already formatted at the starting point of modelling and simulation, meaning that the device, from the beginning, reaches its maximum possible capacity appropriate for a new, healthy device. The influence of potential inappropriate formatting or lack of this activity after the first device installation on the degradation of performances during usage was omitted from this work. This is dictated by the fact that some of the battery technologies considered here do not require to be formatted at all after the installation, and for those that require, it is assumed to be done during installation or shortly after to ensure the device is fully ready to perform its function from the beginning of usage.
3. The equalizing charges were not needed to be included in the battery scheduling. The battery was cycled according to the available resources and demand requirements only. It was assumed that the developed model automatically recognizes the maloperation due to the lack of application of equalizing charges because this functionality was covered during rule formulation.

The operational preferences summarised in Table 4 are used to create rules which will label exemplar charge schedule actions according to the resulting impact on the battery health. Based on Table 4, the example rule consequents that are used to train the prediction model of the lead-acid battery are as follows:

- “do not overcharge”
- “do not over-discharge”

- “do not under-charge”
- “charge BES to full SoC before discharging is allowed”
- “do not forget to apply equalizing charge”.

The knowledge of the battery preferences and resulting rules led to the composition of the lookup tables with preference indexes for different battery technologies considered in this work, namely: Lead-acid, NiCd, NiMH, Zn/Br_2, NaS, Lithium-ion and VRFB batteries. The lookup tables are shown in Tables 5 - 11.

Table 5 Lead-acid battery preference index lookup table.

State of Charge at time t (SoC_t)	Scheduled action at a time (t)	Scheduled action at previous time step (t-1)	Preference index	Rule	Additional note
Discharged	charge	charge	+1	*'do not over-discharge'*	Preferred action when empty
		discharge	+1		
		no action	+1		
	discharge	charge	-1	*'do not over-discharge'*	This battery type does not like over-discharging
		discharge	-1		
		no action	-1		
	no action	charge	-1	*'do not over-discharge'*	Self-discharge leads to over-discharging, leading to hydration
		discharge	-1		
		no action	-1		
Partially charged	charge	charge	+1	*'do not under-charge'*	Prefer to be charged to full capacity
		discharge	0		
		no action	+1	*'do not under-charge'*	Prefer to be charged to full capacity
	discharge	charge	-1	*'do not under-charge'*	Does not like to be discharged before being charged to full capacity
		discharge	0		
		no action	0		
	no action	charge	-1	*'do not under-charge'*	Does not like to be discharged before being charged to full capacity
		discharge	-1	*'charge BES to full SOC before discharging is allowed'*	When not fully charged, possible sulphation
		no action	-1		
Fully charged	charge	charge	-1	*'do not overcharge'*	Does not like to be overcharged
		discharge	-1		
		no action	-1		
	discharge	charge	+1	*'charge BES to full SOC before discharging is allowed'*	Preferred way of operating when fully charged
		discharge	+1		
		no action	+1		
	no action	charge	-1	*'do not forget to apply equalizing charge'*	Keeping the battery too long without topping charge leads to sulphation
		discharge	-1		
		no action	-1		

Table 6 Lithium-ion battery preference index lookup table.

State of Charge at time t (SoC_t)	Scheduled action at a time (t)	Scheduled action at previous time step (t-1)	Preference index	Rule	Additional note
Discharged	charge	charge	+1	*'Charge when empty'*	Preferred action when empty
		discharge	+1		
		no action	+1		
	discharge	charge	-1	*'do not over-discharge'*	Dangerous - safety issue
		discharge	-1		
		no action	-1		
	no action	charge	-1	*'do not over-discharge'*	Can lead to over-discharging, which is dangerous
		discharge	-1		
		no action	-1		
Partially charged	charge	charge	0		
		discharge	+1	*'micro cycle'*	Prefer micro cycling as it can prolong battery life
		no action	0		
	discharge	charge	+1	*'micro cycle'*	Prefer micro cycling as it can prolong battery life
		discharge	0		
		no action	0		
	no action	charge	0		
		discharge	0		
		no action	0		
Fully charged	charge	charge	-1	*'do not overcharge'*	Does not like to be overcharged
		discharge	-1		
		no action	-1		
	discharge	charge	+1	*'discharge when fully charged'*	Preferred action when Fully charged
		discharge	+1		
		no action	+1		
	no action	charge	0		No impact on the chemistry
		discharge	0		
		no action	0		

Table 7 NiMH battery preference index lookup table.

State of Charge at time t (SoC_t)	Scheduled action at a time (t)	Scheduled action at previous time step (t-1)	Preference index	Rule	Additional Note
Discharged	charge	charge	+1	*"charge when empty"*	Preferred action when empty
		discharge	+1		
		no action	+1		
	discharge	charge	-1	*"do not over-discharge"*	This battery type does not like over discharging
		discharge	-1		
		no action	-1		
	no action	charge	-1	*"do not leave in an empty state for too long"*	High self-discharging can quickly lead to over-discharge
		discharge	-1		
		no action	-1		
Partially charged	charge	charge	0		
		discharge	0		
		no action	0		
	discharge	charge	0		
		discharge	0		
		no action	0		
	no action	charge	0		
		discharge	0		
		no action	0		
Fully charged	charge	charge	-1	*"do not overcharge"*	Does not like to be overcharged
		discharge	-1		
		no action	-1		
	discharge	charge	+1	*"discharge when fully charged"*	Preferred way of operating when fully charged
		discharge	+1		
		no action	+1		
	no action	charge	0		No impact on chemistry
		discharge	0		
		no action	0		

Table 8 NiCd battery preference index lookup table.

State of Charge at time t (SoC_t)	Scheduled action at a time (t)	Scheduled action at previous time step (t-1)	Preference index	Rule	Additional note
Discharged	charge	charge	+1	*"charge when empty"*	Preferred action when empty
		discharge	+1		
		no action	+1		
	discharge	charge	-1	*"do not over-discharge"*	This battery type does not like over discharging
		discharge	-1		
		no action	-1		
	no action	charge	-1	*"do not leave in an empty state for too long"*	Possible over-discharge
		discharge	-1		
		no action	-1		
Partially charged	charge	charge	0		
		discharge	-1	*"fully discharge before recharging again"*	Prefers to be discharged completely before recharging due to possible memory effect
		no action	0		
	discharge	charge	0		
		discharge	+1	*"fully discharge when partially charged"*	Prefers to be discharged completely before recharging
		no action	+1		
	no action	charge	0		
		discharge	0		
		no action	0		
Fully charged	charge	charge	-1	*"do not overcharge"*	Does not like to be overcharged, possible thermal runaway
		discharge	-1		
		no action	-1		
	discharge	charge	+1	*"discharge when fully charged"*	Preferred way of operating when fully charged
		discharge	+1		
		no action	+1		
	no action	charge	0		No impact on chemistry
		discharge	0		
		no action	0		

Table 9 VRFB battery preference index lookup table.

State of Charge at time t (SoC_t)	Scheduled action at a time (t)	Scheduled action at previous time step (t-1)	Preference index	Rule	Additional note
Discharged	charge	charge	+1	*"charge when empty"*	Preferred action when empty
		discharge	+1		
		no action	+1		
	discharge	charge	-1	*"do not over-discharge"*	Prefers to be not over-discharged, but over-discharge is possible if within the limits of the capacity of the electrolytes
		discharge	-1		
		no action	-1		
	no action	charge	0		Can be stored long time empty without negative influence on its performance
		discharge	0		
		no action	0		
Partially charged	charge	charge	0		
		discharge	+1	*"charge even if not fully discharged yet"*	Can be micro-cycled without negative influence on performances
		no action	0		
	discharge	charge	+1	*"discharge even if not fully charged yet"*	Can be micro-cycled without negative influence on performances
		discharge	0		
		no action	0		
	no action	charge	0		
		discharge	0		
		no action	0		
Fully charged	charge	charge	-1	*"do not overcharge"*	Overcharging must be avoided
		discharge	-1		
		no action	-1		
	discharge	charge	+1	*"discharge when fully charged"*	Preferred action when fully charged
		discharge	+1		
		no action	+1		
	no action	charge	0		No effect on the chemistry
		discharge	0		
		no action	0		

Table 10 Zn/Br2 battery preference index lookup table.

State of Charge at time t (SoC_t)	Scheduled action at a time (t)	Scheduled action at previous time step (t-1)	Preference index	Rule	Additional note
Discharged	charge	charge	+1	*"charge when empty"*	Preferred action when empty
		discharge	+1		
		no action	+1		
	discharge	charge	-1	*"do not over-discharge"*	'Tolerates' over-discharging to some extend
		discharge	-1		
		no action	-1		
	no action	charge	-1	*"do not over-discharge"*	High self-discharge
		discharge	-1		
		no action	-1		
Partially charged	charge	charge	0		
		discharge	-1	*"fully discharge before recharging again"*	Prefers to be discharged to an empty state before recharging
		no action	0		
	discharge	charge	0		
		discharge	+1	*"fully discharge before recharging again"*	Prefers to be discharged to an empty state before recharging
		no action	+1		
	no action	charge	0		
		discharge	0		
		no action	0		
Fully charged	charge	charge	-1	*"do not overcharge"*	Overcharging must be avoided
		discharge	-1		
		no action	-1		
	discharge	charge	+1	*"discharge when fully charged"*	Preferred action when fully charged
		discharge	+1		
		no action	+1		
	no action	charge	0		
		discharge	0		
		no action	-1	*"do not store fully charged"*	Self-discharge leads to the decline of battery charge when stored fully charged

Table 11 NaS battery preference index lookup table.

State of Charge at time t (SoC_t)	Scheduled action at a time (t)	Scheduled action at previous time step (t-1)	Preference index	Rule	Additional note
Discharged	charge	charge	+1	*"charge when empty"*	Preferred action when empty
		discharge	+1		
		no action	+1		
	discharge	charge	-1	*"do not over-discharge"*	Over-discharging leads to irreversible chemical changes in the battery cell
		discharge	-1		
		no action	-1		
	no action	charge	-1	*"do not over-discharge"*	Even with low self-discharge, keeping the battery fully discharged without recharging it can lead to irreversible chemical changes in the battery cell
		discharge	-1		
		no action	-1		
Partially charged	charge	charge	0		
		discharge	0		
		no action	0		
	discharge	charge	0		
		discharge	0		
		no action	0		
	no action	charge	0		
		discharge	0		
		no action	0		
Fully charged	charge	charge	-1	*"do not overcharge"*	Does not like to be overcharged as it can lead to damage to electrolyte
		discharge	-1		
		no action	-1		
	discharge	charge	+1	*"discharge when fully charged"*	Preferred action when fully charged
		discharge	+1		
		no action	+1		
	no action	charge	0		
		discharge	0		
		no action	0		

The lookup tables describe the battery preferences for the action to be performed in relation to the previous actions and the state of charge of this device, which is dictated by the chemistry of the battery. Three preference indexes were considered in this work. The battery can either:

- prefer to perform a particular action - positive index (+1),
- dislike action - negative index (-1)
- be neutral to the action - zero index (0).

The positive index describes the situation when the battery is run in a way that can actually prolong device life (operation in agreement with the rules); the negative index is the observation emitted when the battery is operated in a way contrary to preference dictated by its chemistry leading to the performance deterioration (operation against the rules). Zero index is emitted in a situation when the executed action has no negative influence on the battery performance but also does not prolong battery life (no rule regulating this action). The composed lookup tables were then used to generate preference indexes due to the random charging/discharging schedule of the BES that constitutes the entry data required for model training. As can be seen in Tables 5 to 11, preference indexes are unweighted and always equal ±1 or 0. Each maloperation event is treated equally. It can be expanded in the future to include varied weights. However, more detailed knowledge about battery chemistry and suitable data sets would be essential to provide these scaled indexes. This would constitute a possible collaboration platform with experts in battery chemistry.

In summary, this chapter provided insight into the complexity of the battery's internal processes that take place inside this device during its operation and are governed by the battery chemistry. It indicated that there is not possible to observe those processes and changes directly, and this information is hidden from the observer. It also provided a useful summary of battery preferences for reviewed battery technologies that have potential applicability during the process of battery type selection for a given application. Based on the battery operational preferences listed in Table 4, a set of rules dictating the

favoured operation from the battery health point of view were formulated for each battery type. This in turn, led to the definition of the new health index in terms of maloperation level. Using maloperation level as the potential measure of the battery health is dictated by the strong influence misuse has on the internal chemical state of the battery. These rules allowed the generation of the data of maloperation level due to the random charge /discharge schedule of the battery, which then is used to train the proposed state-based BES model.

CHAPTER 3

This chapter, the previous and the following chapters constitute an extended version of a journal paper published in IEEE Access Journal in 2021 by Joanna Sobon and Bruce Stephen, titled: "Model-Free Non-Invasive Health Assessment for Battery Energy Storage Assets" [32].

3. Battery Models Review, Shortcomings and Proposed Solution

The development of accurate models of battery conditions is important from both a power systems operation and asset management point of view. The resulting model can allow studying in a safe way the behaviour of a modelled power network under different operating conditions and assessing the operating limits of the device. The model can also support the development of new efficient battery management systems, can help in assessing the application of battery technologies and help in optimizing its operation in the analysed application such as for example, ancillary services, peak shaving and others. The most important aspect of battery modelling is the ability to capture the ageing processes of a real device by a developed model. Ageing of the battery can be defined as the processes associated with the changes that occur in the electrodes, anode and cathode due to chemical reactions taking place during battery operation and when the battery is not used over an extended period of time, leading to a deterioration of battery performances [33][34]. There are two main types of ageing processes. The first type called the degradation-ageing process, is associated with the gradual deterioration of battery performances over time. The second type is associated with a sudden, unexpected drop in battery performance or device failure. This type of ageing process is called a "bursty" ageing process and has no impact on the performance of the battery until it suddenly leads to a major problem, such as device failure and even fire and explosion [16][34]. The

physical and chemical changes in the batteries, and the associated ageing processes, are significantly affected by the operating condition such as rate of charge and discharge, ambient temperature, length of the break in the device operation and other stress factors such as: how long battery remains at a low state of charge (SoC), cycling at partial-SoC and others [16][17]. Taking the chemistry of the battery into account is important when formulating operational strategies that preserve the longevity of the device. From the power grid perspective, where BES becomes an integral part of the system, considering battery health is crucial as the failure of the battery can lead to loss of operation and reduced capability of the power network comprising this device. It is also important for the stability of the power network comprising this device to ensure that the failure of the battery is prevented to guarantee continuous electricity supply to consumers. The health of the battery has an impact on its capabilities, thus influencing the operation of the whole system this device is part of.

3.1 State of Art in Battery Modelling

The most basics properties of the battery are its voltage, in volts (V), and capacity often expressed in the ampere-hour (Ah). In the ideal scenario (ideal battery), the battery voltage would remain constant during the discharge process until the device becomes completely discharged when it instantly drops to zero, Fig. 10(a).

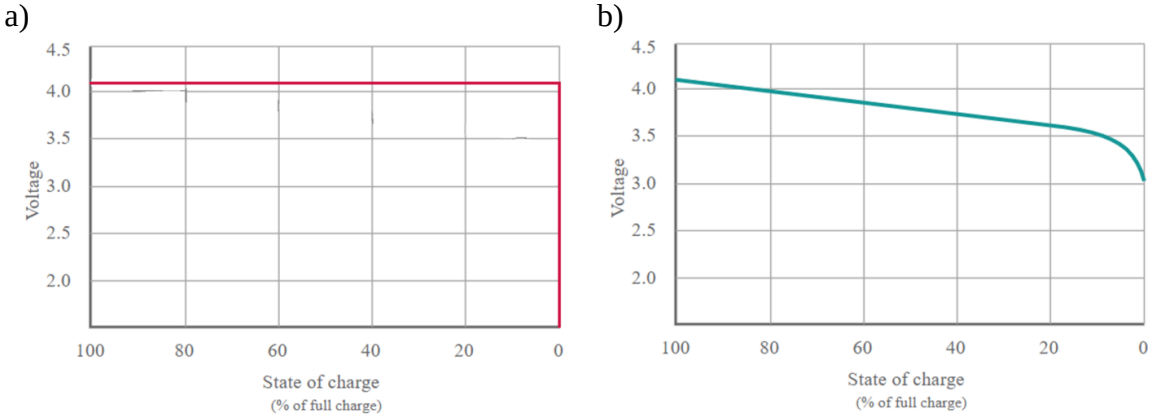

Figure 10 Voltage discharge curve of Lithium-ion cell for the ideal battery (a) and a typical lithium-ion battery cell (b)

Due to non-linear chemical reactions, that take place inside the battery, the voltage drops during discharge in a non-linear manner, see Fig 10(b), this phenomenon is called the rate capacity effect. Another important characteristic of the battery is a process called the recovery process, which is the recovery of some capacity 'lost' during a fast discharge when the battery is at rest (idle). For the ideal battery, the lifetime of this device could be described by a simple equation (5) [97]:

$$L=C/I \tag{5}$$

Where: L – is the lifetime [h],
C – is the capacity [Ah],
I – is the load current [A].

As we deal with the real battery, a complex electrochemical device, inside which the complex non-linear physical changes and the chemical reactions take place during cycling operation, predicting its lifetime is a more complex task, similarly to predicting its capacity fading with time and other phenomena taking place inside this device. This non-linearity makes the modelling of this device a challenging task. To ensure that model will be useful, it needs to catch important phenomena, such as:

- ***State of charge***

  The ability to capture changes in the SoC of the battery during cycling is a very important aspect of managing this asset properly. It supports informed decisions about the next available action to be performed and increases understanding of how much energy is still available for discharge and how much energy can be accommodated in this device to store and use later on.

- ***Self-discharge mechanisms***

  These mechanisms result in a gradual reduction of stored charge when the battery is in an open circuit state. They are battery type-dependent and governed by the different chemical reactions taking place inside the battery cell, influenced by battery chemistry. For example, sulphation process is responsible for the self-discharge processes of the lead-acid battery due to its storing [18][52].

- ***Dynamic I-V characteristics***

  They describe the dynamic characteristics of the battery, such as non-linear open-circuit voltage [98] and voltage and current behaviour of the battery cell during the charging and discharging processes. The example of the voltage discharge curve for a lithium-ion battery is shown in Fig. 10(b).

- ***Rate capacity effect***

  This phenomenon describes the effect of the rate at which the battery is discharged on the device's capacity. The amount of charge (effective capacity) that is drawn from the battery with a low discharge current rate is higher than when a higher discharge rate is applied to the battery [99].

- ***Ageing effect and associated battery state of health*** (SoH)

  The ageing effect is an important phenomenon that needs to be captured to ensure the proper operation of BES. Due to the ageing effect, the internal resistance of the battery is rising, reducing the mobility of ions between the cathode and anode, and the available capacity is decreasing. The ageing effect can have a very important influence on battery operation when not predicted properly. It can lead to overcharging the battery when the battery is being charged to its nominal capacity (capacity of the brand new battery) that due to ageing processes was substantially reduced. This can result in catastrophic device failure, fire and explosion. The SoH denotes the battery health condition that is in use, compared to its ideal condition (condition of the brand new device). The SoH cannot be measured directly but can be computed using the capacity of the battery [100][101]. The SoH can be estimated using equation (6) [102].

$$SoH(t) = \frac{C_t}{C_{new\_batt}} \times 100\% \quad (6)$$

Where: C_t – is the nominal capacity of the battery at time t

C_{new_batt} – is the nominal capacity of the brand-new device.

- ***Recovery effect***

  The electroactive species are homogeneously distributed on the electrodes of the battery cell when it is fully charged [103]. During the discharge process, the particles that are closer to the electrode are consumed first then those further from the electrode are used. When the cell of the battery is subject to a long, continuous discharge process, then the species further from the electrode do not have enough time to travel towards the electrode. This results in the battery appearing as quickly depleted even actually not all species were consumed yet. When the battery is allowed to rest between discharges, additional ions can travel toward the electrodes increasing the number of species that participate in redox reactions. This idle time permitting this process is termed the recovery effect [103][104]. This phenomenon depends on the material used for the cathode and anode and thus cannot be generalized for all the battery chemistries [103]. It can increase the useful power of the battery when the battery is allowed to rest between the discharging cycles [105].

- ***Memory effect***

  This effect occurs due to the incomplete discharges in previous uses of the battery leading to a build-up of residual charge until the point where the battery can store only a small amount of useful charge.

- ***Capacity fade mechanisms***

  The available capacity decreases with time. For lithium-ion batteries, this is the result of lithium deposition during overcharging [106]. For Lead-acid batteries, this phenomenon is caused by electrolyte decomposition, passive film formation, phase change in the electrode material, and active material dissolution (sulphation and grid corrosion) [76].

- ***Remaining useful life***

  The remaining useful life (RUL) is the length of time the battery will operate before its performance drops to the point that this device is no longer viable for a given application and requires replacement.

There is no model developed yet that covers all of the above-mentioned phenomena. Usually, the developed, up-to-date models focus on one or more phenomena in the modelling. Including all the above-mentioned battery features would substantially increase model complexity and its computation time/effort, which is not optimal from the model application point of view. Additionally, it would require suitable data sets to be freely available, covering all life cycles for the battery. Currently, suitable data resources are very limited.

The review of battery models carried out in this chapter is focused on those that provide the ability to predict the state of health, which is dictated by the fact that knowledge about this quantity is critical to ensure proper and safe battery operation. Accurate prediction of SoH is critical for battery management systems as it can prevent overcharging and over-discharging of this device, the processes that can lead to premature battery failure or even catastrophic hazards, which in turn negatively affect the power system encompassing this device. Numerous battery models have been developed to date that capture battery performance for various purposes, such as battery management systems [107], investigating battery design and performance, circuit analysis, electric vehicle applications [108] and others. They can be divided into four groups, namely physical (electrochemical) models [109][110], semi-empirical models comprising equivalent circuits models [111][112], analytical models [113][114] and self-adaptive models [115][116], empirical models comprising models employing probabilistic [117][118] and non-probabilistic [119][120] approaches, and hybrid (mixed) models [121] that combine two or more other modelling techniques to model battery behaviour. The classification of the models used in this work is similar to those used in [122][123] and is shown in Fig. 11. The hybrid models are not reviewed here as a separate model group; instead, they are reviewed under the model group they are closest to in design in the corresponding sections.

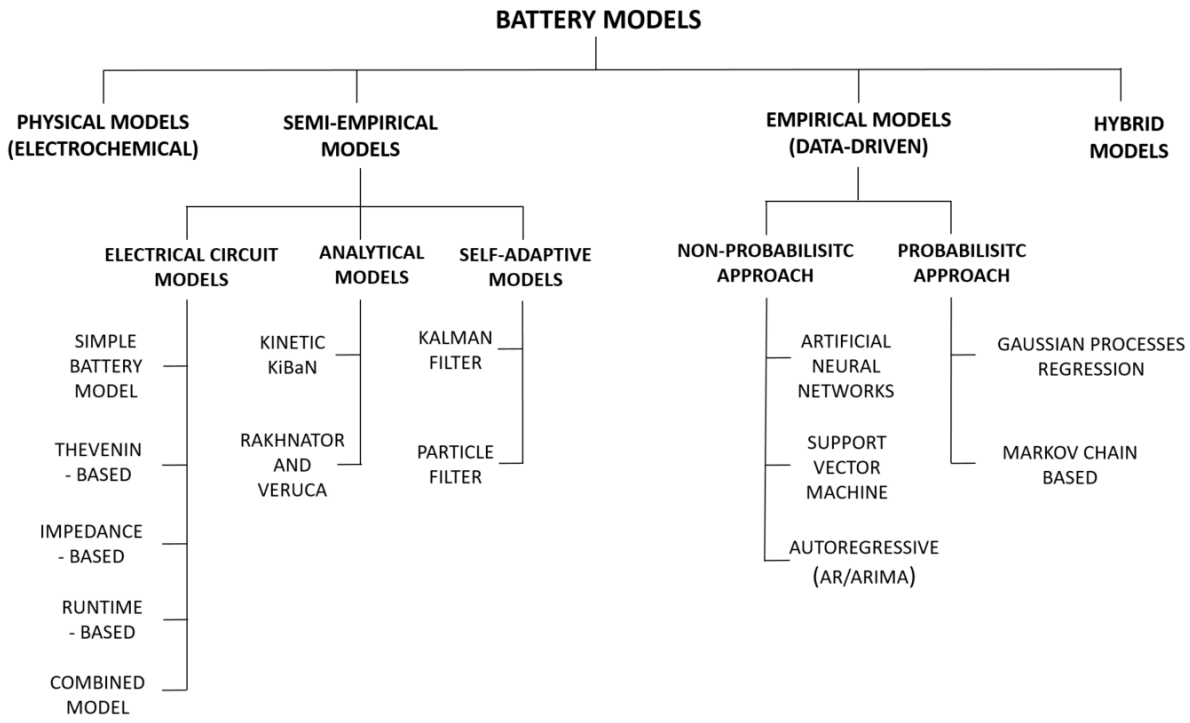

Figure 11 Taxonomy of battery models.

3.1.1 Physical Battery Models

The first group of physical models are also called electrochemical models [44], [45], [59]–[61]; being of the first principles in nature, they also are one of the most accurate models. These models have been developed to understand the mechanisms of degradation that take place inside the battery cell. They are based on the highly non-linear, partial differential equations that model the physics of the battery and the chemical reactions taking place inside this device. The examples of modelled reactions and processes taking place in the battery during its operation are the following:

- diffusion process in the solid material of the electrodes and transport of ions in the electrolyte during the charging/discharging of the lithium-ion cell modelled in [109] and [124],

- relaxation phenomena (also called recovery effect) in Lithium-ion cells that depend on changes in the distribution of the material on the electrodes and inside the solution, modelled in [110].

The electrochemical models require detailed knowledge of the battery chemistry and its design. These models are accurate but also very complex and difficult to configure. They typically require a large number of parameters, which must be obtained from domain knowledge (reasonable estimates) or obtained independently from a series of laboratory experiments [125]. For example, the models developed in [109] and [127] require over 50 battery parameters to be set. Moreover, the number of parameters can differ from one battery to another and even between the cycles of the same battery [128]. This further complicates the applicability of first-principles models to the SoH prediction and implies additional requirements to find new accurate and fast methods of parameters estimation [129]. Physical battery models are also characterised by long simulation times, often in days [130][131], which is not suitable for online model applications. Electrochemical models do capture nonlinear battery behaviour but do not directly address the estimation of the SoC or SoH [130][132], which is crucial in battery storage management systems.

3.1.2 Semi-Empirical Battery Models

The next group of battery models considered in this work are semi-empirical models. This group of models are based on experimental results as in the case of the empirical models, but also some of the real physical effects are implemented in this type of model so that these models encode also some of the underlying theoretical assumptions. The semi-empirical model can be further divided into analytical models, electric circuit models and self-adaptive models.

Two analytical battery models are considered in this work, namely the Rakhmatov and Vrudhula diffusion model [113][133] and the Kinetic battery model [134][114]. These models describe the battery operation at a higher level of abstraction compared to physical models and electrical circuit models. The diffusion model is based on the diffusion of the

ions in the electrolyte, describing the evolution of the ion concentration in the electrolyte while the battery is charged or discharged. This model predicts the battery lifetime under a given load and is capable of modelling the recovery effect taking place inside the battery. Unfortunately, it does not account for the capacity fading characteristics [135]. Accurate prediction of capacity fading for battery energy storage during its life is important in battery management systems as it can prevent overcharging or over-discharging of this device, helping to avoid battery failures. The second battery model that belongs to the analytical model group, and is considered in this work, is the kinetic battery model (KiBaM) shown in Fig. 12.

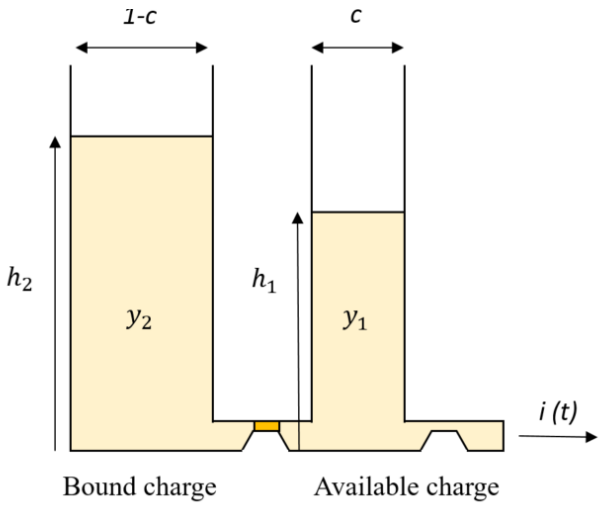

Figure 12 Kinetic battery model – KiBaM.

This model assumes that battery charge is distributed between two connected wells from which the first one (bound charge in Fig. 12) supplies charge to the second one (available charge in Fig. 12), which in turn supplies the load. The dynamic between the wells models the recovery effect and rate capacity effect. This model is capable of capturing the non-linear capacity behaviour of the battery but unfortunately cannot capture the dynamic of I-V battery characteristics that are crucial when considering the battery as an integral part of the electrical system [136]. Summarising the analytical models, while

easily implemented, they are unable to accurately capture the potential battery degradation that is important to storage asset health.

The second group of semi-empirical models reviewed in this work are the electrical-circuit models [111], [137]–[145] that attempt to provide the equivalent representation of the battery. The electrical properties of the battery cell in these models are modelled by using the electronic components mimicking the battery cell characteristics, ranging from the simple capacitor, resistor and voltage source representing battery charge storing capacity, internal resistance (electrolyte resistance and charge transfer resistance) and open-circuit voltage respectively, through more sophisticated, complex elements like Warburg diffusion element[2] (Warburg impedance) modelling slow voltage diffusion process [140][146] or ZARC element [141], which is the parallel configuration of Warburg element with resistor and models the depression in impedance response of battery cell. Warburg impedance and ZARC elements are shown in Fig. 13.

To examples of electrical-circuit models belong; the simple battery model [144], Thévenin-based electrical model [111][142][145], Impedance-based electrical model [28–32] and Runtime-based electrical model [138][139][151], shown in Fig. 14. Most of these models are able to accurately predict the state of charge of the battery, but they do not account for battery degradation [152]. The simple battery model, Fig. 14 (d), consists of the voltage source V_{OC} in series with an internal resistance R_{Series} where V_{OC} gives the voltage across the ideal battery while V_{Batt} is the terminal voltage of the battery, and R_{Series} models the electrolyte resistance.

[2] Warburg diffusion element (Warburg impedance) is an equivalent electrical circuit composed of multiple resistor-capacitor networks in series, as shown in Fig. 13, which models the diffusion processes taking part in the battery during charging and discharging processes.

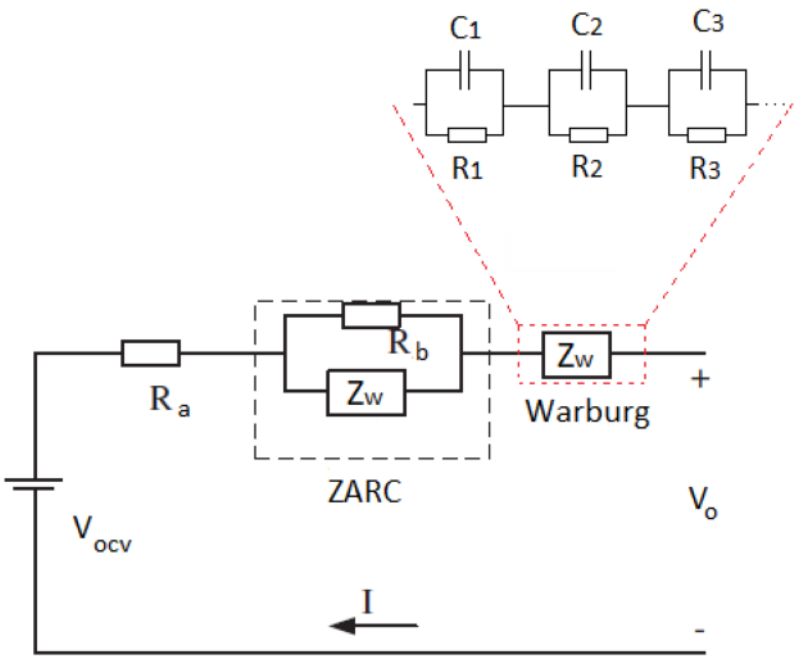

Figure 13 Warburg diffusion element Z_w and ZARC element in the impedance-based electric circuit model.

This model does not account for the SoC of the battery and thus is only suitable for simulations assuming infinite release of the energy from the device and for which the SoC is not important [143][153]. It makes this model unsuitable for modelling batteries for energy storage purposes. Moreover, this model does not take into account the changes in internal resistance with varying states of charge and electrolyte concentration, and also it does not consider the diffusion phenomena that take place in the battery. Furthermore, this model is only valid for steady-state load conditions [144].

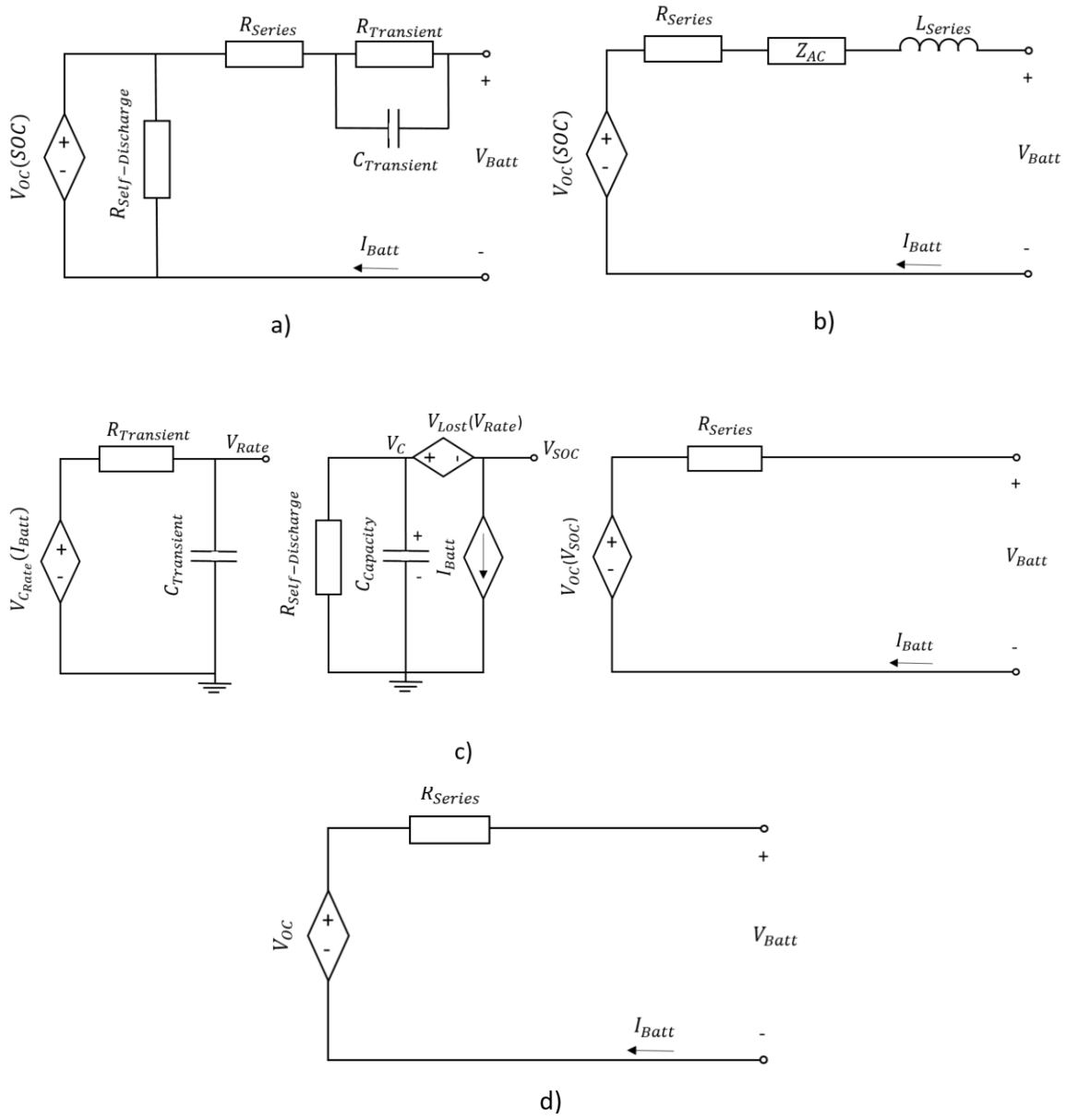

Figure 14 Electrical-circuit battery models: (a) Thévenin -based battery model, (b) impedance-based model, (c) Runtime-based model, (d) Simple battery model.

Thévenin battery model [143][145], Fig. 14 (a), consists of the ideal voltage source (V_{OC}) in series with internal resistance (R_{Series}) and $R_{Transient}C_{Transient}$ parallel circuit that models the voltage diffusion process (voltage diffusion is caused by ions diffusion after

removing the load when the ions try to reach equilibrium[3]). $R_{Transient}$ in this figure is the charge-transfer resistance that models voltage drop over the electrode-electrolyte interface due to load. $C_{Transient}$ is a double-layer capacitance that models the effect of charges building up in the electrolyte at the electrode surface (represents the charge stored in the battery), and R_{Series} is internal resistance that models the electrolyte resistance. This model is capable of simulating the behaviour of the battery under dynamic load conditions [130] and can predict the voltage transient response of the battery due to changes in the load current [154]. The assumption that all model parameters are constant in the Thévenin battery model is a disadvantage of this type of model. In reality, all the parameters values are a function of the battery condition, so they depend inter alia on the rate of charge and discharge, the storage state of charge and temperature [143]. Due to this assumption, the model is not able to capture steady-state battery variations, runtime information and capacity fading due to thermal and degradation impacts [100][130][155].

The impedance-based electrical model [112][150], Fig. 14 (b), consists of the equivalent circuit (Z_{AC}) that models an AC-equivalent impedance, open-circuit voltage (V_{OC}) and internal resistance (R_{Series}) modelling the resistance of electrolyte. The impedance elements in this model are estimated using electrochemical impedance spectroscopy (EIS) measurements to achieve the alternating current (AC) response of a cell at certain frequency spans [147][112][150]. Measuring the EIS spectrum of the battery is a time-intensive task. It requires the steady-state condition to be maintained during the whole time of measurement, which is challenging to achieve for the battery cell. Any shift in battery cell conditions, such as a build-up of the reaction products in solution, temperature changes and others, can lead to inaccurate cell response measurements resulting in an imprecise impedance-based model fitting. The modern battery devices are characterised by a low internal impedance. The lower the impedance, the more difficult it is to accurately measure the EIS response of the cell [156]. The

[3] Chemical equilibrium is the state in the chemical system where there are no net changes in the concentration of the reactants and products of the chemical reactions in time. It does not mean that there are no reactions inside the system; it means that the forward reaction and the reverse reaction in the system proceed at the same rate, resulting in no net change in the system properties.

impedance-based electrical model cannot predict DC response and battery runtime as it works only for fixed SoC and fixed temperature settings [148]; this makes it unsuitable for battery energy storage modelling applications, as predicting runtime is crucial for this application.

The last group of the electrical circuit models presented in this work is runtime-based models [130][138][139]. In those models, a more complicated circuit network is used to model battery runtime and DC voltage responses. The model proposed by Hagman in [138], Fig 14(c), models the battery runtime and DC voltage response for constant current discharge. This model is capable of predicting capacity fading due to ageing and thermal effect but, unfortunately, is not able to predict the runtime and voltage response under dynamic load conditions [100][130]; what is the limiting factor if we want to use the model in energy storage application characterised by load variability in time.

The combined electric model proposed in [130], Fig. 15, is composed of the runtime model (Fig. 15(a)) and the RC network that is similar to the Thévenin-based model (Fig. 15(b)). RC part of the developed model is responsible for simulating the transient response of terminal battery voltage under dynamic load. In this model, the capacity is no longer infinite like it was in a simple battery model or constant. Instead, it is now the function of the cycle number and battery temperature [130]. The combined electrical circuit model is able to predict to acceptable accuracy battery runtime and the I-V performances but is not able to predict battery SoH and update parameters automatically, leading to a decrease in accuracy in the time of simulation as the battery degrades [100].

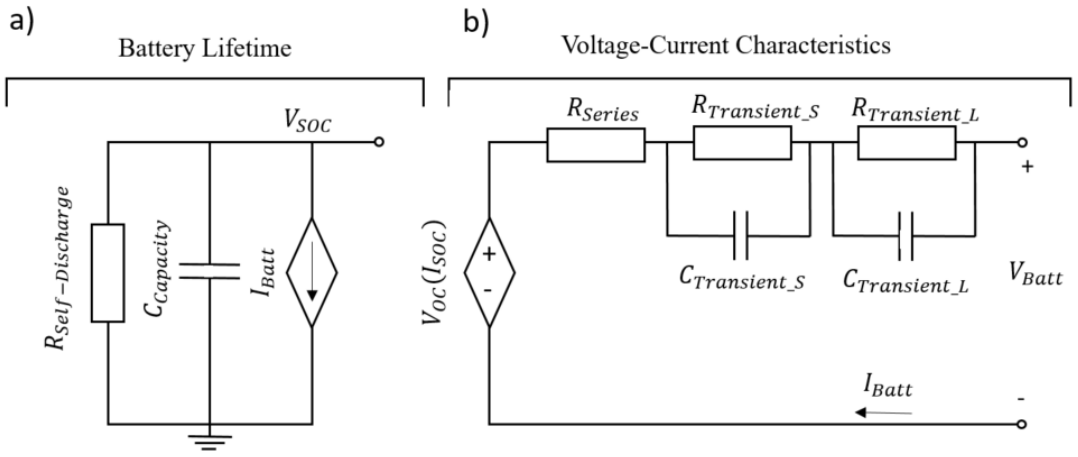

Figure 15 Combined electrical circuit model.

In summary, electrical-circuit models [108][130][157] describe battery behaviour with simple electrical circuits where different electrical components like resistors, capacitors and voltage sources mimic the battery cell characteristics. Most of these models capture I-V characteristics; some can predict the runtime and can track the SoC [158]. The simplified electric-circuit models [130][157][143] are computationally fast and can be easily incorporated into more complex systems and simulation tools [159]. Unfortunately, they do not integrate non-linear capacity behaviour, which leads to inaccurate predictions of the remaining battery capacity and operating time [130], which is crucial for battery management systems. Imprecise prediction of remaining battery capacity can lead to battery over-discharging and over-charging, limiting its lifespan. To overcome this issue, Zhang et al. [121] developed an enhanced electric circuit model by combining the electric circuit model developed in [130] with Rachmatov's diffusion analytical model developed in [113]. The resulting model is capable of capturing the battery recovery effect, but its applicability for performance prediction for battery management systems is limited due to the complexity of the analytical part of the model. Another enhanced electrical circuit model was developed in [136]. This model combines the electrical circuit model proposed by Chen et al. [130] with the kinetic analytical battery model proposed in [134], Fig.16(b) and Fig.16(a), respectively. The resulting model is capable of predicting battery dynamics

with the nonlinear capacity effect of the battery due to the application of the KiBaM module that is capable of capturing this nonlinearity in the capacity behaviour. Additionally, this model has a lower computational requirement than the enhanced model proposed in [121] which makes it more feasible for real-time applications. The drawback of the electric circuit models and two mixed models aforementioned [121] and [136] is that they do not consider the influence of uncertainty in the load profile during dynamic battery operation, which constitutes a limiting factor for applications of this type of models in real applications. From the system operator's point of view, it is important to plan BES operation based on the prediction characterised by high confidence.

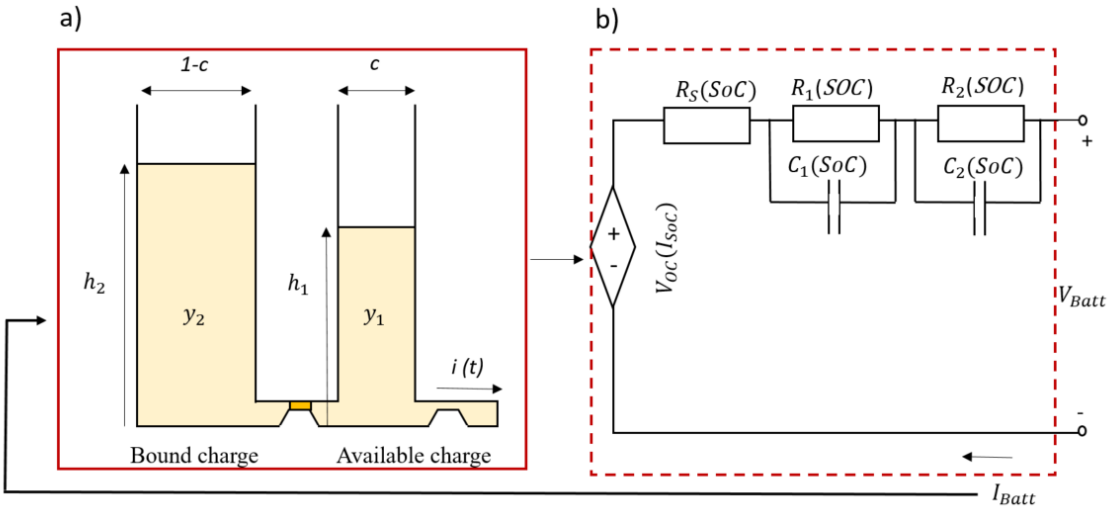

Figure 16 Electrical circuit model combined with a kinetic battery model.

The next group of battery models reviewed in this work are models employing an adaptive approach to predict battery health such as the Kalman filter (KF) [160]–[162] and Particle filter (PF) [115][116][163]. Those models combine electrical circuit models with a data-driven framework and are focused on the prediction of SoH and the remaining useful life (RUL) of the battery. Kalman filter is an approach used in the estimation of the state of health of the battery. It belongs to the Bayesian family of filters and provides the method of filtering the measurements of input and outputs to produce an intelligent

estimation of the dynamic system's state, used for linear systems. The main assumption of this method is that measured noise and process noise have Gaussian distribution with a zero mean and that both types of noise are independent of each other. Depending on how the battery model is defined, the process (a linear function that estimates the value of a variable based on its previous value) can for example estimate SoH. The measurement is used to correct the estimated value from the process equation to converge it to its actual value and can be defined for example in terms of battery voltage. When the system considered is non-linear, the Extended Kalman filter can be used (EKF). It is implemented by applying the linearization process of every time step to estimate the non-linear system with a linear time-varying system [13][154]. Andre et al. in their work [160] used the electrical circuit model shown in Fig. 17 combined with EKF in battery SoH prediction. SoH in this work was measured in terms of ohmic resistance (internal resistance changes compared to resistance at the beginning of battery life).

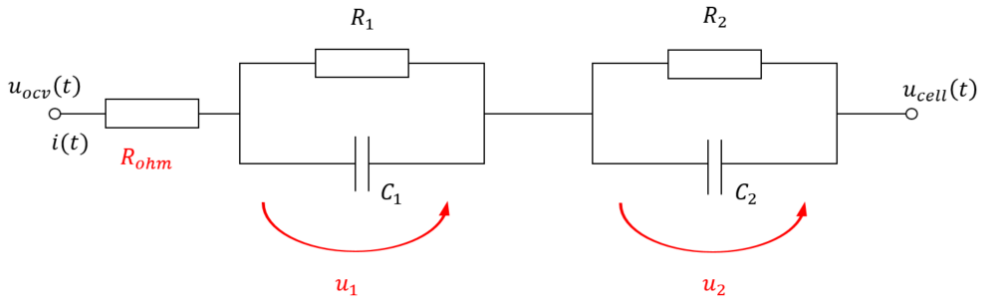

Figure 17 Equivalent Electrical Circuit battery model used in the ensemble model presented in [164]. The parameters shown in red are estimated using EKF.

In this work, EKF was used in the estimation of internal model parameters (in red in Fig. 17). The internal states in the presented model were first estimated using EKF based on the available data; the current and voltage response of the battery was measured at the beginning, in the middle and at the end of the life of the battery. The output of the electrical circuit model applying estimated state parameters by EKF is then compared to the true measured voltage value. The EKF recursively updates the parameter states at each step. The model in [164] was then compared with a structured Neural Network (SNN) approach

to predict the SoH of the lithium-ion battery. The results showed that although both methods performed well in estimating SoH, employing EKF was most promising due to the simpler structure, lower number of inputs required and no need to implement a function that described dependencies in the system as it was required for the SNN model. In [165] the EKF method was also applied to predict battery SoC simultaneously with SoH. Bhangu et al. proposed in [166] the SoH and SoC prediction model for lead-acid battery with the structure of the model originally used for modelling a Lithium-ion battery with modifications. In this approach, SoC has been estimated with KF and SoH prediction with EKF. KF can be applied to the state estimation of linear Gaussian systems; however, it cannot address systems with nonlinear/non-Gaussian properties [164] to which EKF was shown to be more suited. Both methods, KF and EKF, have achieved very good performance. The SoH estimation based on KF and EKF requires modelling of the battery cell, which is realised in both cases by implementation of electrical equivalent circuit models of battery cell for which the parameters are estimated using KF or EKF. Moreover, EKF accumulates significant prediction error for long-term SoH prediction due to its recursive character [129].

Particle filtering belongs to the Bayesian filters framework. They are used for dynamical systems that are nonlinear with non-Gaussian noise. For PF, like in the case of KF, two models are required. First one needs to describe the changes of the states that take part over time, and second model that relates the measurements to the state. More details about this method can be found in [165]. The PF is applied to the SoH estimation and RUL prediction. PF combines the available information from system measurements and other models (usually electric circuit models) and represents uncertainty in the prognostics of degradation processes taking place in the battery in the form of a probability density function for RUL and SoH [129]. Unlike the KF, the source of uncertainty in this model is assumed to be non-Gaussian, which is a more appropriate assumption when characterising phenomena such as the recovery effect [115]. This approach was employed in [115][163] to predict the SoH and RUL of the energy storage device. In both works, the equivalent electric circuit, which models the electrochemical processes, was combined

with the statistical models of state transition and ageing processes for the purpose of probabilistic estimation of the SoH and RUL of the battery energy storage, with simultaneous detection of regeneration phenomena in [115]. Nevertheless, the accuracy of these models relies to a great extent on the quality of the model that was used to model the electrochemical processes (how accurate the model was, how well trained it was) in conjunction with PF. This SoH estimation technique is model-based, and the accuracy of the model used in conduction with PF has a significant impact on the accuracy of the SoH estimation. Similarly, it is in the case of KF models.

3.1.3 Empirical Battery Models

In the remaining part of this section, the empirical models (data-driven models), mostly focused on predicting the SoH, will be considered. The data-driven models are widely used for battery SoH estimation and prediction due to their flexibility (ability to approximate many kinds of functions) and their freedom from modelling assumptions. Among these models, numerous approaches to predict battery SoH and remaining operating life have been used, such as Artificial Neural Networks (ANN) [166][167], Support Vector Machines (SVM) [168] and Gaussian Process Regression (GPR) [169]. Data-driven models, mainly taking the form of regression models, are a type of model that uses observation data to produce the prediction of the state of the battery without the implementation of any physical model. The dependency between the input variable(s) and the output prediction is modelled by a particular mathematical model with parameters that are obtained based on the training data. In other words, these models are a functional approximation of the input/output relation and are widely applied to estimate the SoH of the battery. Two groups can be distinguished among the data-driven models predicting battery health, namely models applying non-probabilistic and probabilistic approaches. The difference between these two approaches is that probabilistic modelling uses probability theory to express the uncertainty in the SoH model (uncertainty in input and output), while non-probabilistic modelling (deterministic modelling) does not consider randomness. Examples of non-probabilistic models that predict SoH of the battery include

Artificial Neural Network[4] models, autoregressive models and support vector machine [170]. The second group constitute the models applying the probabilistic approach (stochastic models) to predict battery health using Gaussian process regression [171][172] and Markov Chain-based stochastic battery models [173][174].

The autoregressive-based models belong to the non-probabilistic models that are used to predict the battery state of health and state of charge. In simple terms, those methods implicitly assume that the future resembles the past; thus, they use previous observations of variables to predict subsequent ones. Long et al. in [117] proposed an autoregressive (AR) based battery degradation model predicting capacity fade. This model has a simple structure and is easy to implement but unfortunately, due to the AR model linearity, it is not capable of fitting the non-linear characteristics of battery capacity fade leading to the model under-fitting. This model has poor long-term prediction and poor generalization ability [175]. The problem of the non-linearity of capacity fade was addressed by Liu et al. in [118]. In this work, the AR model was combined with a non-linear degradation process. The acceleration factor, which is correlated with a number of cycles, was added to the output of the AR model to allow this non-linearity to be captured by the model. The resulting model, the nonlinear degradation AR approach (ND-AR), was able to predict remaining useful life with greater precision in comparison to the AR model in [117] by accommodating the non-linearity of battery degradation processes (the battery degradation rate accelerates with the increasing number of cycles). The problem of battery degradation process non-linearity was also addressed in the work of Zhou et al. [176] by application of an autoregressive integrated moving average (ARIMA) framework. The ARIMA is a time series forecasting. This framework is based on a combination of two concepts, namely AR, which captures the linear trend in time series of battery data, and moving average (MA) represents uncertainty through the previous error regression. To remove the trend present in the data, the initial differentiating step is applied in this

[4] Family of Neural Networks include also the probabilistic approach, Probabilistic Neural Network, but the focus in this work is only on the non-probabilistic ANN and their application in battery health modelling.

framework [177]. In [176], ARIMA model was used along with the Empirical Mode Decomposition (EMD)[5] in the SoH prediction. The assumption of using the EMD in this work was based on the fact that the SoH series can be considered as a hybrid signal with multiple underlying processes occurring at different timescales, such as capacity regeneration and global deterioration [129]. In this work, the EMD was applied to raw SoH data to decouple the effect of global deterioration and capacity regeneration in observations. Then, an ARIMA model was trained for each decomposed time series. The predictions from the resulting models were then added and based on the resulting SoH the remaining useful life was predicted.

ARIMA-based models are not capable of predicting a non-linear relationship which is an important aspect in predicting SoH as the degradation of the battery has a non-linear characteristic. The computational complexity of this type of model depends on its order[6] (the size of the training vector increases with the order increase). Additionally, ARIMA is a 'sparse' modelling method. It only takes a few parts of datasets to fit the model but the relevance of using the part of past data for long-time predictions is questionable [187]. It is because the battery's health changes dynamically over time under different stress factors and operational regimes that the battery is subject to. Additionally, the loss of capacity and other health indexes under given conditions is different for new and aged cells [178].

The next group of data-driven models employing a non-probabilistic approach are Artificial Neural Networks[7]. The ANN are machine learning algorithms that mimic the operation of the neurons in human brains. These types of algorithms are very flexible and can fit any function, given that enough training examples are provided. The numbers of inputs feed each neuron of the ANN. The input is then transferred by the activation

[5] Empirical Mode Decomposition is the tool used to decompose the signals that are non-linear and non-stationary into the sum of oscillating components with zero mean and the composition is performed without leaving time domain [231].
[6] The parameters p, d and q in ARIMA model represent the order of autoregressive model (AR), differencing order (I) and moving average (MA) respectively.
[7] Family of Neural Networks include also the probabilistic approach, Probabilistic Neural Network, but the focus in this work is only on the non-probabilistic ANN and their application in battery health modelling.

function and the resulting signal is propagated to the next layers. At the end of the process, the output signal is generated. The ANN can be divided into deep neural networks (DNN) and shallow neural networks. The DNN requires substantially more data for training than shallow neural networks, where the model is trained on selected features. The feature selection increase requirements for a better understanding of the modelled system. More information about ANN can be found in [179]. The ANN is widely used in battery modelling, especially in SoH and RUL of battery estimation. Among the ANN types, two were successfully applied to the estimation of the SoH and RUL, namely, feed-forward neural network (FFNN), also called backpropagation neural network (BPNN) and recurrent neural network (RNN). The difference between RNN and FFNN is in the way the signal propagates through the network. In the FFNN network, information travels only in one direction from the input to the output layer. RNN also implements feedback connections. More information about the differences in the architecture and implementation of these NN models can be found in [180]. Thanks to feedback connection, the RNN is able to learn the long-term dependencies in data, making it a promising model for battery degradation modelling [175]. The advantage of the ANN methods in battery modelling is, as universal approximators, they do not need an estimation of explicit regression parameters and coefficients. They are used in modelling the RUL of the battery [119], SoC [181] and in the prediction of SoH in [182][183][184].

Eddahech et al. [182] proposed an electric circuit model based on the EIS measurements integrated with the RNN to estimate the RUL and SoH of the lithium-ion battery. In this model, the prediction is based on knowledge of the previous system behaviour and multiple inputs such as temperature, current and state of charge variations. This model is able to accurately predict variations that occur in the battery performance that takes place with ageing [182]. The drawback of this method is a dependency of SoH estimation accuracy on the accuracy of the electric circuit model used. As it is a deep neural network model, it also requires a substantial amount of training data; consequently, training this model is time-intensive. Zhang et al. proposed in [185] battery SoH and SoC estimation based on long-short-term memory (LSTM) recurrent neural network (RNN)

combined with the particle filtering (PF) to smooth the SoH estimation result from RNN. LSTM - RNN is used to learn long-term non-linear relations between states of the battery and the measured battery current, voltage, terminal voltage difference and temperature. Particle filtering is employed to improve the SoC estimation accuracy of the developed model. The model developed in [185] showed improvement in the accuracy of SoH prediction compared to the models based on LSTM-RNN or RNN alone. As the previously reviewed model [182], it also belongs to the deep neural network group of models; thus, it also requires a substantial amount of data for training.

Dai et al. [184] proposed a novel model of estimating SoH based on the Prior-Knowledge Neural Network (PKNN) combined with the Markov Chain[8] that is used to modify the PKNN estimation. This model belonged to the shallow neural network group and was trained on the features selected as the most important in SoH prediction, namely average voltage, change in voltage and dSOC/dV (rate of change of SoC with change in voltage). The FFNN architecture was employed for this model. The prior knowledge was transferred into constraints, and feature constraints, which were added to the loss function of NN to optimise FFNN training. Finally, the Markov chain, which was established on the prediction error, was used to improve the SoH prediction effectiveness of the developed PKNN model. This approach significantly improved the effectiveness of SoH prediction compared to PKNN alone. Improvement of SoH estimates was in the range of 15-30% [184]. This model requires fewer data for training compared with the models based on deep NN reviewed earlier but in turn, requires more knowledge about modelled systems to ensure proper feature selection.

In summary, the SoH modelling method based on neural networks has the ability to learn from experience and examples and does not require the identification of the model parameters and coefficients. These models are simply established by training – estimating of weight vector of the NN based on available training data. However, in the case of DNN, the development of those models requires a substantial amount of data for training

[8] Markov Chain is defined in the Section 3.2 of this thesis.

and verification of the model operation [175]. The quality of data available has a significant impact on the model's accuracy. The uncertainty in noise and bias in training data, for example caused by sensors, and calibration errors, are important issues for DNN [24]. Moreover, the model based on DNN is characterised by the high computational cost and lack of ability to quantify uncertainty in the system. Furthermore, the DNN framework is prone to overfitting and being stuck in local minima [177], meaning that the models learn a suboptimal representation of relationships, thus leading to developed models not reflecting reality. In the case of the battery models predicting SoH, this can mean that the trained model will not be able to predict the battery health of the actual device that the model was based on.

The Deep Neural Network models are able to model non-linearity, but they still require a substantial amount of data for modelling. The modelling method employing Support Vector Regression (SVR)/ Support Vector Machine (SVM) can overcome this issue, as it requires fewer data samples when compared to deep NN [186]. This method is very good in handling small training datasets [175]. SVR is a non-parametric machine learning technique that uses regression analysis to recognise patterns of non-linear systems. The basic idea behind this method is to map data in input space, and using a non-linear transfer function, transform them into a higher dimensional feature space. After this step, the linear function can be used to fit the data in the feature space. More information about this method can be found in [187]. The accuracy of the SVR model depends on the data available in the testing region [188]. Nuhic et al. proposed in [168] the SVR model that estimates the SoH of Lithium-ion battery followed by the same approach to predict remaining useful life. In this method, a very important step is pre-processing of data to ensure the SVR converge. Also, the scaling of features is crucial to remove the potential dominance of some variables that can push the SVR to converge to an unsatisfactory result [168]. The drawback of this method is that it cannot include likelihood prediction, which is an important feature in battery health prediction for the BES. As the operational decisions for BES in the power network are based on model prediction, the system

network operator would prefer to base his/her decision about the operation of this device based on the results characterised by high confidence.

In the [189], Zhao et al. implemented the feature vector selection (FVS)[9] with SVR to cut down training data size by removing redundant data and selecting points that can represent the whole training set [189]. Due to the applied approach, the modelling complexity was diminished compared to standard SVR and the computational performance for model training was improved. The reduced complexity of this model results in better scalability. This approach allowed for improving model training and SoH prediction efficiency and RUL estimation accuracy. The SVR is not affected by the problem of local minima [177] compared to the ANN framework. It has a high generalization ability. This method is additionally particularly suitable when limited training data are available [190]. However, this model lacks uncertainty management in the SoH prognostics, which is important for Battery management systems. Neural network and SVM models both require extensive offline training and a high amount of data to perform it.

The next group of data-driven models that are used in estimating the battery state of health constitutes the models based on the probabilistic approach. In those approaches, the different types of uncertainties are considered during the modelling, namely originating from the measurement, operational environment and the model itself. This type of model aims to capture the stochastic behaviour of parameters that influence the battery SoH, and it utilises probability distribution to model uncertainty in those parameters and their influence on the battery [175]. The models based on the Gaussian Process Regression (GPR) are an example of data-driven, probabilistic battery models considered in this work. Additionally, the stochastic models based on the Markov chain framework are mentioned here, regardless of the lack of their application in SoH prediction in the past. This choice is dictated by the fact that this framework is applied in

[9] Is the pre-processing step when building a machine-learning model that aims to find the best possible set of features based on which then the model is trained.

this work to model the battery maloperation level that constitutes a proxy of the SoH of the battery. These models were included to show how Markov Chain-based methods have been used in the battery modelling field so far.

Gaussian Process Regression has wide application in the battery prognostic analysis due to its flexibility, being nonparametric and providing a probabilistic output [175]. The GPR is a machine-learning method that employs the Bayesian approach for prediction [171]. The GPR is in some way similar to linear regression as in both regression methods, we have the explanatory "signal" and the "noise" signal (error term), and both methods try to find the relationship between the dependent variable and the explanatory (independent) variable (learn the mapping from inputs to outputs given a training data set comprising labelled data). The difference is that in the GPR, the explanatory variable is assumed to be a random variable that follows a particular distribution which eliminates the requirements for the application of parameters that need to be estimated in the case of linear regression, which makes the GPR model a non-parametric regression method [171]. Richardson et al. [172] proposed the multi-output GPR model for the state of health and RUL estimation based on capacity estimation as the measure of the battery SoH. The base for this model constituted the assumption that when we have multiple battery cells that are subject to a similar charge/discharge regime, we can expect a correlation in the capacity trends between the battery cells. The multi-output GPR model in this work [172] was implemented as having a single output with the additional outputs treated as the labels for the associated output. The advantage of multi-output GPR is that this method allows capturing of similarities between battery cells. The disadvantage of the approach applied in this work is the high computational cost due to handling a large number of outputs [172]. He et al. [129] also proposed the application of the GPR for SoH prediction. In this work, instead of applying the GPR to the original SoH time-series data, the global deterioration trend and sudden capacity recovery components were decoupled from the

original data using the wavelet decomposition method[10]. The resulting decoupled signals were then used as input data to the GPR, subsequently leading to separate models fitted for each decoupled signal that predicts SoH. Both models were then combined to achieve SoH prediction [129]. The proposed method outperformed the standard GPR in the SoH estimation (Standard GPR does not use trend extraction) [129]. In summary, the GPR method is used in the battery health prognostic to predict the RUL and SoH of the modelled devices. It provides the probabilities for the prediction that is useful when deciding how BES will be operated. Additionally, the GPR is capable of capturing nonlinearity, but unfortunately, the prediction is done with a high computational cost [187]. Moreover, the GPR does not scale well due to the non-parametric nature of GPR [191].

The last group of probabilistic, data-driven battery models considered in this work are the stochastic models of battery discharging and charging processes based on discrete-time Markov Chains. The first battery models based on the Markov chain were proposed by Chiasserini et al. [120][192] for primary batteries, which are out of the scope of this work, followed by the models proposed for secondary batteries in [173][174]. These models assumed a fully observable state space where the SoC was represented as a Markov Chain whose state transitions captured the charging and discharging process. Bucciarelli proposed in [173] a stochastic model based on the Markov Chain (MC) with N states for a rechargeable battery., Fig. 18 (a). In this model, the transition is only allowed between adjacent states with two possible energy transfer values, Δ and $-\Delta$. This makes this model not suitable for most of the storage applications in the power network where the load has not a constant value and changes in time. This model was extended in [174], Fig 18 (b), by incorporating the possibility for the energy transfer values to be within a finite set value instead of just two which makes this more realistic for modelling real batteries in use.

[10] Wavelet analysis is the method of decomposition of a nonstationary time series data into time-frequency space. This method is capable of determining both the dominant mode of variability and their variation in time. [232]

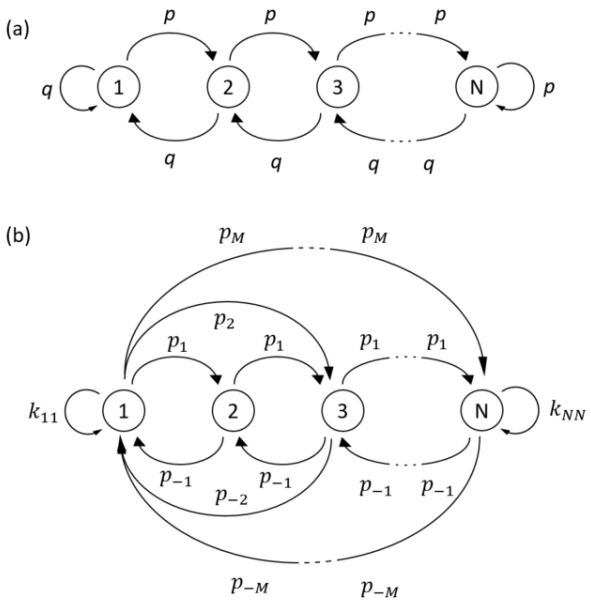

Figure 18 Markov chain model of a rechargeable battery. N is the number of discrete states describing the battery state of charge, where one represents fully discharged, and N represents the fully charged state of the battery. The probability of transition between states in (b) is represented by p, with M indicating the transition between the most outer states. In (a), p represents the probability of increasing the amount of energy in the storage by amount Δ, and q represents the probability of decreasing energy in the battery by Δ.

Unfortunately, the aforementioned two stochastic models proposed in [173][174] do not consider capacity fading during cycling life, which is very important for the battery in use as it impacts the availability of charge for the load and available space for storing that change. The MC-based battery models discussed in this section, due to their narrow focus, do not provide the overall characteristics of the battery; thus their application is limited [159]. In the case of models in [120][192], this narrow focus is mostly dictated by the application of the developed model, battery for pulsed discharge condition in [192], where key performance that needs to be considered by the model is the recovery effect in idle periods. For models in [173] and [174], the limited focus is dictated by the way the MC model is defined and used, which reduces the possibility of incorporating more battery characteristics at once in device modelling. In both models, [173] and [174], the SoC is

represented by MC with the transitions allowed only to adjacent states in [173], extended in [174] to allow transition also to other states.

In summary, the advantage of data-driven models is that they require little or no knowledge of the complex electrochemical mechanisms taking place in the battery cell [177], and they have good performance for nonlinear problems [193]. The drawback of those methods is that they require a significant amount of curated exemplar data from extensive and often complex laboratory tests, which is time-consuming to obtain [177][186] and often requires high fidelity monitoring. The testing of long-term ageing effects in real operating conditions may span 6-11 years, depending on the battery technology. It can be accelerated to 1-2 years under laboratory conditions [194]; however, with the current development of high-performance batteries [195][196][197] characterised by an extended lifetime, obtaining a sufficient amount of ageing data becomes a more resource-intensive task. Another drawback of these models is that their performance heavily depends on the quality and quantity of data available for modelling and applying the modelling technique [193]. Moreover, it is difficult to reproduce realistic operating regimes in laboratory settings, thus, the resulting model can be more error-prone in online prediction [177].

3.2 Challenges in Battery Health Monitoring and Proposed Solution

The monitoring of battery health is a crucial aspect of battery asset management to ensure its safe, reliable operation. There are multiple indicators of battery health that currently are used to assess and describe battery health, with capacity and rise of internal resistance used the most often. The capacity is subject to ageing processes and degrades over time. Similarly, the increase in battery internal resistance changes over time and results from plating the chemical compounds, different for different battery technology, on the battery plates [11][198].

The other less frequently used measures of battery health are the following:

- State of health (describing the state of the battery compared to the state of a brand-new device) [13],
- Available power (proportionally related to capacity fading, as capacity decreases in time, the available power for usage also drops) [199],
- State of function (express a battery performance during operation in a particular application (ex. peak shaving), how this device meets real power demand – in other words, it describes to which extent the battery is capable of providing the function it was intended for) [100].

Health indicators (HI) can be either measured/calculated based on direct (online) observation of the voltage, current, and temperature of the battery or estimated with an application of the battery health model. With the rising number of BES incorporated within the power system, direct measurements of the HI introduces the need for the installation of numerous sensor to measure indicative variables, which can introduce a high cost of telemetry installation and increase the level of maintenance required to ensure proper operation of the system with numerous sensors. It also introduces a substantial amount of data to be gathered and processed. With the BES aggregation, there can be problems with the synchronisation of such a substantial amount of measurements. Additionally, the missed reading by sensors can constitute a problem of the lack of information about the battery's health at a particular time. Moreover, some HI, such as the internal resistance of the battery, is very difficult to be measured. For example, to measure the capacity, the battery needs to be taken out of the normal duties to perform a reference cycle to enable credible measurements to be taken. Estimation of the battery health with the application of the developed model is also not free from its challenges and limitations. For this option, there are two major problems. The first one is related to the limited availability of suitable data from laboratory experiments or lifetime battery usage data required for modelling purposes. As the modelling is based mostly on the measured critical battery variables, such as voltage, internal battery resistance, current, battery and ambient temperature, operating time and others, a substantial amount of information needs to be gathered to allow the model to be defined and implemented. The second problem is

related to the way most of the models are defined with respect to the number of inputs required to enable health estimation. Most of the models often require multiple input variables for predicting battery health, such as current, voltage, temperature and others, depending on how the model was structured, introducing the need for the installation of additional telemetry for gathering the required input data for the model to allow its application. The potential lack of data synchronisation or missed reading can affect battery model operation and the ability to accurately estimate battery health based on available measurements. With the BES aggregation, the application of the models estimating health indicators that require multiple input variables for estimation introduces the need for the installation of numerous sensors to gather the required information. This in turn introduces the significant cost of necessary telemetry installation and introduces the significant volume of data to be gathered and processed.

As the current battery health monitoring solutions are not ideal, they often add extra telemetry installation costs, require impractical volumes of data, or are burdened with high computational costs; there is a need for a new health metric for batteries that will:

- Minimise input data requirements,
- Eliminate the necessity of installation of extensive telemetry and associated with it maintenance of the system with additional sensors installed,
- Reduce/minimise the amount of data to be processed that are introduced due to the aggregation of battery energy storage in the power system,
- Be able to provide information if the battery is operated in a way that can prolong its life based only on the limited information available.

This work aims to provide a solution to the battery health prognostics problem by proposing alternative health indicator in terms of maloperation level. This work proposes capturing cumulative maloperation as a proxy for cell health, motivated by the strong influence misuse has on the internal state of the battery. The necessity for extensive laboratory data required for modelling is eliminated when applying the proposed approach. The proposed model minimizes requirements for training data by simply

reusing available generation and demand data in conjunction with battery operating preferences, summarised in Table 4, to generate training data. Additionally, the requirement for the availability of the measurements of indicative variables, needed as input for the model to allow its operation, is minimized by the proposed approach. The estimation of the proposed HI is simply based only on the operating regime imposed on the device (e.g. actions set by a BES controller), which is usually available (battery schedule is planned in advance in the power system to support energy balance in the system).

3.3 Research Questions

As discussed in the preceding section, many challenges in battery health monitoring need to be still addressed to ensure the successful expansion of the battery energy storage within the power network. To support the process of integration of BES with the power network following questions will be addressed in this work:

- Can we propose an alternative battery health metric to the currently used metrics? Can we measure battery health in terms of device maloperation level, and this HI will be comparable with commonly used indicators, for example, capacity fading?
- Can we reduce the data needs for suitable datasets for battery health modelling?
- Is it possible in the battery health modelling to use only knowledge about battery operating preferences and reused demand and the electrical generation data to train a model that will be able to assess the health of this device? This approach could potentially eliminate the necessity of using extensive laboratory data or data from long-term battery operations in battery health modelling.
- Can we minimize the requirement for increasing telemetry installation to measure indicative variables needed to enable the application of the models estimating battery health based on multiple inputs? Can we imply the battery's state of health based simply on information about implemented battery charging/discharging schedule?

- Does the model trained on a limited number of data could be still representative of the general case?
- Can the Hidden Markov Model framework be suitable for battery health modelling?

This work aims to provide answers to the above questions in the consecutive chapters.

3.4 Proposed Model

The graphical summary of the reviewed battery model types carried out in Section 3.1 is shown in Fig.19. This summary focuses on the knowledge requirement of the model, its computational effort, data requirements and the model complexity.

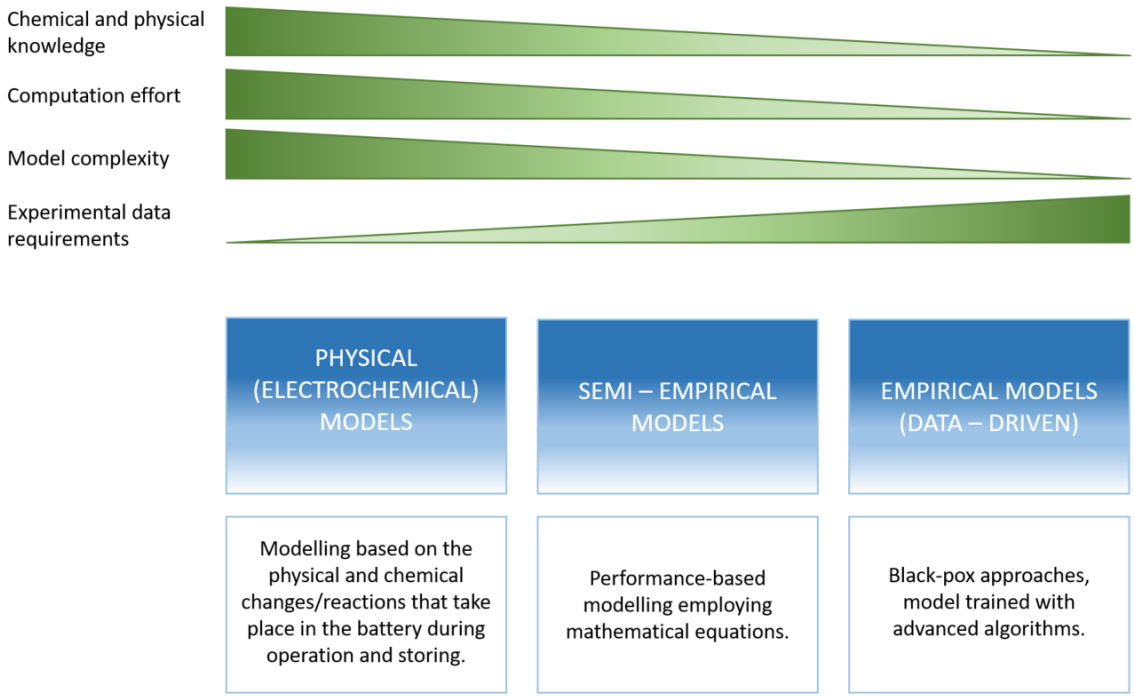

Figure 19 The graphical summary of the model types used in the prediction of battery state of health.

The model proposed in this work belongs to the data-driven, machine-learning models group and is a subset of the family of Hidden Markov models. It is a state space model with hidden discrete states and addresses the unobservability of the state space, in this case, the internal battery chemical reactions and the state of health. As was shown in the

battery technology review carried out in the preceding chapter, the chemical processes that take place inside this device are very complex and cannot be observed directly, as it is also in the case of the state of health of this device. The proposed model addresses this issue by application of Hidden Markov framework in the modelling. Additionally, the application of the modelling approach proposed in this work, namely reusing available demand and generation data in conjunction with battery operational preferences to prepare data for modelling, eliminates the need for intensive laboratory data required for testing and training. Moreover, the proposed model allows the prediction of the battery health based only on limited knowledge of the system, namely based only on information about the battery schedule, eliminating the need for installation of additional telemetry in the system that will gather all required variables required for other models to be applied.

3.4.1 Proposed Model Versus Existing Models

In contrast with the electrochemical models that require detailed knowledge of chemical processes and reactions taking place in the battery cell, the proposed model uses only an understanding of the battery operational preferences governed by battery chemistry, summarized in Table 4. It is also significantly faster in the estimation of battery health than physics-based models, for which running time can often be measured in days. The faster running time is important for the model's applicability. The introduced model is also characterised by significantly lower complexity. Compared to 50 or more battery parameters that need to be set to enable physical battery models to be implemented, the proposed model requires only three low dimensional probability matrices to be defined based on available data, namely state transition probability, emission probability and initial state distribution.

The proposed model also has advantages over reviewed semi-empirical battery models. In comparison to the Vrudhula diffusion model and the Kinetic battery model, analytical models, it can capture potential battery degradation measured in terms of novel maloperation level, which was shown in the following chapter to be strongly correlated with capacity fading of the battery due to ageing processes. In contrast to most of the

electrical circuit models, the proposed model is able to catch the battery degradation, and additionally, it considers the influence of uncertainty in the load profile during dynamic battery operation. The lack of this ability in electrical circuit models constitutes a limiting factor for applications of those types of models in real applications. From the system operator's point of view, it is important to plan BES operation based on the prediction characterised by high confidence. Other semi-empirical models that were reviewed in Section 3.1 are models employing adaptive approaches to predict battery health, such as Kalman Filter, Extended Kalman filter and Particle Filtering. For PF, like in the case of KF and EKF, two models are required for SoH estimation. The first one needs to describe the changes in the states that take part over time, usually in the form of an electrical circuit battery model, and a second model that relates the measurements to the state. On the contrary, the proposed model does not require a separate model to describe a change of states as it is described by the state transition probability matrix, which is learned during the model training. Nevertheless, the accuracy of KF and PF-based models rely to a great extent on the quality of the model that was used to model the electrochemical processes (how accurate the model was, how well trained it was), and there is no such dependency in the proposed approach.

Finally, some of the limitations of data-driven models were addressed by the battery modelling approach proposed in this work, namely the limited availability of extensive suitable battery datasets needed for modelling and the requirement of installation of additional telemetry to allow application of data-driven models often characterised by multiple inputs to allow health estimation. The models employing deep neural networks in battery health estimation that were reviewed in the preceding section require a substantial number of training and testing data, meaning there is a need for extensive laboratory test data or data from long-time battery operation to allow proper modelling. The quality of available data can have an important impact on the model training. The model proposed in this work overcomes this issue by re-using available generation and demand data in conjunction with knowledge of battery operational preferences summarised in Section 2.3 to generate data for battery health modelling. The DNN-based

models are also characterised by the high computational cost, which is reduced by the proposed approach due to reducing amount of data required to be processed during the training. Contrary to DNN models that require multiple input variables to allow the application of the model in the battery health estimation, the proposed approach estimates the battery health only using the information about the battery charge schedule as the input to the model. This in turn, decreases the requirements for the installation of additional telemetry to measure multiple variables when applying the developed battery model.

Another data-driven model group that was reviewed in this work are models based on SVM. These models require fewer data samples when compared to deep NN but still substantially more than the model proposed in this work. The SVM modelling also does not include likelihood estimation, which is an important feature in battery health estimation for the BES, and that is addressed by the proposed modelling approach presented in this work. An additional drawback of models based on SVM is that they require pre-processing of data to ensure the SVR converge, and the scaling of features is also required to remove the potential dominance of some variables that can push the SVR to converge to unsatisfactory results. In contrast, the proposed model does not require pre-processing in the modelling.

Another group of data-driven models reviewed in this chapter constituted the probabilistic battery model based on Gaussian Process Regression. Both reviewed models in this work provided the probabilities for the prediction that is useful when deciding how BES will be operated, and both are capable of capturing nonlinearity. The model presented in [172], due to handling a large number of outputs, is characterised by a high computational cost. The proposed model in this work has only single input and output, making it less computationally expensive than the model presented in [172]. The model presented in [129] as first decouples the deterioration trend and sudden capacity recovery from the original data and then fits the separate models for each decoupled signal, which make the structure of the model more complex. In contrast, the proposed model has a much simpler

structure and does not require data pre-processing to enable modelling as it is in the case of the abovementioned model.

The last group of the probabilistic data-driven models considered in this work are models based on Markov Chain. The model introduced in this work belongs to the Markov Models family and is based on the Hidden Markov Model (HMM), which stochastically models the battery limitations imposed by its chemistry as a combination of present and previous sequential charging actions, and articulates the preferred operating regime as a measure of health consequence. In contrast to models based on the Markov Chain introduced in earlier works that assume full state-space observability, it addresses the issue of the partially observable state-space. The states that the battery can be in cannot be observed directly as they are hidden. This is a more realistic assumption in battery modelling due to the inability to observe the internal battery state and chemical processes taking place inside the cell. Additionally, the Markov Chain-based models were not used in the battery health modelling, and the developed model filled this niche.

3.4.2 Model Requirements

All of the battery models in the battery health modelling field today have demonstrated that they require either a great amount of knowledge and high computational effort, as it is in the case of physics-based models or a large amount of data that need to be captured in the case of data-driven models. However, from the practical perspective, there is a necessity for a model that does not require these levels of detail. From the asset management perspective, what is required is a broad general model, which will capture the health index of battery storage assets allowing more informed scheduling of this device with regard to preserving battery operational integrity. This model would need to run on the minimum data, repurposing existing data for the purpose of formulating those health indexes, and need to have the minimum computational expense. With scalability in mind, the approach applied in this work requires no telemetry other than would be required to meter the use of the battery. Unlike other data-driven methods, the model developed does not require extensive or invasively captured laboratory battery performance data; training

data is instead generated based on simplified knowledge of operating regime preference dictated by the battery chemistry and reused available PV generation and electrical demand data. Additionally, only a single input is required for the prediction of the maloperation level, which approximates the SoH of BES, compared to multiple inputs required in other data-driven models. For example, three inputs are required in the model based on a Bayesian network proposed in [200], which are temperature, discharge current and end-of-discharge voltage. In the model proposed in [167] that is based on the probabilistic neural network, the charging time, the instantaneous voltage drop at the start of discharge and the open-circuit voltage of a fully discharged battery are required to provide battery health estimation. It can constitute a disadvantage of the model due to the requirement of measuring needed variables by multiple sensors or systems, which have to be available simultaneously and synchronised. Additionally, requirements of measuring multiple variables can introduce the need to install additional telemetry when not already installed in the system incurring additional costs. The resulting model developed here makes predictions simply based only on the operating regime imposed on the device (e.g. actions set by a BES controller), thus minimising requirements for extensive monitoring of battery parameters across an asset fleet. This is achieved thanks to the ability of IOHMM to encapsulate all required knowledge of the time-dependent chemical processes taking place inside the battery during operation in the hidden states and describe it in the form of a state probability matrix, thus eliminating requirements of measuring the battery performance that may indicate the condition of the battery.

3.5 A Short Introduction to the Family of Markov Models

Before the proposed model is defined in detail, some knowledge about Markov models will be introduced in this section to enable a better understanding of subsequent parts of this thesis.

Markov Models are stochastic models involving a random transition from state to state. The probability of going from one state to another one, in these models, depends

only on the current state, meaning the present state of the system is independent of the past (Markov property) [200] and is described by state transition probabilities. Markov Models can be either continuous-time or discrete-time. In this work, only discrete-time models will be considered. Classification of the Markov Models is based on the autonomy and observability of the system. Considering the observability of the state space, the Markov models can be divided into two groups:

1. Models with a fully observable state space where all information is available in the model at any state. Markov Chain and Markov Decision Process (MDP) belong to this group.
2. Models with not directly observable state space. The information about the state is not observable directly in these models but through observing the emission produced by the hidden state. The Hidden Markov Model and Partially Observable Markov Decision Process (POMDP) belong to this group.

Taking into consideration the autonomy of the system, Markov models can be divided into two groups:

1. Autonomous models where the system cannot be modified by the action of the agent[11]. There is no control over state transition. Markov Chain, and Hidden Markov Model are the members of this group.
2. The controlled models where the agent has control by actions. In this group, we have Markov Decision Process and Partially Observed Markov Decision Process.

The taxonomy of Markov Models is summarized in Table 12. The autonomous Markov models with full and partial observability of the states are the subject of this section and will be discussed here. The controlled Markov models are out of the scope of this work and will not be further considered. First, the MC will be introduced, followed by the

[11] Agent (decision-maker) refers to the system that is responsible for making decision and performing actions based on the state of the system and the reward generated due to the actions performed by agent.

definition of the HMM. At the end of this section the IOHMM, an extension to the HMM, will be discussed in more detail as this is the main subject of this chapter.

Table 12 Taxonomy of Markov models [200].

		Observability of states	
		Full	**Partial**
Autonomy	**Autonomous**	Markov Chain (MC)	Hidden Markov Model (HMM)
	Controlled	Markov Decision Process (MDP)	Partially Observation Markov Decision Process (POMDP)

A graphical representation of those models, with the required elements to fully define them, is presented in Fig. 20.

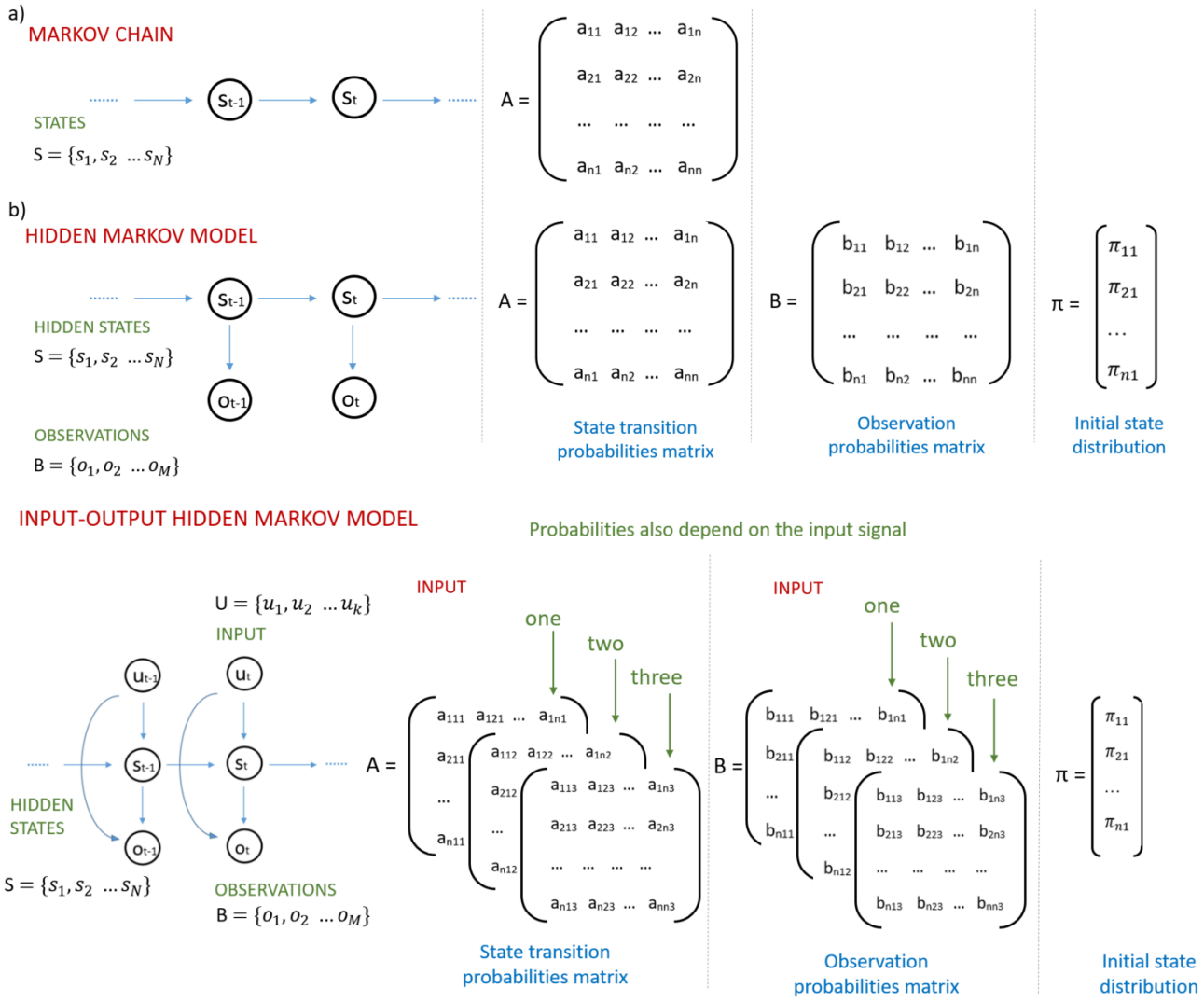

Figure 20 Graphical representation of Autonomous Markov models showing the required elements to fully define the model for (a) Markov Chain, (b) Hidden Markov Model and (c) Input-Output Hidden Markov Model

3.5.1 Markov Chain

Markov Chain, Fig 20(a), is an autonomous stochastic process, a type of Markov Process that has fully observed discrete state space satisfying the Markov property (7) (prediction of the future state can be made based only on the present state and this prediction is as good as it could be when based on the full history of the process).

$$P(S_n = s_n | S_0 = s_0, S_1 = s_1, \dots, S_{n-1} = s_{n-1}) = P(S_n = s_n | S_{n-1} = s_{n-1}) \quad (7)$$

MC has applications as a stochastic model of many real-world processes. A full definition of MC requires:

- a finite set of N[12] sates, sate space[13] $S = \{s_1, s_2, s_3 \dots s_N\}$,
- transition probability matrix $A = a_{ij}$ where a_{ij} is the probability of going from state i to state j, $a_{ij} = Prob[S_{n+1} = j \mid S_n = i]$,
- the initial state distribution $\pi = \pi_i$, where the π_i is the probability that the system starts in a state s_i.

As the transition matrix is stochastic, all its elements are non-negative, and all rows sum to unity, $\sum_j a_{ij} = 1$ [200].

3.5.2 Hidden Markov Model

The Hidden Markov Model, Fig 20(b), also belongs to the autonomous Markov models like MC, but in contrast to MC, it has partial observability of state space, meaning that the states are not observed directly but implied through the observables emitted by the hidden states. The HMM assumption is that the underlying process is the MC with states hidden from the observer. In other words, we can define the HMM as a doubly stochastic process in which the underlying dynamic process cannot be observed directly;

[12] N is positive integer.
[13] Depending on how the problem is defined, the states can be either natural number, or for example simple descriptions such as cloudy, sunny, raining.

instead, it is observed through another stochastic process as a function of the first one. The full definition of the HMM requires like in the case of MC the following:

- the finite set of N states, state space $S = \{s_1, s_2, s_3 \dots s_N\}$, but this time not observed directly,
- transition probability matrix $A = a_{ij}$ where a_{ij} is the probability of going from state i to state j, $a_{ij} = Prob[S_{n+1} = j \mid S_n = i]$
- the initial state distribution $\pi = \pi_i$, where the π_i is the probability that the system starts in the state s_i.

The additional components required to fully define HMM constitute:

- a finite set of M[14] possible observations, $\Omega = \{o_1, o_2, \dots, o_M\}$
- observation probability distribution B= $b_j(o_k)$ where $b_j(o_k)$ is the probability of emitting observable o_k given the system is in state j, $b_j(o_k) = Prob[O_n = o_k \mid S_n = j]$, Fig. 20(b).

Matrices A and B are stochastic matrices, and they have to satisfy the following conditions:

$$\sum_{j=1}^{N} a_{ij} = 1, \forall \text{ for each } i = 1, \dots, N \tag{8}$$

$$\sum_{k=1}^{N} b_j(k) = 1, \forall \text{ for each } j = 1, \dots, N \tag{9}$$

For HMM, each probability transition in the state transition matrix and probability of emission in the observation emission matrix is time-independent, meaning they do not change the structure as the system evolves in time.

HMM can be used to solve three different types of problems, namely:

- *evaluation problem (pattern recognition problem)*

[14] M and k are positive integers.

Here we want to find the probability of an observed sequence $O = \{O_1, \dots O_T\}$ given the HMM model $\Theta = (A, B, \pi)$, meaning we want to find $P(O|\Theta)$.

- *decoding problem (also originated from the area of recognition problem)*
  Here the goal is to find the sequence of hidden states that most probably generates an observed sequence $O = \{O_1, \dots O_T\}$.
- *the learning problem*
  Here the aim is to determine the HMM model $\Theta = (A, B, \pi)$ given a training sequence of observations $O = \{O_1, \dots O_T\}$. This means finding such Θ that $P(O|\Theta)$ is maximized.

3.5.3 Input-Output Hidden Markov Model

The last type of autonomous Markov model (model that is not controlled by the action of an "agent" and all information is available from the model at any state), and the main subject of this chapter, is the input-output Hidden Markov Model, Fig. 20(c). As it was mentioned, one of the assumptions of HMM is that each probability transition in the state transition matrix and probability of emission in the observation emission matrix is time-independent, meaning they do not change the structure as the system evolves in time. In practice, the time independence assumption is unrealistic for real-world processes. IOHMM is the extension of HMM to the domain of supervised learning for sequential data that allows the dependency on time to be incorporated into the model. Similarly to HMM, IOHMM is a doubly stochastic process in which the underlying dynamic process, state process, is hidden and thus cannot be observed directly. It is observed through another stochastic process, an observation process that produces the sequence of observations. Like in the case of MC and HMM, the Markov Property also holds for this model. Contrary to MC and HMM, the latent (hidden) variables[15] and output variables of the IOHMM are influenced by the input variable, often called the control signal, resulting in a non-homogeneous (time-dependent) Markov chain [201]. In consequence, the

[15] Latent variables are the hidden states of the model/system that cannot be observed directly.

dynamics of the system defined by the transition probability in IOHMM change with time according to the input signal, meaning state transition probabilities and emission probability by state differ depending on the input signal, as it is illustrated in Fig. 20. The difference between HMM and IOHMM is that while the HMM aims to define the distribution of output sequence, $P(y_1, \dots, y_T)$, the IOHMM aims to define the conditional distribution of the output sequence given the input sequence, $P(y_1, \dots, y_T | u_1, \dots, u_T)$. The main difference from the HMM is the capability of the IOHMM to learn an output sequence instead of just the distribution of the output sequence [202].

In summary, the IOHMM is used for supervised learning of time series data with exogenous inputs and defines the conditional distribution $P(y_1, \dots, y_T | u_1, \dots, u_T)$ of an output sequence $y_1^T = y_1, y_2, \dots, y_T$ given an input sequence $u_1^T = u_1, u_2, \dots, u_T$ and is defined as a tuple:

$$H = \langle S, \Omega, \mathrm{U}, \mathrm{A}, \mathrm{B}, \pi \rangle \tag{10}$$

Where:

S= $\{s_1, s_2, \dots, s_N\}$ is a set of N states

$\boldsymbol{\Omega}$ = $\{o_1, o_2, \dots, o_M\}$ is the observation sequence with M observables

U = $\{u_1, u_2, \dots, u_K\}$ is the input signal sequence with K input signals

A=$\{a_{ijk}\}$ is the transition probability matrix where a_{ijk} is the probability of transition from state i to j at time t, given input signal u_t=k, a_{ijk} =P(s_{t+1} = j|s_t = i, u_t=k) (conditional probability of ending in state j given the Markov process was in the previous step in state i and the input signal is k).

B=$\{b_{lj}(k)\}$ is the observation distribution probability, also called emission probabilities of an observation o_t = k being generated by state s_t=j given input u_t=l, $b_{li}(k)$=P(o_t=k|s_t = j, u_t=l) (conditional probability of observing symbol k given the Markov process is in state j and the input signal is l).

$\pi=\{\pi_i\}$ is the initial state distribution where π_i is the probability that the system starts in state s_i.

Matrices A and B are stochastic matrices, so they have to satisfy the following conditions:

$$\sum_{j=1}^{N} a_{kij} = 1, \forall \text{ for each } k = 1, \dots, M \text{ and } i = 1, \dots, N \quad (11)$$

$$\sum_{k=1}^{N} b_{lj}(k) = 1, \forall \text{ for each } l = 1, \dots, M \text{ and } j = 1, \dots, N \quad (12)$$

Note that index t is not required in the A and B matrices. The transition and emission probabilities vary with time as a function of an input signal. Meaning that A and B are defined for the input signal (different probabilities matrixes correspond to each input signal). The dependency on time is through the input signal occurring at time t.

IOHMM have previously been used in a variety of applications ranging from sequence processing in grammatical inference problems [26], synthesis of facial animation from audio [27], hand gesture recognition [28], modelling of financial returns series [29], modelling of forecasting of electricity prices [30] and fault diagnosis and prognosis of diesel generators [31].

3.5.4 Issues When Learning of HMM Parameters

There are two major problems when attempting to learn the HMM and IOHMM models. Prior to the model learning, both the number of hidden states (the size of the model) needs to be decided, and the transition, emission probabilities and initial state distribution need to be initialized. The wrong choice of initial parameters may lead to the risk of falling into a local optimum and a low convergence speed. An incorrectly chosen number of hidden states can lead to an inaccurate model when the number of states is too low and increases the complexity of the model, thus increasing computational time (affecting generalisation capability) when too many states are selected. There are three approaches often used that can help to overcome issues related to requirements of probabilities initialization prior to the learning of the model, namely:

1. The parameters can be initialized by using a sample of fully labelled data (The transition and emission probability can be calculated based on the fully labelled data and then used as initial parameters).
2. The Markov dependencies can be initially ignored, and estimation of the parameters can be performed by using the standard mixture model estimation method such as EM (estimation maximization algorithm) or K-means.
3. The parameters can be randomly initialized. Using multiple restarts of the model with different randomly initialized parameters, the parameters that give the best solution can be found and then applied in the modelling.

More information about those three approaches can be found in [203]. Another problem in IOHMM is choosing the right model size and the number of hidden states. The state-of-art approach to tackle this problem is multiple runs with a changing number of states.

3.5.5 Example of Input-Output Hidden Markov Model

For a better understanding of the Hidden Markov Model framework, the simple example of IOHMM will be described here. In our bodies, we have numerous different hormones that circulate in our bloodstream and regulate different body functions. Let's take as an example a hormone called leptin. Leptin is the hormone regulating our appetite. In this example, only the influence of the food on this hormone level will be considered for simplicity and the influence of the body fat and interaction with other hormones, such as oestrogen, on its level is excluded. Let's define two states that relate to the level of leptin in our blood, namely high leptin level and low leptin level. These comprise the finite state space of the example model.

S = {low leptin level, high leptin level}

Without taking a blood test, we cannot directly observe the leptin level in the blood; this information is hidden. We can imply what level of leptin is in our body by observing our feelings, namely if we feel the sensation of satiety (feel full) or if we feel hungry. These are our observations. We define a finite set of possible observations as follows.

Ω = {feel hungry, feel full}

We can influence the leptin level by simply eating the food, and this constitutes our input. We define a finite set of possible inputs, namely: had a meal and did not have a meal.

U = {had a meal, did not have a meal}

It should be noted that normally with a high level of leptin, we feel full and do not have an appetite for food, and when the leptin level drops, we feel hungry. In some people, the leptin resistance condition develops and then, as a result, this mechanism is disturbed. For this reason, in the analysed example, when one has a high leptin level in the blood, one still can feel hungry, even should feel full in such a case. Other elements required to define the IOHMM for this case are the state transition probability matrix A and the observation distribution probability B. In the IOHMM, both A and B depend on the input signal. As this example has defined two input signals, there will be two sets of probability matrices, and they will differ for each input signal, as it was shown in Fig.21.

As can be seen in Fig. 21, the probability of transition from state to state depends on the input signal, if we had or did not have the meal. In addition, the probability of observation generated by the state depends on the input signal.

The remaining element for the full IOHMM definition is the initial state distribution. For this example, the initial state distribution is defined as follows; there is a 0.56 probability that the system starts in the low leptin level state and 0.44 that it will start in the high leptin state.

$$\pi = \begin{pmatrix} 0.56 \\ 0.44 \end{pmatrix}$$

Note that the probabilities used in this example do not reflect real cases and are given here only for illustrating purposes.

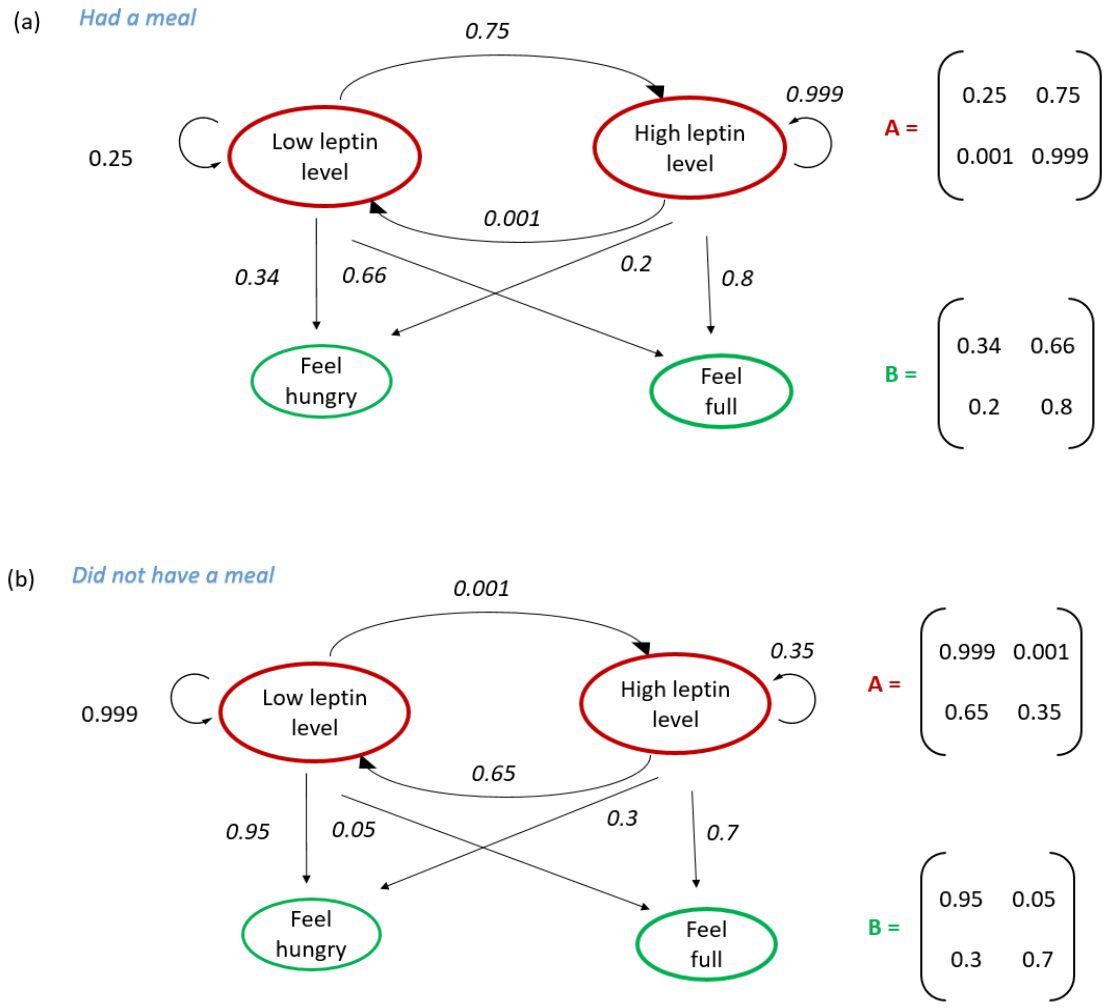

Figure 21 Graphical representation of elements defining the IOHMM for leptin level example showing state transition probability matrix A and the observation distribution probability B for the input: (a) had a meal and (b) did not have a meal.

CHAPTER 4

This chapter and two previous chapters constitute an extended version of a journal paper published in IEEE Access Journal in 2021 by Joanna Sobon and Bruce Stephen, titled: "Model-Free Non-Invasive Health Assessment for Battery Energy Storage Assets" [32].

4. Battery Maloperation Model Development and Validation

The growing portfolio of battery energy storage in today's power network entails the need for a robust method of measuring and/or predicting the health of this device, as it is vital for safe battery operation and the safe operation of the energy network comprising this device. Unfortunately, the models and methods of predicting battery health currently developed require, as was discussed in the preceding chapter, extensive telemetry to be installed, introduce an additional volume of data that has to be processed - this can constitute a limiting factor for the introduction of this device into the system. In this work, an alternative way of measuring the battery state of health was proposed that addresses those issues. This chapter covers in detail the development of the proposed maloperation model, followed by testing and validation of its operation. A case study of a community low voltage distribution feeder with photovoltaic (PV) generation was also covered in this section.

4.1 Model Development Procedure and Data Preparation for the Modelling Stage

The availability of battery operational data that are suitable for modelling is limited due to the fact that measuring the parameters of this device in long-term operation is costly and often difficult, for example:

- accurate measurement of the changes in the internal resistance of the battery during operation is often impossible without introducing additional disturbances to the battery's normal operation [100][204]
- production of full lifetime operational data takes a long time (some batteries like VRFB has cycle life as long as 12000 cycles [45]).

Moreover, this type of data is heavily operating regime and system dependent. The way the battery is operated has a key impact on battery property degradation. This work aimed to exclude system-dependent impact (e.g. charging regime dictated by application) on the performance deterioration of the battery so that the performance deterioration only due to misuse dictated by battery preferences could be caught by the developed model. The application of the knowledge of battery operating preferences dictated strictly by battery technology, reviewed in Chapter 2, in conjunction with re-used demand and generation data for generation of data required for model training and testing, namely maloperation/health indexes, helped to overcome the limitation of the availability of suitable data sets for battery health modelling.

All model development stages will be briefly introduced in this section, with an in-depth description covered of each stage in the following sections of this chapter. Only the generation of data required for model development is discussed here in more detail. The flow chart showing the procedure of modelling stages starting from data generation (data preparation stage), training of the model (model training stage) and ending with model testing (testing stage), including the flow of the information between stages, is shown in Fig. 22. In the first step of the data preparation stage, Fig. 22, the random battery charge/discharge schedule was generated based on the available renewable generation resources, with volatile characteristics (PV generation), and uncertain demand. At this point, the battery itself was not considered, meaning the technical constraints of the device were not included in schedule production, resulting in the battery schedule being unbounded from the technical limitations of this device and its function in the system (such as for example peak shaving), and only dictated by the availability of resources and

energy demand. Explaining further, the charge action was chosen when there was a surplus of renewable energy generated in the system in relation to the energy demand, so potentially, this energy could be accommodated in the battery when present in the system.

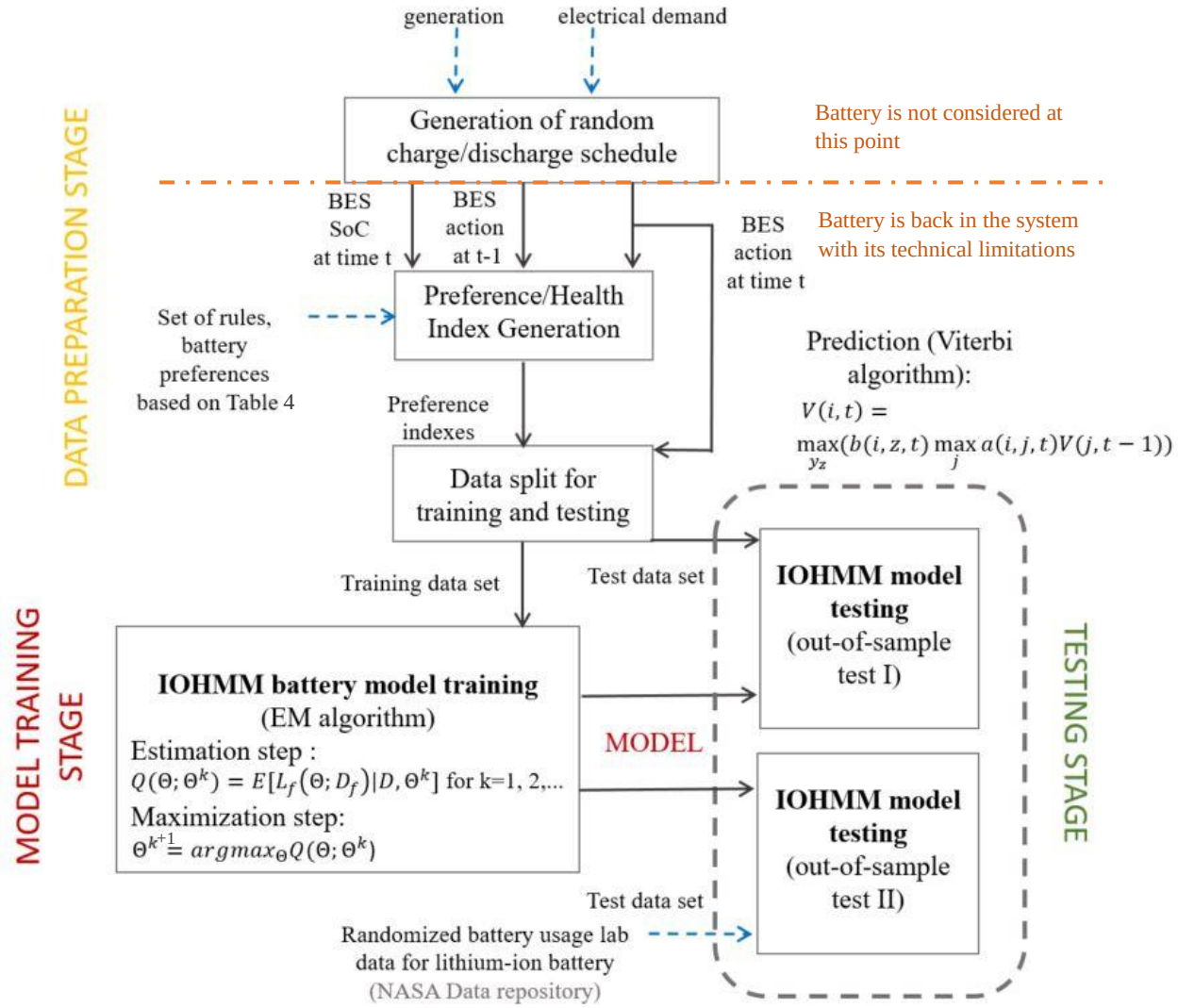

Figure 22 Flow chart of model development procedure with the flow of information in the system. The blue arrows indicate the external inputs required, black arrows indicate the internal flow of information and data. (For all battery types except lithium-ion battery in the test stage, only out-of-sample test I was performed due to unavailability of suitable test data).

The discharging action was chosen when there was deficit of renewable energy generated in relation to the energy demand. There was no limitation on how much energy the storage could accommodate and how much energy it could provide, as its presence in the system was not considered at this stage. Data used to generate data for modelling purposes has a 30-minute resolution and comprises data of electrical demand and photovoltaic generation measured at a community low voltage (LV) feeder (data come from the EU FP7 ORIGIN project). Available data covered the period from 3rd May to 5th July. Only 63 days of data were used in this work (49 for training and 14 for testing) to investigate if the low number of data for training and testing can result in a good-performing model characterised by generalisation ability when applying the proposed modelling approach combined with the Hidden Markov framework. More information about data for modelling and testing will be discussed further in Section 4.5. The example of three days of generation and demand data with the resulting charge schedule is shown in Fig. 23.

In the second step of the data preparation stage, the battery maloperation/health indexes due to the applied random charge/discharge schedule were generated. In this step, the battery was considered back in the system with its technical limitations. The maloperation indexes were produced by applying the random schedule generated in the first stage of data preparation to the battery energy storage in conjunction with the lookup tables, Tables 5 – 11, covering rules for battery dictated by battery operational preferences dependent on battery chemistry. The technical description of BES used in the considered case was discussed in Section 4.5. The battery included back in the system did not serve any particular functions, such as peak shaving, apart from accommodating the energy that was set to be stored or releasing the energy that was set to be removed from the storage according to the random charge prepared in the first stage of the data preparation. This step aimed to produce maloperation/health index data that caught the potential level of misuse (maloperation) of the battery energy storage when a random charged/discharged schedule was applied to the device characterised by its technical limitations.

As the system requirements and limitations were not applied when generating a schedule, the resulting maloperation indexes generated with battery in the system reflected only the misuse level due to violation of preference battery dictated by device chemistry.

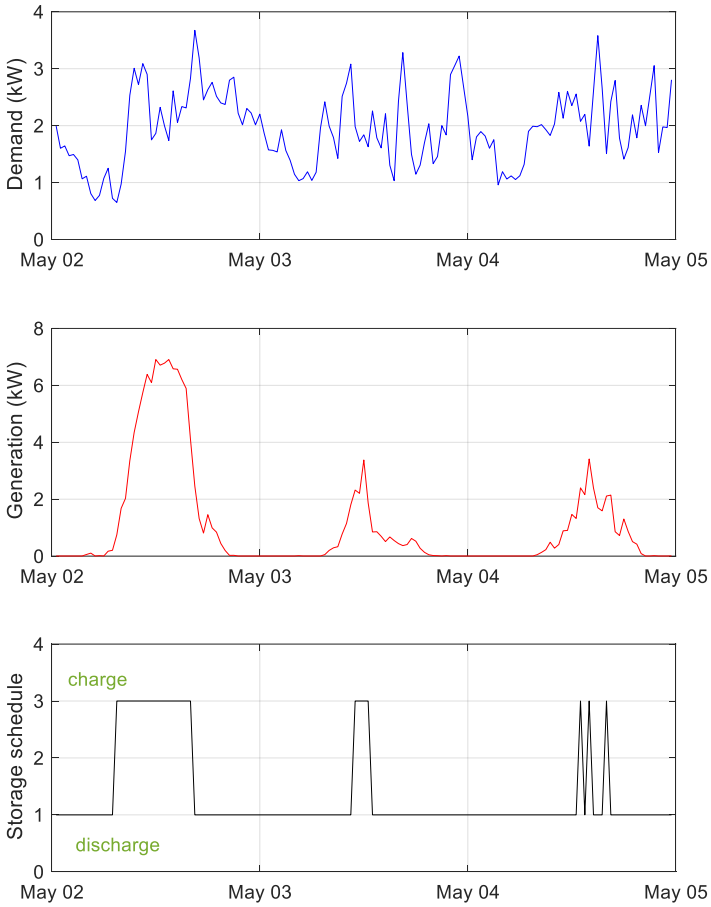

Figure 23 Three days of time series of demand, PV generation with the resulting discrete schedule for the BES based on the forecast of demand and generation under criteria of maximization of self-supply (storing excess generated energy and using it to meet demand).

After data was generated, it was split into training and testing sets. As was mentioned previously in this section, only 49 days were used to train the model, and then the model was tested on the remaining 14 days. The number of data applied in this work was chosen purposefully low to test one of the thesis questions, namely if the battery health model trained on the limited number of data, using the proposed in this work modelling approach,

can be characterised by the ability to generalise. In Section 4.2, the model features, structure and how it was defined was described in detail.

The next stage in the model development (model training stage in Fig. 22) includes the learning of the IOHMM model based on the generated training data using an algorithm similar to the Baum-Welch applied for the learning of HMM parameters [205], discussed in detail in Section 4.3. After model training, in the testing stage (grey dashed rectangle in Fig. 22), the Viterbi algorithm for IOHMM was implemented for the purpose of predicting the maloperation indexes due to the applied schedule of the BES, discussed in detail in Section 4.4. The model selection is discussed in Section 4.6. To evaluate the performance of the developed model, out-of-sample validation was performed using the testing dataset, discussed in Section 4.7. For all battery types except lithium-ion battery in the test stage (Fig. 22, grey dashed rectangle), only out-of-sample test one was performed (using test data generated in the data preparation stage) due to the unavailability of suitable laboratory battery data. For lithium-ion battery, the second validation of the proposed battery model as a proxy for actual battery degradation measure was performed on the publicly available lab battery test data accessible from the NASA Prognostics Centre of Excellence Data repository [206]. This is covered in Section 4.8.

4.2 IOHMM Specialization to Battery Operating State

The model framework proposed in this work consists of the set of actions that comprise the input signal to the model, observables that are emitted by the unobservable states and hidden states that encapsulate the time-dependent chemical processes taking part inside the battery during operation. Among the input signal to the model (u), there are three possibilities, namely: 'perform charge action', 'perform discharge action' and 'hold action'. The model observables (o) are the battery preference/maloperation indexes emitted by the unobservable chemical internal states of the battery due to the performed action. These observed indexes could be either positive, negative or zero. The positive index indicates that the performed action had a positive influence on battery health. The negative index indicates that performed action was against battery preferences dictated by

its chemistry, leading to potential battery performance deterioration. The last preference index, zero index, indicates that the battery is neither positively nor negatively affected by performed action, meaning there was no benefit to battery health due to performed action but also this action did not degrade the device either. Dependencies between the states and transitions between states resulting from a particular action are modelled as the IOHMM with the information flow in the developed model shown in Fig. 24.

The introduction of a latent variable in the model implicitly captures phenomena such as:

- micro-cycling,
- preferences of battery to be fully discharged before consecutive charging,
- preferences of battery to be fully charged before discharging again,

and others.

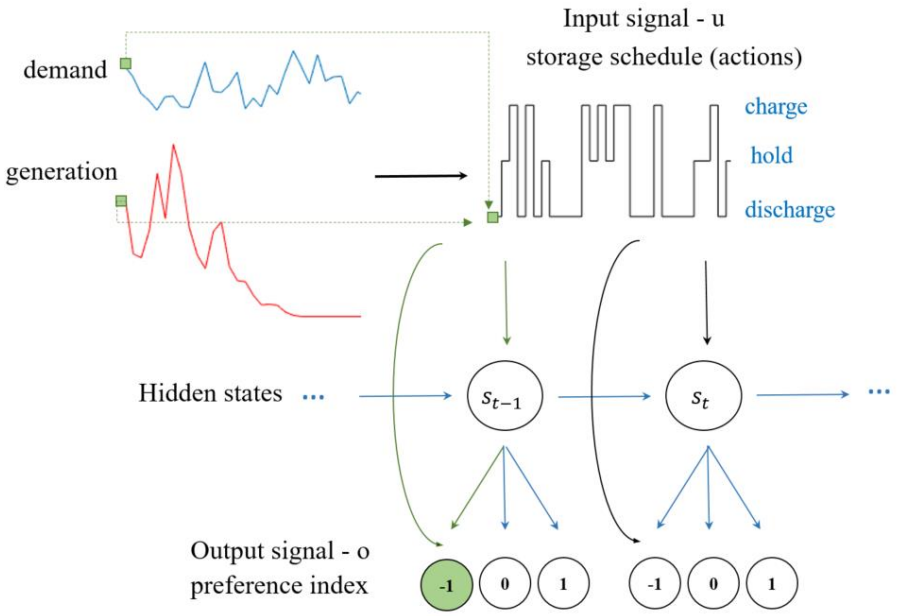

Figure 24 Diagram of IOHMM indicating the information flow in the developed model.

Training data *D*, which preparation was described in Section 4.1, was then used to find optimal parameters of the IOHMM. *D* was the set of *R* pairs of input/output sequences, where the input described the action that was scheduled to perform by BES, and the output

of the model was the resulting preference/maloperation index describing the battery preference to the performed action dictated by cell chemistry:

$$D \stackrel{\text{def}}{=} \{(u_1^{T_r}(r), o_1^{T_r}(r)); r = 1 \dots R\} \quad (13)$$

Where:

R - is the number of output/input pairs (2352 in this work)

$u_1^{T_r}$ - is the input sequence

$o_1^{T_r}$ - is the output sequence

T_r – is the length of the rth input/output sequence

The training data D were generated based on the set of rules formulated in Section 2.3 (Table 5 - 11) and on the available resources in the system comprising renewable generation. The preparation of the training data is summarized in Fig. 22.

4.3 Learning the Model Parameters

As was stated in Section 3.5.2, three problems can be solved using HMM, namely evaluation, decoding and learning of time series data. The same applies to the IOHMM, the extension of HMM to the domain of supervised learning for sequential data. In this section, the learning of the parameters will be discussed in more detail. As it was discussed in Section 3.5.4, there are two issues when learning model parameters that need to be considered. The first problem is related to the choice of model parameters (initial parameters for transition, emission probability matrices and initial state distribution) and the second one with the choice of the model size (number of hidden states). To tackle the first problem, the usual practice of replications with random restarts was chosen in this work. Fifty restarts with randomly initialised initial parameters were performed. This procedure aimed to find the parameters that resulted in the best performance of the model after learning, where model log-likelihood and Sum Squared Errors (SSE) were applied as the selection criterion. To tackle the issue with the choice of the number of hidden states

(right model size), the state-of-art approach of multiple runs with a changing number of states was applied in this work. A set of IOHMM with states in the range of 2-50 were trained, and the selection of the most optimal number of states was based on the Bayesian Information Criterion (BIC). The BIC is a penalised measure of the model likelihood. Here we try to find the most likely fit with the least number of parameters, where model parameters are regarded as equivalent to model complexity.

Determining the IOHMM means finding optimum IOHMM parameters Θ that best reflect the observed data. In other words, training of IOHMM (learning problem) is estimating the optimal parameters $\Theta = (A, B, \pi)$ that maximizes the conditional likelihood $P(o^T|u^T, \Theta)$; probability of observing output sequence O = (o_1, o_2 ,…, o_T) given the input sequence U = (u_1, u_2,…, u_T) and model parameters Θ. The optimal parameters of the IOHMM model, which are transition and observation probability matrices, were learned using the formulation of the Expectation-Maximization (EM) algorithm proposed in [26][207] for training IOHMM. The EM algorithm applied in this work is similar to the Baum-Welch algorithm used to train the HMM [205]. EM is a general technique that is used in the estimation of the distribution with hidden data. The aim of EM here is to maximize the log-likelihood function (14).

$$l(\Theta; D) = log(L(\Theta; D)) \tag{14}$$

Where Θ are the model parameters, T_r is the length of the r^{th} input/output sequence, D are training data and $L(\Theta; D)$ is likelihood function, defined as:

$$L(\Theta; D) \stackrel{\text{def}}{=} \prod_{r=1}^{R} P\left(o_1^{T_r}(r) \middle| (u_1^{T_r}(r); \Theta)\right) \tag{15}$$

As the state variables s_t (describing the path in the state space) are not observed, (15) is treated as parameter estimation with missing data. Let D_f be the complete data set defined as (16)

$$D_f \stackrel{\text{def}}{=} \left\{\left(u_1^{T_r}(r), o_1^{T_r}(r), s_1^{T_r}(r)\right); r = 1 \dots R\right\} \tag{16}$$

and corresponding complete-data likelihood is

$$L_f(\Theta; D_f) = \prod_{r=1}^{R} P\left(o_1^{T_r}(r), s_1^{T_r}(r) \middle| (u_1^{T_r}(r); \Theta)\right) \quad (17)$$

Due to the unobservable character of state variables S, the $L_f(\Theta; D_f)$ cannot be maximized directly. The solution requires the introduction of the auxiliary function

$$Q(\Theta; \widehat{\Theta}) = E[l_f(\Theta; D_f)|D, \widehat{\Theta}] \quad (18)$$

and iterating it over the distribution of S in two steps (estimation and maximization) until a local maximum of the likelihood is found. Where $Q(\Theta; \widehat{\Theta})$ is the expected value of complete data log-likelihood given model parameters computed at the end of the previous iteration $\widehat{\Theta}$ and observed data *D*.

The EM algorithm iterates in two following steps for k=1,2,.. until the point when the maximum likelihood is found.

1st step – Estimation, comprises computation of $Q(\Theta; \Theta^k) = E[l_f(\Theta; D_f)|D, \Theta^k]$,

2nd step – Maximization, comprises parameters updates as $\Theta^{k+1} = argmax_{\Theta} Q(\Theta; \Theta^k)$.

4.4 Decoding Problem Implementation

For a given cell chemistry, the trained model can be used to predict an observation sequence of preference/maloperation indices (health index) given an input sequence of charge actions *u*. The direct computation of the output sequence, which is more likely given the input signal, is computationally expensive as the computation time grows exponentially with the sequence length [208]. For this reason, the approach using the complete data model was applied in this work, as in the Viterbi algorithm, to calculate the joint values of the states and outputs that are the most likely. The algorithm (19) for asynchronous IOHMM proposed by [208] was used.

$$V(i,t) = \max_{n}(b(i,n,t) \max_{j} a(i,j,t)V(j,t-1)) \quad (19)$$

Where:

$V(i,t)$ is the probability of the best state and output subsequence ending up in state i at time t,

$a(i,j,t) = P(s_{t=1} = i|s_{t-1} = j, u_t)$ - is the probability of transition from state j to state i at time t and given input u_t

$b(i,n,t) = P(o_n|s_t = i, u_t)$ - is the probability of observation o_n being generated by state s_t= i at time t, given input u_t. (n is the length of the output sequence o_1^n)

4.5 Case Study: Community Low Voltage Distribution Feeder with Photovoltaic Generation

The developed model was trained and tested on 63 consecutive days of historical data of electrical demand and photovoltaic generation measured at a community low voltage (LV) feeder (data come from the EU FP7 ORIGIN project). The available data has a 30-minute resolution and covers the period from the 3rd of May to the 5th of July 2015. Only 63 days of data were used in this work (49 for training and 14 for testing) to show that the applied battery health modelling framework proposed in this work is able to deal with the low number of data for training, thus addressing the limited availability of suitable battery data for battery health modelling. As an illustration of data used in this study case, a sample of seven consecutive days of demand and PV generation is shown in Fig. 25. Demand data (Fig. 25(a)) has a noisy and volatile character due to the low level of load aggregation typical at the LV level. This exhibits a peak value of 6.9 kW within a considered period of 63 days. The generation data available (Fig. 25(b)) has an intermittent nature across its daily pattern, consistent with small PV installations. These characteristics of demand and generation data make the forecasting task challenging. To capture and demonstrate the identification of maloperation level, a BES of 10 kWh was assumed with a naïve persistence generation forecast and a day ahead Gradient Boost Machine forecast for the demand [209][210]. The naïve persistence forecasting of the PV generation assumes that the energy generated today at a given time *t* is the same as it was on a preceding day at the corresponding time. Gradient Boost Machines (GBM) is an ensemble method which has applications in regression and classification problems [211].

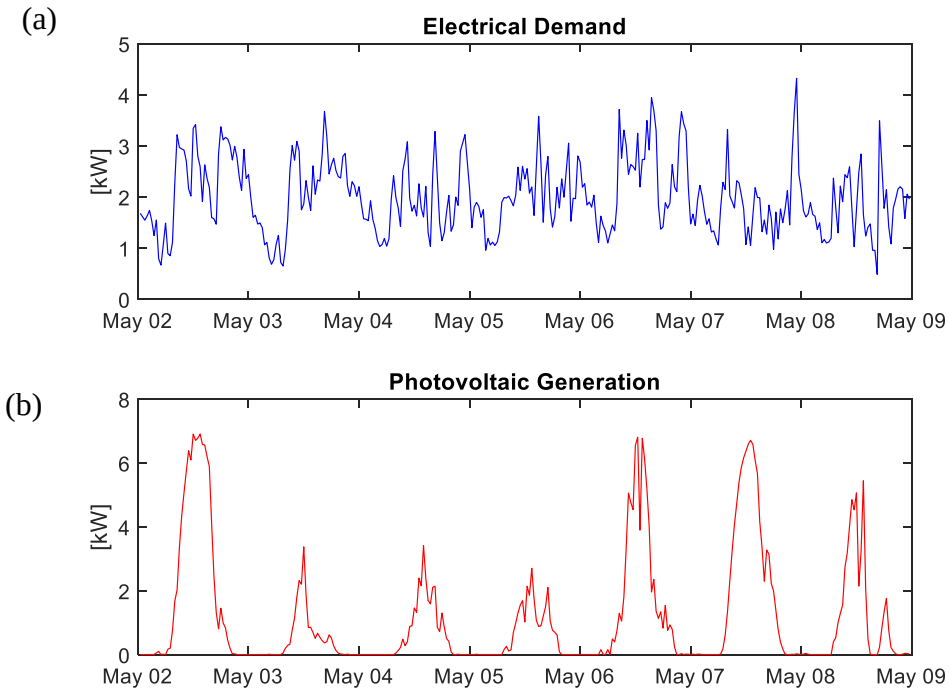

Figure 25 Seven consecutive days of electrical demand at LV level and PV generation data starting from the 2nd of May until the 9th of May.

GBM gives the model that is in the form of an ensemble of multiple 'weak' models. The 'weak' models are learned and added in stages to produce a strong model. The 'weak' learners are fitted into the residuals of the model developed in the previous step to improve the resulting model. The loss function used during training was a mean square error, and the shortcomings in the accuracy of the simple model used in this work were identified based on the gradient descent learning procedure[16] [210]. More information about gradient descent learning can be found in [203]. The scenario described above has been designed to capture frequent opportunities for maloperation due to the excess of generation with respect to demand.

[16] In simple terms gradient decent is an optimization algorithm that is used to find the parameters of the function that minimizes a cost function in the case when parameters cannot be calculated analytically by for example using the linear algebra, and they must be searched with application of the optimization algorithm.

4.6 Model Selection

The Bayesian Information Criterion (BIC) approach was used to select the optimal number of hidden states for the IOHMM-based battery model. The BIC was developed by Gideon E. Schwarz in 1978 [212], and it constitutes a penalised measure of the model likelihood that allows a tradeoff between the model likelihood and its computational complexity [213]. The BIC can be evaluated using equation (20) [203].

$$BIC = -\log\left(L_f\left(\Theta; D_f\right)\right) + \frac{k}{2} * \log(T) \tag{20}$$

Where: L_f denotes a model likelihood (17), k is the degree of freedom or number of parameters in the model, and the length of the training data is T. The first term of the equation (20) is a measure of a fit of the model, and it decreases with the number of parameters (number of states in this model). The second term is a "penalty term" that penalizes the model for the increasing number of parameters. This term depends on the sample size and is an increasing function of the number of estimated parameters (it rises with the increasing number of parameters). The second term in equation (20) discourages overfitting by penalizing model complexity. In short, the BIC is the form of penalized log-likelihood that allows a tradeoff between the model likelihood and its computational complexity [213]. When fitting IOHMMs, the increase in the number of states, leads to an increase in model likelihood, the goodness of fit, but also increases the chance of model overfitting when too many parameters are used (limiting the model's ability to generalize) [214]. The Bayesian Information Criterion is minimized to decide the optimal number of hidden states for the IOHMM-based battery models.

Some further explanation of the terms in the BIC equation (20) is required for a full understanding of the application of this criterion in the selection of an optimal number of hidden states in the IOHMM. As the complexity of the model or degree of freedom, k, in BIC is model specific, its choice depends strictly on the model that is investigated, IOHMM in this work, to ensure the appropriate application of the penalty term in BIC. The degree of freedom for HMM has been used previously [214][215] as follows:

$$k = (N-1)N + Nm \tag{21}$$

Where k is called the degree of freedom or complexity term, N and m are free parameters of the model. *N* represents the number of hidden states of the HMM model, and *m* is the number that represents the number of parameters of the underlying distribution of the observation process. This expression was modified for the purpose of this work by incorporating an additional dimension to the IOHMM over the HMM, namely the input signal. Both terms of equation (21) were multiplied by a number of possible input signals in the modelled system (three possible actions), resulting in equation (22).

$$k = 3(N-1)N + 3Nm \tag{22}$$

The limitation of the BIC is that this approximation is only valid when the sample size is larger than the number of parameters in the model [216].

The change in BIC values with an increasing number of hidden states is shown in Fig. 26 for the lead-acid battery, Fig. 27 for lithium-ion (a) and NaS (b) batteries, Fig. 28 for NiMH (a) and NiCd (b) batteries and Fig. 29 for Zn/Br_2 (a) and VRFB (b) batteries.

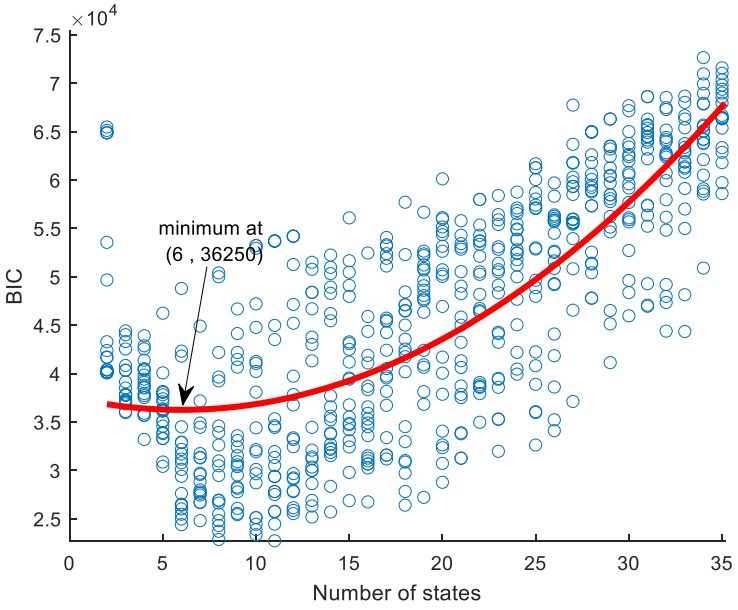

Figure 26 Change in BIC with increasing model complexity for the IOHMM model of the lead-acid battery.

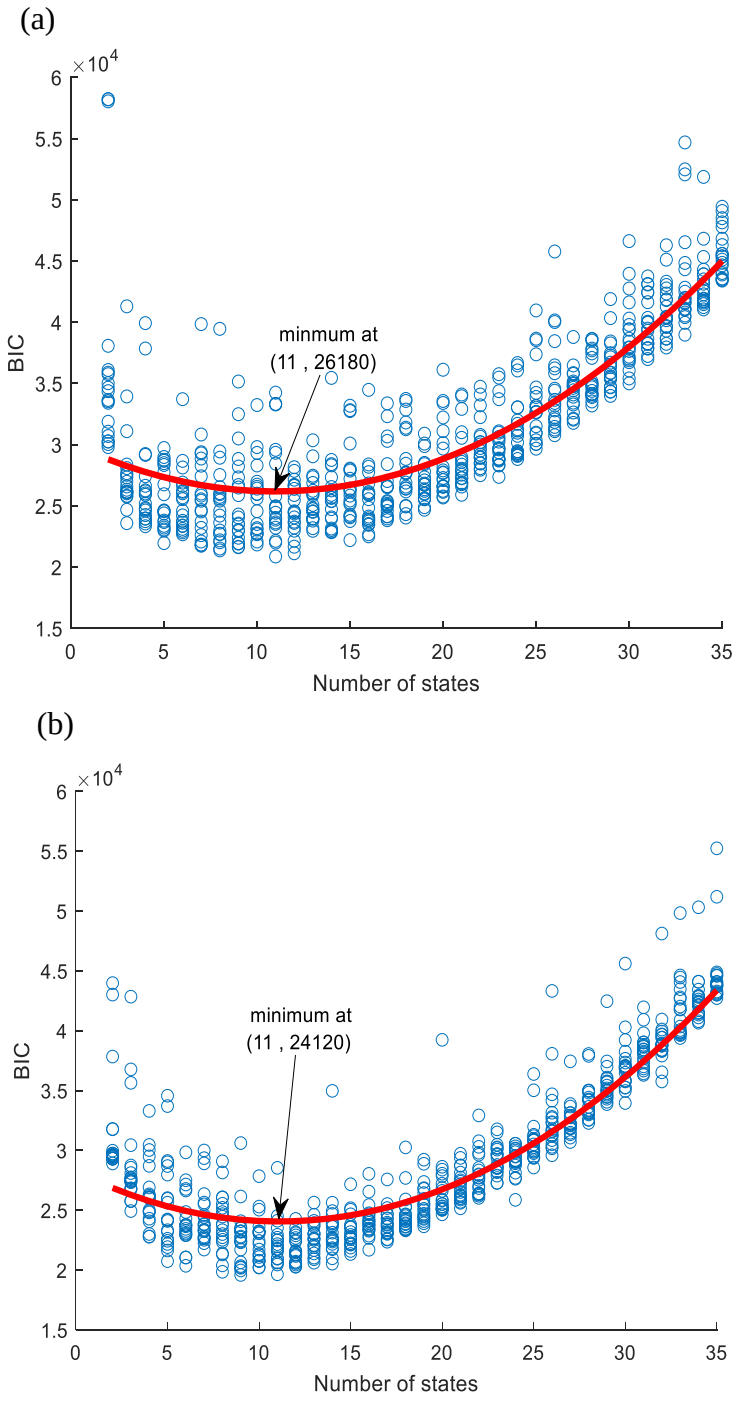

Figure 27 Change in BIC with increasing model complexity for the IOHMM model of lithium-ion battery (a) and the IOHMM model of NaS battery (b).

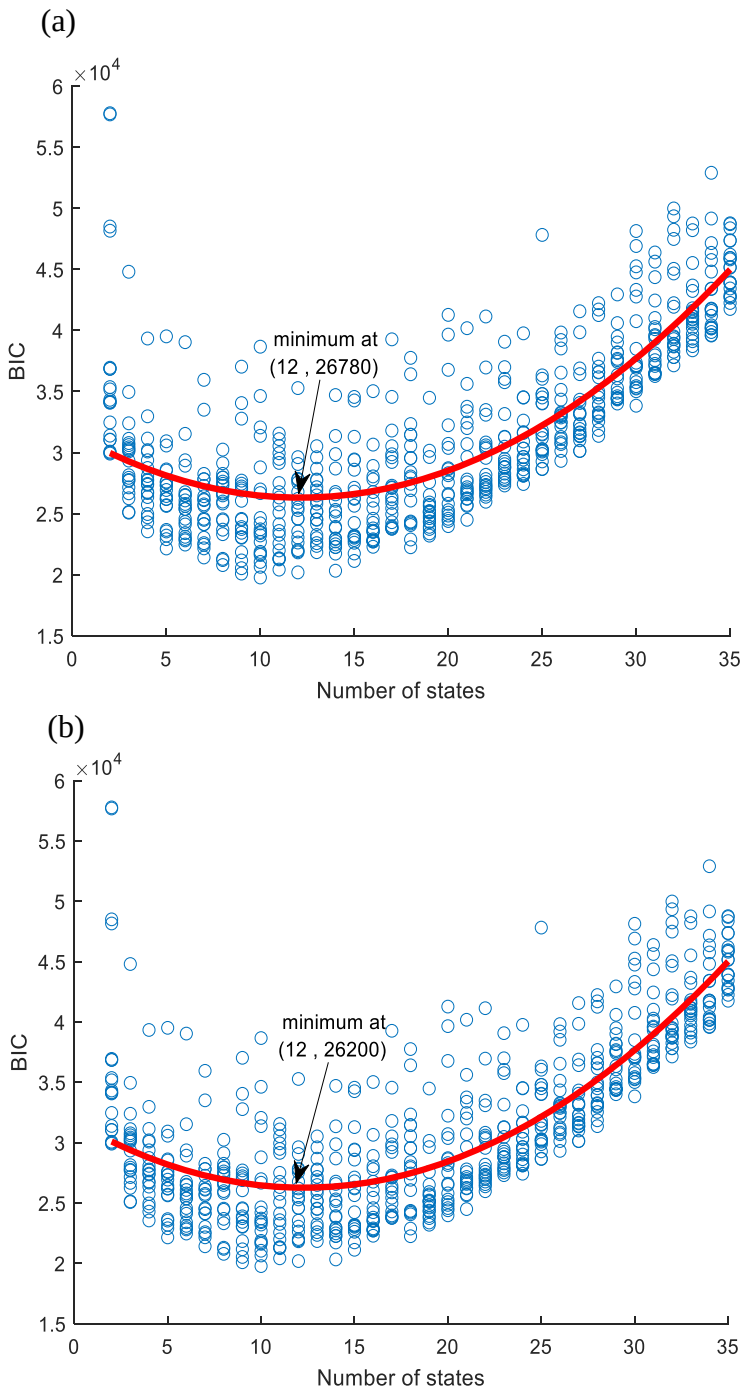

Figure 28 Change in BIC with increasing model complexity for the IOHMM model of NiMH battery (a) and the IOHMM model of NiCd battery (b).

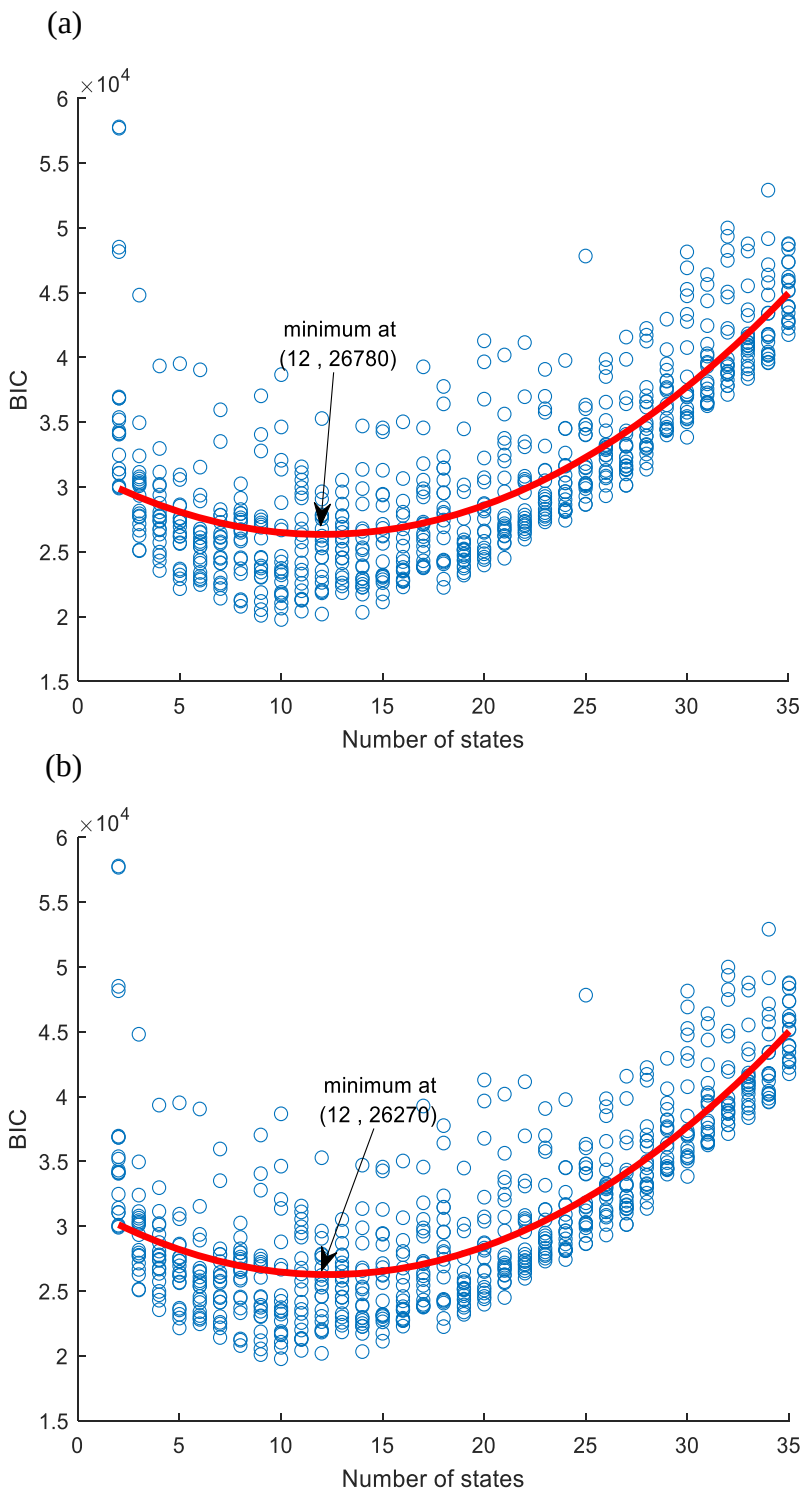

Figure 29 Change in BIC values with increasing model complexity for the IOHMM model of Zn/Br_2 battery (a) and the IOHMM model of VRFB battery (b).

The minimum values of BIC in Fig. 26-29 indicate the fewest number of states for the IOHMM battery model that was chosen as optimal for given battery technology. The choice of the number of states was based on the fitted average curve. Applying BIC different battery chemistries resulted in different optimal numbers of states: 11 states for Lithium-ion and NaS batteries, 12 states for NiMH, NiCd, Zn/Br_2 and VRFB batteries, and 6 states for Lead-acid battery.

4.7 Testing and Validation of Developed Model.

The trained models of battery maloperation consist of a hidden state transition probability matrix, observation distribution probability and initial state distribution. The developed models for seven battery technologies considered in this work are included in Appendix A. The chemical processes taking place inside the battery during operation and associated degradation processes are encapsulated in the state probability matrix. As the battery's internal state is not observable directly, it cannot be stated, if any, or by how much the battery was degraded based on the state transition probabilities. Instead, it is captured in the observation distribution probability. The probabilities in state transition matrices differ for different battery types due to the differences in the battery chemistries and their preferences that models captured, as can be seen in Appendix A. However, there is no way of relating this difference to the particular preference for the battery technology or battery health state due to the hidden nature of the states. Similarly, when examining observation distribution probabilities for different battery types, it is difficult to say which preference of battery results in the emitted preference index by a particular state due to its unobservable character.

In the IOHMM, the input variable can influence either the distribution of the latent variable, output variable or both. It was found that in the trained models, the input signal (the action that was set to be performed by the energy storage) always had an impact on the emission of the battery maloperation/health index by the state, irrespective of the battery type, but has little or no impact on the distribution of the latent variable. The

transition probabilities distributions, in graphical form, for three battery models, NaS, NiMH and Lithium-ion, for which the influence of input signal on transitions probabilities was not observed, are illustrated in Fig. 30.

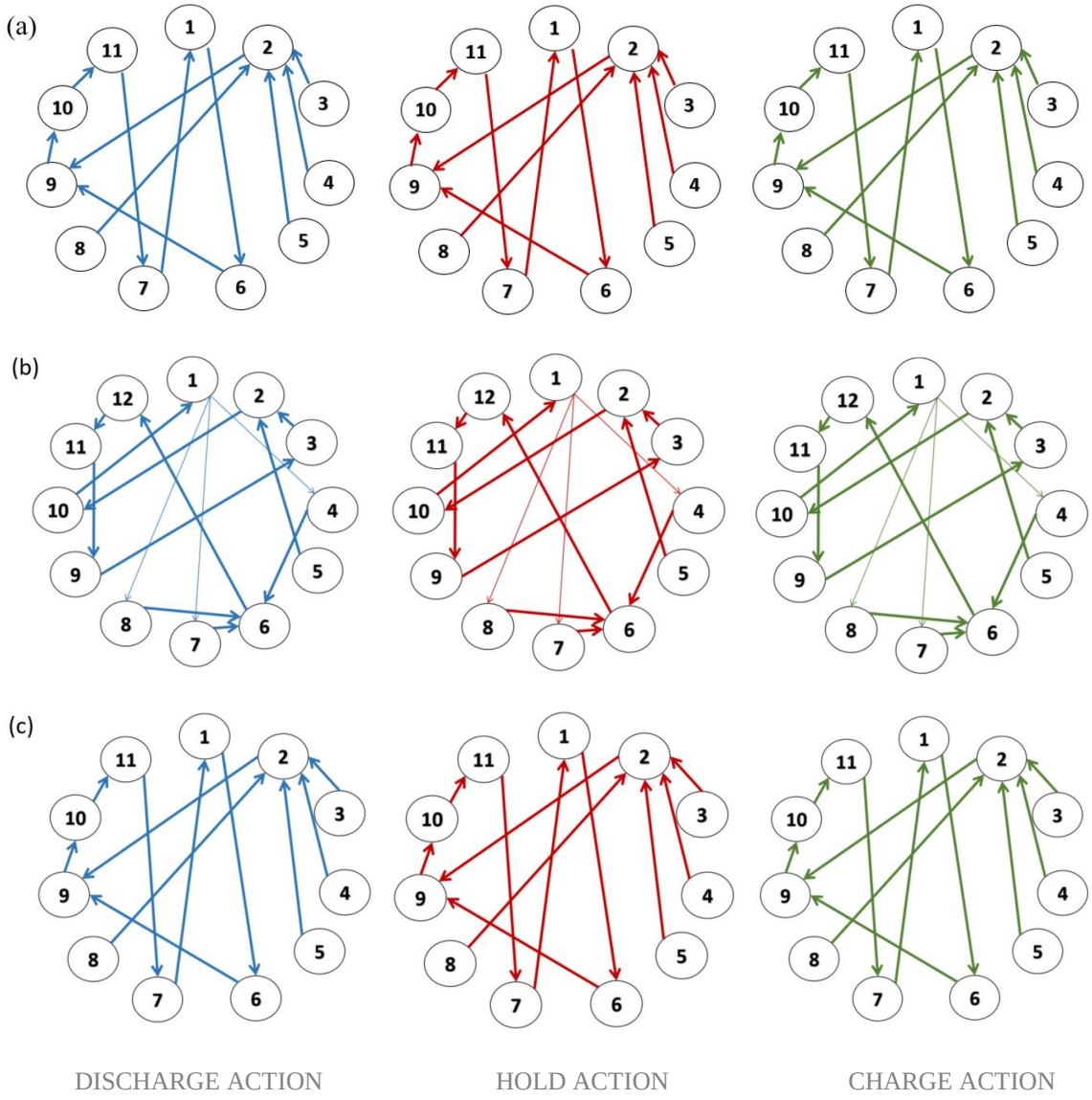

Figure 30 The comparison of the state transition probability distribution for input signal 'discharge action' (blue), 'hold action' (red) or 'charge action' (green) for the batteries for which the state transition was found to be independent of the input signal: Lithium-ion (a), NiMH (b) and NaS (c). The thickness of the arrows indicates an increased probability of transition between the states.

The transition probabilities distributions for the Lead-acid, Zn/Br_2, VRFB and NiCd battery models, where this dependency was observed, are illustrated in Fig. 31. Taking, for example, the Zn/Br_2 battery model, Fig. 31 (b), when the battery is in state eight for the input signal three ('charge action') the probability of transition to state ten is 0.98 and to state six is 0.02. For the input signal one ('discharge action') and two ('hold action'), the only allowed transition from state eight is to state six with a probability of 1. The difference or similarities in the impact of the input signal on the distribution of the latent variables may be dictated by the chemical differences or similarities between batteries. Further research is required to find the battery characteristics governing those differences or similarities, which are not in the scope of this work but constitute a potential collaboration platform with the experts in the battery chemistry area in the future.

For all developed battery models, the emission probability from the state depended on the input signal (action set to be performed) and this dependency is reflected in the emission probability matrix. The probabilities in the emission probability matrix are different for different input signals, which can be seen when examining the models' parameters summarised in Appendix A1-A7. As it was stated above, due to the hidden nature of the states, when examining observation distribution probabilities for different battery types, it is difficult to say which preference of battery results in the emitted preference index by a particular state. The dependency of the input signal on the emission probabilities is illustrated in Fig. 32 in the example of the Lead-acid battery model. From that figure, we can see differences between emissions from states depending on the input signal. We can see a significant difference between the emitted health index by the state when comparing the possible emission from states when 'discharge action' (blue in Fig. 32) or 'charge action' (green in Fig. 32) was set to be performed by battery energy storage. For example, when the battery was in state six and 'discharge action' was set to be performed by this device, the state can emit '-1' index with a probability of 0.001 and '1' with the probability of 0.999, but if 'charge action' was as the input signal, only possible emission by this state was -1 with the probability of 1.

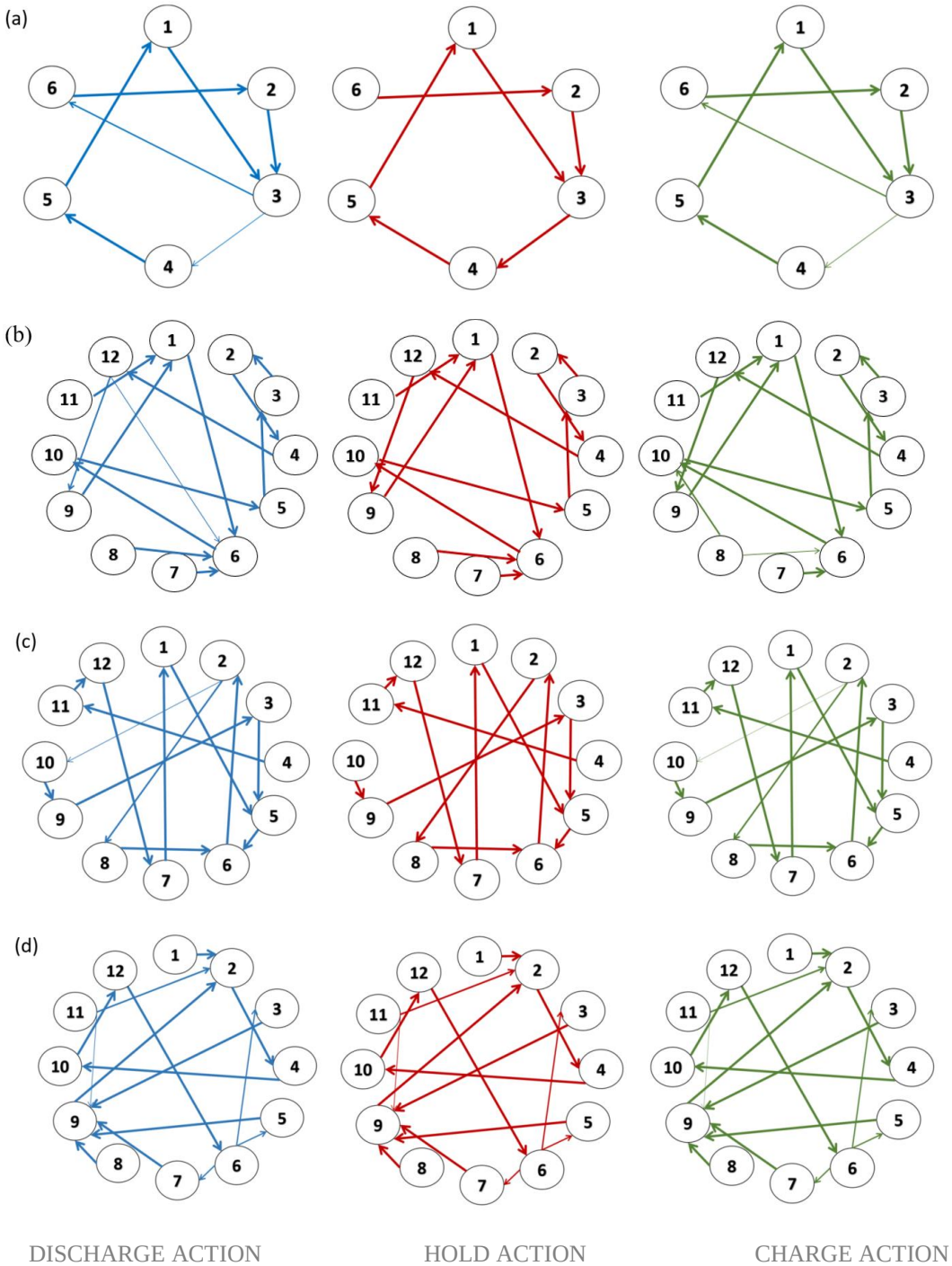

Figure 31 The comparison of the state transition probability distribution for input signal 'discharge action' (blue), 'hold action' (red) or 'charge action' (green) for the batteries with the observed dependency of the input signal on the state transition: Lead Acid (a), Zn/Br_2 (b), NiCd (c) and VRFB (d). The thickness of arrows indicates an increased probability of transition between the states.

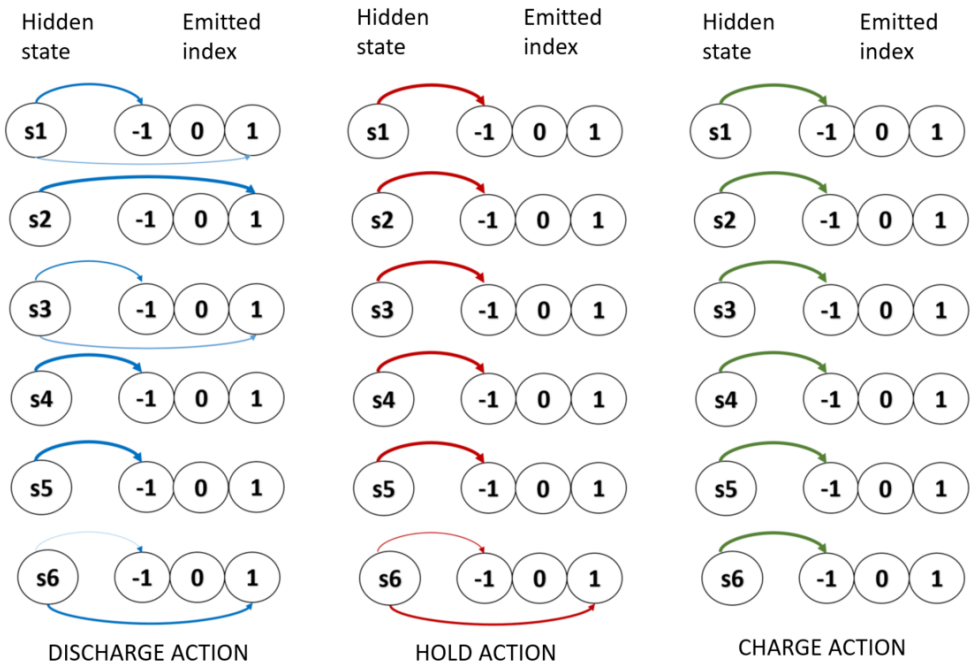

Figure 32 Graphical representation of the maloperation index emission by the hidden state of the IOHMM Lead-acid battery model. The arrows point to the possible emission by state, given the system is at this state and the input signal 'discharge action' (blue), 'hold action' (red) or 'charge action' (green). The thickness of the arrow is proportional to the probability of state emission of the health index the arrow is pointing at, where the thickest arrow is an equal one. ('-1' indicates that the battery operates contrary to its preferences dictated by device chemistry, '+1' indicates that performed action is in agreement with battery chemistry and '0' there is no positive or negative influence on battery health due to performed action).

The results indicating the significant impact of the input signal on the emission probabilities are in agreement with the knowledge of the influencing factors on battery well-being. The battery health is closely influenced by the action that is performed by the storage with a particular state of health and the preceding action that storage was subject to, and this is reflected in the emission dependency on input that was found in each model of battery developed in this work. As was said previously, there is not possible for sure to describe what each state represents and how the emission indexes are correlated with battery preferences learned by the developed model due to the unobservable character of model states (the information about states is hidden). With some assumptions and with general knowledge about battery chemistry and operational preferences reviewed in

Chapter 2, we can imply to some extent that, for example, state two for Lead-acid battery (S2), see Figure 32, might correspond to a fully charged and not perfectly healthy state of this device. When discharging action is performed, the positive health index is generated, and when charging action is performed, the negative index is generated. This is linked with the battery preference 'to not being overcharged' (when it is charged, negative index is generated) or 'not being left idle' ('no action' performed) (when the battery is discharged, positive index is generated). The negative maloperation index generated at state 2 when 'no action' is performed is linked to the battery preference being prone to build up of sulphate crystal due to self-discharge processes leading to performance deterioration or even device failure when the health of the battery was compromised. However, it should be remembered that the battery states assignment and links with preferences described here cannot be taken for granted. Transition probabilities matrices, emission probability matrices and the initial state probability for all IOHMM developed are included in Appendix A.

The operational purpose of the developed battery models in this work is to predict the most likely output sequence (health/maloperation index) given the input signal (scheduled action for the BES). The prediction is based on the Viterbi approach that was discussed in Section 4.4. The choice of trained model was based on the model log-likelihood and the value of the Sum of Squared Errors calculated on the cumulative preference/maloperation index[17] predicted by the trained model and the actual values of this index using equation (23)

$$SSE = \sum_{i=1}^{n} \left(y_i - f(x_i)\right)^2 \tag{23}$$

Where:

SSE is the sum of squared error,

[17] Cumulative health index was calculated by successive additions of generated health indexes by the IOHMM model during simulation.

y_i is the actual value of the variable to be predicted,

$f(x_i)$ is predicted value

To clarify at this point how the 'original' and 'generated' health indexes were produced, a visual summary of the procedure is shown in Fig. 33. For more details on how the series of health indexes were generated in the first place, please refer to Section 4.1 where it was discussed in more detail and summarized in Fig. 22.

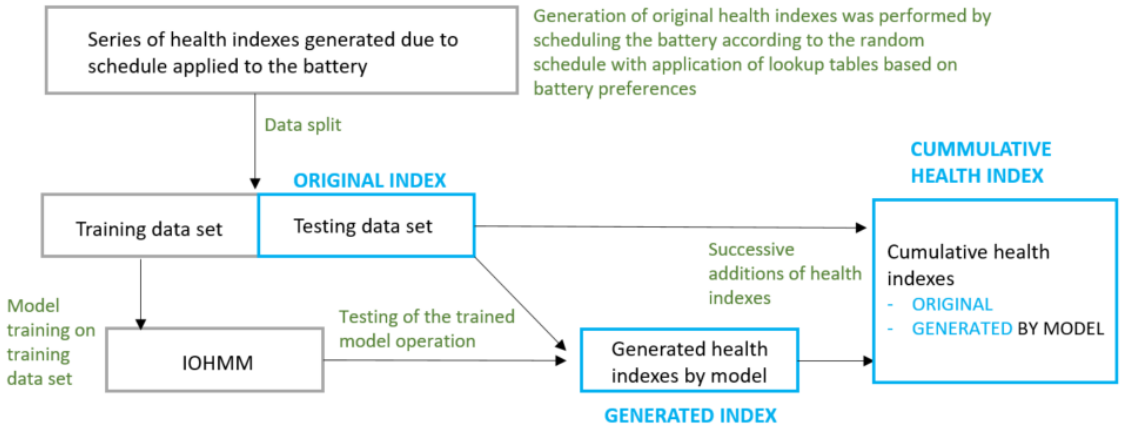

Figure 33 Flow chart of generation of the 'original' and 'generated' cumulative health indexes.

The comparison of the original cumulative preference index with the cumulative index generated by developed battery models is shown in Fig. 34 (Lithium-ion battery), Fig. 35 (NaS, NiCd and NiMH batteries), Fig. 36 (Lead-acid, Zn/Br_2 and VRFB batteries) and are summarized in Table 13.

The actual cumulative health index, the blue line in Fig 34 - 36, is characterized by diurnal patterns observed in the photovoltaic generation data as well as monotonic decrease. The higher peak on the graph corresponds to the time when the generation drops below the load requirements, and the lower one is when the generation starts to exceed demand. In the case study being analysed, energy demand is much lower than the available generation.

Table 13 Cumulative health index out of sample prediction.

Type	NiCd	NiMH	Li-Ion	NaS	VRFB	Zn/Br_2	Lead Acid
States	12	12	11	11	12	12	6
SSE [10^3]	49	51	77	99	98	46	109
Final index	-234	-234	-234	-234	-132	-234	-234
Predict index	-242	-244	-248	-250	-110	-240	-230
Over/underestimation [%]	-3.42	-4.27	-5.99	-6.84	16.66	-2.56	1.71

The battery is to be charged according to available resources without consideration of technical constraints or its limited capacity. For this reason, when energy is generated in excess, the battery becomes stressed due to extensive charging, resulting in a maloperation/health index decrease. When there is no excess of energy in the system, the stress on the battery due to overcharging drops; therefore, the value of the HI increases. For this worst-case scenario, the forecasted generation dominates the battery health impact in this case study.

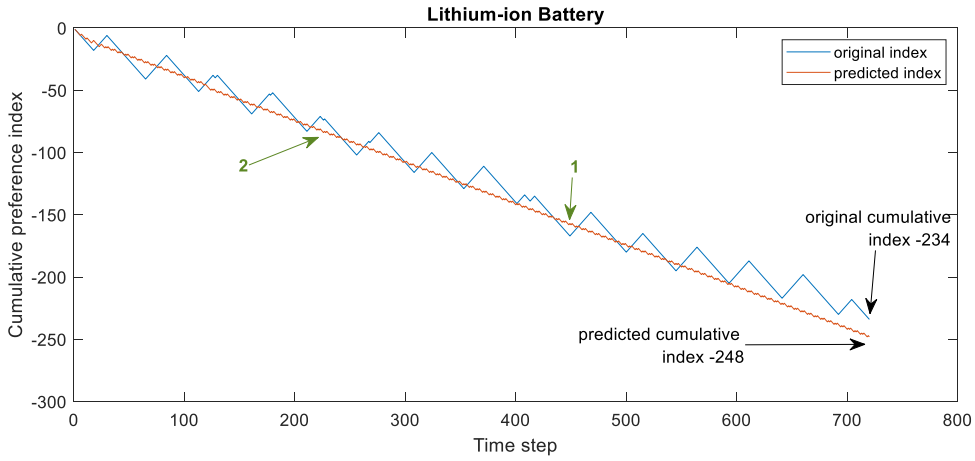

Figure 34 Comparison of the original cumulative preference index and index predicted by the developed model of Lithium-ion battery.

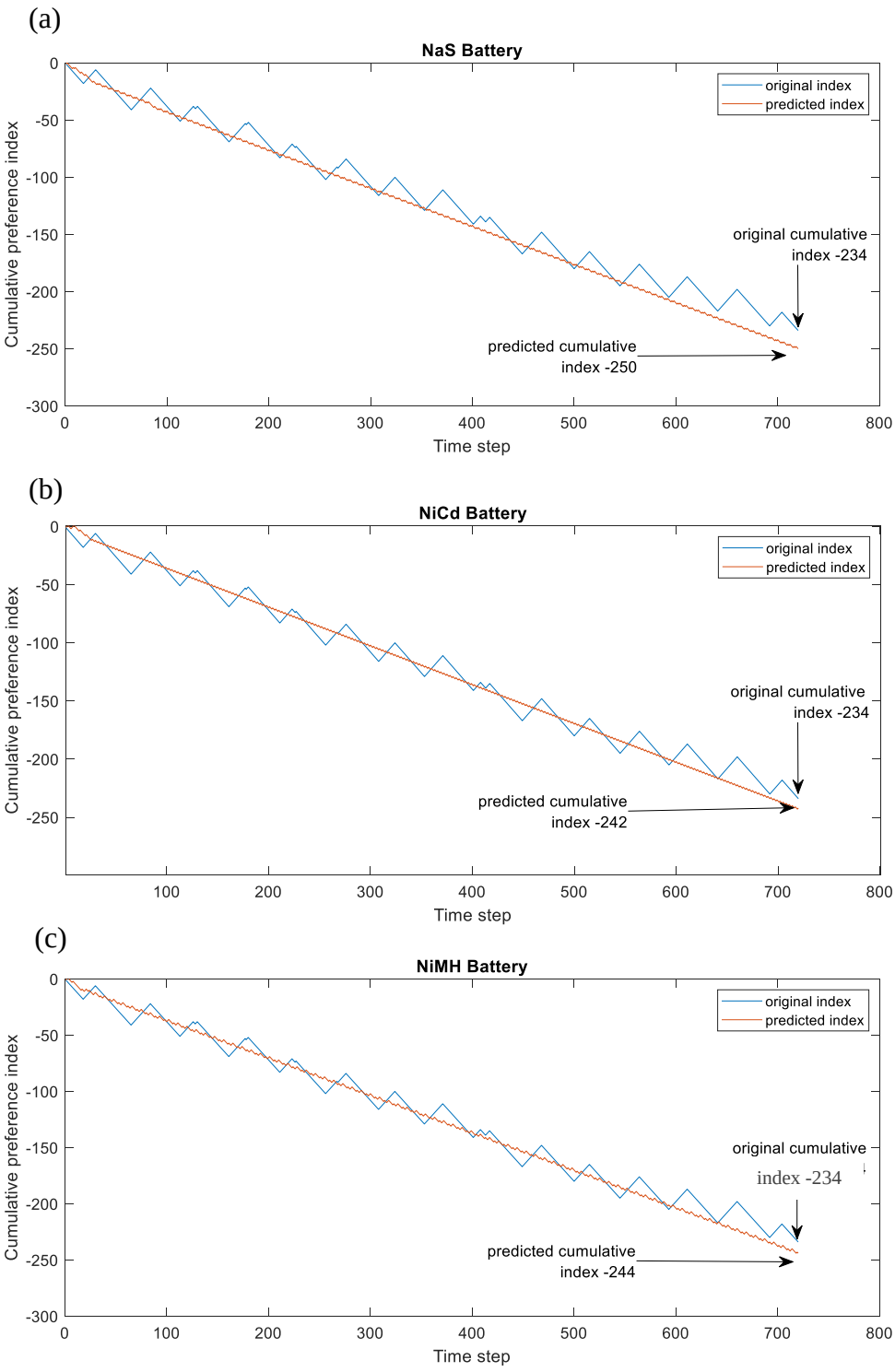

Figure 35 Comparison of the original cumulative preference index and index predicted by the developed model of NaS (a), NiCd (b) and NiMH (c) batteries.

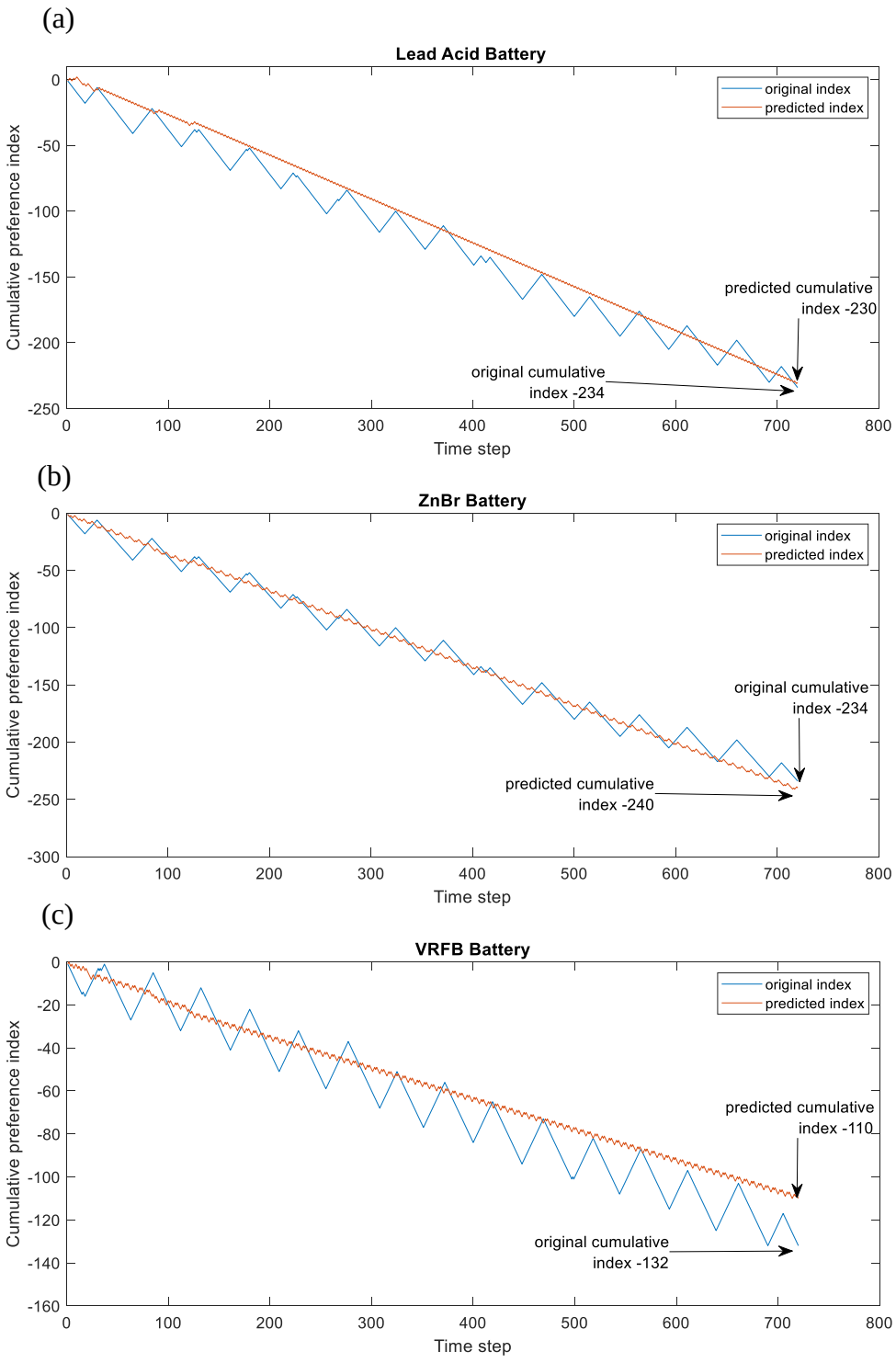

Figure 36 Comparison of the original cumulative preference index and index predicted by the developed model of Lead-Acid (a), Zn/Br_2 (b) and VRFB (c) batteries.

The results presented in Fig 34 - 36 show that the health index predicted by the models, the red line in Fig 34 - 36, does not follow the short-term diurnal patterns of the actual index, although a general long-term trend is recovered, providing valuable knowledge about the impact of the unbounded charging/discharging strategy has on the health of the battery. The estimation of battery health produced by models seems to follow the linear trend, but this seen linearity is the result of batteries being subject to schedule carried out in a consistent way based on the PV generation. The model is capable of predicting the non-linear trends in the battery health due to the random charge/discharge schedule that is shown in Fig. 38 in the following section. For most of the battery models, except for the Lead-acid and VRFB battery models, the predicted index alternately overperforms and underperforms the original index throughout the whole test period, which is illustrated in the example of Lithium-ion battery in Fig. 34 (points 1 and 2 on Fig. 34, respectively). For the VRFB battery model, the predicted preference index behaved in a similar fashion to that observed for most battery models until day six, then starts to increasingly underestimate the health index, Fig. 36(c). For the Lead-acid battery model, Fig. 36(a), until day eleven, the model slightly underestimates the battery health by predicting the health index to be higher than the actual one, then it starts to alternately overperform and underperform the original index in a similar fashion as it was observed for other battery models. The poorer performance of both models can potentially be a result of poor initialization of the initial conditions. It is possible that during 50 random restarts, the suboptimal initialization of model parameters was found, leading to a suboptimal model.

Comparing the original health index for all battery chemistries considered in this work, Table 13, observation can be made that the value of the original index is the same for all battery models with the exception of VRFB. The occurrence of a similar value for this index indicates that the batteries degrade at the same pace, indicating that the maloperation metric is reflective of the physical degradation process. The actual cumulative health index of the VRFB, with the value of -132, indicates that this battery is more robust and the least prone to damage from maloperation compared with the rest of the batteries achieving an index of -234. This result aligns with the domain knowledge and can be

explained by the difference in battery construction that affects device health. In VRFB, the reactants and products are in the solution phase during charging; therefore, no metal deposition occurs on the plates compared with conventional secondary batteries and hybrid flow batteries. The changes that occur in the electrodes materials of conventional batteries and hybrid flow batteries result in their degradation over time, which is accelerated by running the battery against its preferences. The VRFB battery is free of the processes leading to mechanical breakdown of the active material, as the active material is stored in separate tanks dissolved in liquid, which makes them less prone to degradation due the maloperation and this is reflected in much lower maloperation level at the end of the simulation.

Most of the developed battery models overestimated battery degradation/maloperation by predicting the cumulative maloperation, at the end of the test period, to be lower than the original by the difference between 2.56% (Zn/Br_2 battery) to 6.84% (NaS battery model), Table 13. The lead-acid battery only slightly underestimated battery degradation/maloperation by 1.71%. VRFB IOHMM battery model significantly underestimated the maloperation index by 16.66%. Overestimating the battery degradation level can have less severe consequences than underestimating it, but it could lead to loss of the opportunity to use the BES or needless replacement of the asset ahead of the end of its life. In contrast, the underestimating of battery degradation level can lead to battery failure due to using a device that is more degraded than it is anticipated.

Comparing the predictions, the model of the Zn/Br_2 battery achieved the best performance in predicting the preference index given the input sequence, the lowest value of SSE and the worst performing model of all was the model of the Lead-acid battery, which achieves the highest SSE value.

4.8 Validation of Health Metric Against Laboratory Test Data for Lithium-ion Battery Model

Due to the limited availability of suitable battery data for testing, only validation of the developed Lithium-ion battery model will be carried out in this section. To assess the effectiveness of the proposed battery maloperation model as a proxy for actual battery degradation, out-of-sample testing was performed using publicly available randomized battery usage lab data accessible from the NASA Prognostics Centre of Excellence Data repository [206]. Data come from laboratory tests of Lithium-ion batteries over the period of seven months (from August 2014 to February 2015). Batteries were continuously cycled at high or low temperatures with randomly generated current profiles to better represent practical battery usage. As the influence of temperature on battery health was excluded in this work, the set of data from experiments at low temperatures was chosen for comparison (ambient temperature between 21 and 33°C). The dataset also included data from reference charging and discharging cycles, which were performed after a fixed interval of randomized usage (every 50 random charge/discharge cycles) to provide reference benchmarks for battery state of health measured in terms of capacity fading. The NASA data set consists of detailed electrical measurements of current, voltage, temperature, and battery capacity measured every 50 random charge/discharge cycles and charge schedule information from the period of seven months. The 10 hours of NASA battery data is shown in Fig. 37 as a reference.

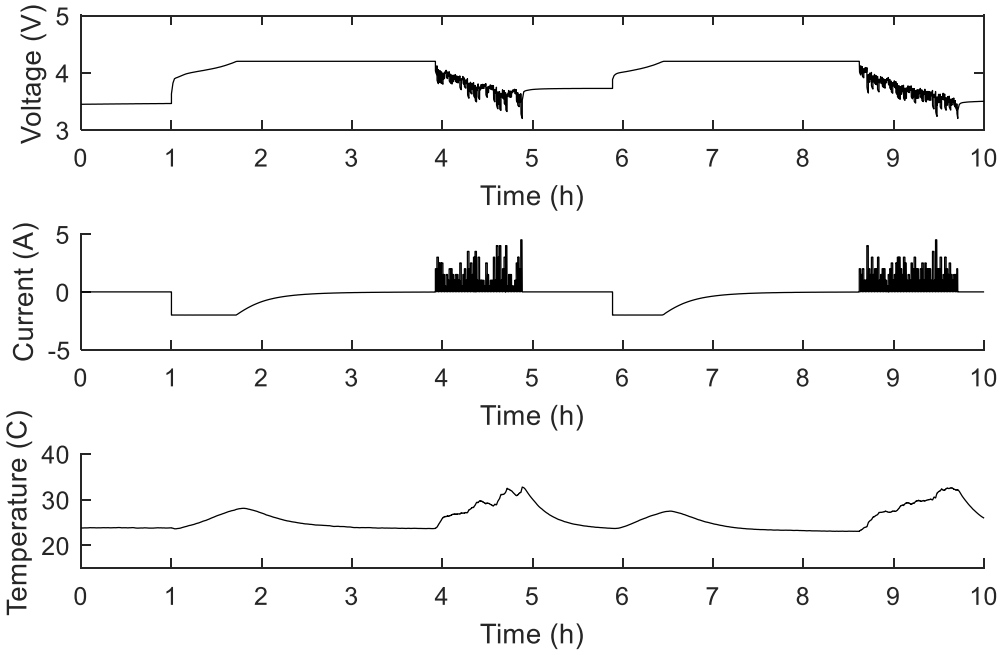

Figure 37 One hour of data from random battery charging/discharging at low temperature (NASA battery experiment [206]).

Since the developed Lithium-ion battery maloperation model has minimal input requirements, only the sequence of charge actions from the NASA dataset was used as the input to the developed IOHMM maloperation model of Lithium-ion battery. The IOHMM model output, maloperation index, is compared against the measurement of battery capacity taken every 50 random charging/discharging cycles from the NASA experimental dataset. A comparison of capacity fade, and cumulative maloperation/health index produced by the IOHMM is shown in Fig. 38.

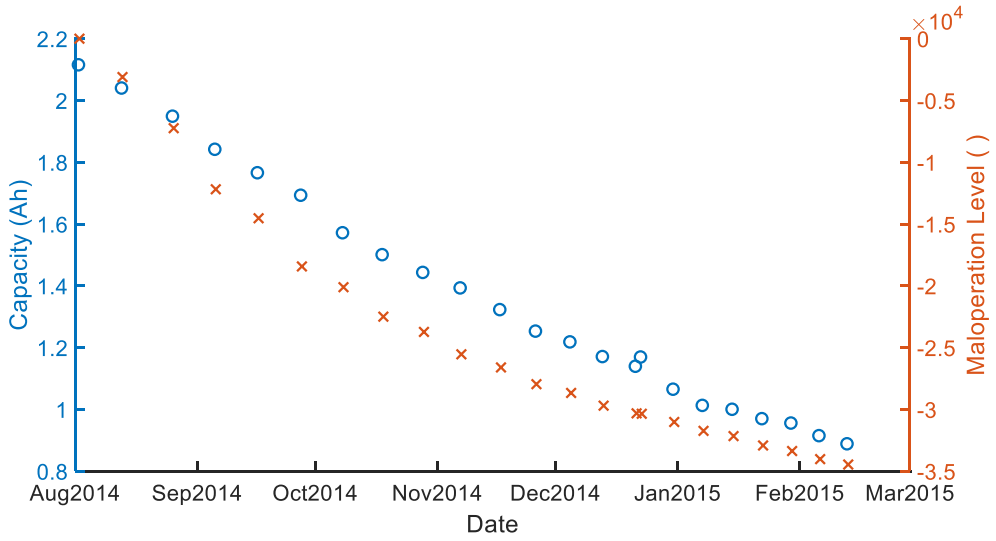

Figure 38 Degradation of Measured Capacity (capacity fade) versus Maloperation Level (cumulative maloperation index) predicted by developed IOHMM model of Lithium-ion battery. (Maloperation level is dimensionless quantity)

The IOHMM maloperation measure proposed in this work follows the trend observed in the capacity fading of lithium-ion battery operated under random charging/discharging, see Fig. 38, indicating that the level of battery maloperation reflects battery capacity degradation due to ageing processes. This makes the IOHMM proposed here a potential tool for assessing battery degradation levels due to the applied charging/discharging schedule without requirements for extensive measurements to be carried out. It is worth mentioning that the battery under test showed a substantial drop in its capacity over a period of seven months when charged and discharged randomly without considering battery preferences to the way of operation dictated by its chemistry, as shown in Fig. 38. This fast property deterioration in capacity of the actual device shows how important is the proper battery schedule that will consider this device's preferences when charging/discharging to ensure its health and lifetime are not too quickly compromised leading to the battery's premature degradation and the need for early replacement of this device. The health management of batteries is an important aspect of this asset management, thus a decision support tool increasing knowledge about the potential influence of planned action on battery health can

be beneficial for asset managers, supporting the decision process in battery schedule planning. The model of battery maloperation level presented in this work can be used in such types of applications as the decision support tool.

From Fig. 38, it is clear that there is some level of association between capacity fading and maloperation level predicted by the developed model. To assess this relationship and its strength, the correlation analysis between those two variables was performed. The scatter plot of the cumulative maloperation index and measured capacity is shown in Fig. 39.

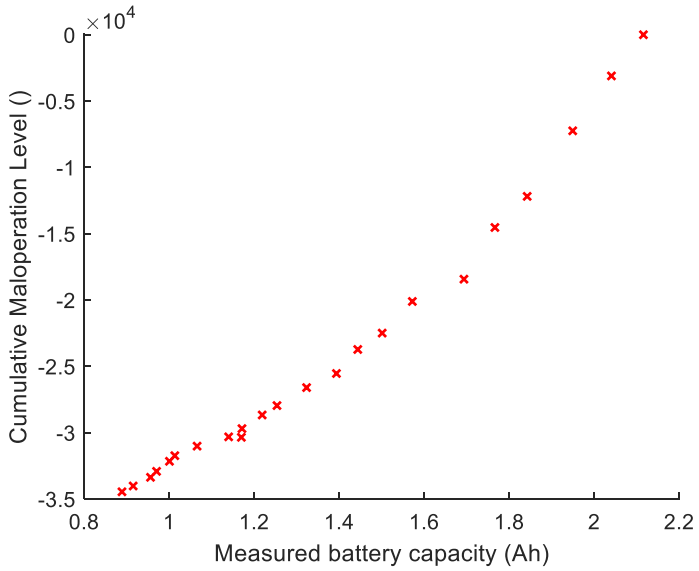

Figure 39 Scatter plot of cumulative maloperation index produced by the proposed IOHMM model and measured capacity fading of Lithium-ion battery from the NASA lab test.

From Fig. 39, it can be seen that there is a strong relationship between variables, but the relationship is not linear, which violates one of Pearson's correlation assumptions (assumption of the linear relationship between the variables), thus making this method of relationship measure not appropriate in this case. To evaluate the strength of the relationship shown in Fig. 39 between the maloperation/health index predicted by the IOHMM battery model and measured battery capacity fading of Lithium-ion from the NASA data set, the Spearman's rank correlation was applied. Charles Spearman, a psychologist, introduced the Spearman Rank correlation in 1904 [217] as the non-

parametric measure of the correlation between two variables that assess the strength and direction of the monotonic association between them. Spearman's formula for rank correlation between variables X and Y is given by equation (24).

$$r_s = 1 - \frac{6\sum D^2}{N(N^2-1)} \tag{24}$$

Where D represents the difference between the ranks of corresponding values of X and Y, N is the number of pairs of values (X, Y) in data. Spearman correlation between the IOHMM Lithium-ion battery model output and the capacity fade from the lab experiment was 0.99 with a corresponding p-value of $1.42*10^{-4}$. This indicated that the IOHMM metric, developed in this work, can determine a measure of the battery degradation with minimal knowledge of battery state, without invasive measurements or an intensive physics-based model. The capacity fade measurement from the NASA lab experiment required a reference cycle to be performed and measurements to be taken. Every 50 random charge/discharge battery cycles, the reference charge and discharge were performed to observe the battery capacity. This included the following four steps: constant current charging (reference charging) followed by rest after reference charging and constant current reference discharge followed by the rest after reference discharge. The battery capacity was then benchmarked by integrating current over reference cycles. This required a special reference cycle to be performed to enable the gathering of required data to estimate battery capacity. In contrast, the developed IOHMM model estimates battery health by taking only the battery charge/discharge schedule as the input. The developed model does not require any additional measurements to be taken or reference cycles to be performed to estimate devise maloperation level. The battery can be used as demanded with no requirements of taking it from normal operation to perform the reference charge/discharge cycle, as it was needed in the case of the NASA laboratory test.

4.9 Discussion

The research in the science and technology area is constantly evolving and moving forward, with new developments in the area of battery health estimation and prognostics being published each day. The visibility of the work presented in this thesis versus the ongoing research up to date in the battery energy storage area will be shortly summarised in this section. Moreover, the capabilities of the developed model, the problems in battery health prognostics it addressed, and the main findings of Chapter 4 will be discussed here.

- Currently, there is a clear trend in the increasing application of machine learning techniques in battery health modelling [170][218]. Battery health modelling based on machine learning techniques provides a non-invasive approach that is characterised by low computation, reduced requirement for knowledge and high accuracy with an increased ability to model scalability, which is very important for battery health modelling due to the increase of this device penetration in modern power systems [218]. The work presented in this thesis sits within the currently very fast-developing area of application of machine learning techniques for non-invasive battery health modelling.
- One of the very important advantages of the developed model over other models for battery health estimation, such as presented in [219][220][221][222], is its minimum system knowledge requirement for the prediction of device health. The majority of the models require a substantial amount of knowledge about the system to predict the battery health, such as information about battery capacity, current and voltage in the [219]; current, voltage profiles and battery temperature in [220][222]; temperature, voltage, capacity and information about the cycle in [221]. This required knowledge increases costs, such as the additional cost of installation of required telemetry and the cost of maintenance of such installation to ensure its proper operation. The model presented in this work, on the contrary, requires only information about the battery regime to make a prediction, which is available as the fiscal meters are already installed. A minimal requirement of

knowledge of the system is important with the increasing level of battery aggregation in the energy system. The aggregation of battery devices in the system can lead to the substantial amount of data required to be gathered and processed when models with higher data requirements are used in battery health prognostics. This leads to the requirement for the installation of numerous sensors, which has financial implications. The more sensors, the more possibility of missed reading and more difficulties with synchronisation of all reading and more data to work with when estimating battery health that is crucial in the battery asset management.

- As discussed earlier, one of the important limitations of battery modelling is the shortage of suitable data sets for modelling purposes. The necessity for extensive laboratory data required for modelling is eliminated when applying the approach proposed in this work. The proposed model minimizes requirements for training data by simply reusing available generation and demand data in conjunction with battery operating preferences, discussed in Chapter 2, to generate training data. The resulting developed model is capable of predicting of maloperation level of the real battery that was strongly correlated with the currently used HI measure - capacity fading as can be observed in Fig. 26. This indicates that the IOHMM metric, developed in this work, determines a measure of the battery degradation with minimal knowledge of battery state, without invasive measurements or an intensive physics-based model.
- The proposed framework of battery health modelling based on IOHMM can be easily applied to the new battery technology. It can be also extended by incorporating new battery preferences for existing technologies or can be adjusted if technology will change by updating existing battery preferences. It can be simply implemented by:
    - Creation of heuristic rules based on the preferences of new battery technology and composition of a new lookup table for this device,
    - Addition of new or modifications of existing heuristic rules that are governed by battery preference and adjusting the lookup tables with

maloperation index accordingly, based on new and existing preferences.

The remaining steps in model development, namely: data generation, training, model selection and testing, can be applied without modification for each of the above cases.

- The data used in this work come from the EU FP7 ORIGIN project and has 30- minute resolution. Data with higher granularity, if available, also can be used in the battery health modelling using the proposed modelling approach and IOHMM framework. The internal changes in the battery state and chemical reactions taking place inside this device are dynamic processes that may change very rapidly. The higher resolution of data could help catch these types of changes during the modelling and could further help to improve the model. However, the usage of data with higher granularity can substantially increase the model training time. The running time of the developed model, when battery health is estimated on higher granularity data will also increase, with the running time depending on the resolution of the data available and the length of the testing data set. The training time of the model will be substantially more impacted than the time required to run the trained model due to multiple reruns required to deal with issues associated with learning the model, namely: choice of the model size and initialization of transition, emission and initial state distributions.
- For the application of BES in the power system, an important aspect is how to plan the charging/discharging of this device to meet the energy network requirement while also considering battery health. Each action can incur positive or negative consequences on the health of the battery, which can generate costs for the battery asset owner (premature battery replacement) or energy system operator (costs due to failure to deliver services when required). Many studies ignore battery degradation while dispatching BES and do not take the degradation cost into consideration [224]. The developed model can act as the proxy of the degradation

costs, as it generates a health index indicating if the battery is maloperated (operated against its chemistry and preferences leading to battery health degradation). The developed model constitutes the degradation metric that can be used as the policy function in an automated scheduler that accommodates battery health in the dispatch process.

- Proposed battery health metrics, in terms of maloperation level, is an abstract HI measuring the battery health. It was shown that it is strongly correlated with battery capacity fading. With an available suitable data set covering the lifetime of the lithium-ion battery, it would be possible to derive a scaling factor enabling the developed measure in maloperation level to be directly translated into the capacity fading term. This can extend the potential application of the developed model from only informative (information if performed action is against battery preferences leading to the health deterioration that will support decision when preparing battery schedule) to the actual application (recalculating the capacity fading level based on the battery schedule with the application of the developed model in conjunction with the scaling factor).
- The proposed approach is applicable to a range of battery ages. With the knowledge of battery health at the starting point, it can be used to estimate the consecutive levels of maloperation due to the battery application.
- The 'weightings' of each mal-operation are treated equally in the developed model. There is a possibility of changing these weightings to ensure that the length of the action performed against battery preferences would be reflected in the index; for example, the longer action is performed against battery preferences, the lower the index should be generated. More detailed knowledge of chemical processes taking place inside the battery during operation and more data would be essential in order to provide these varied weightings.
- The model proposed in this work excluded the system-dependent impact (e.g. charging regime dictated by application) on the performance deterioration of the battery in the modelling so that the resulting model caught the performance

deterioration only due to misuse dictated by battery preferences. Thanks to this approach, the resulting model is characterised by high generalisation in battery health estimation and can be potentially used to estimate battery health regardless of the function it performs in the system.

4.10 Conclusions of the Chapter

As storage aggregation becomes more commonplace, the management of the constituent battery assets will require health metrics in order to ensure ongoing contractual turn-up and turn-down commitments are fulfilled to their agreed capacity. To support this, a non-invasive approach has been presented that predicts the extent to which a battery asset has been maloperated. The proposed IOHMM captures the differences in the preferred operation of the battery, dependent on its chemistry, that allows the incorporation of preferences like micro cycling, deep cycling, and storing full or empty. These preferences were encapsulated in the state transition probability matrix and observation probability matrix as the model was trained on the maloperation/health indexes that considered those events. By capturing the information on how well the battery is operated in regard to its chemical preferences, the model becomes a potential decision support tool for planning and asset management tasks by increasing knowledge about the suitability of this BES for its intended application or suitability of the planned charging/discharging regime of this device. The minimal knowledge requirement also makes the model suitable when dealing with practical cases where storage installations may comprise heterogeneous cell chemistries. While this can undoubtedly be developed to support condition monitoring and estimate remaining useful life, the wider interest could be from using this as the policy function in an automated scheduler – this can be used to diversify the impact of maloperation across a portfolio of battery assets, prolonging their life and reducing the capital expenditure costs for storage aggregators.

CHAPTER 5

This chapter constitutes an updated and extended conference paper that was published in the Proceedings of the 52nd International Universities Power Engineering Conference in 2017 by Joanna Sobon, Andrew Roscoe and Bruce Stephen, titled: "Energy storage day-ahead scheduling to reduce grid energy export and increase self-consumption for micro-grid and small power park applications," [209].

5. Influence of Demand Forecast Error on the BES Schedule Effectiveness and the Level of Device Maloperation

Accurate and timely forecasting of demand and forecasting of renewable generation has an important influence on the operation of the power network. Due to undergoing changes in the GB's power system, namely introducing a greater share of decentralised renewable generation that is closer to the end user, balancing the system becomes more challenging. The increase in embedded generation on distribution networks means that power must be balanced close to the end-user point. Due to the low aggregation of these loads, the noise caused by routine behaviour dominates load profiles, making them harder to predict [2], but they still need to be balanced; hence new forecasting approaches are needed [225]. With the decrease in load aggregation, the forecasting error increases significantly from around 3% for the National level through 10% for the secondary substation to 30% for a single premise [2][226]. The significantly lower accuracy of demand prediction and the uncertainty originating from unknown generation outputs become an important challenge for the system operators that need to be addressed to ensure continuity of energy provision and the stability of the system to be maintained. One of the solutions to help tackle the problem of intermittency of renewable generation is an introduction into the system battery storage that can shift surplus energy to times when it is in deficit. This solution is promising, although it introduces additional

unknowns when planning system operation and balancing energy. The BES need to be scheduled in a way that allows exploiting its capability with simultaneous provision of required functions and additionally ensuring its long life span and device-safe operation. As the balancing energy in the power system is planned in advance and is based on the demand and generation forecasts, the scheduling of the battery energy storage, which becomes an integral part of the system, will also be performed based on those variables. For the system operator's informed decisions and to fully exploit BES technology, it is important to gain more understanding on:

- How does the applied demand forecasting method influence the BES schedule and effectiveness of provision required functions by this device?
- Which demand forecasting method is the most promising in tackling the problem of disaggregated load prediction to support energy balancing in the system comprising battery energy storage and renewable generation?
- How does the BES schedule based on the different prediction methods influence the battery maloperation level, thus device health?
- How effective can be battery energy storage schedule prepared using the disaggregated demand forecast?
- Can we determine how good potentially would be BES schedule produced based on forecasted demand by simply examining the accuracy of the demand forecast used in schedule production?

The main aim of the work covered in this chapter is to investigate some of the aforementioned problems to help asset operators in increasing knowledge of the influencing factors on the BES schedule and battery maloperation level due to the applied schedule. The influence of increased levels of uncertainty in demand forecast on the BES schedule will be investigated in this work, followed by an examination of the effect of the demand forecast accuracy on the provision of the required function by the BES scheduler. Moreover, the impact of the schedules generated by the scheduling tool employing different forecast models on the battery maloperation level, and thus its health, will be

studied here by using the IOHMM battery model developed and discussed in the previous chapter. The additional contribution of this chapter is a design of generic parametrized forecasting and BES scheduling tool for small power parks and microgrid applications. The availability-based scheduler developed produces day-ahead energy storage charging and discharging schedules that decrease electrical energy export to the main grid and increases the self-consumption of energy resources within a local system.

This chapter is structured as follows: Section 5.1 covers the formulation and implementation of the developed BES scheduler model. The case study and evaluation of the performance, the effectiveness of the proposed model and the influence of the demand forecasting model on the BES schedule are performed in section 5.2. In the subsequent section, the effect of applied schedules that were based on different demand forecasting models on battery maloperation level, thus battery health, was examined for the purpose of finding the demand forecast method which application in schedule preparation resulted in the lowest level of battery degradation with simultaneous high schedule effectiveness[18]. Finally, the last section concludes this chapter.

5.1 Model Formulation and Implementation

As power networks evolve to accommodate low carbon aspirations, new concepts helping in this transformation emerge, and the advances in technology may bring solutions to tackle the problems of load growth, increase the level of intermittent generation integrated with the system, prolonged power outages due to network failures (due to ageing equipment) or network updates, and supporting the governmental targets for low carbon economies. One of those concepts is the integration of decentralised groups of renewable generation sources, energy storage and loads to form a microgrid that is normally connected to a public distribution network but is also capable of working in an autonomous state called 'islanding mode' [223][224]. If microgrids become more often

[18] The schedule effectiveness here means how effective is a scheduler in setting particular action when schedule prepared based on the forecasted demand compared to the action set for BES in schedule prepared on original demand data (perfect demand case).

an element of the power network [223] it is important to study further their capabilities and operation.

A grid-connected system, microgrid, with 'behind the meter' PV generation, battery energy storage and an availability-based scheduler, proposed in this chapter, was simulated here. The scheduler tool operation is based on the available resources in the system (predicted amount of generated energy by PV system installation) and demand requirements (predicted level of load). The scheduler controls energy flow within the system to achieve a reduction in energy export to the grid and an increase in self-consumption. A 40kWh lithium-ion battery energy storage with a rated power of 10kW, efficiency of 98%, and discharge rate of 0.001% per half-hour (corresponding to ~1.5% per month) is part of the simulated system along with the 8.6kWp PV installation. This size of battery was chosen on purpose to provide high self-consumption, around 90.3 % in the analysed system. The battery was not sized perfectly to allow originally also some export to the grid. More information about the demand and PV generation data used in this experiment will be discussed in Section 5.2. The energy flow and information exchange within the considered system are presented in Fig. 40. In the system, the energy generated by the photovoltaic generator can either flow to the load (E_{PV_Load}), to the battery energy storage to be used to charge this device ($E_{PV\_battery}$) or can be exported to the grid (E_{PV_Grid}) when generated energy is not needed, and the BES is fully charged. To meet the demand, apart from energy originating from the PV panels, if there is not enough generation, the energy can be imported from the grid ($E_{battery\_load}$), or BES is used to provide energy (E_{grid_load}) if enough energy is available in the storage.

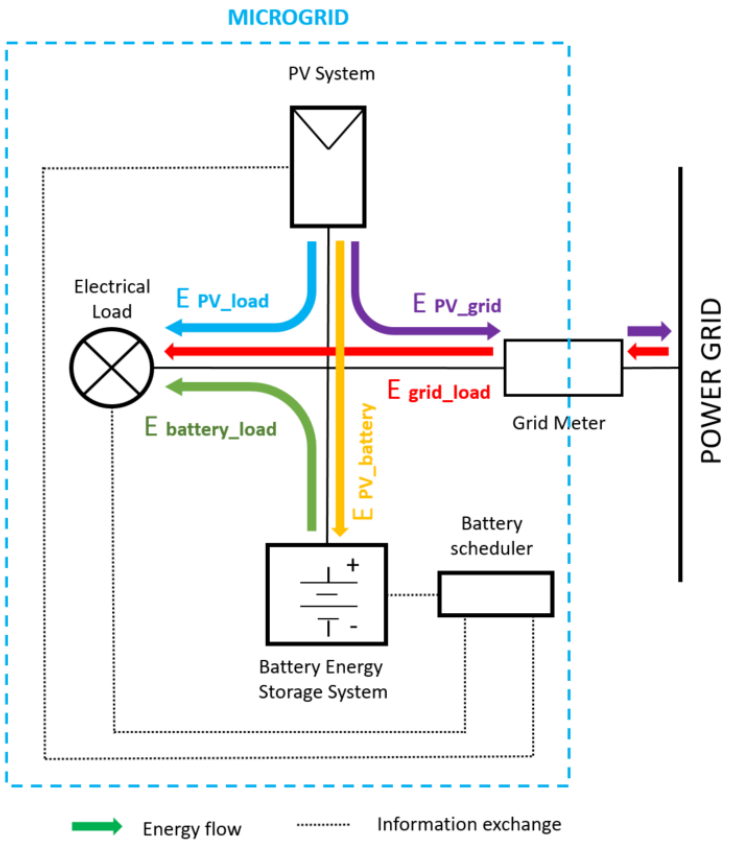

Figure 40 Energy flow and information exchange within the simulated system.

The full procedure of the model implementation and testing is shown in Fig. 41.

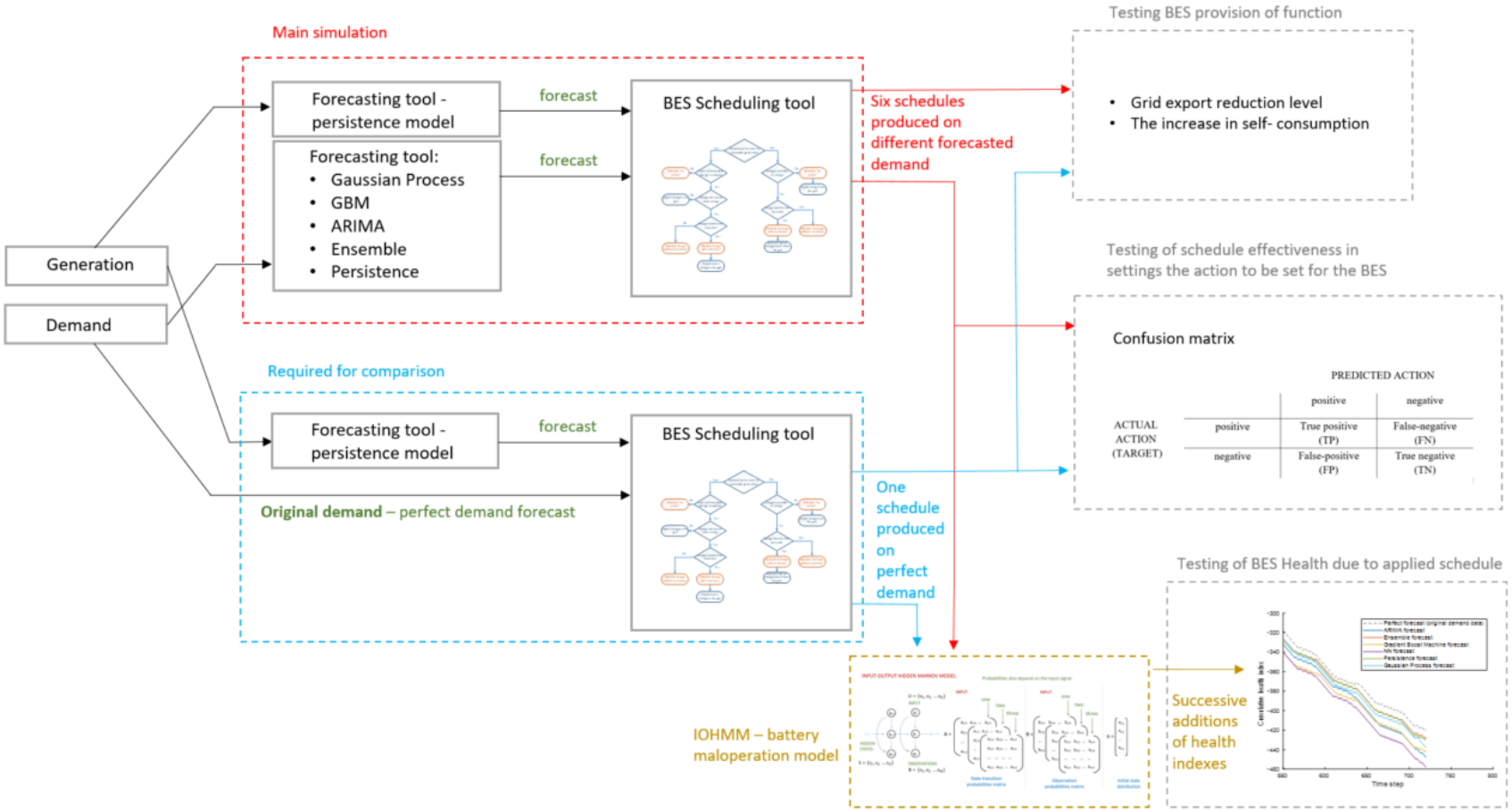

Figure 41 The summary of the model implementation process for analysis of the demand forecast influence on the BES schedule and its effectiveness in providing required functions and effectiveness in assigning the required storage actions.

5.1.1 Generation and Demand Forecast Models

The developed scheduler model makes use of the day-ahead demand forecasting method previously used in this area of research [210], [225]–[228]. Different methods for demand forecasting are employed to investigate the influence of forecast on the performance of developed BES schedule tool and its effectiveness in providing grid export reduction, increase in self-consumption functionality and influence on battery health. These models were previously tested on the disaggregated demand data (LV feeder level disaggregation). The available data has a half-hourly resolution. Due to the lack of numerical weather prediction data, purely data-driven forecast methods are used.

1. Demand forecasting: Different methods of demand forecasting are implemented in the model. These are an ARIMA model with lags of 48 samples (a conventional time-series approach), a shallow feed-forward Neural Network with 48 output nodes, 49 input nodes and 20 neurons (one hidden layer) (non-linear and generally black-box approach) as used in [227], model based on the Gaussian Process and Gradient Boost Machine (GBM) used by [228] (two contemporary machine learning approaches), Ensemble Forecast (the combination of all demand forecasting methods used via a simple unweighted average) [226][229] and finally a Persistence forecast which is a naïve week ahead forecast.
2. PV generation forecasting: In the absence of any other information, the PV generation forecast used in this work is based on the persistence model. This naïve method assumes that the energy generated today at a given time is the same as it was the previous day at the corresponding time.

5.1.2 Battery Energy Storage Model

The parameterised model of battery energy storage based on the energy balance equation (25) was developed.

$$E_{stored\_t+1} = (1 - \alpha)*E_{stored\_t} - \eta* E_{storage\_flow\_t} \quad (25)$$

Where: E_{stored_t} - energy stored in BES at time t

$E_{storage\_flow}$ - energy exchanged between storage and the rest of the system

α - self-discharge rate of BES

η - efficiency of the BES

The energy stored in the BES system is reduced by the value associated with the self-discharge rate α over an interval of time t. The efficiency η associated with the charging and discharging processes of energy storage reduces the potential energy, $E_{storage\_flow}$, which is available to flow from and to the storage. During model development, the following parameters were considered: state of charge of BES, minimum and maximum SoC, rated power (10kW), capacity (40kWh), efficiency (98%) and self-discharge rate (0.001% per half-hour). The energy flow from storage at any given interval of time in the proposed model is constrained by the rated power of the used storage technology as follows in (26).

$$E_{flow\_min} \leq E_{storage\_flow\_t} \leq E_{flow\_max} \quad (26)$$

Where:

$$E_{flow\_max} = P_{rated} * \Delta t \quad (27)$$

$$E_{flow\_min} = - P_{rated} * \Delta t \quad (28)$$

Where: E_{flow_min} – minimum allowed energy flow to the storage

E_{flow_max} – maximum allowed energy flow to the storage

Δt – the time interval (half-hour in this work)

P_{rated} – rated power of BES

Additionally, the energy stored in the energy storage is limited by maximum and minimum allowed values (29) resulting from the storage specification.

$$E_{\_stored\_min} \leq E_{\_stored\_t} \leq E_{\_stored\_max} \quad (29)$$

Where the $E_{\_stored\_max}$ is related to the maximum allowed level of energy in the BES and $E_{\_stored\_min}$ is the minimum allowed energy stored for simulated technology (corresponding to the allowed depth of discharge).

5.1.3 Scheduling of Battery Energy Storage

The day-ahead scheduling of the BES is performed based on the forecasted daily profile of electricity demand and renewable generation forecast. The output of the scheduling are periods of time and corresponding actions to be performed by BES during these periods (a charge, discharge or ”no action”). The logic that controls charge and discharge regimes is based on the available renewable energy resources in the system and the technical limitations of the energy storage to be simulated - a Lithium-ion battery in this case. The scheduler decision making applied in this work is shown in Fig 42. The objective of the algorithm controlling the schedule is to reduce export energy to the grid and increase self-consumption within the system.

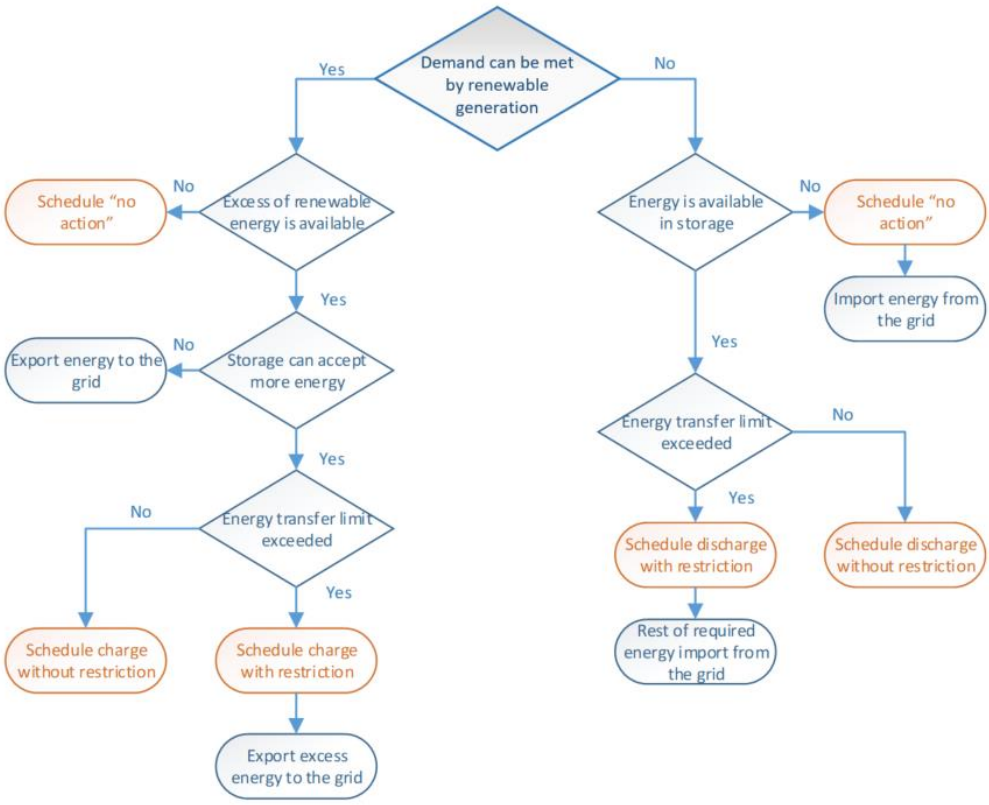

Figure 42 Availability-based scheduler decision flow chart.

5.2 Case Study and Results

To assess the performance and effectiveness of the proposed scheduler model and examine the influence of the demand forecasting model used to produce the schedule on its effectiveness and battery health, the case study of an actual community feeder with significant PV generation installed is presented. Half-hourly historical data of electrical demand and PV generation covering 126 days were used in the case study. As an illustration of data used in this study case, a sample of seven consecutive days of demand and PV generation, Monday to Sunday in March, is shown in Fig. 43. Half of the data were used for training and half for testing. The impact of the different PV generation forecasts on the BES schedule and device health is not investigated in this work. The PV

generation based on a naïve persistence model was used for all the scenarios. To understand the impact of PV generation on the produced schedule and battery health, the scenario with the schedule produced based on the original data versus the schedule based on the perfect demand data (original demand data) and forecasted generation was used in this work. A more throughout investigation of the PV generation forecast on the battery schedule is treated as a potential future extension to the research and is not in the scope of this work.

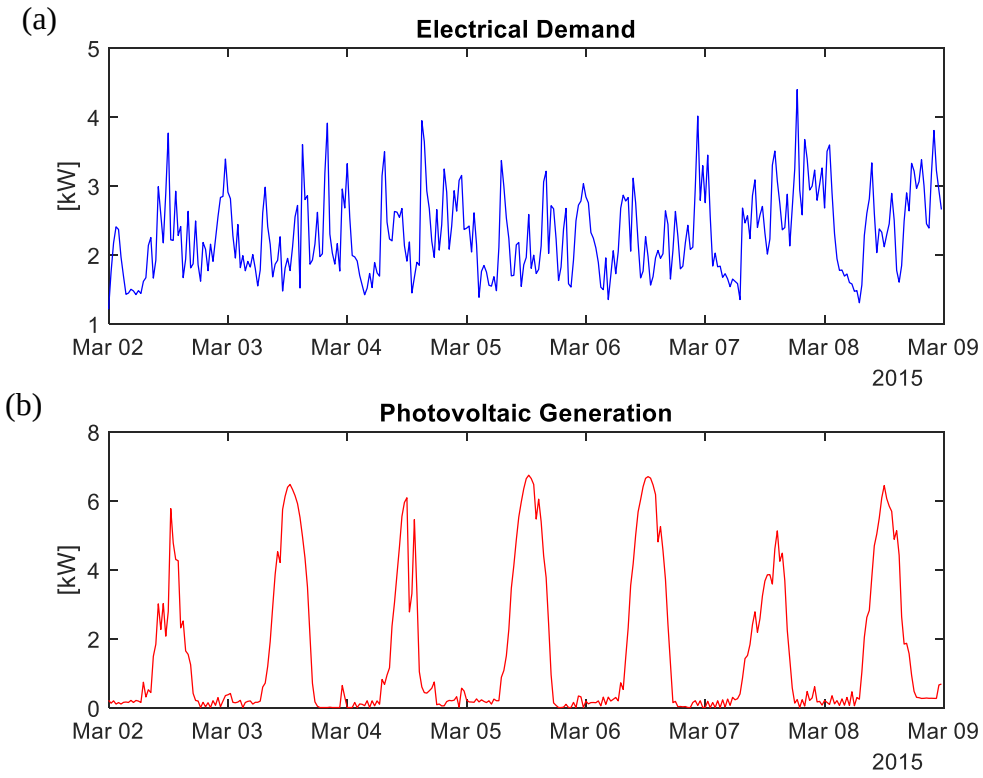

Figure 43 Seven consecutive days of electrical demand at LV level and PV generation data starting from Monday 2nd of March until Sunday 9th of March.

5.2.1 Effect of Demand Forecast Methods Accuracy on the Battery Scheduler Performance

The simulations, with six different forecasting methods employed, were considered to study the effect of the error in demand forecasting on the level of reduction in electricity export to the grid and the increase of self-consumption within the simulated system comprising BES. The same naïve PV generation forecasting method was used in all scenarios to keep this variable unchanged throughout the study resulting in a similar impact of the PV generation forecast on the produced schedule. The schedule for comparison was based on the perfect demand forecast (actual demand data) in conjunction with the PV generation forecast based on the persistence method. Additionally, the perfect case when all original data were used in schedule generation was also included here to give some indication of the influence of the PV generation forecast error on scheduler effectiveness. The results of the simulations are given in Table 14. The example of the electrical energy storage charging and discharging schedule produced by the model is illustrated in Fig. 44. When examining the schedules produced by the scheduling tool, Fig. 44, we can observe the differences in actions that were set to be performed by BES depending on the demand forecasting model used by the scheduler, against the schedule based on the actual demand data. As can be seen, in Fig. 44, the schedule generated is dominated by the diurnal pattern of PV generation. During the day, when the amount of generated energy by PV installation exceeds the requirements of the load, the generated schedule mostly consists of ‘charge actions’ set to the storage, with sporadic ‘discharge’ and ‘no action’ actions set (in the case when the generation is lower than required energy to meet demand or storage cannot accept more energy as it is fully charged). Conversely, during the night, the dominant operation for the battery energy storage is ‘discharge’ as PV generation cannot provide any energy during this period of the day, and there is still energy required in the system. The body plots of daily error in forecasting for each demand forecasting method considered in this work are shown in Fig.45 and Fig.46. The body plot of daily error in PV generation forecasting is shown in Fig.47.

Table 14 Performance of Scheduler Tool that employs different demand forecasting models for lithium-ion battery.

Forecasting model	Demand forecasting error		PV Generation error	Performance of the scheduler model	
	Mean absolute percentage error (MAPE) [%]	Mean squared error (MSE)	Mean squared error (MSE)	Grid export reduction [%]	The increase in self-consumption within the system [%]
Perfect case (original demand and generation) [19]	-	-	-	89	90.3
Perfect forecast (original demand)	-	-	1.83	**87.8**	**87**
Ensemble forecast (all)	27.4	0.4047	1.83	82.2	80.1
Gradient boost machine	29	0.4152	1.83	83.8	**82.8**
Persistence forecast	29.7	0.5361	1.83	**85.4**	76
Gaussian Process	30.6	0.4289	1.83	85.1	80.9
ARIMA model	48.2	1.1648	1.83	75.8	75.4
Neural network	50	1.0774	1.83	76.9	74.5

NOTE: For all simulations with a different type of demand forecast, including the perfect forecast case when original demand data was used, the PV generation was based on the persistence forecast. Perfect forecast is used for comparison in this work, and the perfect case (original demand and generation data) is used here to show the impact of the PV generation on the schedule (comparison between perfect demand case and perfect case).

NOTE: The PV generation forecast error was added to the table to stress that the generation forecast error was kept constant for all considered scenarios.

[19] Please note that performance measured for this case originate from comparison system without and with BES as the part of the system.

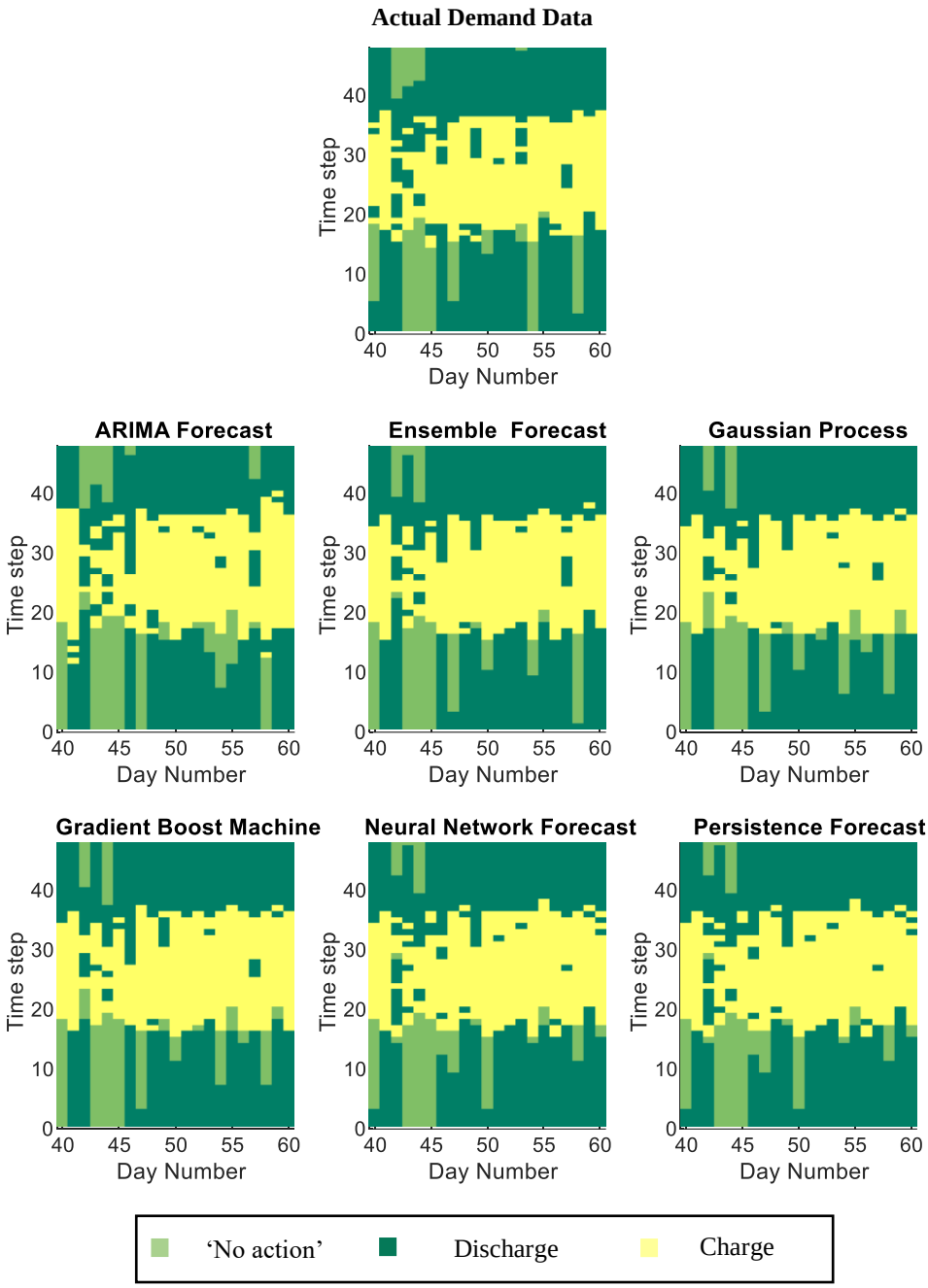

Figure 44 Day-ahead schedule of lithium-ion BES achieved for twenty days when different demand forecasting models were used in schedule planning and schedule based on actual data. The colours indicate the appropriate action to be performed by BES. Colours represent the charging, discharging and "no action" functions of energy storage. (Actual data correspond to the case when actual demand data were used in schedule production, in all cases the forecasted generation was used)

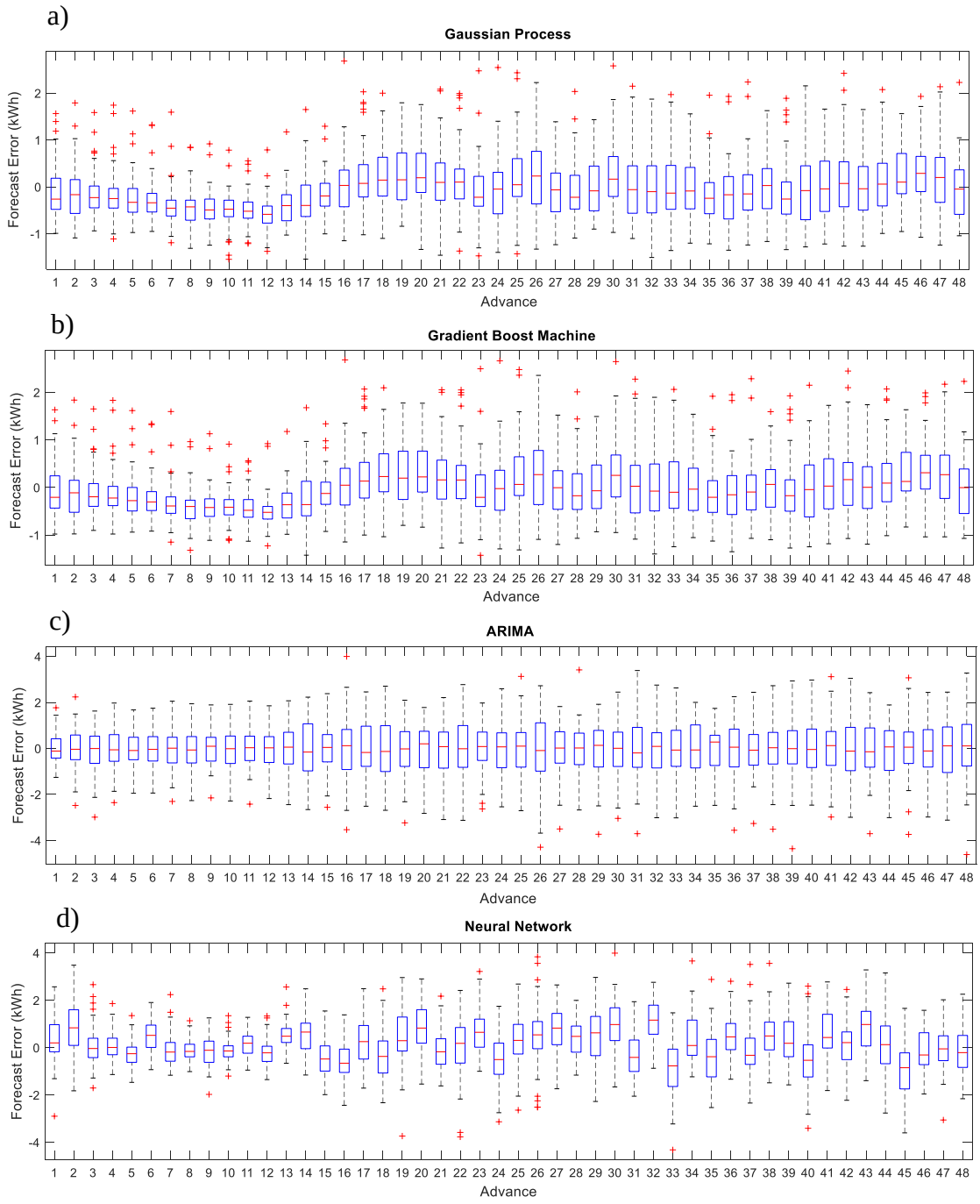

Figure 45 Error boxplot by the time advances for the demand forecasting based on: a) Gaussian Process, b) Gradient Boost Machine, c) ARIMA model, d) Neural Network.

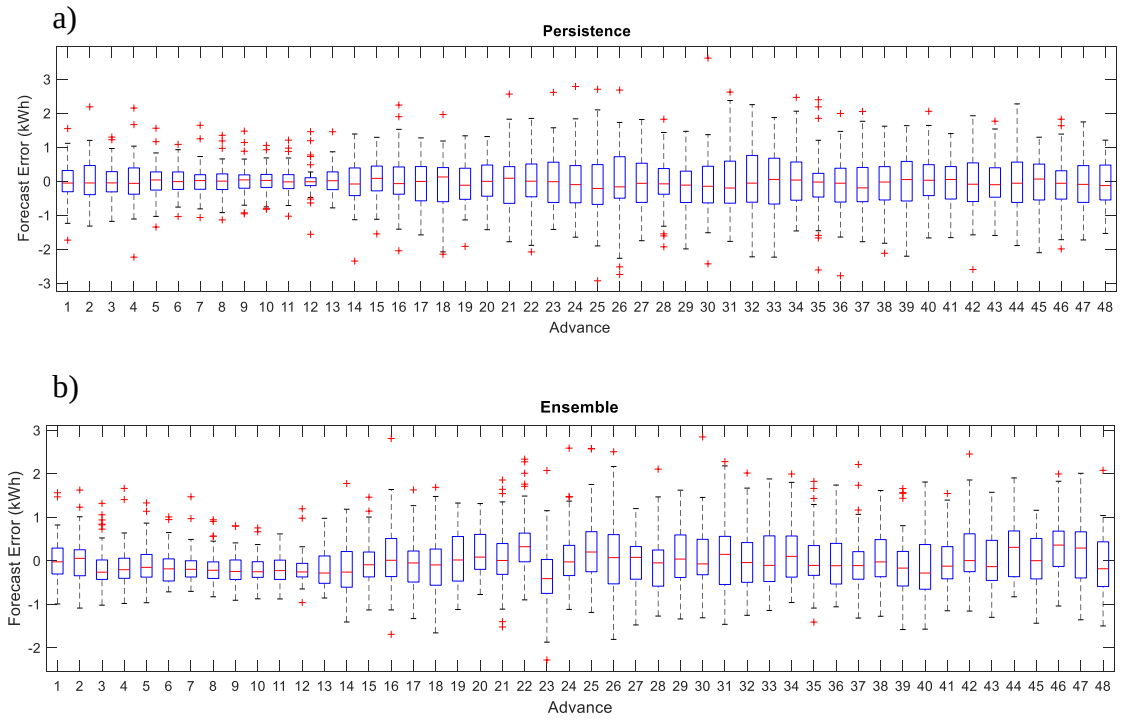

Figure 46 Error boxplot by the time advances for the demand forecasting based on: a) Persistence method, b) Ensemble model.

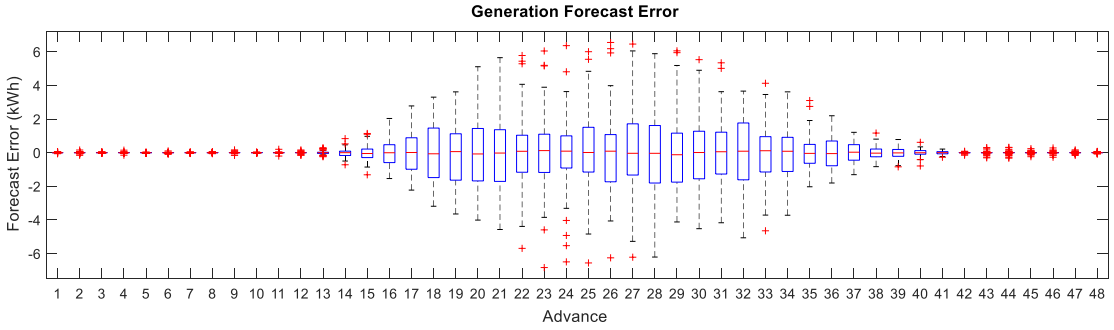

Figure 47 Error boxplot by the time advances for the PV generation forecast (persistence forecast).

The mean absolute percentage error measure was used in this work to allow comparison across different forecasting methods used in this work. As MAPE is not sensitive to outliers, the mean squared error was also calculated and included in Table 14. The MSE is an error measure that emphasizes larger errors, penalizing models that make significant mistakes more heavily.

A perfect case was added in this work to show how the PV generation forecast itself influences battery schedule effectiveness in grid export reduction and the self-consumption increase. From Table 14, can be seen that when perfect data is used in the generation of the schedule, the grid export reduction is 89% and self-consumption increases by 90.3% compared to the case when the battery was not in the system. Both variables were reduced when the schedule was prepared based on the perfect demand and forecasted generation. The grid export reduction was lower by 1.2%, and the self-consumption increase was reduced by 3.3% compared to the perfect case.

For the scenarios employing different demand forecasting models, the reduction in grid export achieved by the developed model is in the range of 75.8% - 85.4% and the self-consumption is increased by between 74.5-82.8%, compared to 87.8% and 87% for the grid export reduction and increase in self-consumption respectively, achieved by perfect demand forecasting case. The model employing persistence and Gradient Boost Machine demand forecasting model achieved the best results among other for the export reduction and self-consumption increase respectively, Table 14. The worst performance in export reduction and self-consumption compared with the perfect demand forecast achieved the model employing the ARIMA demand forecast and applying the NN demand forecast, respectively. The NN model used in this work was shallow feed-forward NN. The low accuracy of this model is the result of not proper tuning of the model to the available data that resulted in a high error in the demand prediction, thus low export reduction and self-consumption compared to the perfect demand forecast. Additionally, the low number of training data also influenced the accuracy of this model as it was trained only on 63 days of data.

To measure the strengths of the correlation between the export reduction and forecast error and the self-consumption and demand forecast error, both Spearman and Pearson correlations were applied. The examination of the scatter plots with only six points did not give a clear indication if the relationship is linear or monotonic; for this reason, both measures of correlation were checked here. The simulation results show that there is a very strong negative Pearson correlation between the forecasting error and the reduction in export to the grid, equalling -0.92 with a corresponding p-value of 0.008, Table 15. This indicates that with the reduction of the forecasting error, the export of energy to the grid is increasing. There was also found negative strong Pearson correlation between the forecasting error and the increase in self-consumption, equal to -0.76, but due to the corresponding p-value of 0.08 (the significance level of 0.05 is applied in this work), this result is treated as inconclusive evidence of an association between these two variables (there is no statistically significant relationship between variables). The correlation between the reduction of grid export and the forecast error indicates that the accuracy of the employed forecasting method has a significant influence on model performance. The Spearman correlation for both export reduction and self-consumption increase have corresponding p values above a significance level of 0.05 and are treated as inconclusive evidence of an association between these variables and forecasting error.

Table 15 Correlation between the forecast error and grid export reduction, forecast error and the self-consumption increase.

MAPE association with	Spearman Correlation		Pearson Correlation	
	Correlation coefficient	Corresponding p-value	Correlation coefficient	Corresponding p-value
Grid export reduction	-0.43	0.42	-0.92	0.008
Self-consumption increase	-0.71	0.14	-0.76	0.08

The naïve method, Persistence demand forecasting, used in the developed tool, gives the higher export reduction among all used models, but it does not perform so well with the increase in self-consumption. The model employing the Ensemble forecast has the lowest mean absolute percentage error (MAPE) but does not introduce a higher percentage increase in the analysed quantities than other models. Ensemble forecast calculates the unweighted average of all other forecasts and uses it as forecasted value. During the process of averaging, some errors cancel each other; this is a reason why the MAPE is improved. This method, regardless of the lowest MAPE, does not provide better performance in grid export and self-consumption; this indicates that other performances of the forecasting method need to be analysed, and their influence on the performance of the developed model should be evaluated.

5.2.2 Evaluation of the Storage Scheduler Effectiveness

The analysis of the BES scheduler's effectiveness in predicting required storage actions is presented in this section. The method based on binary classification (the confusion matrix) is proposed. The confusion matrix is the table of true and false positives (TP, FP, respectively) and true and false negatives (TN, FN, respectively) that are results of comparing the outcomes of classification, hypothesis testing, and object/event detection with the available target/ true/ actual outcomes [203]. It is a way to describe the performance of the classification model or classifier [203][229]. The example of the confusion matrix with its notation is shown in Fig.48. The rows of the matrix represent the actual (target) occurrences of the particular storage action, and the columns correspond to predicted instances of this action. This method enables the evaluation of the scheduler model's capability to predict the occurrence of a particular action of the electrical energy storage. In this work, the target value were the actions set to be performed by BES when actual demand data were used during schedule generation. The predicted results came from simulations with different demand forecasting methods employed in the model. For each case, the three separate matrices were prepared for predicting charging, discharging

and the “no action” (hold action) actions with a comparison to the target schedule, included in Appendix B.

		PREDICTED ACTION	
		positive	negative
ACTUAL ACTION (TARGET)	positive	True positive (TP)	False-negative (FN)
	negative	False-positive (FP)	True negative (TN)

Figure 48 Confusion matrix notation. Separate matrices were replicated for each of the three considered charge actions (charging, discharging and ‘no action’).

The assessment of the effectiveness of the schedule was performed based on different performance measures derived from those matrices, such as sensitivity, specificity, false-positive rate, and precision/positive predicted value. All these indicators “describe the level at which the evaluated classifier succeeds or fails to correctly detect a positive class” [229]. In this case, the positive class is an action set by the scheduling tool to be performed by BES (either charging, discharging or “no action”). The sensitivity gives the proportion of actual positive instances that are correctly identified. The specificity gives the proportion of actual negative instances that are correctly identified. The false-positive rate indicates the proportion of the number of negative occurrences that were predicted to be positive. Finally, precision is the proportion of positive instances that were correctly identified [203][229]. Based on the confusion matrix notation from Fig. 48, these performance measures can be calculated as follows:

$$\text{sensitivity} = TP/(TP+FN) \tag{30}$$

$$\text{specificity} = TN/(TN+FP) \tag{31}$$

$$\text{false-positive rate} = FP/(TN+FP) \tag{32}$$

$$precision=TP/(TP+FP) \quad (33)$$

As stated in [229], using all performance measures derived from the confusion matrix at the same time leads to significant informational redundancy. Usually, the performance measure is performed by assessing a complementary pair of indicators such as sensitivity with specificity, precision with sensitivity or true positive rate with the false positive rate. It is because one of the indicators describes the ability to detect the positive occurrence, and the other one describes the capability to detect negative instances [229]. In this work, the analysis of sensitivity and specificity is carried out to evaluate the schedule effectiveness.

When selecting the best classification method, ideally, both its sensitivity and specificity should be high; in practice, it is a compromise based on application-specific criteria. The method with very high sensitivity does not perform well if it is characterised by poor specificity and vice versa. These two quantities have complementary characteristics; hence, it is necessary to achieve high values for both of them to ensure effectiveness in classification. The sensitivity indicates how good a method is in predicting positive outcomes (performing the required action: charging/discharging and hold actions in this case), and the specificity gives information on how good the model performs with the prediction of "not performing this action" (not performing either charging, discharging or 'hold action' in this case). When specificity is high, it means that the scheduler sets fewer cases of actions to be executed even if they should not be executed at a particular time. For the BES, it is crucial that charging and discharging actions, set by the charge scheduler, are not executed when they should not be performed, as it can reduce the ability of this device to achieve system goals (grid export reduction and increase in self-consumption in this case). More importantly, this situation can negatively influence the health of the battery due to misuse. For this reason, specificity is treated as the leading criterion for assessing the schedule effectiveness in this work and sensitivity is treated as the subsequent criterion.

In the presented work, the effectiveness of the scheduler model employing a different method of demand forecasting was evaluated compared to the schedule based on a perfect demand forecast. The analysis of effectiveness was based on the performance of predictions for the three possible actions that storage can perform: discharge, charge or 'no action' in a given interval of time. The calculated performance measures for all possible simulated cases are summarised in Table 16. According to Table 16, the scheduler model employing GP forecast of demand achieves the highest specificity in the prediction of the energy storage actions except for predicting the "no action" state (hold action for the storage), for which the model employing GBM demand forecasting performs the best. The scheduler model that uses GP regression to forecast demand was chosen as the potential candidate with good effectiveness in the charge and the discharge action prediction. It also achieves a higher sensitivity in predicting the "no action" state than the GBM model. The analysis of the model performance in the grid export reduction for the model employing GP shows that the grid export reduction achieved by this model compared to the schedule based on perfect demand forecast is lower only by 2.7%. It is the second-best result after the persistence model, which was off only by 2.4% in grid export reduction compared to the perfect forecast demand case. The model employing the GP forecast also achieved the second-best increase in self-consumption after the GBM model. The self-consumption increase of the GP model was lower by 6.1% compared to the perfect demand forecast case. In the case of the GBM model, the increase in self-consumption decreases by 4.2% compared to the perfect demand case. The persistence forecast does not perform well with respect to the increase in self-consumption, which was lower by 11% compared to the perfect demand forecast case, and thus was rejected as the potential candidate. In the case of the GBM model, which performed better in self-consumption than the GP model in comparison to the perfect demand case, this model achieved lower grid export reduction than GP and additionally has lower specificity in the prediction of the charge and discharge actions, the chosen leading criterion of schedule effectiveness, thus also was rejected. The above analysis of the model performance in the

grid export reduction and self-consumption increase can support the choice of the GP model as the most promising candidate.

Table 16 Performance measure values for prediction of action of the BES for Lithium-ion battery.

Action	Performance Measure		The demand forecasting model used					
			Gaussian Process	Gradient boost machine	Persistence	ARIMA	Neural Network	Ensemble forecast (all)
Discharge	Sensitivity	(%)	90.8	91.7	90.9	78.9	87.5	91.5
	Specificity		**91.6**	90.9	91.5	87.3	86.9	91.5
	False-positive rate		8.4	9.1	8.5	12.7	13.1	8.5
	Precision		91.8	91.2	91.6	86.5	87.3	91.7
Charge	Sensitivity	(%)	93.9	94.4	92.7	88.4	85.7	93.1
	Specificity		**96.4**	96	96.3	92.2	94	96.2
	False-positive rate		3.6	4	3.7	7.8	6	3.8
	Precision		92.4	91.7	92.1	84.2	87	91.9
No action	Sensitivity	(%)	81.7	78.8	83.4	74.2	79.4	82.4
	Specificity		96.2	**97**	96.2	91.2	95.3	96.7
	False-positive rate		3.8	3	3.8	8.8	4.7	3.3
	Precision		81.7	84.6	82.3	63.9	77.9	83.9

The most accurate forecasting of demand does not necessarily provide the most effective schedule for all possible BES actions. It indicates that further work on the influencing

factors on the schedule effectiveness should be performed. Furthermore, the influence of the performance of the forecasting model used in the scheduling tool should be more closely investigated.

5.2.3 Effect of the Error in Demand Forecasting on the Maloperation Level of a Lithium-ion Battery

In this section, the examination of the influence of the BES schedule produced by the scheduling tool employing different demand forecasting models on the level of maloperation of this device for the Lithium-ion battery was carried out. For this purpose, the IOHMM model of the Lithium-ion battery (maloperation model) developed in the previous chapter was used. The charging/discharging battery schedules generated were run through the IOHMM model, and the output of the model, health/maloperation indexes, were compared. The cumulative health indexes generated by the battery model due to the applied schedule based on different forecasting methods and perfect cases[20] are presented in Fig. 49 and Fig. 50 (which shows the cumulative health index change from the time step 550 onwards). The maloperation level of the battery due to the applied schedule based on the perfect demand forecast and PV generation forecast (persistence-based) was included in the simulations to allow comparison of the simulation with different demand forecasts against the perfect forecast demand case. The maloperation level of the battery operated using a schedule prepared based on original demand and original generation was also included. The purpose of this addition was to show the effect of the PV generation forecast error alone on the maloperation level of BES (perfect forecast demand case versus perfect case). The cumulative health indexes at the end of the simulation period are summarized in Table 17.

[20] Perfect demand case – perfect demand data with PV generation forecasted
Perfect case – original demand and original PV generation data used

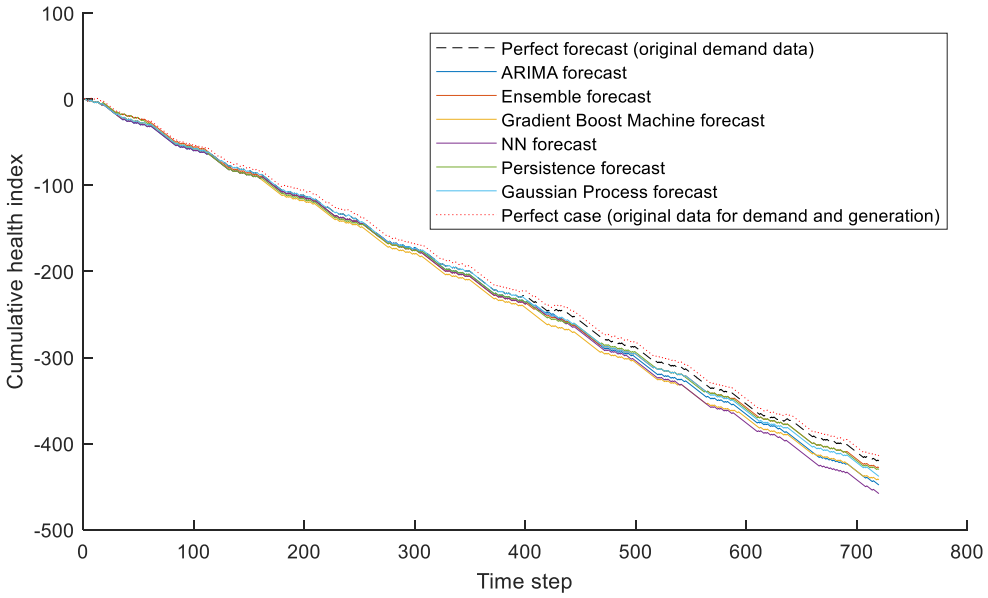

Figure 49 Comparison of cumulative health indexes generated by Lithium-ion battery model based on the schedules prepared by scheduler employing different demand forecasting models.

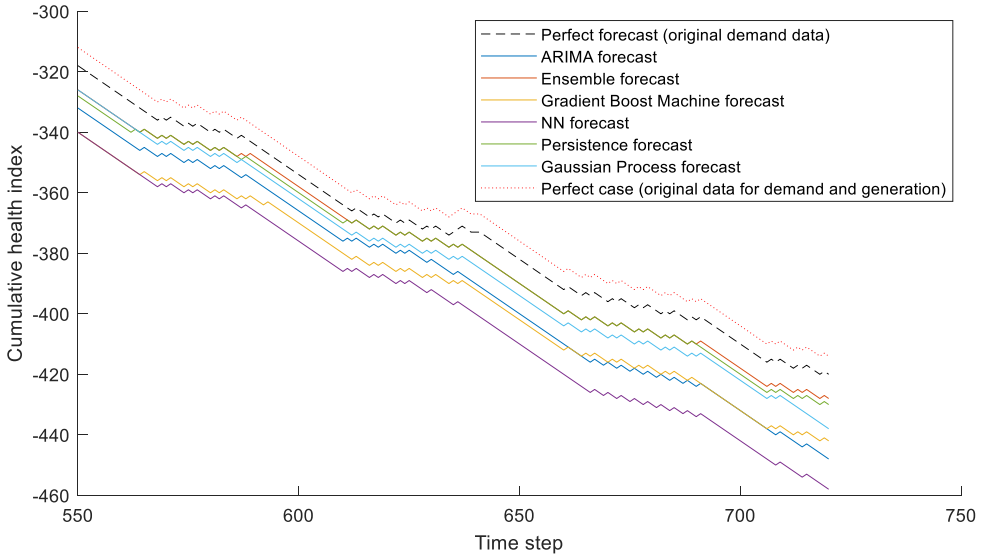

Figure 50 Detail of comparison of cumulative health indexes, from time step 550 to the end of the simulation, generated by Lithium-ion battery.

From Fig. 49, it is clear that the batteries are degraded in a similar fashion by the first 200 steps, where the level of maloperation starts to diverge for schedules based on different forecasting methods. The increasing spread between the estimated cumulative health indexes produced based on the schedule generated employing different demand forecasting models is due to the accumulation of the error in the demand prediction. This indicates that accuracy in demand prediction is very important as it can affect battery health. The schedule based on the ensemble forecast and persistence forecast similarly influenced the battery health and resulted in the lowest level of maloperation among all schedules considered compared to the perfect demand case.

Table 17 Forecasting error and the Maloperation level of the battery due to the applied operating regime generated based on the different demand forecasting models while charging/discharging schedule generation.

Forecasting model	Forecasting error	Health measure of battery
	Mean absolute percentage error	Cumulative health index generated due to applied schedule
	[%]	[ ]
Perfect case (original demand and generation data)	-	**-414**
Perfect forecast (original demand data)	-	**-420**
Ensemble forecast (all)	**27.4**	-428
Gradient boost Machine	29	-442
Persistence forecast	29.7	-430
Gaussian Process	30.6	-438
ARIMA model	48.2	-448
Neural network	50	-456

From Table 17, it can be seen that the degradation level of the battery that was run with the schedule produced when employing the perfect demand data reached -420 compared to -414 for the schedule based on actual data. In Fig. 49 and Fig. 50, the cumulative maloperation level curve for the perfect demand case is pushed down compared to the case with the original demand and original generation data used in the simulation. The health of the battery in this case becomes negatively impacted due to the applied schedule and the impact on health is solely due to the influence of the generation forecast error on the produced schedule. As the PV generation forecast is kept the same in all remaining scenarios, except the perfect case, the health changes when compared to the perfect demand case are due to the influence of the demand forecast method used in schedule generation. The degradation level for the schedule based on ensemble and persistence forecast reached -428 and -430 levels, respectively, compared to -420 for the perfect demand case, Table 17. The highest level of maloperation due to the applied schedule, -456, achieved the schedule based on the neural network demand forecast model, which is lower by -36 from the perfect demand case. When analysing the most promising forecast model to be used in the scheduling tool, considering the influence on the health of this device, the schedule based on ensemble and persistence forecast performed the best compared to all other considered methods with respect to the perfect demand case. The GP model, which was chosen as the most promising model when the effectiveness of prediction and providing the grid reduction export and self-consumption functions were used as a criterion of choice, achieved the third-lowest maloperation level of -438, which was lower by – 18 compared to perfect demand case. When including all remaining criteria (specificity and sensitivity) in conjunction with the level of maloperation in assessment, the GP model will keep its position as the most promising method among all considered in this work. The ensemble forecast provides the lowest level of maloperation, but it does not do so well with providing the required function by the scheduler (i.e. export to grid reduction and self-consumption increase). In turn, a schedule based on the persistence demand forecast achieves a much lower self-consumption level compared to GP and GBP models. Additionally, it has lower specificity

and sensitivity in predicting charge and discharge actions than the GP model, thus is also rejected as a potential candidate.

The Pearson and Spearman correlations were applied are applied here to measure the association between the maloperation level and the battery performance measures used in this work to assess schedule effectiveness. The Pearson correlation only evaluates the linear relationship between two variables. From the examination of data, there was not clear whether linear or monotonic relationships existed between analysed variables; for this reason, also the Spearman correlation was used (this method measures the monotonic association between two variables). The summary of this analysis is included in Table 18.

Table 18 Association strength between cumulative health index at the end of simulation and variables describing the performance of the scheduler.

Cumulative index association with		Pearson correlation		Spearman correlation	
		Correlation coefficient	P-value	Correlation coefficient	P-value
Demand forecast error (MAPE)		**-0.79**	**0.05**	**-0.94**	**0.001**
Reduction of export to the grid		0.76	0.08	0.60	0.24
Increase in self-consumption		0.43	0.39	0.48	0.35
Specificity for predicting action	Discharge	0.77	0.07	0.63	0.19
	Charge	0.063	0.18	0.60	0.20
	‘no action’	0.43	0.38	0.72	0.10
Sensitivity for predicting action	Discharge	0.57	0.24	0.60	0.24
	Charge	0.79	0.06	0.49	0.36
	‘no action’	0.70	0.12	0.77	0.10

The analysis was carried out for the MAPE, export to grid reduction, increase of self-consumption, specificity and sensitivity of prediction charge, discharge and 'no action' by the scheduler. The export to grid reduction and increase in self-consumption were the main performance measure of the developed scheduler tool hence, they were included in this analysis. The two last variables, specificity and sensitivity, were selected as they were treated as leading and subsequent criteria respectively for assessing schedule effectiveness in prediction actions, as mentioned in Section 5.2.2.

From Table 18, it is clear that only the correlation between the forecast error -MAPE and the cumulative health index can be treated as statistically significant. In the rest of the cases, the p-values associated with the correlation coefficients are greater than the significance level of 0.05; thus, the results were treated as inconclusive evidence of an association between variables. A high negative Pearson correlation[21] was found between error in demand forecasting and the inferred battery level of maloperation at the end of the simulation with a value of -0.79 and a corresponding p-value of 0.05. There was also a very strong negative monotonic correlation (Spearman)[21] between those two variables, -0.94, with a corresponding p-value of 0.001. This result indicates that with the increase in the demand forecasting error, the level of battery degradation increases (reflected by a decrease in the health metric). This kind of relationship between forecast error and battery degradation was expected. If the battery performs the action that was scheduled by 'mistake' due to a wrong demand prediction, it could potentially harm this device. This result can imply that the demand forecasting error influences battery health by introducing in the schedule of this device the actions that misuse this device. This misuse instance might lead to battery performance deterioration and potential hazards for this device and the whole power system comprising it.

[21] Note that the correlations were calculated based only on six available pair of values of error and battery maloperation level.

5.3 Summary of Chapter Findings

This chapter has presented an availability-based algorithm for producing day-ahead electrical energy storage schedules that reduce the energy export to the grid and additionally increase self-consumption in the modelled system. It has also discussed the influence of the demand forecasting methods used to generate the BES schedule on its effectiveness, provision of required functions by this device and level of maloperation of BES due to the applied schedule.

The most significant findings of chapter four can be summarised in the following points.

1. The most accurate demand forecasting models do not necessarily give the most effective schedule for all possible BES actions. This can have important implications for this device and the system comprising it. Performing charging/discharging actions of BES when they should not be performed can reduce the ability of this device to provide required functions due to the accelerated deterioration of battery performances, potentially resulting in device failures or safety hazards in the system. Other important implications of not appropriately scheduled action of the BES, this time from the system operator's point of view, are the potential reduction of power system capability for continuous energy provision to the consumers. For example, when demand in the system is much higher than a generation available at a particular time, and the discharge action for BES was not scheduled at this time, the required energy for the user may not be provided to him due to the wrongly assigned action to be performed by the BES. This finding indicates that further work on the influencing factors on the schedule effectiveness should be performed. Furthermore, the influence of the performance of demand forecasting models used in schedule generation should be more closely investigated, and their impact on the generated BES schedule needs to be evaluated.
2. The strong dependency between the MAPE of the demand forecasting method used, and energy export reduction (shown by high negative Pearson and Spearman

correlation) indicates that a forecasting method with low MAPE is preferred as it can improve the overall storage system performance. Although the exception of schedule based on ensemble load forecast, which despite the lowest MAPE achieved, did not provide the highest reduction in the energy export to the grid, indicates that further research on the influence of the performances of the forecasting methods on the performance of the BES schedule should be investigated and more closely evaluated.

3. The observed increasing spread between the estimated cumulative health indexes produced based on the schedule generated employing different demand forecasting models that resulted from the accumulation of the error in the demand prediction indicates that accuracy in demand prediction is very important as it can affect battery health.

CHAPTER 6

6. Conclusions and Further Work

This thesis contributed to the development of a novel Battery Energy Storage health measure, which requires nothing more than only operational monitoring to support its operation. This non-invasive approach, based on the Input-Output Hidden Markov Model, predicts the extent to which a battery asset has been maloperated based only on the battery operating regime imposed.

Chapter Two has contributed to the formulation of rules based on an in-depth review of seven battery technologies and underlying degradation mechanisms which constituted the basis for the novel health index generation required for model training. In this chapter, the battery operational preferences dictated by its chemistry and physics were translated into the novel health index, maloperation level, which then was learned by the proposed Input-Output Hidden Markov Model, enabling automatic future recognition of such events by the developed model using only the limited data observed from the battery operational regime. In this chapter, the battery operational preferences were summarised in tabular form, constituting a potential guide when selecting battery technology for considered application.

Chapter Three contributed to an increased understanding of the current challenges in battery health prognostics. In this chapter, the state of art in the modelling of battery health prognostics was reviewed with a discussion about the advantages and disadvantages of currently used approaches in battery health modelling. Based on this review, the niche in battery modelling was found. This work has filled this niche. This chapter also summarised the research questions answered in chapter four of this thesis.

Chapter Four contributed to the design of a novel machine-learning model employing the IOHMM, which captures battery degradation mechanisms without considering the detailed chemistry and physics of the asset. The applicability of the developed model to predict battery asset degradation level was assessed against randomised battery usage lab data accessible from the NASA Prognostic Centre of Excellence Data repository [206]. It was shown that the battery degradation level expressed in the novel metric proposed in this thesis is comparable to capacity fading, a commonly used metric for battery degradation and ageing. The advantage of the proposed approach over using capacity fade is the minimal data requirements for operation. The developed model does not require intensive measurements for its operation, and health/maloperation prediction is comparable with currently used metrics.

Chapter Five demonstrated the operational practicality of the developed model. It looked at how the demand forecast error influenced the effectiveness of the battery schedules generated based on this forecast and how it is reflected in the battery maloperation level. The availability-based scheduler was designed in this chapter, which employed different forecasting methods. Multiple schedules were generated based on different forecast methods. Those schedules were then assessed to determine how the accuracy of each forecasting method affected the effectiveness of the BES schedule and its performance in the export to the grid reduction and self-consumption increase. This chapter also looked if there is any association between the uncertainty due to the forecast of demand and the battery degradation level.

In summary, this thesis contributed to the development of non-invasive battery energy storage health metrics based on revised battery technologies and degradation mechanisms linked to chemistry and battery physics, supported by the development of a machine-learning model of maloperation level capturing degradation mechanisms, which requires nothing more than only operational monitoring to support its assessment. It also investigated how the forecast error, from demand forecasting, propagates to the

maloperation matrix and how much uncertainty in the forecast influences the maloperation level.

6.1 Recommendations

No model includes every aspect of the real world or real system [230], as it constitutes only its representation. In this section, some recommendations regarding possible improvements to the developed battery maloperation/health model are discussed. Implementing proposed enhancements, such as including additional variables impacting battery asset wellbeing, can further extend the ability of the model to predict battery health. Additionally, in this section, some potential collaborative multidisciplinary research topics are recommended to further enhance the developed battery health/maloperation model and to increase understanding of the impact of the demand forecasts on the BES health, schedule and its ability to provide required functions. Further understanding of the influence of demand forecasts on the BES health and schedule can be beneficial for more informed battery management, especially when scheduling its operation in advance.

6.1.1 Recommended Battery Maloperation Model Improvements

The battery maloperation model developed in this work can be further improved by:

- Using a 'weighted' preference index to accommodate the different levels of influence of the particular operation on the battery health. Currently, the model uses indexes with the same weight at any given time. More appropriate could be to use a scaled index to be able to accommodate, for example, prolonged action against the battery preferences. For example, the longer we charge the Zn/Br2 battery before discharging it to the empty state, the higher probability of growing dendrites and a higher level of deterioration of device performance or even device damage. It would be beneficial if the length of the action performed against battery preferences would be reflected in the index. The longer the negative action

is performed, the lower the index should be generated. In the developed model, it is always a negative one in such a situation regardless of the length of action performed against battery preferences. This requires a deeper understanding and more complex knowledge of battery chemical processes and ways of modelling them than it is currently in a state of research and constitutes a potential collaboration platform with experts in battery chemistry.

- The temperature of the battery and ambient temperature has a significant influence on the battery degradation processes. In the developed model, this dependency was excluded from the modelling. It was assumed that the battery operating environment was not hostile to this device and that the sole threat to asset life was through misuse. This is dictated by the fact that in the grid storage applications, regardless if the battery is stored in containers, dedicated rooms in the building or if we deal with ready-to-install systems, the system is always equipped with a temperature management system, which maintains the optimum conditions for the batteries. Adding this information to the model can allow extending the application of the developed model to those where the battery is not used in the temperature-controlled environment.
- In addition to the improvements in the developed models, it would be beneficial to perform the second out-of-sample test and validation of the battery models for all battery technologies covered in this work, as it was not implemented due to the lack of available suitable datasets with the exception of lithium-ion battery for which this test was performed.

6.1.2 Proposed Collaborative Research

The work proposed in this thesis opens the numerous possible direction for further research, with possible cross-field collaboration. Some of the possibilities are as follows:

- Collaborative research with the experts in the area of battery chemistry to improve the developed battery maloperation model by including the weighted preference index to catch dependency on the length of action performed

against battery preference on device degradation and health, which can even further enhance the model capabilities to predict battery maloperation level.

- Further research on the influence of the forecasting model (used in the prediction of electrical demand) on the generation of the BES schedule, its effectiveness and battery health constitutes potential collaboration with experts in the forecasting area. This research will be beneficial for smart grid applications as the outcome can improve the understanding of the forecasting influence on the BES health and ability to provide required functions due to operation dictated by schedule based on the forecast of demand and generation.
- The research on the influence of the PV generation forecasting model on the generation of the BES schedule, its effectiveness and battery health constitutes potential collaboration with experts in the forecasting area.
- Development of a novel charging and discharging scheduler that plans the charging regime of BES under uncertainties (uncertain output of renewable generation, high prediction error of disaggregated demand, battery itself), reinforcement learning-based (for example, using Partially Observable Markov Decision Processes). The developed battery maloperation model can help accommodate the uncertainty related to the battery technology in the scheduler and can act as the policy function in an automated scheduler based on POMDP or another type of algorithm. The developed model can act as the proxy for the degradation costs in terms of maloperation level. It is not monetary cost but rather some measure of battery maloperation level that, by impacting the battery health, can generate monetary costs due to, for example, premature replacement of this device. In other words, the maloperation index indicates that the battery was operated against its chemistry and preferences, leading to battery health degradation, which can incur some additional costs in the system.
- Joining efforts with the researchers proposing the battery health prediction based solely on the temperature to produce a hybrid model incorporating the

health prediction based on battery maloperation proposed in this work with a model based on device temperature. This can result in a more complete model for battery health estimation.

7. Appendices

Appendix A.1 IOHMM Lead-acid battery model parameters.

A is the transition probability matrix, B is the observation probability matrix and π is the initial state probability.

For input signal:

'discharge action'

$$A = \begin{pmatrix} 0 & 0 & 1 & 0 & 0 & 0 \\ 0 & 0 & 1 & 0 & 0 & 0 \\ 0 & 0 & 0 & 0.4025 & 0 & 0.5975 \\ 0 & 0 & 0 & 0 & 1 & 0 \\ 1 & 0 & 0 & 0 & 0 & 0 \\ 0 & 1 & 0 & 0 & 0 & 0 \end{pmatrix}$$

'hold action'

$$A = \begin{pmatrix} 0 & 0 & 1 & 0 & 0 & 0 \\ 0 & 0 & 1 & 0 & 0 & 0 \\ 0 & 0 & 0 & 1 & 0 & 0 \\ 0 & 0 & 0 & 0 & 1 & 0 \\ 1 & 0 & 0 & 0 & 0 & 0 \\ 0 & 1 & 0 & 0 & 0 & 0 \end{pmatrix}$$

'charge action'

$$A = \begin{pmatrix} 0 & 0 & 1 & 0 & 0 & 0 \\ 0 & 0 & 1 & 0 & 0 & 0 \\ 0 & 0 & 0 & 0.4968 & 0 & 0.5032 \\ 0 & 0 & 0 & 0 & 1 & 0 \\ 1 & 0 & 0 & 0 & 0 & 0 \\ 0 & 1 & 0 & 0 & 0 & 0 \end{pmatrix}$$

For input signal:

'discharge action'

$$B = \begin{pmatrix} 0.8367 & 0 & 0.1633 \\ 0 & 0 & 1 \\ 0.5025 & 0 & 0.4975 \\ 1 & 0 & 0 \\ 1 & 0 & 0 \\ 0.001 & 0 & 0.999 \end{pmatrix}$$

'hold action'

$$B = \begin{pmatrix} 1 & 0 & 0 \\ 1 & 0 & 0 \\ 1 & 0 & 0 \\ 1 & 0 & 0 \\ 1 & 0 & 0 \\ 0.0299 & 0 & 0.9701 \end{pmatrix}$$

'charge action'

$$B = \begin{pmatrix} 1 & 0 & 0 \\ 1 & 0 & 0 \\ 1 & 0 & 0 \\ 1 & 0 & 0 \\ 1 & 0 & 0 \\ 1 & 0 & 0 \end{pmatrix}$$

$$\pi = \begin{pmatrix} 0 \\ 0 \\ 0 \\ 0 \\ 0 \\ 1 \end{pmatrix}$$

Appendix A.2 IOHMM Lithium-ion battery model parameters.

A is the transition probability matrix, B is the observation probability matrix and π is the initial state probability.

For input signal:

'discharge action'

$$A = \begin{pmatrix}
0 & 0 & 0 & 0 & 0 & 0 & 0 & 1 & 0 & 0 & 0 \\
0 & 0 & 0 & 0 & 0 & 0 & 0 & 0 & 0 & 1 & 0 \\
1 & 0 & 0 & 0 & 0 & 0 & 0 & 0 & 0 & 0 & 0 \\
0 & 0 & 0 & 0 & 0 & 0 & 0 & 1 & 0 & 0 & 0 \\
1 & 0 & 0 & 0 & 0 & 0 & 0 & 0 & 0 & 0 & 0 \\
0 & 0 & 0 & 0 & 0 & 0 & 0 & 1 & 0 & 0 & 0 \\
1 & 0 & 0 & 0 & 0 & 0 & 0 & 0 & 0 & 0 & 0 \\
0 & 0 & 0 & 0 & 0 & 0 & 0 & 0 & 0 & 0 & 1 \\
0 & 1 & 0 & 0 & 0 & 0 & 0 & 0 & 0 & 0 & 0 \\
0 & 0 & 0 & 0.3742 & 0 & 0.6258 & 0 & 0 & 0 & 0 & 0 \\
0 & 0 & 0 & 0 & 0 & 0 & 0 & 0 & 1 & 0 & 0
\end{pmatrix}$$

For input signal:

'discharge action'

$$B = \begin{pmatrix}
1 & 0 & 0 \\
0.7143 & 0 & 0.2857 \\
0.9967 & 0 & 0.0033 \\
0.5201 & 0 & 0.4799 \\
0.9967 & 0 & 0.0033 \\
0.4880 & 0 & 0.5120 \\
0.9967 & 0 & 0.0033 \\
0.4000 & 0 & 0.6000 \\
0.2497 & 0 & 0.7503 \\
0.5000 & 0 & 0.5000 \\
0.6000 & 0 & 0.4000
\end{pmatrix}$$

$$\pi = \begin{pmatrix}
0 \\ 0 \\ 0 \\ 0 \\ 0 \\ 0 \\ 1 \\ 0 \\ 0 \\ 0 \\ 0
\end{pmatrix}$$

'hold action'

$$A = \begin{pmatrix}
0 & 0 & 0 & 0 & 0 & 0 & 0 & 1 & 0 & 0 & 0 \\
0 & 0 & 0 & 0 & 0 & 0 & 0 & 0 & 0 & 1 & 0 \\
1 & 0 & 0 & 0 & 0 & 0 & 0 & 0 & 0 & 0 & 0 \\
0 & 0 & 0 & 0 & 0 & 0 & 0 & 1 & 0 & 0 & 0 \\
1 & 0 & 0 & 0 & 0 & 0 & 0 & 0 & 0 & 0 & 0 \\
0 & 0 & 0 & 0 & 0 & 0 & 0 & 1 & 0 & 0 & 0 \\
1 & 0 & 0 & 0 & 0 & 0 & 0 & 0 & 0 & 0 & 0 \\
0 & 0 & 0 & 0 & 0 & 0 & 0.0018 & 0 & 0 & 0 & 0.9982 \\
0 & 1 & 0 & 0 & 0 & 0 & 0 & 0 & 0 & 0 & 0 \\
0 & 0 & 0 & 0.3742 & 0 & 0.6258 & 0 & 0 & 0 & 0 & 0 \\
0 & 0 & 0 & 0 & 0 & 0 & 0 & 0 & 1 & 0 & 0
\end{pmatrix}$$

'hold action'

$$B = \begin{pmatrix}
1 & 0 & 0 \\
1 & 0 & 0 \\
1 & 0 & 0 \\
1 & 0 & 0 \\
1 & 0 & 0 \\
1 & 0 & 0 \\
1 & 0 & 0 \\
1 & 0 & 0 \\
1 & 0 & 0 \\
1 & 0 & 0 \\
0.4995 & 0 & 0.5005
\end{pmatrix}$$

'charge action'

$$A = \begin{pmatrix}
0 & 0 & 0 & 0 & 0 & 0 & 0 & 1 & 0 & 0 & 0 \\
0 & 0 & 0 & 0 & 0 & 0 & 0 & 0 & 0 & 1 & 0 \\
1 & 0 & 0 & 0 & 0 & 0 & 0 & 0 & 0 & 0 & 0 \\
0 & 0 & 0 & 0 & 0 & 0 & 0 & 1 & 0 & 0 & 0 \\
1 & 0 & 0 & 0 & 0 & 0 & 0 & 0 & 0 & 0 & 0 \\
0 & 0 & 0 & 0 & 0 & 0 & 0 & 1 & 0 & 0 & 0 \\
1 & 0 & 0 & 0 & 0 & 0 & 0 & 0 & 0 & 0 & 0 \\
0 & 0 & 0 & 0 & 0 & 0 & 0 & 0 & 0 & 0 & 1 \\
0 & 1 & 0 & 0 & 0 & 0 & 0 & 0 & 0 & 0 & 0 \\
0 & 0 & 0 & 0.3742 & 0 & 0.6258 & 0 & 0 & 0 & 0 & 0 \\
0 & 0 & 0 & 0 & 0 & 0 & 0 & 0 & 1 & 0 & 0
\end{pmatrix}$$

'charge action'

$$B = \begin{pmatrix}
1 & 0 & 0 \\
1 & 0 & 0 \\
1 & 0 & 0 \\
1 & 0 & 0 \\
1 & 0 & 0 \\
1 & 0 & 0 \\
1 & 0 & 0 \\
1 & 0 & 0 \\
1 & 0 & 0 \\
1 & 0 & 0 \\
1 & 0 & 0
\end{pmatrix}$$

Appendix A.3 IOHMM Nickel Cadmium battery model parameters.

A is the transition probability matrix, B is the observation probability matrix and π is the initial state probability.

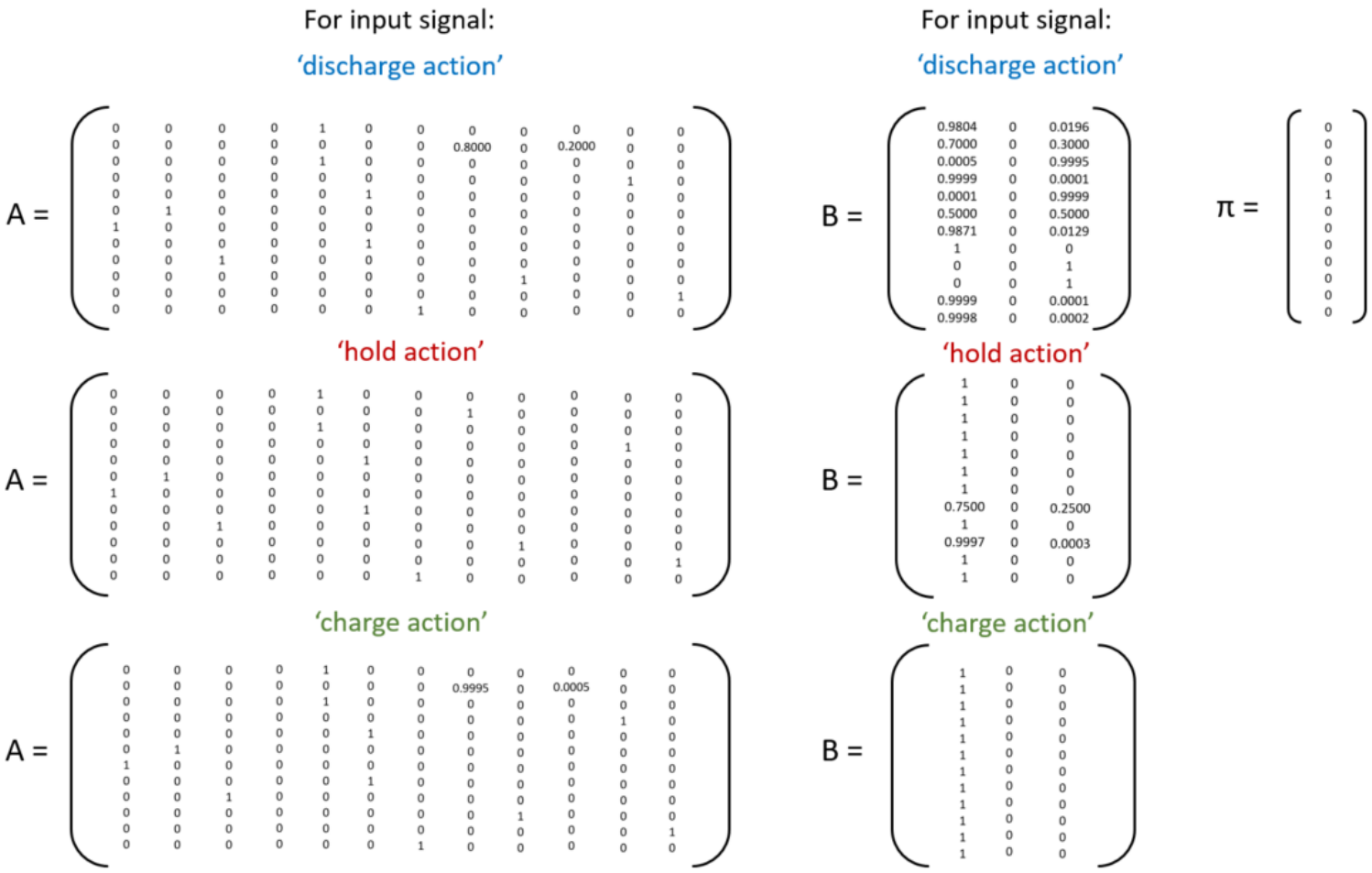

Appendix A.4 IOHMM NiMH battery model parameters.

A is the transition probability matrix, B is the observation probability matrix and π is the initial state probability.

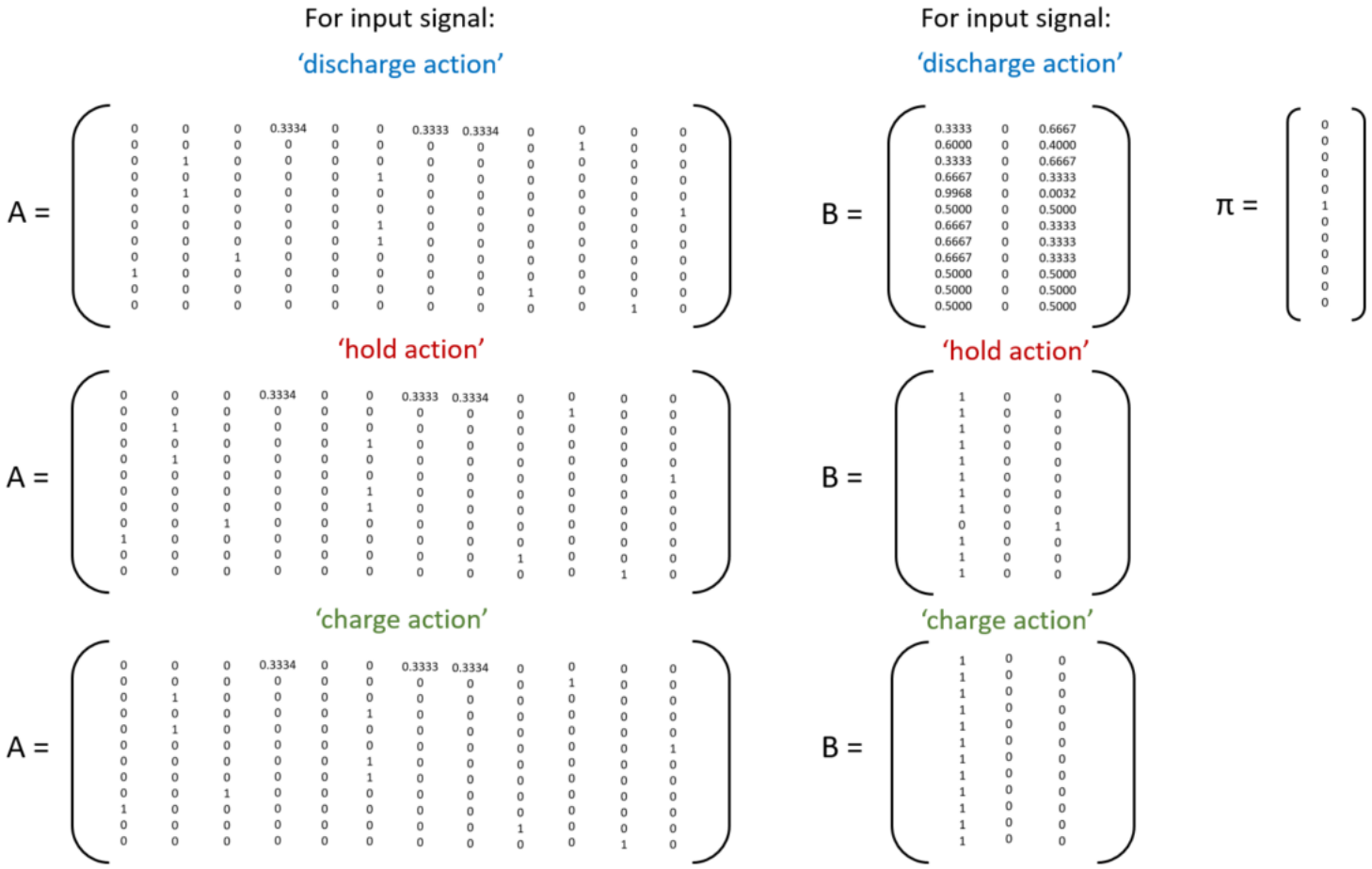

Appendix A.5 IOHMM sodium-sulphur battery model parameters.

A is the transition probability matrix, B is the observation probability matrix and π is the initial state probability.

For input signal:

'discharge action'

$$A = \begin{pmatrix} 0 & 0 & 0 & 0 & 0 & 1 & 0 & 0 & 0 & 0 & 0 & 0 \\ 0 & 0 & 0 & 0 & 0 & 0 & 0 & 0 & 1 & 0 & 0 & 0 \\ 0 & 1 & 0 & 0 & 0 & 0 & 0 & 0 & 0 & 0 & 0 & 0 \\ 0 & 1 & 0 & 0 & 0 & 0 & 0 & 0 & 0 & 0 & 0 & 0 \\ 0 & 1 & 0 & 0 & 0 & 0 & 0 & 0 & 0 & 0 & 0 & 0 \\ 0 & 0 & 0 & 0 & 0 & 0 & 0 & 0 & 1 & 0 & 0 & 0 \\ 1 & 0 & 0 & 0 & 0 & 0 & 0 & 0 & 0 & 0 & 0 & 0 \\ 0 & 1 & 0 & 0 & 0 & 0 & 0 & 0 & 0 & 0 & 0 & 0 \\ 0 & 0 & 0 & 0 & 0 & 0 & 0 & 0 & 0 & 1 & 0 & 0 \\ 0 & 0 & 0 & 0 & 0 & 0 & 1 & 0 & 0 & 0 & 1 & 0 \\ 0 & 0 & 0 & 0 & 0 & 0 & 0 & 0 & 0 & 0 & 0 & 0 \end{pmatrix}$$

'hold action'

$$A = \begin{pmatrix} 0 & 0 & 0 & 0 & 0 & 1 & 0 & 0 & 0 & 0 & 0 & 0 \\ 0 & 0 & 0 & 0 & 0 & 0 & 0 & 0 & 1 & 0 & 0 & 0 \\ 0 & 1 & 0 & 0 & 0 & 0 & 0 & 0 & 0 & 0 & 0 & 0 \\ 0 & 1 & 0 & 0 & 0 & 0 & 0 & 0 & 0 & 0 & 0 & 0 \\ 0 & 0 & 0 & 0 & 0 & 0 & 0 & 0 & 0 & 0 & 0 & 0 \\ 1 & 0 & 0 & 0 & 0 & 0 & 0 & 0 & 1 & 0 & 0 & 0 \\ 0 & 1 & 0 & 0 & 0 & 0 & 0 & 0 & 0 & 0 & 0 & 0 \\ 0 & 0 & 0 & 0 & 0 & 0 & 0 & 0 & 0 & 1 & 0 & 0 \\ 0 & 0 & 0 & 0 & 0 & 0 & 1 & 0 & 0 & 0 & 1 & 0 \\ 0 & 0 & 0 & 0 & 0 & 0 & 0 & 0 & 0 & 0 & 0 & 0 \end{pmatrix}$$

'charge action'

$$A = \begin{pmatrix} 0 & 0 & 0 & 0 & 0 & 1 & 0 & 0 & 0 & 0 & 0 & 0 \\ 0 & 0 & 0 & 0 & 0 & 0 & 0 & 0 & 1 & 0 & 0 & 0 \\ 0 & 1 & 0 & 0 & 0 & 0 & 0 & 0 & 0 & 0 & 0 & 0 \\ 0 & 1 & 0 & 0 & 0 & 0 & 0 & 0 & 0 & 0 & 0 & 0 \\ 0 & 0 & 0 & 0 & 0 & 0 & 0 & 0 & 0 & 0 & 0 & 0 \\ 1 & 0 & 0 & 0 & 0 & 0 & 0 & 0 & 1 & 0 & 0 & 0 \\ 0 & 1 & 0 & 0 & 0 & 0 & 0 & 0 & 0 & 0 & 0 & 0 \\ 0 & 0 & 0 & 0 & 0 & 0 & 0 & 0 & 0 & 1 & 0 & 0 \\ 0 & 0 & 0 & 0 & 0 & 0 & 1 & 0 & 0 & 0 & 1 & 0 \\ 0 & 0 & 0 & 0 & 0 & 0 & 0 & 0 & 0 & 0 & 0 & 0 \end{pmatrix}$$

For input signal:

'discharge action'

$$B = \begin{pmatrix} 0.5000 & 0 & 0.5000 \\ 0.9982 & 0 & 0.0018 \\ 0.9967 & 0 & 0.0033 \\ 0.9967 & 0 & 0.0033 \\ 0.9967 & 0 & 0.0033 \\ 0.5000 & 0 & 0.5000 \\ 0.7143 & 0 & 0.2857 \\ 0.9967 & 0 & 0.0033 \\ 0.4000 & 0 & 0.6000 \\ 0.6000 & 0 & 0.4000 \\ 0.2500 & 0 & 0.7500 \end{pmatrix}$$

'hold action'

$$B = \begin{pmatrix} 1 & 0 & 0 \\ 1 & 0 & 0 \\ 1 & 0 & 0 \\ 1 & 0 & 0 \\ 1 & 0 & 0 \\ 1 & 0 & 0 \\ 1 & 0 & 0 \\ 1 & 0 & 0 \\ 1 & 0 & 0 \\ 0.5000 & 0 & 0.5000 \\ 1 & 0 & 0 \end{pmatrix}$$

'charge action'

$$B = \begin{pmatrix} 1 & 0 & 0 \\ 1 & 0 & 0 \\ 1 & 0 & 0 \\ 1 & 0 & 0 \\ 1 & 0 & 0 \\ 1 & 0 & 0 \\ 1 & 0 & 0 \\ 1 & 0 & 0 \\ 1 & 0 & 0 \\ 1 & 0 & 0 \\ 1 & 0 & 0 \end{pmatrix}$$

$$\pi = \begin{pmatrix} 0 \\ 0 \\ 0.4118 \\ 0.2352 \\ 0.0710 \\ 0 \\ 0 \\ 0.2821 \\ 0 \\ 0 \\ 0 \end{pmatrix}$$

Appendix A.6 IOHMM Zn/Br_2 battery model parameters.

A is the transition probability matrix, B is the observation probability matrix and π is the initial state probability.

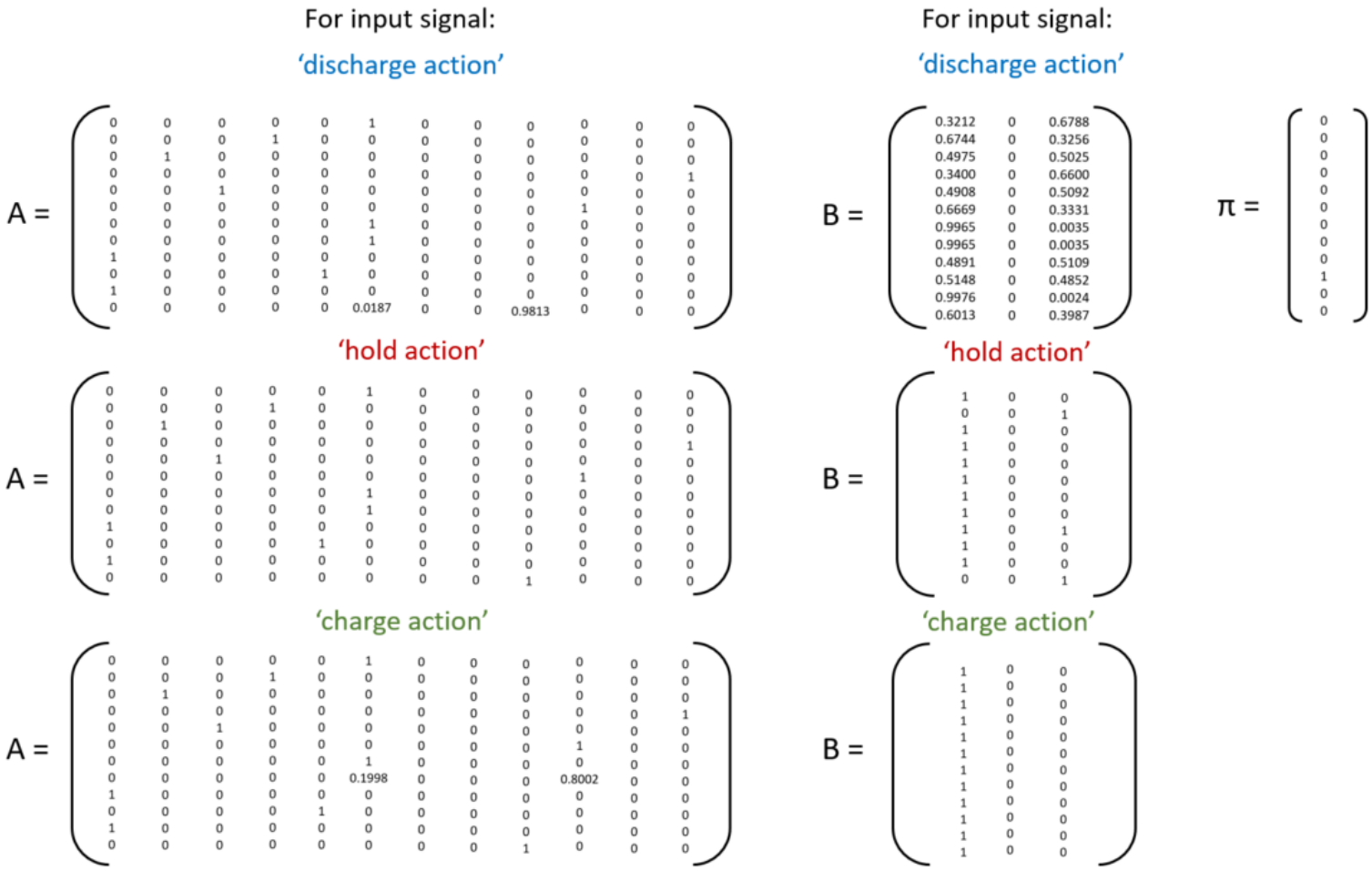

Appendix A.7 IOHMM VRFB model parameters.

P is the transition probability matrix, B is the observation probability matrix and π is the initial state probability.

For input signal:

'discharge action'

$$A = \begin{pmatrix}
0 & 1 & 0 & 0 & 0 & 0 & 0 & 0 & 0 & 0 & 0 & 0 \\
0 & 0 & 0 & 1 & 0 & 0 & 0 & 0 & 0 & 0 & 0 & 0 \\
0 & 0 & 0 & 0 & 0 & 0 & 0 & 0 & 1 & 0 & 0 & 0 \\
0 & 0 & 0 & 0 & 0 & 0 & 0 & 0 & 0 & 1 & 0 & 0 \\
0 & 0 & 0 & 0 & 0 & 0 & 0 & 0 & 1 & 0 & 0 & 0 \\
0 & 0 & 0.3333 & 0 & 0.3333 & 0 & 0.3333 & 0 & 0 & 0 & 0 & 0 \\
0 & 0 & 0 & 0 & 0 & 0 & 0 & 0 & 1 & 0 & 0 & 0 \\
0 & 0 & 0 & 0 & 0 & 0 & 0 & 0 & 1 & 0 & 0 & 0 \\
0 & 1 & 0 & 0 & 0 & 0 & 0 & 0 & 0 & 0 & 0 & 0 \\
0 & 0 & 0 & 0 & 0 & 0 & 0 & 0 & 0 & 0 & 0 & 1 \\
0 & 0.7126 & 0 & 0 & 0 & 0 & 0 & 0 & 0.2874 & 0 & 0 & 0 \\
0 & 0 & 0 & 0 & 0 & 1 & 0 & 0 & 0 & 0 & 0 & 0
\end{pmatrix}$$

$$B = \begin{pmatrix}
0.9994 & 0 & 0.0006 \\
0.5000 & 0 & 0.5000 \\
0.5000 & 0 & 0.5000 \\
0.2500 & 0 & 0.7500 \\
0.5000 & 0 & 0.5000 \\
0.4000 & 0 & 0.6000 \\
0.5000 & 0 & 0.5000 \\
0.9985 & 0 & 0.0015 \\
0.2500 & 0 & 0.7500 \\
0.6000 & 0 & 0.4000 \\
0.9991 & 0 & 0.0009 \\
0.4000 & 0 & 0.6000
\end{pmatrix}$$

$$\pi = \begin{pmatrix}
0 \\ 0 \\ 0 \\ 0 \\ 0 \\ 0 \\ 0 \\ 1 \\ 0 \\ 0 \\ 0 \\ 0
\end{pmatrix}$$

'hold action'

$$A = \begin{pmatrix}
0 & 1 & 0 & 0 & 0 & 0 & 0 & 0 & 0 & 0 & 0 & 0 \\
0 & 0 & 0 & 1 & 0 & 0 & 0 & 0 & 0 & 0 & 0 & 0 \\
0 & 0 & 0 & 0 & 0 & 0 & 0 & 0 & 1 & 0 & 0 & 0 \\
0 & 0 & 0 & 0 & 0 & 0 & 0 & 0 & 0 & 1 & 0 & 0 \\
0 & 0 & 0 & 0 & 0 & 0 & 0 & 0 & 1 & 0 & 0 & 0 \\
0 & 0 & 0.3333 & 0 & 0.3333 & 0 & 0.3333 & 0 & 0 & 0 & 0 & 0 \\
0 & 0 & 0 & 0 & 0 & 0 & 0 & 0 & 1 & 0 & 0 & 0 \\
0 & 0 & 0 & 0 & 0 & 0 & 0 & 0 & 1 & 0 & 0 & 0 \\
0 & 1 & 0 & 0 & 0 & 0 & 0 & 0 & 0 & 0 & 0 & 0 \\
0 & 0 & 0 & 0 & 0 & 0 & 0 & 0 & 0 & 0 & 0 & 1 \\
0 & 0.7234 & 0 & 0 & 0 & 0 & 0 & 0 & 0.2766 & 0 & 0 & 0 \\
0 & 0 & 0 & 0 & 0 & 1 & 0 & 0 & 0 & 0 & 0 & 0
\end{pmatrix}$$

$$B = \begin{pmatrix}
0.9993 & 0 & 0.007 \\
0.5000 & 0 & 0.5000 \\
0.5000 & 0 & 0.5000 \\
1 & 0 & 0 \\
0.5000 & 0 & 0.5000 \\
0.9994 & 0 & 0.0006 \\
0.5000 & 0 & 0.5000 \\
1 & 0 & 0 \\
0.5000 & 0 & 0.5000 \\
0.5000 & 0 & 0.5000 \\
0.9995 & 0 & 0.0005 \\
1 & 0 & 0
\end{pmatrix}$$

'charge action'

$$A = \begin{pmatrix}
0 & 1 & 0 & 0 & 0 & 0 & 0 & 0 & 0 & 0 & 0 & 0 \\
0 & 0 & 0 & 1 & 0 & 0 & 0 & 0 & 0 & 0 & 0 & 0 \\
0 & 0 & 0 & 0 & 0 & 0 & 0 & 0 & 1 & 0 & 0 & 0 \\
0 & 0 & 0 & 0 & 0 & 0 & 0 & 0 & 0 & 1 & 0 & 0 \\
0 & 0 & 0 & 0 & 0 & 0 & 0 & 0 & 1 & 0 & 0 & 0 \\
0 & 0 & 0.3333 & 0 & 0.3333 & 0 & 0.3333 & 0 & 0 & 0 & 0 & 0 \\
0 & 0 & 0 & 0 & 0 & 0 & 0 & 0 & 1 & 0 & 0 & 0 \\
0 & 0 & 0 & 0 & 0 & 0 & 0 & 0 & 1 & 0 & 0 & 0 \\
0 & 1 & 0 & 0 & 0 & 0 & 0 & 0 & 0 & 0 & 0 & 0 \\
0 & 0 & 0 & 0 & 0 & 0 & 0 & 0 & 0 & 0 & 0 & 1 \\
0 & 0.9716 & 0 & 0 & 0 & 0 & 0 & 0 & 0.0284 & 0 & 0 & 0 \\
0 & 0 & 0 & 0 & 0 & 1 & 0 & 0 & 0 & 0 & 0 & 0
\end{pmatrix}$$

$$B = \begin{pmatrix}
1 & 0 & 0 \\
1 & 0 & 0 \\
1 & 0 & 0 \\
1 & 0 & 0 \\
1 & 0 & 0 \\
1 & 0 & 0 \\
1 & 0 & 0 \\
1 & 0 & 0 \\
1 & 0 & 0 \\
1 & 0 & 0 \\
1 & 0 & 0 \\
1 & 0 & 0
\end{pmatrix}$$

Appendix B.1 Confusion matrices for Gradient Boost Machine and Persistence demand forecasts.

The confusion matrices for charging, discharging and "no action" state prediction of energy storage schedule for model employing (a) the Gradient Boost Machine demand forecast, (b) Persistence forecast

(a)

		PREDICTED ACTION	
	DISCHARGE	yes	no
ACTUAL ACTION (TARGET)	yes	1405	128
	no	135	1356

		PREDICTED ACTION	
	CHARGE	yes	no
ACTUAL ACTION (TARGET)	yes	913	54
	no	83	1974

		PREDICTED ACTION	
	NO ACTION	yes	no
ACTUAL ACTION (TARGET)	yes	413	111
	no	75	2425

(b)

		PREDICTED ACTION	
	DISCHARGE	yes	no
ACTUAL ACTION (TARGET)	yes	1393	140
	no	127	1364

		PREDICTED ACTION	
	CHARGE	yes	no
ACTUAL ACTION (TARGET)	yes	896	71
	no	70	1980

		PREDICTED ACTION	
	NO ACTION	yes	no
ACTUAL ACTION (TARGET)	yes	437	87
	no	94	2406

Appendix B.2 Confusion matrices for ARIMA and Neural Network demand forecasts.

The confusion matrices for charging, discharging and "no action" state prediction of energy storage schedule for model employing (a) ARIMA model, (b) Neural Network forecast.

(a)

		PREDICTED ACTION	
	DISCHARGE	yes	no
ACTUAL ACTION (TARGET)	yes	1210	323
	no	189	1302

		PREDICTED ACTION	
	CHARGE	yes	no
ACTUAL ACTION (TARGET)	yes	855	112
	no	161	1896

		PREDICTED ACTION	
	NO ACTION	yes	no
ACTUAL ACTION (TARGET)	yes	389	135
	no	220	2280

(b)

		PREDICTED ACTION	
	DISCHARGE	yes	no
ACTUAL ACTION (TARGET)	yes	1342	191
	no	195	1296

		PREDICTED ACTION	
	CHARGE	yes	no
ACTUAL ACTION (TARGET)	yes	829	138
	no	124	1933

		PREDICTED ACTION	
	NO ACTION	yes	no
ACTUAL ACTION (TARGET)	yes	416	108
	no	118	2382

Appendix B.3 Confusion matrices for Gaussian Process regression and Ensemble demand forecasts.

The confusion matrices for charging, discharging and "no action" state prediction of energy storage schedule for model employing (a) Gaussian Process Regression Model, (b) Ensemble forecast.

(a)

		PREDICTED ACTION	
	DISCHARGE	yes	no
ACTUAL ACTION (TARGET)	yes	1392	141
	no	125	1366

		PREDICTED ACTION	
	CHARGE	yes	no
ACTUAL ACTION (TARGET)	yes	908	59
	no	75	1982

		PREDICTED ACTION	
	NO ACTION	yes	no
ACTUAL ACTION (TARGET)	yes	428	96
	no	96	2404

(b)

		PREDICTED ACTION	
	DISCHARGE	yes	no
ACTUAL ACTION (TARGET)	yes	1403	130
	no	127	1364

		PREDICTED ACTION	
	CHARGE	yes	no
ACTUAL ACTION (TARGET)	yes	900	67
	no	79	1978

		PREDICTED ACTION	
	NO ACTION	yes	no
ACTUAL ACTION (TARGET)	yes	432	92
	no	83	2417

8. Bibliography

[1] D. A. Halamay, T. K. A. Brekken, A. Simmons, and S. McArthur, "Reserve Requirement Impacts of Large-Scale Integration of Wind, Solar, and Ocean Wave Power Generation," *IEEE Trans. Sustain. Energy*, vol. 2, no. 3, pp. 321–328, 2011.

[2] B. Hayes, J. Gruber, and M. Prodanovic, 'Short-Term Load Forecasting at the local level using smart meter data,' in 2015 IEEE Eindhoven PowerTech, 2015, pp. 1–6.," in *2015 IEEE Eindhoven PowerTech*, 2015, pp. 1–6.

[3] A. A. Muzumdar, C. N. Modi, G. M. Madhu, and C. Vyjayanthi, "Designing a Robust and Accurate Model for Consumer-Centric Short-Term Load Forecasting in Microgrid Environment," *IEEE Syst. J.*, vol. 16, no. 2, pp. 2448–2459, Jun. 2022.

[4] N. Mlilo, J. Brown, and T. Ahfock, "Impact of intermittent renewable energy generation penetration on the power system networks – A review," *Technol. Econ. Smart Grids Sustain. Energy*, vol. 6, no. 1, pp. 1–19, Dec. 2021.

[5] A. J. Roscoe and G. Ault, "Supporting high penetrations of renewable generation via implementation of real-time electricity pricing and demand response," *IET Renew. Power Gener.*, vol. 4, no. 4, pp. 369–382, 2010.

[6] A. Sharma and H. Sharma, "Demand Side Response: Drivers, Challenges, and Opportunities," in *Proceedings of International Conference on Advancements in Computing & Management (ICACM)*, 2019.

[7] J. P. Barton and D. G. Infield, "Energy Storage and Its Use With Intermittent Renewable Energy," *IEEE Trans. Energy Convers.*, vol. 19, no. 2, pp. 441–448, Jun. 2004.

[8] G. Carpinelli, G. Celli, S. Mocci, F. Mottola, F. Pilo, and D. Proto, "Optimal Integration of Distributed Energy Storage Devices in Smart Grids," *IEEE Trans. Smart Grid*, vol. 4, no. 2, pp. 985–995, 2013.

[9] D. Greenwood, N. Wade, P. Taylor, P. Papadopoulos, N. Heyward, and S. Alilat, "A Forecasting, Optimization and Scheduling System for Energy Storage Systems in distribution networks," in *2016 IEEE Power and Energy Society General Meeting (PESGM)*, 2016, pp. 1–5.

[10] X. Hu, R. Xiong, and B. Egardt, "Model-based dynamic power assessment of lithium-ion batteries considering different operating conditions," *IEEE Trans. Ind. Informatics*, vol. 10, no. 3, pp. 1948–1959, 2014.

[11] M. Ecker *et al.*, "Calendar and cycle life study of Li(NiMnCo) O2- based 18650 lithium- ion batteries," *J. Power Sources*, vol. 248, pp. 839–851, 2014.

[12] Y. Ye, Z. Zhou, Z. Cai, Z. Zhang, and Z. Li, “State of Health Estimation of Lithium-ion Batteries based on Indirect Health Indicators and Gaussian Process Regression Model,” *Proc. 2021 IEEE 10th Data Driven Control Learn. Syst. Conf. DDCLS 2021*, pp. 929–934, May 2021.

[13] S. B. Sarmah *et al.*, “A Review of State of Health Estimation of Energy Storage Systems: Challenges and Possible Solutions for Futuristic Applications of Li-Ion Battery Packs in Electric Vehicles,” *Journal of Electrochemical Energy Conversion and Storage*, vol. 16, no. 4. 2019.

[14] D. Qing, J. Huang, and W. Sun, “SOH estimation of lithium-ion batteries for electric vehicles,” in *31st International Symposium on Automation and Robotics in Construction and Mining, ISARC 2014 - Proceedings*, 2014, pp. 925–928.

[15] J. Wei, G. Dong, and Z. Chen, “Remaining Useful Life Prediction and State of Health Diagnosis for Lithium-Ion Batteries Using Particle Filter and Support Vector Regression,” *IEEE Trans. Ind. Electron.*, vol. 65, no. 7, pp. 5634–5643, Jul. 2018.

[16] H. Wenzl *et al.*, “Life prediction of batteries for selecting the technically most suitable and cost effective battery,” *J. Power Sources*, vol. 144, no. 2, pp. 373–384, Jun. 2005.

[17] V. Svoboda *et al.*, “Operating conditions of batteries in off- grid renewable energy systems,” *Sol. Energy*, vol. 81, no. 11, pp. 1409–1425, 2007.

[18] P. Ruetschi, “Aging mechanisms and service life of lead–acid batteries,” *J. Power Sources*, vol. 127, no. 1–2, pp. 33–44, Mar. 2004.

[19] H. A. Catherino, F. F. Feres, and F. Trinidad, “Sulfation in lead–acid batteries,” *J. Power Sources*, vol. 129, no. 1, pp. 113–120, Apr. 2004.

[20] R. R. Richardson, P. T. Ireland, and D. A. Howey, “Battery internal temperature estimation by combined impedance and surface temperature measurement,” *J. Power Sources*, vol. 265, pp. 254–261, Nov. 2014.

[21] Z. Li *et al.*, “Examining temporal and spatial variations of internal temperature in large-format laminated battery with embedded thermocouples,” *J. Power Sources*, vol. 241, pp. 536–553, Nov. 2013.

[22] M. S. K. Mutyala, J. Zhao, J. Li, H. Pan, C. Yuan, and X. Li, “In-situ temperature measurement in lithium ion battery by transferable flexible thin film thermocouples,” *J. Power Sources*, vol. 260, pp. 43–49, Aug. 2014.

[23] R. Mortel *et al.*, “Smart Cells - Battery monitoring via internal sensors,” in *2022 IEEE 13th International Symposium on Power Electronics for Distributed Generation Systems (PEDG)*, 2022, pp. 1–6.

[24] D. An, N. H. Kim, and J. H. Choi, “Options for prognostics Methods: A review of data-driven and physics-based prognostics,” in *54th AIAA/ASME/ASCE/AHS/ASC Structures, Structural Dynamics, and Materials Conference*, 2013.

[25] E. Meissner and G. Richter, “Battery Monitoring and Electrical Energy Management precondition for future vehicle electric power systems,” in *Journal of Power Sources*, 2003, vol. 116, no. 1–2, pp. 79–98.

[26] Y. Bengio and P. Frasconi, “Input-output HMMs for sequence processing,” *IEEE Trans. Neural Networks*, vol. 7, no. 5, pp. 1231–1249, 1996.

[27] Y. Li and H.-Y. Shum, “Learning dynamic audio-visual mapping with input-output Hidden Markov models,” *IEEE Trans. Multimed.*, vol. 8, no. 3, pp. 542–549, 2006.

[28] S. Marcel, O. Bernier, J. E. Viallet, and D. Collobert, “Hand gesture recognition using input- output hidden Markov models,” in *Fourth IEEE International Conference on Automatic Face and Gesture Recognition*, 2000, pp. 456–461.

[29] Y. Bengio, V. P. Lauzon, and R. Ducharme, “Experiments on the application of IOHMMs to model financial returns series,” *IEEE Trans. Neural Networks*, vol. 12, no. 1, pp. 113–123, 2001.

[30] A. M. González, A. Muñoz, S. Roque, and J. García-gonzález, “Modeling and Forecasting Electricity Prices with Input / Output Hidden Markov Models,” vol. 20, no. 1, pp. 13–24, 2005.

[31] T. Klingelschmidt, P. Weber, C. Simon, D. Theilliol, and F. Peysson, “Fault diagnosis and prognosis by using Input-Output Hidden Markov Models applied to a diesel generator,” in *2017 25th Mediterranean Conference on Control and Automation, MED 2017*, 2017, pp. 1326–1331.

[32] J. Sobon and B. Stephen, “Model-Free Non-Invasive Health Assessment for Battery Energy Storage Assets,” *IEEE Access*, vol. 9, pp. 54579–54590, 2021.

[33] D. Linden and T. B. Reddy, *Handbook of batteries*, 3rd ed. McGraw-Hill, 2002.

[34] A. Khor *et al.*, “Review of zinc-based hybrid flow batteries: From fundamentals to applications,” *Mater. Today Energy*, vol. 8, pp. 80–108, Jun. 2018.

[35] G. Tomazic and M. Skyllas-Kazacos, “Redox Flow Batteries,” in *Electrochemical Energy Storage for Renewable Sources and Grid Balancing*, Elsevier Inc., 2015, pp. 309–336.

[36] F. Li, Z. Wei, A. Manthiram, Y. Feng, J. Ma, and L. Mai, “Sodium-based batteries: from critical materials to battery systems,” *J. Mater. Chem. A*, vol. 7, no. 16, pp. 9406–9431, Apr. 2019.

[37] P. J. Tsai and S. L. I. Chan, “Nickel-based batteries: materials and chemistry,”

Electr. Transm. Distrib. Storage Syst., pp. 309–397, Jan. 2013.

[38] P. Bernard and M. Lippert, “Nickel-Cadmium and Nickel-Metal Hydride Battery Energy Storage,” in *Electrochemical Energy Storage for Renewable Sources and Grid Balancing*, Elsevier, 2015, pp. 223–251.

[39] C. Ponce de León, A. Frías-Ferrer, J. González-García, D. A. Szánto, and F. C. Walsh, “Redox flow cells for energy conversion,” *J. Power Sources*, vol. 160, no. 1, pp. 716–732, Sep. 2006.

[40] K. Lourenssen, J. Williams, F. Ahmadpour, R. Clemmer, and S. Tasnim, “Vanadium redox flow batteries: A comprehensive review,” *J. Energy Storage*, vol. 25, p. 100844, Oct. 2019.

[41] Electropaedia, “Cell Mechanical Construction,” *Woodbank Communications Ltd.*, 2005. [Online]. Available: https://www.mpoweruk.com/cell_construction.htm. [Accessed: 03-Jul-2020].

[42] R. Gundlapalli, S. Kumar, and S. Jayanti, “Stack Design Considerations for Vanadium Redox Flow Battery,” *Ina. Lett.*, vol. 3, no. 3, pp. 149–157, Sep. 2018.

[43] B. R. Chalamala, T. Soundappan, G. R. Fisher, M. R. Anstey, V. V. Viswanathan, and M. L. Perry, “Redox Flow Batteries: An Engineering Perspective,” *Proc. IEEE*, vol. 102, no. 6, pp. 976–999, Jun. 2014.

[44] A. Z. Weber, M. M. Mench, J. P. Meyers, P. N. Ross, J. T. Gostick, and Q. Liu, “Redox flow batteries: a review,” *J. Appl. Electrochem.*, vol. 41, no. 10, pp. 1137–1164, Oct. 2011.

[45] H. Chen, T. N. Cong, W. Yang, C. Tan, Y. Li, and Y. Ding, “Progress in electrical energy storage system: A critical review,” *Prog. Nat. Sci.*, vol. 19, no. 3, pp. 291–312, Mar. 2009.

[46] N. Kularatna and N. Kularatna, “Rechargeable battery technologies: an electronic engineer’s view point,” *Energy Storage Devices Electron. Syst.*, pp. 29–61, Jan. 2015.

[47] Z. Yang *et al.*, “Electrochemical energy storage for green grid,” *Chem. Rev.*, vol. 111, no. 5, pp. 3577–3613, May 2011.

[48] I. Hadjipaschalis, A. Poullikkas, and V. Efthimiou, “Overview of current and future energy storage technologies for electric power applications,” *Renew. Sustain. Energy Rev.*, vol. 13, no. 6, pp. 1513–1522, 2009.

[49] D. Pavlov, *Lead-acid batteries : science and technology : a handbook of lead-acid battery technology and its influence on the product*. Elsevier, 2017.

[50] “History Of Batteries: A Timeline - News about Energy Storage, Batteries, Climate Change and the Environment.” [Online]. Available:

https://www.upsbatterycenter.com/blog/history-batteries-timeline/. [Accessed: 21-Jun-2020].

[51] D. A. J. Rand and P. T. Moseley, “Lead–acid battery fundamentals,” *Lead-Acid Batter. Futur. Automob.*, pp. 97–132, Jan. 2017.

[52] H. A. Catherino, F. F. Feres, and F. Trinidad, “Sulfation in lead–acid batteries,” *J. Power Sources*, vol. 129, no. 1, pp. 113–120, Apr. 2004.

[53] A. Jossen, J. Garche, and D. U. Sauer, “Operation conditions of batteries in PV applications,” *Sol. Energy*, vol. 76, no. 6, pp. 759–769, Jan. 2004.

[54] H. Karami and R. Asadi, “Recovery of discarded sulfated lead-acid batteries,” *J. Power Sources*, vol. 191, no. 1, pp. 165–175, Jun. 2009.

[55] R. M. Dell and D. A. J. Rand, “Energy storage - A key technology for global energy sustainability,” *J. Power Sources*, vol. 100, no. 1–2, pp. 2–17, Nov. 2001.

[56] G. J. May, A. Davidson, and B. Monahov, “Lead batteries for utility energy storage: A review,” *Journal of Energy Storage*, vol. 15. 2018.

[57] D. M. Akhil, Abbas A., Georgianne Huff, Aileen B. Currier, Benjamin C. Kaun, “DOE/EPRI 2013 electricity storage handbook in collaboration with NRECA,” California, 2013.

[58] “Section 4 - Sealed Lead Celles and Batteries,” in *Rechargeable batteries applications handbook / [internet resource], EDN Series for Design Engineers*, Newnes, 1998, pp. 153–235.

[59] B. Culpin, “Thermal runaway in valve-regulated lead-acid cells and the effect of separator structure,” *J. Power Sources*, vol. 133, no. 1, pp. 79–86, May 2004.

[60] C. M. Hoff and K. Steeves, “New Insights into Thermal Runaway of Valve Regulated Lead-Acid Batteries,” 2005.

[61] Y. Guo, S. Tang, G. Meng, and S. Yang, “Failure modes of valve-regulated lead-acid batteries for electric bicycle applications in deep discharge,” *J. Power Sources*, vol. 191, no. 1, pp. 127–133, Jun. 2009.

[62] H. A. Catherino, “Complexity in battery systems: Thermal runaway in VRLA batteries,” *J. Power Sources*, vol. 158, no. 2, pp. 977–986, Aug. 2006.

[63] N. Galushkin, N. Yazvinskaya, D. Galushkin, and I. Galushkina, “The Reasons of Thermal Runaway in Nickel-Cadmium Batteries,” *Recent Patents Eng.*, vol. 11, no. 1, pp. 4–9, Feb. 2017.

[64] Y. Guo, “Safety | Thermal Runaway,” in *Encyclopedia of Electrochemical Power Sources*, Elsevier, 2009, pp. 241–253.

[65] N. E. Galushkin, N. N. Yazvinskaya, and D. N. Galushkin, “Thermal runaway as

a new high-performance method of desorption of hydrogen from hydrides," *Int. J. Hydrogen Energy*, vol. 41, no. 33, pp. 14813–14819, Sep. 2016.

[66] N. N. Yazvinskaya, N. E. Galushkin, D. N. Galushkin, and I. A. Galushkina, "Hydrogen Amount Estimation in Electrodes of Nickel-Cadmium Batteries Depending on Their Operating Life," *Int. J. Electrochem. Sci*, vol. 11, pp. 7843–7848, 2016.

[67] N. E. Galushkin, N. N. Yazvinskaya, and D. N. Galushkin, "The Mechanism of Thermal Runaway in Alkaline Batteries," *J. Electrochem. Soc.*, vol. 162, no. 4, pp. A749–A753, Feb. 2015.

[68] W. K. Hu *et al.*, "Effect of long-term overcharge and operated temperature on performance of rechargeable NiMH cells," *J. Power Sources*, vol. 159, no. 2, pp. 1478–1483, Sep. 2006.

[69] J. C. Viera, M. Gonzalez, J. Anton, J. C. Campo, F. J. Ferrero, and M. Valledor, "NiMH vs NiCd Batteries under High Charging Rates," in *INTELEC 06 - Twenty-Eighth International Telecommunications Energy Conference*, 2006, pp. 1–6.

[70] Z. Ye and D. Noréus, "Oxygen and hydrogen gas recombination in NiMH cells," *J. Power Sources*, vol. 208, pp. 232–236, Jun. 2012.

[71] R. Spotnitz and J. Franklin, "Abuse behavior of high-power, lithium-ion cells," *J. Power Sources*, vol. 113, no. 1, pp. 81–100, Jan. 2003.

[72] L. Lu, X. Han, J. Li, J. Hua, and M. Ouyang, "A review on the key issues for lithium-ion battery management in electric vehicles," *J. Power Sources*, vol. 226, pp. 272–288, Mar. 2013.

[73] D. P. Abraham, E. P. Roth, R. Kostecki, K. McCarthy, S. MacLaren, and D. H. Doughty, "Diagnostic examination of thermally abused high-power lithium-ion cells," *J. Power Sources*, vol. 161, no. 1, pp. 648–657, Oct. 2006.

[74] H. U. Escobar-Hernandez, R. M. Gustafson, M. I. Papadaki, S. Sachdeva, and M. S. Mannan, "Thermal Runaway in Lithium-Ion Batteries: Incidents, Kinetics of the Runaway and Assessment of Factors Affecting Its Initiation," *J. Electrochem. Soc.*, vol. 163, no. 13, pp. A2691–A2701, 2016.

[75] Q. Wang, P. Ping, X. Zhao, G. Chu, J. Sun, and C. Chen, "Thermal runaway caused fire and explosion of lithium ion battery," *J. Power Sources*, vol. 208, pp. 210–224, Jun. 2012.

[76] P. Arora, R. E. White, and M. Doyle, "Capacity Fade Mechanisms and Side Reactions in Lithium-Ion Batteries," *J. Electrochem. Soc.*, vol. 145, no. 10, p. 3647, Oct. 1998.

[77] T. M. Bandhauer, S. Garimella, and T. F. Fuller, "A Critical Review of Thermal

Issues in Lithium-Ion Batteries," *J. Electrochem. Soc.*, vol. 158, no. 3, pp. R1–R25, 2011.

[78] D. Miranda, C. M. Costa, and S. Lanceros-Mendez, "Lithium ion rechargeable batteries: State of the art and future needs of microscopic theoretical models and simulations," *J. Electroanal. Chem.*, vol. 739, pp. 97–110, Feb. 2015.

[79] B. Dunn, H. Kamath, and J.-M. Tarascon, "Electrical Energy Storage for the Grid: A Battery of Choices," *Science (80-.).*, vol. 334, no. 6058, pp. 928–935, 2011.

[80] D. Kumar, S. K. Rajouria, S. B. Kuhar, and D. K. Kanchan, "Progress and prospects of sodium-sulfur batteries: A review," *Solid State Ionics*, vol. 312, pp. 8–16, Dec. 2017.

[81] T. Oshima, M. Kajita, and A. Okuno, "Development of Sodium-Sulfur Batteries," *Int. J. Appl. Ceram. Technol.*, vol. 1, no. 3, pp. 269–276, Jan. 2005.

[82] K. B. Hueso, M. Armand, and T. Rojo, "High temperature sodium batteries: Status, challenges and future trends," *Energy Environ. Sci.*, vol. 6, no. 3, pp. 734–749, 2013.

[83] J. L. Sudworth, "The sodium/sulphur battery," *J. Power Sources*, vol. 11, no. 1–2, pp. 143–154, Jan. 1984.

[84] R. Holze, "SECONDARY BATTERIES–HIGH TEMPERATURE SYSTEMS| Sodium–Sulfur," *Encycl. Electrochem. Power Sources*, pp. 302–311, 2009.

[85] H. S. Yang, J. H. Park, H. W. Ra, C.-S. Jin, and J. H. Yang, "Critical rate of electrolyte circulation for preventing zinc dendrite formation in a zinc–bromine redox flow battery," *J. Power Sources*, vol. 325, pp. 446–452, 2016.

[86] R. L. Largent, M. Skylas-Kazacos, and J. Chieng, "Improved PV system performance using vanadium batteries," in *Conference Record of the IEEE Photovoltaic Specialists Conference (1993)*, 1993, pp. 1119–1124.

[87] M. Rychcik and M. Skyllas-Kazacos, "Characteristics of a new all- vanadium redox flow battery," *J. Power Sources*, vol. 22, no. 1, pp. 59–67, 1988.

[88] K.-L. Huang, X. Li, S. Liu, N. Tan, and L. Chen, "Research progress of vanadium redox flow battery for energy storage in China," *Renew. Energy*, vol. 33, no. 2, pp. 186–192, Feb. 2008.

[89] A. Tang, J. Bao, and M. Skyllas-Kazacos, "Studies on pressure losses and flow rate optimization in vanadium redox flow battery," *J. Power Sources*, vol. 248, pp. 154–162, 2014.

[90] G. Kear, A. A. Shah, and F. C. Walsh, "Development of the all- vanadium redox flow battery for energy storage: a review of technological, financial and policy aspects," *Int. J. Energy Res.*, vol. 36, no. 11, pp. 1105–1120, 2012.

[91] M. Skyllas-Kazacos, D. Kasherman, D. R. Hong, and M. Kazacos, "Characteristics and performance of 1 kW UNSW vanadium redox battery," *J. Power Sources*, vol. 35, no. 4, pp. 399–404, Sep. 1991.

[92] B. R. Williams and T. Hennessy, "Energy oasis [vanadium redox battery system in power distribution application]," *Power Eng.*, vol. 19, no. 1, pp. 28–31, 2005.

[93] D. M. Rose and S. R. Ferreira, "Performance Testing of Zinc-Bromine Flow Batteries for Remote Telecom Sites," 2013.

[94] S.-C. Yang, "An approximate model for estimating the faradaic efficiency loss in zinc/bromine batteries caused by cell self-discharge," *J. Power Sources*, vol. 50, no. 3, pp. 343–360, 1994.

[95] G. J. May, A. Davidson, and B. Monahov, "Lead batteries for utility energy storage: A review," *J. Energy Storage*, vol. 15, pp. 145–157, Feb. 2018.

[96] V. Svoboda *et al.*, "Operating conditions of batteries in off-grid renewable energy systems," *Sol. Energy*, vol. 81, no. 11, pp. 1409–1425, Nov. 2007.

[97] M. R. Jongerden and B. R. Haverkort, "Which battery model to use?," *IET Softw.*, vol. 3, no. 6, pp. 445–457, 2009.

[98] B. Pattipati, B. Balasingam, G. V. Avvari, K. R. Pattipati, and Y. Bar-Shalom, "Open circuit voltage characterization of lithium-ion batteries," *J. Power Sources*, vol. 269, pp. 317–333, Dec. 2014.

[99] F. Cheng *et al.*, "Porous LiMn 2O 4 nanorods with durable high-rate capability for rechargeable Li-ion batteries," *Energy Environ. Sci.*, vol. 4, no. 9, pp. 3668–3675, Sep. 2011.

[100] J. L. Seyed Mohammad Rezvanizaniani, Zongchang Liu, Yan Chen, "Review and recent advances in battery health monitoring and prognostics technologies for EV," *J. Power Sources*, vol. 256, no. 256, pp. 110–124, 2014.

[101] K. S. Ng, C. S. Moo, Y. P. Chen, and Y. C. Hsieh, "Enhanced coulomb counting method for estimating state-of-charge and state-of-health of lithium-ion batteries," *Appl. Energy*, vol. 86, no. 9, pp. 1506–1511, Sep. 2009.

[102] A. Widodo, M. C. Shim, W. Caesarendra, and B. S. Yang, "Intelligent prognostics for battery health monitoring based on sample entropy," *Expert Syst. Appl.*, vol. 38, no. 9, pp. 11763–11769, Sep. 2011.

[103] H. Arora, R. Sherratt, B. Janko, and W. Harwin, "Experimental validation of the recovery effect in batteries for wearable sensors and healthcare devices discovering the existence of hidden time constants," *J. Eng.*, no. 10, p. 2017, 2017.

[104] D. Rakhmatov and S. B. K. Vrudhula, "Time-to-failure estimation for batteries in

portable electronic systems," in *ISLPED'01: Proceedings of the 2001 International Symposium on Low Power Electronics and Design (IEEE Cat. No.01TH8581)*, pp. 88–91.

[105] C. F. Chiasserini and R. R. Rao, "Improving battery performance by using traffic shaping techniques," *IEEE J. Sel. Areas Commun.*, vol. 19, no. 7, pp. 1385–1394, Jul. 2001.

[106] P. Arora, R. E. White, and M. Doyle, "Capacity Fade Mechanisms and Side Reactions in Lithium-Ion Batteries," *J. Electrochem. Soc.*, vol. 145, no. 10, pp. 3647–3667, Oct. 1998.

[107] J. D. Dogger, B. Roossien, and F. D. J. Nieuwenhout, "Characterization of Li-Ion Batteries for Intelligent Management of Distributed Grid-Connected Storage," *IEEE Trans. Energy Convers.*, vol. 26, no. 1, pp. 256–263, 2011.

[108] P. K. K. Thirugnanam, J. T. P. Ezhil Reena, M. Singh, "Mathematical Modeling of Li-Ion Battery Using Genetic Algorithm Approach for V2G Applications," *IEEE Trans. Energy Convers.*, vol. 29, no. 2, pp. 332–343, 2014.

[109] M. Doyle, T. F. ; Fuller, and J. Newman, "Modeling of Galvanostatic Charge and Discharge of the Lithium/Polymer/Insertion Cell," *J. Electrochem. Soc.*, vol. 140, no. 6, p. 1533, 1993.

[110] T. F. . Fuller, M. Doyle, and J. Newman, "Relaxation Phenomena in Lithium-Ion-Insertion Cells," *J. Electrochem. Soc.*, vol. 141, no. 4, p. 990, 1994.

[111] C. S. Huang and M. Y. Chow, "Accurate Thevenin's circuit-based battery model parameter identification," in *IEEE International Symposium on Industrial Electronics*, 2016, vol. 2016-November, pp. 274–279.

[112] D. Andre, M. Meiler, K. Steiner, H. Waltz, T. Soczka-Guth, and D. U. Sauer, "Characterization of high-power lithium-ion batteries by electrochemical impedance spectroscopy. II: Modelling - ScienceDirect," *J. Power Sources*, vol. 196, no. 12, pp. 5349–5356, Jun. 2011.

[113] D. Rakhmatov and S. B. K. Vrudhula, "An analytical high-level battery model for use in energy management of portable electronic systems," *IEEE/ACM Int. Conf. Comput. Aided Des. ICCAD 2001. IEEE/ACM Dig. Tech. Pap. (Cat. No.01CH37281)*, pp. 488–493, 2001.

[114] J. F. Manwell and J. G. McGowan, "Lead acid battery storage model for hybrid energy systems," *Sol. Energy*, vol. 50, no. 5, pp. 399–405, May 1993.

[115] B. E. Olivares, M. A. Cerda Munoz, M. E. Orchard, and J. F. Silva, "Particle-Filtering- Based Prognosis Framework for Energy Storage Devices With a Statistical Characterization of State-of- Health Regeneration Phenomena," *Instrum. Meas. IEEE Trans.*, vol. 62, no. 2, pp. 364–376, 2013.

[116] ZHE CHEN, “Bayesian Filtering From Kalman Filters to Particle Filters and Beyond,” *Statistics (Ber).*, vol. 37, no. 2, pp. 145–168, 2003.

[117] B. Long, W. Xian, L. Jiang, and Z. Liu, “An improved autoregressive model by particle swarm optimization for prognostics of lithium-ion batteries,” *Microelectron. Reliab.*, vol. 53, no. 6, pp. 821–831, Jun. 2013.

[118] D. Liu, Y. Luo, Y. Peng, X. Peng, and M. Pecht, “Lithium-ion battery remaining useful life estimation based on nonlinear AR model combined with degradation feature,” in *Proceedings of the Annual Conference of the Prognostics and Health Management Society 2012, PHM 2012*, 2012, pp. 336–342.

[119] J. Wu, C. Zhang, and Z. Chen, “An online method for lithium-ion battery remaining useful life estimation using importance sampling and neural networks,” *Appl. Energy*, vol. 173, pp. 134–140, Jul. 2016.

[120] C.-F. Chiasserini and R. R. Rao, “Energy efficient battery management,” *IEEE J. Sel. Areas Commun.*, vol. 19, no. 7, pp. 1235–1245, Jul. 2001.

[121] J. Zhang, S. Ci, H. Sharif, and M. Alahmad, “An enhanced circuit-based model for single-cell battery,” in *Conference Proceedings - IEEE Applied Power Electronics Conference and Exposition - APEC*, 2010, pp. 672–675.

[122] M. S. Hosen, J. Jaguemont, J. Van Mierlo, and M. Berecibar, “Battery lifetime prediction and performance assessment of different modeling approaches,” *iScience*, vol. 24, no. 2, p. 102060, Jan. 2021.

[123] A. Nikolian, J. De Hoog, K. Fleurbay, J. Timmermans, P. Van De Bossche, and J. Van Mierlo, “Classification of Electric modelling and Characterization methods of Lithium-ion Batteries for Vehicle Applications,” *Eur. Electr. Veh. Congr.*, no. December, pp. 1–15, 2014.

[124] L. Song and J. W. Evans, “Electrochemical-Thermal Model of Lithium Polymer Batteries,” *J. Electrochem. Soc.*, vol. 147, no. 6, p. 2095, 2000.

[125] D. W. Dees, V. S. Battaglia, and A. Bélanger, “Electrochemical modeling of lithium polymer batteries,” *J. Power Sources*, vol. 110, no. 1, pp. 310–320, 2002.

[126] D. Stephenson *et al.*, “Electrochemical model of the FE/V redox flow battery,” *J. Electrochem. Soc.*, vol. 159, no. 12, pp. A1993–A2000, 2012.

[127] T. F. Fuller, M. Doyle, and J. Newman, “Simulation and Optimization of the Dual Lithium Ion Insertion Cell,” *J. Electrochem. Soc.*, vol. 141, no. 1, pp. 1–10, 1994.

[128] B. Saha and K. Goebel, “Modeling Li-ion battery capacity depletion in a particle filtering framework,” in *Annual Conference of the Prognostics and Health Management Society, PHM 2009*, 2009.

[129] Y. J. He, J. N. Shen, J. F. Shen, and Z. F. Ma, “State of health estimation of

lithium-ion batteries: A multiscale Gaussian process regression modeling approach," *AIChE J.*, vol. 61, no. 5, pp. 1589–1600, May 2015.

[130] M. Chen and G. A. Rincón-Mora, "Accurate electrical battery model capable of predicting runtime and I- V performance," *Energy Conversion, IEEE Trans.*, vol. 21, no. 2, pp. 504–511, 2006.

[131] D. W. Dees, V. S. Battaglia, and A. Bélanger, "Electrochemical modeling of lithium polymer batteries," *J. Power Sources*, vol. 110, no. 2, pp. 310–320, Aug. 2002.

[132] X. Hu, J. Jiang, D. Cao, and B. Egardt, "Battery health prognosis for electric vehicles using sample entropy and sparse Bayesian predictive modeling," *IEEE Trans. Ind. Electron.*, vol. 63, no. 4, pp. 2645–2656, Apr. 2016.

[133] M. Guo, G. Sikha, and R. E. White, "Single-Particle Model for a Lithium-Ion Cell: Thermal Behavior," *J. Electrochem. Soc.*, vol. 158, no. 2, p. A122, Dec. 2011.

[134] J. G. Manwell, F James. McGowan, "Extension of the kinetic battery model for wind/hybrid power systems," *Proc. 5th Eur. Wind Energy Assoc. Conf. (EWEC '94)*, no. February, pp. 284–289, 1994.

[135] R. Rao, S. Vrudhula, and D. N. Rakhmatov, "Battery Modeling for Energy-Aware System Design," *Computer (Long. Beach. Calif).*, vol. 36, no. 12, Dec. 2003.

[136] T. Kim and W. Qiao, "A hybrid battery model capable of capturing dynamic circuit characteristics and nonlinear capacity effects," *IEEE Trans. Energy Convers.*, vol. 26, no. 4, pp. 1172–1180, Dec. 2011.

[137] M. Dürr, A. Cruden, S. Gair, and J. R. McDonald, "Dynamic model of a lead acid battery for use in a domestic fuel cell system," *J. Power Sources*, vol. 161, no. 2, pp. 1400–1411, Oct. 2006.

[138] S. C. Hageman, "Simple PSpice models let you simulate common battery types," *Electron. Des. News*, vol. 38, pp. 117–129, 1993.

[139] S. Gold, "PSPICE macromodel for lithium-ion batteries," in *Proceedings of the Annual Battery Conference on Applications and Advances*, 1997, pp. 215–222.

[140] N. Kularatna, "Dynamics and modeling of rechargeable batteries: What electrochemists' work tells the electronic engineers," *IEEE Power Electron. Mag.*, vol. 1, no. 4, pp. 23–33, Dec. 2014.

[141] J. Xu, C. C. Mi, B. Cao, and J. Cao, "A new method to estimate the state of charge of lithium-ion batteries based on the battery impedance model," *J. Power Sources*, vol. 233, pp. 277–284, Jul. 2013.

[142] M. & O. Daowd, N. Omar, B. Verbrugge, P. Van den Bossche, and J. Van Mierlo,

"Battery Models Parameter Estimation based on Matlab/Simulink," *The 25th World Battery, Hybrid and Fuel Cell Electric Vehicle Symposium & Exhibition*, Nov-2010. [Online]. Available: https://www.researchgate.net/publication/215553095_Battery_Models_Parameter_Estimation_based_on_MatlabSimulink. [Accessed: 07-Jul-2020].

[143] S. M. Mousavi G. and M. Nikdel, "Various battery models for various simulation studies and applications," *Renew. Sustain. Energy Rev.*, vol. 32, pp. 477–485, Apr. 2014.

[144] V. H. Johnson, "Battery performance models in ADVISOR," *J. Power Sources*, vol. 110, no. 2, pp. 321–329, Aug. 2002.

[145] B. Y. Liaw, G. Nagasubramanian, R. G. Jungst, and D. H. Doughty, "Modeling of lithium ion cells - A simple equivalent-circuit model approach," *Solid State Ionics*, vol. 175, no. 1–4, pp. 835–839, Nov. 2004.

[146] E. Kuhn, C. Forgez, P. Lagonotte, and G. Friedrich, "Modelling Ni-mH battery using Cauer and Foster structures," *J. Power Sources*, vol. 158, no. 2 SPEC. ISS., pp. 1490–1497, Aug. 2006.

[147] P. Suresh, A. K. Shukla, and N. Munichandraiah, "Temperature dependence studies of a.c. impedance of lithium-ion cells," *J. Appl. Electrochem.*, vol. 32, no. 3, pp. 267–273, Mar. 2002.

[148] S. Buller, M. Thele, R. W. A. A. De Doncker, and E. Karden, "Impedance-based simulation models of supercapacitors and Li-ion batteries for power electronic applications - IEEE Journals & Magazine," *IEEE Trans. Ind. Appl.* , vol. 41, no. 3, pp. 742–747, 2005.

[149] G. Pérez, I. Gandiaga, M. Garmendia, J. F. Reynaud, and U. Viscarret, "Modelling of Li-ion batteries dynamics using impedance spectroscopy and pulse fitting: EVs application," in *2013 World Electric Vehicle Symposium and Exhibition (EVS27), Barcelona*, 2013, pp. 1–9.

[150] D. Andre, M. Meiler, K. Steiner, C. Wimmer, T. Soczka-Guth, and D. U. Sauer, "Characterization of high-power lithium-ion batteries by electrochemical impedance spectroscopy. I. Experimental investigation," *J. Power Sources*, vol. 196, no. 12, pp. 5334–5341, Jun. 2011.

[151] K. Sarrafan, D. Sutanto, and K. M. Muttaqi, "An electric circuit based EV battery model for runtime prediction and state of charge tracking," in *2017 IEEE Transportation Electrification Conference, ITEC-India 2017*, 2018, vol. 2018-January, pp. 1–6.

[152] R. Chandrasekaran, W. Bi, and T. F. Fuller, "Robust design of battery/ fuel cell hybrid systems— Methodology for surrogate models of Pt stability and mitigation through system controls," *J. Power Sources*, vol. 182, no. 2, pp. 546–557, 2008.

[153] M. Ceraolo, “New dynamical models of lead-acid batteries,” *IEEE Trans. Power Syst.*, vol. 15, no. 4, pp. 1184–1190, 2000.

[154] S. M. Rezvanizaniani, Z. Liu, Y. Chen, and J. Lee, “Review and recent advances in battery health monitoring and prognostics technologies for electric vehicle (EV) safety and mobility,” *Journal of Power Sources*, vol. 256. Elsevier B.V., pp. 110–124, 15-Jun-2014.

[155] M. Dubarry and B. Y. Liaw, “Development of a universal modeling tool for rechargeable lithium batteries,” *J. Power Sources*, vol. 174, no. 2, pp. 856–860, Dec. 2007.

[156] “Battery Impedance Modeling-EIS Measurement Low Impedance LIB.” [Online]. Available: https://www.gamry.com/application-notes/EIS/eis-measurement-of-a-very-low-impedance-lithium-ion-battery/. [Accessed: 20-Mar-2021].

[157] M. A. Casacca and W. A. Lynch, “A Mathematical Model for Lead-Acid Batteries,” *IEEE Trans. Energy Convers.*, vol. 7, no. 1, pp. 93–98, 1992.

[158] Lijun Gao, Shengyi Liu, and R. A. Dougal, “Dynamic lithium-ion battery model for system simulation,” *IEEE Trans. Components Packag. Technol.*, vol. 25, no. 3, pp. 495–505, Sep. 2002.

[159] R. Suresh, H. Kumar Tanneru, and R. Rengaswamy, “Modeling of rechargeable batteries,” *Current Opinion in Chemical Engineering*, vol. 13. Elsevier Ltd, pp. 63–74, 01-Aug-2016.

[160] D. Andre, A. Nuhic, T. Soczka-Guth, and D. U. Sauer, “Comparative study of a structured neural network and an extended Kalman filter for state of health determination of lithium-ion batteries in hybrid electricvehicles,” *Eng. Appl. Artif. Intell.*, vol. 26, no. 3, pp. 951–961, Mar. 2013.

[161] G. L. Plett, “Dual and joint EKF for simultaneous SOC and SOH estimation,” in *21st International Battery, Hybrid and Fuel Cell Electric Vehicle Symposium and Exhibition 2005, EVS 2005*, 2005, pp. 318–330.

[162] B. S. Bhangu, P. Bentley, D. A. Stone, and C. M. Bingham, “Nonlinear observers for predicting state-of-charge and state-of-health of lead-acid batteries for hybrid-electric vehicles,” *IEEE Trans. Veh. Technol.*, vol. 54, no. 3, pp. 783–794, May 2005.

[163] B. Saha, K. Goebel, S. Poll, and J. Christophersen, “Prognostics methods for battery health monitoring using a Bayesian framework,” *IEEE Trans. Instrum. Meas.*, vol. 58, no. 2, pp. 291–296, 2009.

[164] M. S. Arulampalam, S. Maskell, N. Gordon, and T. Clapp, “A tutorial on particle filters for online nonlinear/non-Gaussian Bayesian tracking,” *IEEE Trans. Signal Process.*, vol. 50, no. 2, pp. 174–188, Feb. 2002.

[165] A. Tulsyan, R. Bhushan Gopaluni, and S. R. Khare, “Particle filtering without tears: A primer for beginners,” *Comput. Chem. Eng.*, vol. 95, pp. 130–145, Dec. 2016.

[166] G. won You, S. Park, and D. Oh, “Real-time state-of-health estimation for electric vehicle batteries: A data-driven approach,” *Appl. Energy*, vol. 176, pp. 92–103, Aug. 2016.

[167] H.-T. Lin, T.-J. Liang, and S.-M. Chen, “Estimation of Battery State of Health Using Probabilistic Neural Network,” *IEEE Trans. Ind. Informatics*, vol. 9, no. 2, pp. 679–685, May 2013.

[168] A. Nuhic, T. Terzimehic, T. Soczka-Guth, M. Buchholz, and K. Dietmayer, “Health diagnosis and remaining useful life prognostics of lithium-ion batteries using data-driven methods,” *J. Power Sources*, vol. 239, pp. 680–688, Oct. 2013.

[169] R. R. Richardson, M. A. Osborne, and D. A. Howey, “Battery health prediction under generalized conditions using a Gaussian process transition model,” *J. Energy Storage*, vol. 23, pp. 320–328, Jun. 2019.

[170] X. Sui, S. He, S. B. Vilsen, J. Meng, R. Teodorescu, and D. I. Stroe, “A review of non-probabilistic machine learning-based state of health estimation techniques for Lithium-ion battery,” *Appl. Energy*, vol. 300, p. 117346, Oct. 2021.

[171] E. Schulz, M. Speekenbrink, and A. Krause, “A tutorial on Gaussian process regression: Modelling, exploring, and exploiting functions,” *J. Math. Psychol.*, vol. 85, pp. 1–16, Aug. 2018.

[172] R. R. Richardson, M. A. Osborne, and D. A. Howey, “Gaussian process regression for forecasting battery state of health,” *J. Power Sources*, vol. 357, pp. 209–219, Jul. 2017.

[173] L. L. Bucciarelli, “Estimating loss-of- power probabilities of stand- alone photovoltaic solar energy systems,” *Sol. Energy*, vol. 32, no. 2, pp. 205–209, 1984.

[174] V. Junseok Song, A. Krishnamurthy, R. Kwasinski, and R. Sharma, “Development of a Markov- Chain- Based Energy Storage Model for Power Supply Availability Assessment of Photovoltaic Generation Plants,” *Sustain. Energy, IEEE Trans.*, vol. 4, no. 2, pp. 491–500, 2013.

[175] Y. Li *et al.*, “Data-driven health estimation and lifetime prediction of lithium-ion batteries: A review,” *Renewable and Sustainable Energy Reviews*, vol. 113. Elsevier Ltd, p. 109254, 01-Oct-2019.

[176] Y. Zhou and M. Huang, “Lithium-ion batteries remaining useful life prediction based on a mixture of empirical mode decomposition and ARIMA model,” *Microelectron. Reliab.*, vol. 65, pp. 265–273, Oct. 2016.

[177] M. Lucu, E. Martinez-Laserna, I. Gandiaga, and H. Camblong, “A critical review on self-adaptive Li-ion battery ageing models,” *J. Power Sources*, vol. 401, pp. 85–101, Oct. 2018.

[178] I. Baghdadi, O. Briat, J. Y. Delétage, P. Gyan, and J. M. Vinassa, “Lithium battery aging model based on Dakin’s degradation approach,” *J. Power Sources*, vol. 325, pp. 273–285, Sep. 2016.

[179] L. Wenshou, P. Atkinson, S. Delamont, A. Cernat, and J. W. Sakshaug, “Neural Networks,” *SAGE Research Methods Foundations*, 2020. [Online]. Available: https://methods.sagepub.com/foundations/neural-networks. [Accessed: 18-Jan-2023].

[180] C. C. Aggarwal, *Neural Networks and Deep Learning*, First edition. Springer International Publishing, 2018.

[181] X. Hu, S. E. Li, and Y. Yang, “Advanced Machine Learning Approach for Lithium-Ion Battery State Estimation in Electric Vehicles,” *IEEE Trans. Transp. Electrif.*, vol. 2, no. 2, pp. 140–149, Jun. 2016.

[182] A. Eddahech, O. Briat, N. Bertrand, J. Y. Delétage, and J. M. Vinassa, “Behavior and state-of-health monitoring of Li-ion batteries using impedance spectroscopy and recurrent neural networks,” *Int. J. Electr. Power Energy Syst.*, vol. 42, no. 1, pp. 487–494, Nov. 2012.

[183] D. Yang, Y. Wang, R. Pan, R. Chen, and Z. Chen, “A Neural Network Based State-of-Health Estimation of Lithium-ion Battery in Electric Vehicles,” in *Energy Procedia*, 2017, vol. 105, pp. 2059–2064.

[184] H. Dai, G. Zhao, M. Lin, J. Wu, and G. Zheng, “A novel estimation method for the state of health of lithium-ion battery using prior knowledge-based neural network and markov chain,” *IEEE Trans. Ind. Electron.*, vol. 66, no. 10, pp. 7706–7716, Oct. 2019.

[185] C. Zhang, Y. Zhu, G. Dong, and J. Wei, “Data-driven lithium-ion battery states estimation using neural networks and particle filtering,” *Int. J. Energy Res.*, vol. 43, no. 14, pp. 8230–8241, Nov. 2019.

[186] D. Yang, Y. Wang, R. Pan, R. Chen, and Z. Chen, “State-of-health estimation for the lithium-ion battery based on support vector regression,” *Appl. Energy*, vol. 227, pp. 273–283, Oct. 2018.

[187] C. M. Bishop, “Sparse Kernel Machines,” in *Pattern Recognition And Machine Learning* , no. 12, 2006, pp. 325–359.

[188] M. A. Patil *et al.*, “A novel multistage Support Vector Machine based approach for Li ion battery remaining useful life estimation,” *Appl. Energy*, vol. 159, pp. 285–297, Dec. 2015.

[189] Q. Zhao, X. Qin, H. Zhao, and W. Feng, “A novel prediction method based on the support vector regression for the remaining useful life of lithium-ion batteries,” *Microelectron. Reliab.*, vol. 85, pp. 99–108, Jun. 2018.

[190] G. Mountrakis, J. Im, and C. Ogole, “Support vector machines in remote sensing: A review,” *ISPRS Journal of Photogrammetry and Remote Sensing*, vol. 66, no. 3. Elsevier, pp. 247–259, 01-May-2011.

[191] E. L. Snelson, “Flexible and efficient Gaussian process models for machine learning,” University College London, London, 2007.

[192] C. F. Chiasserini and R. R. Rao, “A model for battery pulsed discharge with recovery effect,” in *IEEE Wireless Communications and Networking Conference, WCNC*, 1999, vol. 2, pp. 636–639.

[193] Y. Wang *et al.*, “A comprehensive review of battery modeling and state estimation approaches for advanced battery management systems,” *Renew. Sustain. Energy Rev.*, vol. 131, p. 110015, Oct. 2020.

[194] E. Sarasketa-Zabala, E. Martinez-Laserna, M. Berecibar, I. Gandiaga, L. M. Rodriguez-Martinez, and I. Villarreal, “Realistic lifetime prediction approach for Li-ion batteries,” *Appl. Energy*, vol. 162, pp. 839–852, Jan. 2016.

[195] T. Cai *et al.*, “Stable CoSe2/carbon nanodice@reduced graphene oxide composites for high-performance rechargeable aluminum-ion batteries,” *Energy Environ. Sci.*, vol. 11, no. 9, pp. 2341–2347, Sep. 2018.

[196] G. Xu, B. Ding, J. Pan, P. Nie, L. Shen, and X. Zhang, “High performance lithium-sulfur batteries: Advances and challenges,” *Journal of Materials Chemistry A*, vol. 2, no. 32. Royal Society of Chemistry, pp. 12662–12676, 28-Aug-2014.

[197] W. Zhang, Y. Liu, and Z. Guo, “Approaching high-performance potassium-ion batteries via advanced design strategies and engineering,” *Sci. Adv.*, vol. 5, no. 5, pp. 7412–7422, May 2019.

[198] G. Weijun, S. Zechang, W. Xuezhe, and D. Haifeng, “Review of Methods for Battery Life Modeling and Their Applications,” *Appl. Mech. Mater.*, vol. 29–32, pp. 2392–2397, 2010.

[199] R. Jurgen, “Available Power and Energy Prediction Using a Simplified Circuit Model of HEV Li-ion Battery (2010-01-1074),” in *Electric and Hybrid-Elactric Vehicles: Batteries*, SAE International, 2011, pp. 61–66.

[200] O. C. Ibe, *Markov processes for stochastic modeling*, 2nd Edition. Elsevier, 2013.

[201] Y. Bengio and P. Frasconi, “An Input Output HMM Architecture,” in *Proceedings of the 7th International Conference on Neural Information*

Processing Systems, 1994, pp. 427–434.

[202] Y. Bengio, "Markovian Models for Sequential Data,", *Technical Report 1049*, Universite de Montreal, Canada, 1996.

[203] K. P. Murphy, *Machine learning : a probabilistic perspective*. Cambridge, Mass.: Cambridge, Mass. : MIT Press, 2012.

[204] J. de la Peña Llerandi, C. S. de Mingo, and J. C. Ibáñez, "Continuous Battery Health Diagnosis by On-Line Internal Resistance Measuring," *Energies 2019, Vol. 12, Page 2836*, vol. 12, no. 14, p. 2836, Jul. 2019.

[205] L. R. Rabiner, "A tutorial on hidden Markov models and selected applications in speech recognition," *Proc. IEEE*, vol. 77, no. 2, pp. 257–286, 1989.

[206] B. Bole, C. Kulkarni, and M. Daig, "'Randomized Battery Usage Data Set,'" *NASA Ames Prognostics Data Repository (https://ti.arc.nasa.gov/tech/dash/groups/pcoe/prognostic-data-repository/)*. NASA Ames Research Center, Moffett Field, CA.

[207] P. Frasconi and Y. Bengio, "An EM Approach to Grammatical Inference: Input/Output HMMs," in *International Conference on Pattern Recognition*, 2004, vol. 2, pp. 289–294.

[208] S. Bengio and Y. Bengio, "An EM Algorithm for Asynchronous Input/Output Hidden Markov Models," in *International Conference On Neural Information Processing*, 1996, pp. 328–334.

[209] J. Sobon, A. Roscoe, and B. Stephen, "Energy storage day-ahead scheduling to reduce grid energy export and increase self-consumption for micro-grid and small power park applications," in *2017 52nd International Universities Power Engineering Conference, UPEC 2017*, 2017.

[210] B. Stephen, R. Telford, and S. Galloway, "Non-Gaussian Residual Based Short Term Load Forecast Adjustment for Distribution Feeders," *IEEE Access*, vol. 8, pp. 10731–10741, 2020.

[211] T. Hastie, R. Tibshirani, and J. Friedman, "Boosting and Additive Trees," in *The Elements of Statistical Learning*, New York, NY: Springer New York, 2009, pp. 337–387.

[212] G. Schwarz, "Estimating the Dimension of a Model," *Ann. Stat.*, vol. 6, no. 2, pp. 461–464, Mar. 1978.

[213] R. E. Kass and A. E. Raftery, "Bayes Factors," *J. Am. Stat. Assoc.*, vol. 90, no. 430, pp. 773–795, Jun. 1995.

[214] T. Adam, R. Langrock, and C. H. Weiß, "Penalized estimation of flexible hidden Markov models for time series of counts," *Metron*, vol. 77, no. 2, pp. 87–104,

Aug. 2019.

[215] W. Zucchini and I. L. MacDonald, *Hidden Markov Models for Time Series: An Introduction Using R (Monographs on Statistics & Applied Probability)*. Chapman & Hall/CRC, 2009.

[216] C. Giraud, *Introduction to High-Dimensional Statistics*, 1st ed. New York: Chapman and Hall/CRC, 2014.

[217] C. Spearman, "The Proof and Measurement of Association between Two Things," *Am. J. Psychol.*, vol. 15, no. 1, p. 72, Jan. 1904.

[218] H. Rauf, M. Khalid, and N. Arshad, "Machine learning in state of health and remaining useful life estimation: Theoretical and technological development in battery degradation modelling," *Renew. Sustain. Energy Rev.*, vol. 156, p. 111903, Mar. 2022.

[219] T. Sun, B. Xu, Y. Cui, X. Feng, X. Han, and Y. Zheng, "A sequential capacity estimation for the lithium-ion batteries combining incremental capacity curve and discrete Arrhenius fading model," *J. Power Sources*, vol. 484, p. 229248, Feb. 2021.

[220] Z. Deng, X. Hu, P. Li, X. Lin, and X. Bian, "Data-Driven Battery State of Health Estimation Based on Random Partial Charging Data," *IEEE Trans. Power Electron.*, vol. 37, no. 5, pp. 5021–5031, May 2022.

[221] X. Li, C. Yuan, Z. Wang, J. He, and S. Yu, "Lithium battery state-of-health estimation and remaining useful lifetime prediction based on non-parametric aging model and particle filter algorithm," *eTransportation*, vol. 11, p. 100156, Feb. 2022.

[222] X. Y. Yao, G. Chen, L. Hu, and M. Pecht, "A multi-model feature fusion model for lithium-ion battery state of health prediction," *J. Energy Storage*, vol. 56, p. 106051, Dec. 2022.

[223] N. Scott, F. Veryfier: Jeff, and S. Veryfier: Marc, "Prepared For Highlands And Islands Enterprise in Partnership with Scottish Government MICROGRIDS A GUIDE TO THEIR ISSUES AND VALUE," 2016.

[224] "Introduction to microgrids insight | UK Power Networks Services." [Online]. Available: https://ukpowernetworksservices.co.uk/insights-and-news/introduction-to-microgrids/. [Accessed: 05-Feb-2022].

[225] B. Stephen, X. Tang, P. R. Harvey, S. Galloway, and K. I. Jennett, "Incorporating practice theory in sub- profile models for short term aggregated residential load forecasting," *IEEE Trans. Smart Grid*, vol. 8, no. 4, pp. 1591–1598, 2017.

[226] A. Marinescu, C. Harris, I. Dusparic, S. Clarke, and V. Cahill, "Residential

electrical demand forecasting in very small scale: An evaluation of forecasting methods," in *2013 2nd International Workshop on Software Engineering Challenges for the Smart Grid (SE4SG)*, 2013, pp. 25–32.

[227] J. R. Lloyd, "GEFCom2012 hierarchical load forecasting: Gradient boosting machines and Gaussian processes," *Int. J. Forecast.*, vol. 30, no. 2, pp. 369–374, 2014.

[228] C. E. Borges, Y. K. Penya, and I. Fernandez, "Evaluating Combined Load Forecasting in Large Power Systems and Smart Grids," *Ind. Informatics, IEEE Trans.*, vol. 9, no. 3, pp. 1570–1577, 2013.

[229] P. Cichosz, *Data mining algorithms : explained using R / [internet resource]*. Chichester, West Sussex ; Malden, MA : John Wiley & Sons Inc., 2015.

[230] G. E. P. Box, "Science and statistics," in *Journal of the American Statistical Association*, vol. 71, no. 356, 2009, pp. 791–799.

[231] S. Maheshwari and A. Kumar, "Empirical Mode Decomposition: Theory & Applications," *Int. J. Electron. Electr. Eng.*, vol. 7, no. 8, pp. 873–878, 2014.

[232] C. Torrence and G. P. Compo, "A practical Guide to Wavelet Analysis," *Bull. Am. Meteorol. Soc.*, vol. 79, no. 1, pp. 61–78, 1998.